

**IMPLANTABLE TRANSDUCERS FOR  
NEUROKINESIOLOGICAL RESEARCH AND  
NEURAL PROSTHESES**

by

**Klaus Kallesøe**

M.Sc.E.E. Systems Eng., Biomedical, University of Aalborg, Denmark, 1990

THESIS SUBMITTED IN PARTIAL FULFILLMENT OF  
THE REQUIREMENTS FOR THE DEGREE OF  
DOCTOR OF PHILOSOPHY  
IN THE  
SCHOOL OF KINESIOLOGY

© Klaus Kallesøe 1998

SIMON FRASER UNIVERSITY

February 1998

All rights reserved. This work may not be  
reproduced in whole or in part, by photocopy  
or other means, without permission of the author.

## Approval


ii


**NAME :** Klaus Kallesøe

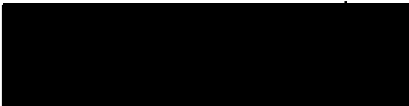
**DEGREE :** Doctor of Philosophy (Applied Sciences, Kinesiology)


**TITLE OF THESIS :** Implantable transducers for neurokinesiological research and neural prostheses


### EXAMINING COMMITTEE :

  
\_\_\_\_\_  
*Dr. Joaquín Andrés Hoffer*, Senior Supervisor  
Professor, School of Kinesiology

  
\_\_\_\_\_  
*Dr. Theodore E. Milner*  
Associate Professor, School of Kinesiology

  
\_\_\_\_\_  
*Dr. Harold Weinberg*  
Professor, School of Kinesiology

  
\_\_\_\_\_  
*Dr. Douglas Cheyne*, Internal Examiner  
Adjunct Professor, School of Kinesiology

  
\_\_\_\_\_  
*Dr. Arthur Prochazka*, External Examiner  
Professor in Physiology, University of Alberta  
Division of Neuroscience, 507 Heritage Bldg.  
University of Alberta, Edmonton, Alberta T6G 2S2  
CANADA

Chair: *Dr. Miriam Rosin*, Professor, School of Kinesiology

**Date Approved:**

24 Feb 1998

**PARTIAL COPYRIGHT LICENSE**

I hereby grant to Simon Fraser University the right to lend my thesis, project or extended essay (the title of which is shown below) to users of the Simon Fraser University Library, and to make partial or single copies only for such users or in response to a request from the library of any other university, or other educational institution, on its own behalf or for one of its users. I further agree that permission for multiple copying of this work for scholarly purposes may be granted by me or the Dean of Graduate Studies. It is understood that copying or publication of this work for financial gain shall not be allowed without my written permission.

**Title of Thesis/Project/Extended Essay**

---

Implantable transducers for neurokinesiological  
research and neural prostheses

---

---

---

**Author:** \_\_\_\_\_

(signature)



Klaus Kallesøe

(name)

16 Feb. 1998

(date)

The objective of this thesis was to develop a family of advanced electrical and mechanical interfaces to record activity of nerves and muscles during natural movements. These interfaces have applications in basic research and may eventually be refined for used in restoring voluntary control of movement in paralyzed persons.

- 1) A muscle length gauge was designed that is based on piezoelectric crystals attached at the ends of a fluid filled extensible tubing. The *in-vivo* performance of these gauges was equal to previous length gauge designs. In addition, the ultrasound based design provided for the first time a direct muscle length calibration method.
- 2) An innovative nerve cuff closing technique was devised that does not require suture closures. The new design uses interdigitated tubes to lock the opening and fix the lumen of a nerve cuff. The cuffs were tested in long-term mammalian implants and their performance matched or surpassed previous closure designs. The nerve cuff was further redesigned to include a more compliant cuff wall and wire electrodes.
- 3) Floating microelectrodes previously used for central nervous system recordings were adapted for chronic use in the peripheral nervous system. These electrodes proved disappointing in terms of signal quality and longevity. The reasons for failure are thought to be of both electrical and mechanical origin.
- 4) An innovative silicon micromachined peripheral single unit electrode was designed and tested. In the *in-vivo* tests, a limited number of recording sites successfully established short-term neural interfaces. However, the quality of the electrode performance, in terms of signal amplitude and ability to discriminate single unit potentials, was insufficient.
- 5) Using a finite difference model, a numerical simulation of static and dynamic electrical interactions between peripheral axons and microelectrode interfaces was derived. The model consisted of resistive and capacitive elements arranged in a 3-dimensional conductive universe (two spatial dimensions and time). Models of intrafascicular fine wire or silicon based electrodes were used to record simulated propagating action potentials. It was confirmed that electrode movement affected the recorded signal amplitude and that a

dielectric layer on a silicon electrode accentuated the recorded potential field. A conducting back plane facing away from axon sources did not have a significant effect on the electrode recording properties.

In conclusion, several novel implantable transducers were developed for use in neurokinesiological research. A numerical simulation of the axonal potentials recorded by intrafascicular electrodes helped interpret various shortcomings found in the *in-vivo* electrode performance. Although not attempted in the present thesis some of the developed technologies may have potential of transferring to clinical neural prostheses applications.

## Acknowledgments

v

Throughout the present thesis work many friends, family members and relatives have been very encouraging and supportive in my efforts and I am sincerely grateful for all of it. This print would not have seen daylight without you.

In chronological order, I would in particular like to thank the following people:

First of all my Danish relatives, especially my parents, Ella Hass and Ole Kallesøe, for supporting and encouraging me throughout all these years away from Denmark.

Secondly, one of my very best friends, Dr. Morten Haugland who is an ever inspiring, enthusiastic and joyful person to be around. I owe him both my interest in biomedical engineering and the initial arrangements for my Canadian adventure.

Thirdly, Dr. Andy Hoffer for initiating, inspiring and supporting my work throughout the years and for enduring and correcting my "Dinglish" accent. On a similar note, I wish to express my gratitude to all the members serving on my supervisor committee, Drs. Ted Milner, Tom Richardson and Hal Weinberg. A special thought goes to Tom, wherever you are.

In addition, many lab-mates have generously shared and contributed their time and expertise. One of these, Ignacio Valenzuela, became a very close and personal friend and Best Man of mine. I am grateful for having experienced his wonderful enthusiasm and ever joyful spirit. You have truly changed my life.

A long list of other lab-mates and friends exist (in alphabetic order): Dr. Gordon Boorman for being an inspiring academic colleague and friend; Dr. Yunquan Chen for many fruitful technical discussions; Paul Christensen and family for keeping the Danish spirit alive; David Crouch for many a good "Duke" discussion; Dr. Janice Eng as an inspiring rising academic star; Myriam El Mouldi for her encouraging Sanja to join me on a canoe trip; Catharine Kendall for a great friendship and showing me how to stay calm; Dr. Haiming Qi for fruitful academic discussions; Teresa Razniewska for her ever present assistance in Calgary; Kevin Strange for supporting friendship and collaboration; Dave Viberg for being a levelheaded, tremendously informative and knowledgeable friend and for providing inspiring technical support, and Dr. Jan Weytjens for exchanging academic opinions.

## Acknowledgments

I apologize for not mentioning everyone here. As friends and colleges, you have all shared my enjoyments and frustrations throughout the years and I certainly appreciate your support.

All this would not have taken place without the generous financial support of several funding agencies in both Canada and Denmark (in chronological order):

"President's Ph.D. research stipend", Canada 1997; "Dean's graduate fellowship, Simon Fraser University", Canada 1996; "Dean's graduate fellowship, Simon Fraser University", Canada 1995; "Government of Canada Awards", Canada 1993; "Knud Højgaards Fond", Denmark 1992; "Thomas B. Thriges Fond", Denmark 1992; "Alberta Heritage Foundation for Medical Research", Canada 1991; "Det Obelske Familiefond", Denmark 1991; "Løvens Kemiske Fabriks Fond", Denmark 1990; "Det Obelske Familiefond", Denmark 1990; "Dr. Techn. A.N. Neergaards og hustrus Fond", Denmark 1990.

Finally, a very special thanks go to Sanja Savic-Kallesøe (Dr. "Wife" and "Mom"), for having shared my frustrations and for invaluable assistance with my writing. - And, of course, for enlightening my life with our daughter Sarah Aleksandra.

# Table of contents

vii

<i>Approval</i>	ii
<i>Abstract</i>	iii
<i>Acknowledgements</i>	v
<i>Table of contents</i>	vii
<i>List of tables</i>	ix
<i>List of figures</i>	x
<b>I. INTRODUCTION</b>	<b>1</b>
A. SCOPE OF THESIS	1
B. FUNCTIONAL NEUROMUSCULAR STIMULATION (FNS)	1
C. PROPRIOCEPTORS	4
Spindles	4
Golgi tendon organ (GTO)	7
D. RECORDING PROPRIOCEPTIVE FEEDBACK DURING NORMAL MOVEMENTS	8
Biomechanical signals	8
Bioelectric signals - EMG	11
Bioelectric signals - ENG	12
E. RATIONALE	14
Biomechanical transducer: Implantable length transducer (Length gauge)	14
Bioelectric transducer: Implantable nerve cuff transducer (Nerve cuff)	15
Bioelectric transducer: Implantable single unit electrode	16
F. OBJECTIVES OF THE THESIS	18
<b>II. GENERAL EXPERIMENTAL DESIGN AND SURGICAL APPROACH</b>	<b>19</b>
<i>Training</i>	19
<i>Experimental design</i>	20
<i>Surgical approach</i>	23
<i>Recording procedures</i>	26
<b>III. MUSCLE LENGTH GAUGE</b>	<b>31</b>
<i>Conventional resistive length gauge</i>	31
<i>Objective</i>	32
<i>The use of piezoelectric transducers</i>	32
<i>Piezoelectric ultrasound based muscle length gauge</i>	34
<i>Application of piezoelectric length gauges</i>	37
<i>Discussion</i>	39
<b>IV. NERVE CUFF RECORDING ELECTRODE</b>	<b>43</b>
<i>Objective</i>	43
<i>Theory of operation</i>	43
<i>Existing recording nerve cuff designs</i>	45
<i>New nerve cuff designs</i>	49
<i>Application of new designs</i>	54
<i>Discussion</i>	58



<b>V. FINE WIRE AND HATPIN SINGLE UNIT ELECTRODE</b>	<b>63</b>
<i>Objective</i>	65
<i>Electrode fabrication and implantation</i>	65
<i>Results of 1<sup>st</sup> and 2<sup>nd</sup> series of implants</i>	71
<i>Discussion of 1<sup>st</sup> and 2<sup>nd</sup> series of implants</i>	74
<i>Hatpin micro-electrode based on commercial electrode tips</i>	78
<i>Results of 3<sup>rd</sup> series of implants</i>	82
<i>Discussion of 3<sup>rd</sup> series of implants</i>	83
<i>Discussion of fine wire or hatpin single unit electrode</i>	84
<b>VI. SILICON BASED SINGLE UNIT ELECTRODE</b>	<b>86</b>
<i>Objective</i>	89
<i>Designing a silicon based electrode</i>	89
<i>Initial experiments with silicon based "Schmidt probe"</i>	92
<i>1<sup>st</sup> Silicon design: PSU-0 probes</i>	96
<i>Iridium activation</i>	102
<i>2<sup>nd</sup> Silicon design: PSU-3 and PSU-4 probes</i>	104
<i>3<sup>rd</sup> Silicon design: PSU-5 and PSU-6 probes</i>	111
<i>Discussion</i>	114
<b>VII. SIMULATION OF SINGLE AXON RECORDING INTERFACES</b>	<b>118</b>
<i>Objectives</i>	118
<i>Analytical modeling</i>	119
<i>Discrete numerical solution to analytical models</i>	122
<i>Formalism</i>	124
Definition of the conductive universe	125
Axon model	127
Neural current source model	129
Boundary specifications	130
<i>Solution method</i>	132
Implementation	136
The interface site, its cabling and preamplification	143
<i>Simulated action potentials</i>	151
Stationary potential along unmyelinated fiber	151
Stationary potential along myelinated fiber	155
Dynamic potential near a myelinated fiber	156
Simulation of silicon recording electrode	161
Simulation of fine wire recording electrode	165
<i>Discussion</i>	168
<b>VIII. DISCUSSION</b>	<b>174</b>
Length gauge	174
Nerve cuff recording electrode	175
Single unit electrodes	177
Simulation of intrafascicular interfaces	181
Final remarks	184
References	185

## List of tables

ix

Table V.1: Hatpin and fine wire experimental series (1 and 2).	72
Table V.2: Hatpin experiments using commercial tip electrodes.	82
Table VI.1: Initial silicon probe experiments using the "Schmidt" probes.	94
Table VI.2: Silicon probe experiments using PSU-0 probes.	98
Table VI.3: Silicon probe experiments using the PSU-3 and PSU-4 probes.	109
Table VI.4: Silicon probe experiments using the PSU-5 and PSU-6 probes.	112
Table VII.1: Measurement of the shunt capacitance	147

## List of figures

x

Figure I.1: Biomechanical transducers implanted on a cat MG muscle	9
Figure I.2: Bioelectric transducers instrumented on a cat MG muscle	13
Figure II.1: Typical devices implanted in a cat's left hindlimb	21
Figure II.2: Recording setup	27
Figure III.1: Predicted ultrasound wave front pattern	33
Figure III.2: Piezoelectric length gauge, Type 1	35
Figure III.3: Piezoelectric length gauge, Type 2	36
Figure III.4: Stiffness characteristics of Type 1 and Type 2 length gauge designs	36
Figure III.5: Chronic measurements using piezoelectric gauge Type 1	37
Figure III.6: Chronic measurements using piezoelectric gauge Type 2	38
Figure III.7: Stiffness characteristics of a Latex based piezoelectric length gauge	41
Figure III.8: Final Type 2 length gauge design, including the double layer shell.	42
Figure IV.1: Extracellular recording methods from peripheral nerves	44
Figure IV.2: Electrical model of the center recording electrode of the nerve cuff	44
Figure IV.3: Traditional nerve cuff with suture closing	45
Figure IV.4: Possible failure points in the traditional suture closed cuff	46
Figure IV.5: Possible failure points in the traditional sewn wire electrodes	48
Figure IV.6: Nerve cuff closing method.	49
Figure IV.7: Nerve cuff installation.	51
Figure IV.8: Casting a nerve cuff using Silastic® medical adhesive.	52
Figure IV.9: Cross-section of a spiral electrode cast in a silicone cuff wall	54
Figure IV.10: Top: Normalized peak-to-peak amplitudes of CAPs	56
Figure IV.11: Top: Normalized conduction latencies of CAPs	57
Figure IV.12: Geometric mean of distal nerve cuff impedances	57
Figure IV.13: Self sizing nerve cuff designs.	60
Figure IV.14: The "gun barrel" cuff design	61
Figure V.1: The hatpin design	66
Figure V.2: Sciatic nerve cuff with hatpin electrodes	68
Figure V.3: The simple fine wire design	69
Figure V.4: The revised fine wire design	71
Figure V.5: An example of a spike triggered average of a 1st series implant hatpin	73
Figure V.6: Spike triggered averaging of 2nd series implant	74
Figure V.7: New hatpin design	79
Figure V.8: A double compartment tibial cuff	80
Figure V.9: Thin wall sciatic cuff	81
Figure V.10: Spike triggered averaging from the new hatpin style.	83
Figure VI.1: Thin film masks for a silicon probe design.	90
Figure VI.2: "Schmidt 2" probe layout.	92
Figure VI.3: Minimal instrumentation of intact left cat hindlimb	93
Figure VI.4: Surgical insertion technique.	94
Figure VI.5: An example of a spike triggered average from a "Schmidt" probe implant	95
Figure VI.6: Layout of the Peripheral Single Unit design PSU-0.	97
Figure VI.7: Spike-triggered averaging of two MG afferent neurons	99
Figure VI.8: Spike-triggered averaging of a MG afferent neuron	99
Figure VI.9: Spike triggered average of several MG	100
Figure VI.10: Activity of 3 simultaneously recorded MG afferents	101

## List of figures

xi

Figure VI.11: Setup for cyclic voltammetry.	103
Figure VI.12: Probe insertion technique.	105
Figure VI.13: Details of the PSU-3 and PSU-4 designs.	107
Figure VI.14: The assembly technique of PSU-3-4-5-6 designs.	108
Figure VI.15: Unwanted electrical connections to the Si-substrate	110
Figure VI.16: The bonding pad sites were redesigned on the PSU-5 and PSU-6 probes	112
Figure VI.17: Spike-triggered averaging of an MG afferent neuron	113
Figure VII.1: Sketch of the conductive universe.	126
Figure VII.2: Electric grid-point model of the "conductive universe".	127
Figure VII.3: Discrete axon model.	128
Figure VII.4: Discrete implementation of nodes of Ranvier.	129
Figure VII.5: Transmembrane current flow	130
Figure VII.6: Test of monopole source	136
Figure VII.7: Test of source-sink combination.	137
Figure VII.8: Test of resistive barrier	138
Figure VII.9: Test of leaky resistive barrier.	139
Figure VII.10: Test of charging capacitive barrier.	140
Figure VII.11: Continued test of charging capacitive barrier.	140
Figure VII.12: Test of discharging capacitive elements.	141
Figure VII.13: Continued test of discharging capacitive elements.	142
Figure VII.14: Potential characteristics of a single point in the computational grid.	142
Figure VII.15: The equivalent circuit of a metal microelectrode,	143
Figure VII.16: Assumed extracellular current pathways in neural tissue.	144
Figure VII.17: Preamplifier stage.	148
Figure VII.18: Simplified equivalent circuitry.	149
Figure VII.19: The finite difference implementation of the recording interface site,	150
Figure VII.20: Stationary fields around an unmyelinated fiber	152
Figure VII.21: Extracellular potentials along an unmyelinated axon	153
Figure VII.22: Stationary fields around an unmyelinated fiber in a bounded environment.	154
Figure VII.23: Extracellular potentials along an unmyelinated axon	154
Figure VII.24: Stationary fields around a myelinated fiber in an unbounded environment.	155
Figure VII.25: Potential amplitudes along a myelinated axon	156
Figure VII.26: The dynamic current source configuration.	157
Figure VII.27: Perpendicular distance related attenuation	158
Figure VII.28: Longitudinal movement of a recording point along an axon membrane	159
Figure VII.29: Simulated dynamic differential recording	160
Figure VII.30: Silicon electrode in simulated dynamic action potential field.	161
Figure VII.31: Detailed view of local field distortion caused by a silicon electrode.	162
Figure VII.32: Cross sectional view of the potential drop	162
Figure VII.33: Dynamic action potentials	163
Figure VII.34: Dynamic action potentials	164
Figure VII.35: Fine wire simulation.	165
Figure VII.36: An example of back ground "noise" potential field..	166
Figure VII.37: Background noise recordings.	166
Figure VII.38: Background noise distortions around a silicon electrode.	167

# I. INTRODUCTION

## *A. Scope of thesis*

This thesis is focused on the development of a family of advanced electrical and mechanical interfaces suitable for recording the activity of nerves and muscles during natural movements. These interfaces have application directly in basic research as well as indirectly in development of prosthetic devices used for restoration of voluntary control of movement in paralyzed persons.

## *B. Functional Neuromuscular Stimulation (FNS)*

Traumatic spinal cord injuries (SCI) or strokes typically damage localized areas of the nervous system, generally leaving the peripheral sensory and motor organs intact. In spite of vigorous ongoing research efforts, at present no methods are available for regenerating or reconnecting severed nerve tracts in the spinal cord. Treatments are limited to assisting spontaneous recovery and providing prosthetic assistance to improve the patient's quality of life and general life expectancy. Some of these prosthetic devices are based on electrical stimulation of muscles (Functional Electrical Stimulation - FES) or motor nerves (Functional Neuromuscular Stimulation - FNS) to elicit functional movement (Peckham 1992, reviewed in Stein et al. 1992, Agnew & McCreery 1990, Crago et al. 1986.)

Totally implanted FES systems have for decades successfully benefited millions of cardiac patients and similar success has lately been shown in thalamic pacemaker implants (Pollak et al. 1996, Benabid et al. 1996). Cochlear FNS systems and partial gait and stance assistance FES and FNS systems have to a lesser extent been used in rehabilitation applications, but strong research efforts are presently advancing these areas (Kralj and Bajd 1989, Kralj et al. 1987).

Application of FNS and FES systems in areas such as control of respiration, bowel and bladder functions, and reproduction have only been available on a more experimental basis (reviewed by Teeter 1992). A similar situation is in the control of upper extremities (reviewed by Billan and Gorman 1992, reviewed in Stein et al. 1992b) and lower extremities (reviewed by Jaeger

1992). Although the potential need for these devices is evident, the number of cases where technology has successfully been transferred from the research environment to clinical applications is very small. This is partly due to insufficient technical performance of the experimental prosthetic devices (Jaeger 1992.)

Early FNS systems were typically implemented using straight feed-forward control (open loop), where no bio-feedback was included to accommodate individual user needs (e.g. cardiac pacemakers with no adjustment of pacing frequency). These systems may be adequate for patients with limited disabilities performing simplified tasks (McNeal et al. 1989), but will in general not be acceptable in situations where instability and inefficient control is not backed up by any remaining physiological control. This is the case in para- or quadriplegic stance and gait, where body posture must depend exclusively on an FNS or FES system. Even a relatively minor technical failure, like inappropriate timing of stimulation, can have a disastrous outcome. In such a system, additional stability and increased efficiency can be obtained through the use of feedback from peripheral sensors and implementation of adequate control algorithms (Stein et al. 1992a, Popovic et al. 1993, Abbas and Triolo 1997).

One of the major obstacles in successfully designing a robust neuromuscular prosthesis system is the availability of feedback transducers. A variety of artificial sensors have been tested, to signal onset and offset of biomechanical events, like shoe switches for detection of heel strike and toe off. Similarly, mechanical linkage devices (goniometers) have been strapped to limbs for measuring ankle, knee, hip, shoulder, elbow, wrist or finger joint angles (Pronk and van der Helm 1991, Arent-Nielsen et al. 1990, Petrofsky et al. 1984, Chao 1979, Townsend et al. 1977, Kettelkamp et al. 1970, Finley and Karpovich 1959). Force and pressure transducers have been mounted on extremities for measuring grasp force or weight bearing foot load (Crago et al. 1986). Accelerometers have been used in applications similar to the electro-goniometer, for measuring limb segment acceleration (Morris 1973, Smidt et al. 1977). Inclometers that measure the tilt of limb segments have recently been applied as a rehabilitation tool (Dai et al. 1996). Hall effect transducers have been used on an experimental basis, for measuring joint angles (Crago et al. 1986).

The initial design of these sensor systems has typically been based on modified industrial transducers. This design approach is adequate for initial trials, with the transducer mounted externally on the patient. However, for continuous long-term use of the system, entirely different requirements need to be met. Although these requirements rarely exceed industrial specifications of range and resolution, they do impose important constraints in terms of size, robustness in harsh environments and user-friendliness.

The ultimate test of any of these rehabilitation devices is in the long term use, i.e. years, decades or the patient's entire life span. In long-term use, patients continuously evaluate the benefits gained from using a prostheses against the inconveniences or "cost" of the system. This cost evaluation obviously includes technical issues like functionality, robustness and stability of the system, but also very important issues like cosmetic appeal and user-friendliness are considered. If the drawbacks, such as being too displeasing and cumbersome to use, outweigh the benefits, the system will simply not be used. In a similar manner, if a simpler device - like a wheelchair or rigid orthosis - performs efficiently and is socially well accepted, a complex, fragile and unusual looking FNS system will not be used.

With reference to the above defined cost-benefit evaluation, designing "cost effective" prosthesis systems is always a priority in rehabilitation engineering. Recent progress in the design of implantable feedback transducers (Hoffer 1990, Hoffer et al. 1996) and the potential uses of natural transducers (Hoffer and Sinkjær 1986, Hoffer 1988, Hoffer and Haugland 1992, Popovic et al. 1993, Haugland 1994, Haugland et al. 1995, Yoshida and Horch 1996), has opened new avenues in prosthetic designs. The use of natural sensors can potentially reduce both cosmetic and technical limitations of existing FNS systems. This will increase the likelihood of successful adoption of a system by patients (Kralj et al. 1993).

When designing FNS systems to replace lost motor control, an obvious approach is to try to mimic the natural control schemes present prior to any injuries. It is evident from neurophysiological research that feedback from a multitude of distributed receptors is a crucial component of physiological motor control systems (reviewed by Hasan and Stuart 1988). These feedback channels include several modalities of signals from muscle, joint and cutaneous mechanoreceptors (Edin 1992) that define sensations of relative position of

individual body segments - i.e. *proprioception* (Rothwell 1994). Proprioceptive feedback has been shown to be a vital feedback parameter in controlling limb movement (van Dijk 1978, McIntyre and Bizzi 1993).

### *C. Proprioceptors*

Two mammalian proprioceptors - muscle spindles and Golgi tendon organs (GTOs) - have for decades been the target of intensive postural and locomotor research (reviewed by Matthews 1972, 1981, Hulliger 1984, Hunt 1990, Jami 1992). The muscle spindle stands out as a unique sensor that follows both mechanical and neural inputs. Its role in the neuromuscular control system is generally assumed to be the transmission of information related to muscle fiber length and rate of change of muscle fiber length. In a similar manner, GTO's are viewed as transmitters of information about the force produced by groups of muscle fibers.

#### *SPINDLES*

The **anatomy** of the mammalian muscle spindle describes a receptor capsule encircling the central section of a set of intrafusal muscle fibers. These smaller muscle fibers run in parallel with larger and more numerous extrafusal muscle fibers, and do not contribute significantly to the force relative to the overall performance of the muscle. The neural output from the spindle capsule has, however, a powerful indirect effect on the activation level of the extrafusal fibers.

The spindle is described as a transducer with two types of input sources - external mechanical stretch, and internal contraction of intrafusal fibers. The output of the transducer is seen in a modulated receptor potential. This potential is encoded in the firing frequency of the group Ia and II afferent nerve fibers innervating the capsule.

*Neural output* from the spindle is transmitted via afferent innervation of the capsule consisting of a primary nerve fiber (group Ia, diam.: 12-20  $\mu\text{m}$ , propagation velocity: 70-120  $\text{m}\cdot\text{s}^{-1}$ ) and a secondary nerve fiber (group II, diam.: 5-12  $\mu\text{m}$ , propagation velocity: 30-70  $\text{m}\cdot\text{s}^{-1}$ ). The afferent nerve fibers stem from three different classes of intrafusal fibers: dynamic bag fibers, static bag fibers and chain fibers. The primary group I originates from all three types, whereas the secondary group II only innervates the static bag fibers and the chain fibers. Each of the



intrafusal muscle fiber type exhibits distinctly different mechanical characteristics, thereby making the transduction of the spindle dependent upon the composition of these fibers. In the cat, typically 1 dynamic bag fiber, 1-2 static bag fibers, and 3-5 chain fibers constitute a spindle, whereas human spindles generally have more chain fibers (Hulliger 1984).

*Neural input* to spindles is transmitted through contraction of the intrafusal fibers. These are innervated by two classes of efferent nerve fibers. The majority of this innervation (>80%) is by fusimotor fibers ( $\gamma$ -fibers, diam.: 3-6  $\mu\text{m}$ , propagation velocity: 15-30  $\text{m}\cdot\text{s}^{-1}$ ) and to a lesser degree by skeletofusimotor fibers ( $\beta$ -fibers, diam.: 12-20  $\mu\text{m}$ , propagation velocity: 70-120  $\text{m}\cdot\text{s}^{-1}$ ). The fusimotor fibers can be either  $\gamma$ -dynamic or  $\gamma$ -static, innervating either the dynamic bag fibers or the static bag and the chain fibers, respectively. The fusimotor fibers are smaller than the primary afferent fibers, whereas the skeletofusimotor fibers overlap in terms of fiber diameter and propagation velocity.

The **physiology** of the spindle describes a receptor sensitive to two different stimuli: *mechanical* stimulation during extension of intrafusal fibers caused by increased external load of the extra- and intrafusal fibers, and *neural* stimulation causing activation and shortening of the polar regions (fiber sections outside the central capsule) of the intrafusal muscle fibers.

*Mechanical stimuli* in terms of spindle stretching, will generate an afferent response depending upon the mechanical characteristics and state of the intrafusal fibers. The three types of intrafusal fibers each exhibit unique mechanical stretch response characteristics and their receptor endings respond accordingly. The sensory regions of the dynamic bag fibers have been shown to be most sensitive to relative fiber length changes, whereas those of static bag fibers and chain fibers are more responsive to changes in absolute length (Matthews and Stein 1969, Hulliger 1984). For the dynamic bag fibers it was shown that the reason for the dynamic sensitivity is a mechanical inhomogeneity in the central and polar regions of the fiber. The elastic central capsule region stretches rapidly and extensively during the initial phase of muscle fiber stretch, whereas the more viscous polar regions stretch more slowly over a longer time interval (Boyd 1976). After the initial mechanical transient, the polar regions not only accommodate the external stretch, they also partially absorb some of the initial stretch in the central region. The settling of this relative length change causes a decrease in the length of

the central region and thereby a drop in the firing rate of the primary afferent fibers. This drop in firing rate is known as a "creep" in the spindle primary afferent response and is not seen to the same extent in the response from either the static bag fibers or the chain fibers. The static fibers are less sensitive to dynamic length changes, probably due to a more homogeneous mechanical match between the central and polar regions of the fibers.

The afferent response to mechanical stimuli is thus dependent upon the properties of the intrafusal fibers. Those innervating dynamic bag fibers exhibit non-linear response characteristics with a high sensitivity to small amplitude, high frequency mechanical stimuli. Those endings on static bag and chain fibers, on the other hand, are more responsive to larger amplitude stretches of longer duration. Both response characteristics can be modified by changing the mechanical state of the intrafusal fibers.

*Neural stimuli* delivered through either type of efferent fibers ( $\gamma$ -static, -dynamic or  $\beta$ -motoneurone) will cause contraction of the polar regions of the spindle. This modifies the transducer characteristics by stretching the central capsule. The resulting effect on afferent discharge rate depends upon the intrafusal fiber type. The effect is most evident in the chain and static bag fibers, where the central equatorial region can stretch up to 20%, significantly increasing the resting discharge rate of the primary afferent (Rothwell 1994). Contrary to extrafusal fibers, neither the dynamic nor the static bag fibers are capable of propagating action potentials. The contractile forces of the intrafusal bag fiber thus depend on the strength of their nonpropagating endplate potentials. This causes the  $\gamma$ -dynamic activation to have a limited mechanical effect on the central spindle capsule (less than 5% length change) (Rothwell 1994).

In addition to changing the transducer sensitivity, intrafusal activation can also adjust the total length of the intrafusal fiber to compensate for decreased extrafusal fiber length during muscle contraction. Without such compensation, shortening of the extrafusal fibers beyond the slack length of the spindles would "unload" the transducer and drastically reduce its sensitivity. Simultaneous activation of  $\alpha$  and  $\gamma$  fibers, " $\alpha$ - $\gamma$  coactivation", is assumed to increase the transducer gain during motor tasks requiring intensive sensory feedback (Hulliger 1984, Murphy et al. 1984, Prochazka 1989, Murphy and Martin 1993). The coactivation would be a desirable feedback control option during gait on challenging terrain (e.g. uneven surfaces or

beam balancing), or when visual or vestibular input is limited (e.g. in dark environments or obstruction of visual pathway).

The fact that the fusimotor fibers are capable of adjusting the transducer sensitivity of the spindle is a unique characteristic among physiological receptors. It allows for very complex neural output from the spindles based on length changes in intrafusal fibers and on fusimotor and skeletofusimotor neural inputs.

### ***GOLGI TENDON ORGAN (GTO)***

The **anatomy** of a GTO is described as a capsule of connective tissue located at the myo-aponeurotic junction in series with a number of individual extrafusal fibers (human: 10-20 fibers, cat: 4-41). It encloses strands of collagen and terminals of a larger diameter afferent nerve fiber (group Ib, diam.: 12-20  $\mu\text{m}$ , propagation velocity: 70-120  $\text{m}\cdot\text{s}^{-1}$  in the cat). Inside the capsule, the nerve breaks up into many fine branches, innervating several collagen fascicles. The afferent receptor branches do not innervate all of the fascicles within the capsule. The number of motor units contributing mechanical input to a single GTO in the cat medial gastrocnemius (MG) is typically 5-6 motor units (Jami 1992). When these motor units contract, GTO receptor endings interwoven in the collagen fibers get compressed or stretched, which results in the opening of stretch-dependent ion channels in the membrane and depolarization of the receptor membrane (reviewed by Jami 1992).

The **physiology** of the GTO describes a highly sensitive force transducer capable of resolving force changes in single muscle fibers (Houk and Henneman 1967). This makes it possible to have a feedback transducer sensitive to mechanical input from only a local compartment of the muscle. It was confirmed in the cat that during voluntary isotonic movements, involving active muscle shortening, the modulation of GTO firing rate was largely determined by single motor unit activity (Prochazka and Wand 1980). The transducer output is thus more dependent upon the contraction state of individual motor units than on the external load on the tendon. This is due to the parallel arrangement of the myo-aponeurotic junctions and surrounding tissue, which effectively shunts out part of the externally applied force. The sensitivity of the GTOs thus appears very low to stretches applied to a passive muscle.

### *D. Recording proprioceptive feedback during normal movements*

Characterizing the functional behavior of the natural control system is done by simultaneously recording information from input and output flowing to and from the peripheral sensors. This requires interfacing to a voluntarily active neuromuscular system, most commonly done in mammalian animal models. This is a challenging task that calls for specially designed recording and stimulation interfaces (reviewed by Lemon 1984 and by Hoffer 1990). These interfaces can be grouped as follows:

- **Biomechanical** interfaces to muscles and tendons, that record such parameters as: tendon force, muscle length, muscle fiber length, aponeurosis deformation, limb acceleration, inter limb angles.
- **Bioelectrical** interfaces to muscles and nerves, that record such signals as: electromyogram (EMG), whole nerve electroneurogram (ENG), or unitary action potentials from single muscle units or single nerve fibers.

These interfaces may be used individually or together to create a more complete picture of a particular biological event.

#### **Biomechanical signals**

Two biomechanical actions are specifically monitored by muscle proprioceptive organs: 1) forces produced by muscles and transferred by tendons and bones; and 2) displacement of limb segments and deformation of connective tissue and muscle structures.

Measurement of tendon *force* can be obtained, for example, with strain gauges mounted on a spring steel "buckle". The buckle is typically shaped like an "E", allowing the tendon to be threaded through the two openings. This epi-tendonous type of force transducer has a limited lifetime (less than 3 months) due to connective tissue growing around the buckle, progressively shunting out force until none is transmitted through the buckle. Other types of endo-tendonous transducers are emerging, possibly extending the transducer lifetime (review by Gregor and Abelew 1994, Platt et al. 1994, Steven 1991, Arms 1991, and 1989).

Recording tendon force in the context of proprioception serves to characterize the mechanical output of a specific muscle. However, due to the above mentioned parallel arrangement of

collagen fibers in the tendon, recordings of total tendon force during normal movements are more a measure of the combined muscle load than the force input to individual GTO's. Estimating the input force to individual GTO's, using a tendon buckle, thus requires tendon force recordings during contraction of single motor units rather than during activity of the total muscle.

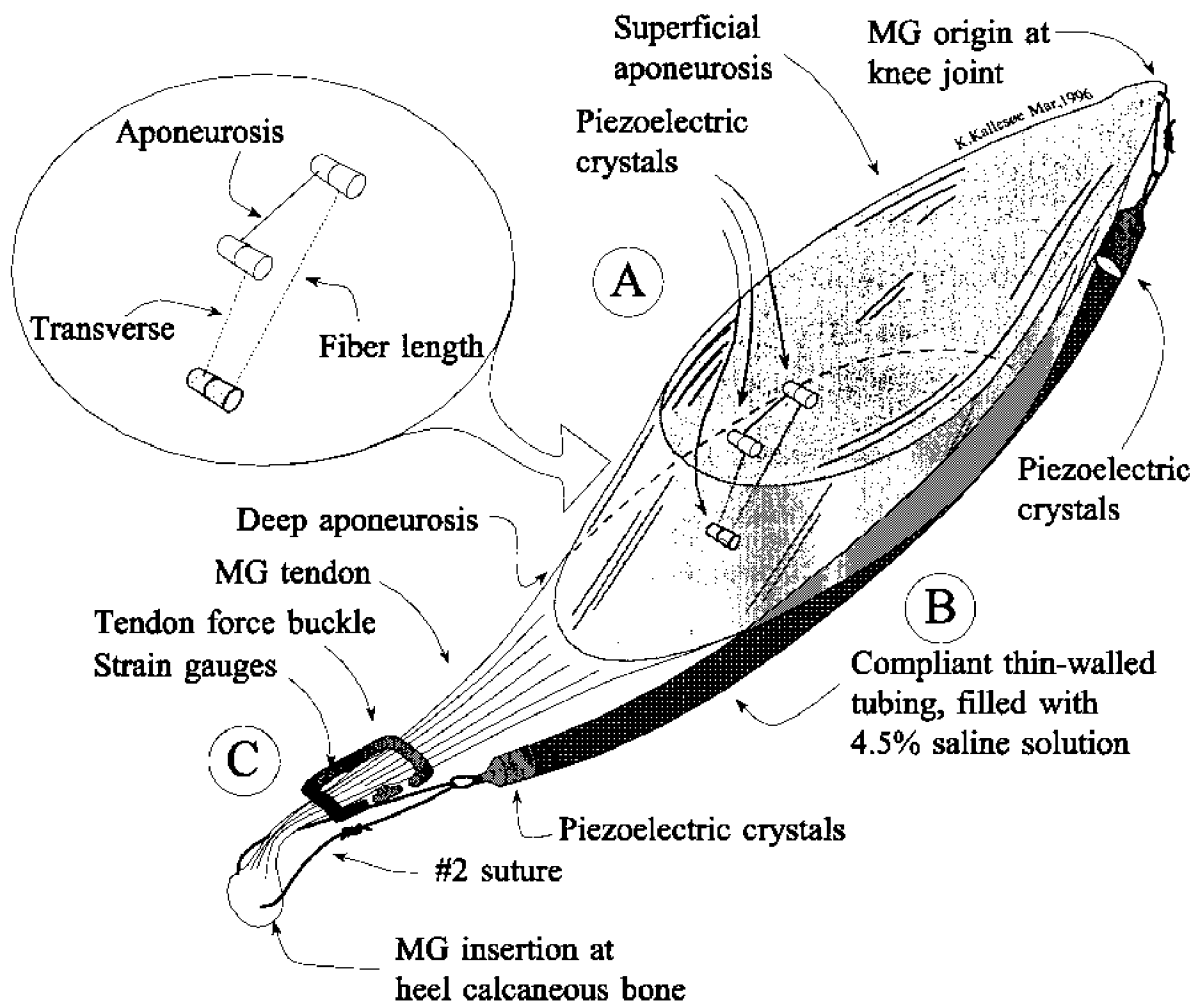


Figure I.1: Biomechanical transducers implanted on a cat MG muscle. (A) Piezoelectric crystals mounted on the MG muscle belly in a triangular configuration allow for measurements of muscle belly deformation in 3 dimensions: Fiber length changes, stretch of aponeurosis and change in belly thickness. (B) Length gauge attached on the medial side of the left MG muscle. Large sutures (#2) are passed through the calcaneous bone of the heel and through the sesamoid bone of the MG origin to provide a mechanically secure anchoring of the transducer. (C) Tendon force buckle installed on the distal section of the MG tendon. The buckle may be locked in place by 5-0 sutures to prevent the tendon from slipping out of the buckle.

Measurements of *displacement*, as in the length changes of individual muscle fibers, in the context of proprioception, helps to characterize the mechanical input to individual spindle receptors. These measurements can be done using ultrasound or reluctance transducers with

sub-millimeter resolution (Steven 1989). The use of ultrasound technology has been transferred from cardio-mechanical recording setups to neurokinesiological research for *in situ* measurements of length changes in groups of muscle fibers (Caputi et al. 1990, 1992). The use of ultrasound to measure deformation of tissue minimizes the constraint and mechanical loading on the source, making this transducer technology an excellent choice for estimating sub-millimeter length changes of muscle fibers. This technique assumes that the ultrasound conductive pathway between two piezoelectric crystals is homogenous, straight, and that the tissue pathway maintains a constant ultrasound conduction velocity. Even "simple" unipennate muscles, like the cat MG muscle, have been found to have muscle fibers curved in S-shapes (Leeuwen and Spoor 1993), and their pinnation changing during muscle contraction (Hoffer et al. 1989). However, in terms of measuring accuracy, these factors were found negligible by Caputi et al. (1992), who successfully used the ultrasound technique in recording the muscle fiber length, deformation of aponeurosis and changes in muscle fiber pinnation angles. The latter was obtained with three crystals arranged in a quasi-planar triangular formation. By using several of these triangular crystal formations, multidimensional recordings of *in vivo* muscle mechanics have been obtained (Qi et al. 1994, Ratcliffe et al. 1995).

Measurement of *displacement* on a larger scale is done when recording total muscle length. Several techniques exist for external estimation of changes of total muscle length (e.g. video analysis of movement of skin markers; externally mounted goniometers). These techniques have limited accuracy due to relative movement of cutaneous and subcutaneous tissue with respect to attached markers or goniometers. Although some transducers have been attached transcutaneously to bone (Prochazka in Lemon 1984), totally implantable transducers are less likely to have secondary complications like skin irritation or transcutaneous infections.

As reviewed by Prochazka (in Lemon 1984) and Hoffer (1990), implantable length transducers using a compliant silicone rubber tube filled with either hypertonic saline or mercury, allow for continuous measurement of the distance between the ends of the tube by recording changes in the electrical resistance of the fluid column inside the tubing.

Recording whole muscle length in the context of proprioception serves to characterize the mechanical output of specific muscles. This length is not directly equivalent to the length

changes of individual muscle spindles, due to changes in pination angles of muscle fibers and compliance in the aponeurosis (Hoffer et al. 1989). When correlating recorded spindle activity to limb movements it is thus important to include not only the overall length of the muscle but also other variables affecting the length of the spindle.

### **Bioelectric signals - EMG**

Contraction of muscles provides a mechanical input to spindle receptors, either directly through the shortening of receptors in the active muscle or indirectly by lengthening of receptors in antagonist muscles. The electrical activity generated by muscle fibers, the electromyogram (EMG), identifies local mechanical activity. In general, different levels of extracellular recording resolution can be obtained depending on the electrode configuration. Skin surface electrodes typically pick up potentials from several muscles. Activity in local regions of a muscle can be recorded with epimysial electrodes or intramuscular electrodes, with the latter technique having the advantage of discriminating activity in local compartments inside a muscle (Griep et al. 1978). These techniques are also capable of recording activity generated by individual muscle fibers (reviewed by Loeb and Gans 1986, Stein et al. 1992b).

Recording EMG in the context of proprioception serves to indirectly identify mechanical activity around muscle proprioceptors. Technical limitations eliminate direct mechanical recording from individual receptors *in vivo*, and the mechanical input to the receptor is therefore derived by indirect recording techniques. One such technique is the recording of EMG activity as an indicator of force production in local regions of the muscle. To maximize the chance of recording activity from compartments where identified receptors are located, several intramuscular electrodes can be distributed throughout the muscle.

**Bioelectric signals - ENG**

Neural activity in peripheral nerves includes both efferent axonal conduction to the muscle (innervating extra- and intrafusal fibers) and afferent conduction from the muscle (originating from proprioceptors like spindles and GTOs). Recording all of these is important for the characterization of the transduction properties of the receptors. Recordings from the surface of peripheral nerves using nerve cuff electrodes reflects mainly mass activity in populations of axons, favoring larger axons located close to the surface of the nerve. Activity of single axons can be recorded using small intraneural electrodes either introduced transcutaneously (microneurography) or implanted permanently (peripheral single unit). This type favors axonal activity in close proximity of the electrode (Schoonhoven and De Weerd 1984).

A *nerve cuff electrode* creates an electrochemical interface with the extracellular space of a group of axons, typically a whole nerve, including multiple fascicles. The extracellular potentials recorded represent the electroneurogram (ENG) of the nerve which is dominated by the activity in large myelinated axons (Hoffer et al. 1981). By encapsulating the nerve in an electrically insulating cuff, a resistive pathway is defined and extracellular potentials generated by individual axons are constrained. Using a tripolar electrode configuration and differential amplification, an ENG signal is discriminable from "noise" generated by electrical sources external to the cuff, such as potentials originating from nearby muscles (reviewed by Hoffer 1990).

Recording the whole nerve electroneurogram in the context of proprioception serves to characterize the neural input and output to and from a specific muscle. This ensemble recording can be used in conjunction with more selective recording techniques, to characterize neural activity related to single proprioceptors.



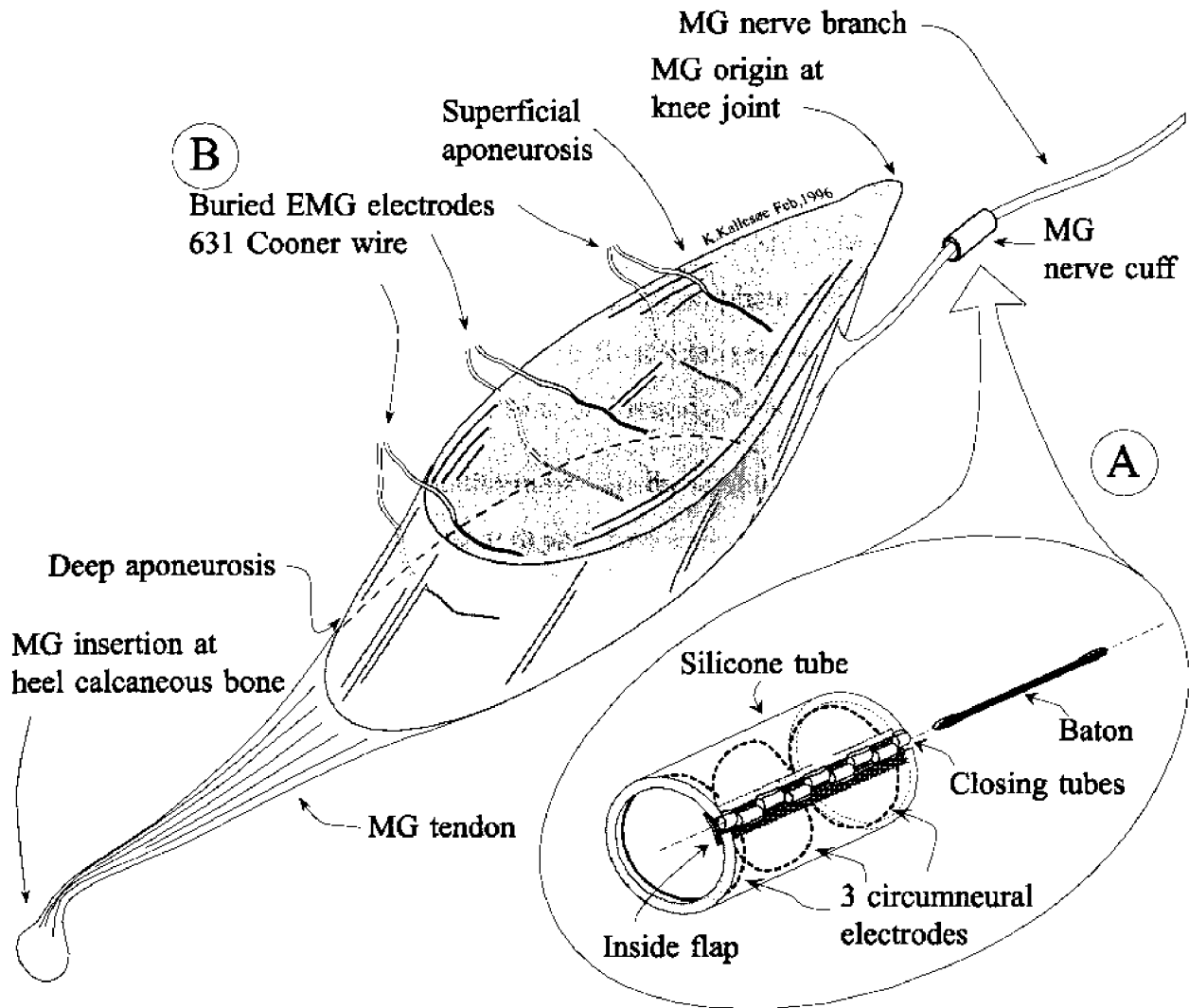


Figure I.2: Bioelectric transducers instrumented on a cat MG muscle and its nerve. (A) MG nerve cuff consisting of a silicone tube with sets of interdigitated closing tubes attached to the opening of the cuff. After the cuff is closed, a baton is inserted through the closing tubes to mechanically lock the cuff. A silicone flap attached on the inside seals the opening. Three circumneural electrodes are sewn or cast into the cuff wall. (B) Buried EMG electrodes evenly distributed along the longitudinal axis of the MG muscle belly. In addition to these recording electrodes, a differential amplification technique is used to limit "crosstalk" from neighboring muscle compartments and other muscles (Lindström and Petersén 1983). This requires one indifferent reference, or so called "ground" electrode.

*Intraneural electrodes* provide an interface to peripheral axons inside a nerve fascicle. In its most rudimentary version, an intraneural electrode consists of an electrically insulated wire with a small exposed conducting surface area which is placed close to an axon. Intraneural electrodes should be small to avoid damaging axons. So called "fine wire electrodes" consist of a miniature gauge wire with a diameter comparable to large myelinated axons (10-20  $\mu\text{m}$ ),

where the cut end of the insulated wire forms the electrochemical interface to neural tissue. Refinements of the fine wire electrode were introduced with the "thumb-tack" or "hatpin" electrodes (Salcman and Bak 1976), where a sharp, short, stiff insulated needle at the end of a fine flexible wire served as a penetrating needle. This needle was electrically insulated, except for a limited section at the tip exposing the conducting surface. The opposite end of the needle was connected to a flexible fine wire, creating a compliant mechanical linkage to external leadout wires. This allowed the electrode to float relatively unrestricted in the neural tissue, giving it the name "floating" microelectrode or "floating hatpin" electrode.

Recording single axon electroneurograms in the context of proprioception serves to characterize the neural input and output to and from a specific mechanoreceptor.

### *E. Rationale*

The transducers described above were all used or developed in neuromuscular research projects aimed at understanding physiology of proprioceptors and testing ways of possibly using these natural sensor feedback in FNS systems (Hoffer: "Muscle proprioceptors and the control of voluntary movement" funded by the Medical Research Council of Canada (MRC) 1990-1996, Hoffer: "Sensory feedback derived from afferent neurons" funded by the National Institutes of Health, USA (NIH) 1992-1999).

This thesis is focused on three applications of these transducers:

- 1) biomechanical measurement of muscle length;
- 2) nerve cuff recording of multiunit activity in peripheral nerves;
- 3) bioelectric measurement of single unit activity in peripheral nerves.

#### **Biomechanical transducer:** *Implantable length transducer (Length gauge)*

Muscle length transducers used in unrestrained, chronically implanted animals have conventionally consisted of a compliant ( $\sim 0.05 \text{ N}\cdot\text{mm}^{-1}$ ) silicone rubber tube filled with either hypertonic saline or mercury. The measurement principle was the continuous change in the electrical resistance of the fluid column inside the tubing (reviewed by Prochazka in Lemon 1984 and by Hoffer 1990). This gauge design had three major disadvantages: 1) the

change in resistance was not only related to a change in length, but depended also on changes in temperature or osmotic dilution of the hypertonic saline, 2) the dependence on length was non-linear, and 3) the absence of a direct and accurate way to calibrate the measurements.

The total length of a muscle could instead be estimated using ultrasound technology if piezoelectric crystals were attached to the origin and insertion of the muscle of interest. However, a limitation in the distance, for which a reliable signal can be obtained *in vivo* eliminated this option for many muscles. This is partly due to the inherently dissipative nature of an *in vivo* preparation and partly due to unavoidable misalignment of the crystals when limb segments are displaced. To alleviate these problems, an improved length gauge is described in this thesis which simultaneously aligned the crystals and defined a conduction pathway for the ultrasound.

**Bioelectric transducer:** *Implantable nerve cuff transducer (Nerve cuff)*

Nerve cuff electrodes have conventionally been closed and sealed with several encircling sutures placed externally along the cuff (reviewed by Hoffer 1990). In using this closing technique, several design flaws were identified: 1) closing sutures do not prevent the cuff wall from collapsing, reducing the volume of the cuff and possibly causing constriction damage to the nerve; 2) if the suture knots become loose or un-done, a pathway is created for connective tissue to grow through the longitudinal slit of the cuff opening which provides an unwanted electrical shunt of neural current flow; 3) braided suture material is difficult to clean and connective tissue adheres excessively to it; 4) tying suture knots during surgical implantation is cumbersome and time consuming.

A recording nerve cuff should be mechanically and electrically well sealed, with the interior of the cuff isolated from the exterior. The cross-section should not be allowed to decrease as this could compromise the integrity of the nerve. The closure should be easy to close and open - like a zipper. A new nerve cuff closing technique that addressed these issues is described in this thesis.

**Bioelectric transducer:** *Implantable single unit electrode*

The "floating fine wire" electrodes described above were first used by Burns et al. (1974) to study central nervous system (CNS) neurons of conscious, freely moving cats, and were later adapted for use in the spinal cord (Cleland and Hoffer 1986) and its dorsal and ventral roots (Loeb et al. 1977, Prochazka et al. 1976, Hoffer et al. 1987a). The "hatpin" electrode design was also adapted in the peripheral nervous system (PNS) by Hoffer and Weytjens (1990), who reported some success in recording efferent discharge from motoneurons. However, their electrode design and implantation technique could not provide a reliable chronic interface with single axons. All of these electrodes were designed with a fairly small recording site ( $\sim 500 \mu\text{m}^2$ ) and an impedance value of approximately 200-300 k $\Omega$  at 1 kHz.

Other styles of peripheral nerve electrodes used for local intraneural stimulation, have larger active surface areas and lower impedances (Bowman and Erickson 1985, Yoshida and Horch 1993). These electrode designs were also used for intraneural recordings of multiunit potentials under anesthetized or decerebrate conditions (Lefurge et al. 1991, Goodall et al. 1991, Yoshida and Horch 1996). Although the electrode design was proven useful for these applications, it is questionable whether unitary discrimination can be done during voluntary movements or during electrical stimulation of nearby nerves and muscles. Reliable long-term recordings (more than 6 month) were reported by Lefurge et al (1991) and Goodall et al. (1991) for anesthetized preparations; however, questions regarding histologically detected neural damage and electrode failure were raised by Schoenberg and Kendell (1993) using the same electrode design.

Low impedance electrodes like those used by Horch and coworkers, recorded potentials from populations of axons rather than from single axons. These multi-unit signals may be adequate and desirable as feedback in certain FNS systems or as mass activity indicators in basic research of neural motor control. Also, human nerve cuff recordings from natural sensors have been used for providing feedback assistance in gait and grasp tasks (Haugland 1994, Haugland et al. 1995), where a composite signal was obtained rather than unitary spike trains. To discriminate unitary spikes with low impedance electrodes, restrictive recording conditions and special analysis methods are needed (Goodall and Horch 1993, Mirfakhraei and Horch 1994). An increased selectivity can also be obtained by targeting specific nerve branches as seen in

the methodology of Yoshida and Horch (1996). Their electrodes were implanted close to the nerve entry point of a selected muscle, but because of the fragility of fine nerve branches, this approach increases the mechanical requirements of the electrode design. Similar mechanical restrictions apply to the bulkier nerve cuff electrode. A typical way to increase selectivity is to reduce the recording surface area, thus limiting the volume from which potentials are picked up. This is the basis for the design of single unit electrodes studied in this thesis.

For FNS applications, an intraneural recording and stimulation electrode should be mechanically and electrically stable for long-term peripheral nerve interfacing. It should be small in size, and preferably interface with a population of axons. A composite neural signal recorded from each interface site should have neural spikes with amplitudes discriminable even during activation of nearby muscles and electrical stimulation of other nerves or muscles.

Advances in silicon micro-machining techniques have opened the possibility of using a new and innovative electrode design suitable for CNS neural recordings (Drake et al. 1988). Silicon based electrodes typically have multiple interface sites located at or near the tip of a relatively small and stiff electrode substrate shank. This design technique was used as basis for a new electrode design for interfacing to peripheral nerves.

### *F. Objectives of the thesis*

The research objectives of this thesis were to develop, improve and evaluate advanced implantable transducers for use in neuromuscular research. The devices employed in this research are required to obtain physiological information from neuromuscular systems. They are used in motor control research, enhancing our understanding of the mammalian neuromuscular physiology. Within the scope of the present project the devices are not directly applied in a clinical rehabilitation environment, although they can potentially become the basis for designs of advanced neural prostheses. Instead, a set of transducers was developed for use in neuromuscular research, and the following questions were addressed:

- A. **Muscle length gauge:** Can problems with the traditional implantable length gauge design be solved with the use of ultrasound as an alternate information carrier ?
- B. **Nerve cuff electrode:** Is it possible to eliminate sutures for the closure of a nerve cuff and improve the long-term electrical and mechanical isolation of the cuff interior ?
- C. **Fine-wire single unit electrode:** Can traditional fine wire and hatpin electrode be used for chronic awake recording of single-unit activity in peripheral nerves ?
- D. **Silicon based single unit electrode:** Can silicon micro machining techniques be used to design multicontact electrodes suitable for intraneural interfacing to individual peripheral axons ?
- E. **Simulation of peripheral nervous system interfaces:** Are existing intraneural electrodes designed adequately for interfacing to single peripheral axons ?

In addressing these questions, the above mentioned implantable transducers and techniques were developed and evaluated for their *in vivo* performance. The thesis outlines the objectives, methods, results and performance assessment of each transducer.

## II. GENERAL EXPERIMENTAL DESIGN AND SURGICAL APPROACH

This thesis is focused on development and improvement of three neuromuscular interfaces. As discussed in *Introduction*, the rationale for these designs was the need for specific interfaces to document the physiology of proprioceptors. Each design built on experience from earlier transducer designs and became an integral part of a general implantation approach in the cat hindlimb.

This chapter has four sections that describe the general experimental approach. The *Training* section describes general training protocols. The *Experimental design* section documents the general purpose of all implanted devices and gives a brief description of device designs and implant locations. The *Surgical approach* section describes the surgical preparation and implant techniques. The *Recording procedures* section describes the recordings that were done before, during and/or after the surgical sessions.

### **Training**

Male cats were trained to walk on a motorized treadmill at level, uphill and downhill inclinations. The training was continued on a daily basis for a period of 2-3 weeks with the goal of sustaining up to  $1.0 \text{ m}\cdot\text{s}^{-1}$  for at least 10 min at level walking. Sprints of up to  $2.0 \text{ m}\cdot\text{s}^{-1}$  were sustained for 30 s. These performance levels were obtained through positive encouragement, such as food rewards and toys. Cats were also familiarized with the cables that were used during recording sessions.

In addition, selected cats were trained to stand on 4 pedestals of which one (left hindlimb) was connected to a perturbation motor as described by Sinkjær and Hoffer (1987). During the stance, the cat was required to produce set levels of background force (up to 20 N) on the perturbation platform. If the force was successfully maintained for a given period of time (200-300 ms), a mechanical perturbation of the limb was delivered where the ankle joint was rotated up to  $8.2^\circ$ . Immediately following the perturbation, the cat was automatically rewarded from a food dispenser system.

## **Experimental design**

A general experimental setup was used in all experiments. Minor variations occurred over time as different devices were developed and fine-tuned.

*Length Gauge transducer:* The total length of the MG muscle was measured by recording the distance from the muscle origin, on the posterior distal end of the femur, to the muscle insertion on the calcaneous bone of the heel. This was done to correlate bio-mechanical dimensions of the muscle with neural signals originating from that muscle.

Length measurements had previously been made using extensible tubes with variable electrical resistance (Lemon 1984, Hoffer 1990). Advances in the use of piezoelectrically generated ultrasound opened the possibility for a new transducer type (Weytjens et al. 1992). The transducer uses the transmission time of ultrasound waves traveling through body tissue, as a measurement of conduction distance. As with the implanted length gauges mentioned above, the new transducer was implanted alongside the MG muscle (Figure II.1-H). The distal end of the gauge was attached through the calcaneous bone of the heel and the proximal end was anchored through the sesamoid bone on the posterior side of the knee joint.

As part of this thesis a novel length gauge design, based on piezoelectrically emitted ultrasound, has been developed (Weytjens et al. 1992).

*Nerve Cuff Electrode:* Neural activity in the sciatic and tibial nerves was measured by recording extraneural potentials along short sections of these nerves. This was done to identify the propagation direction and velocity of single unit action potentials recorded with intraneural electrodes in the MG nerve branch.



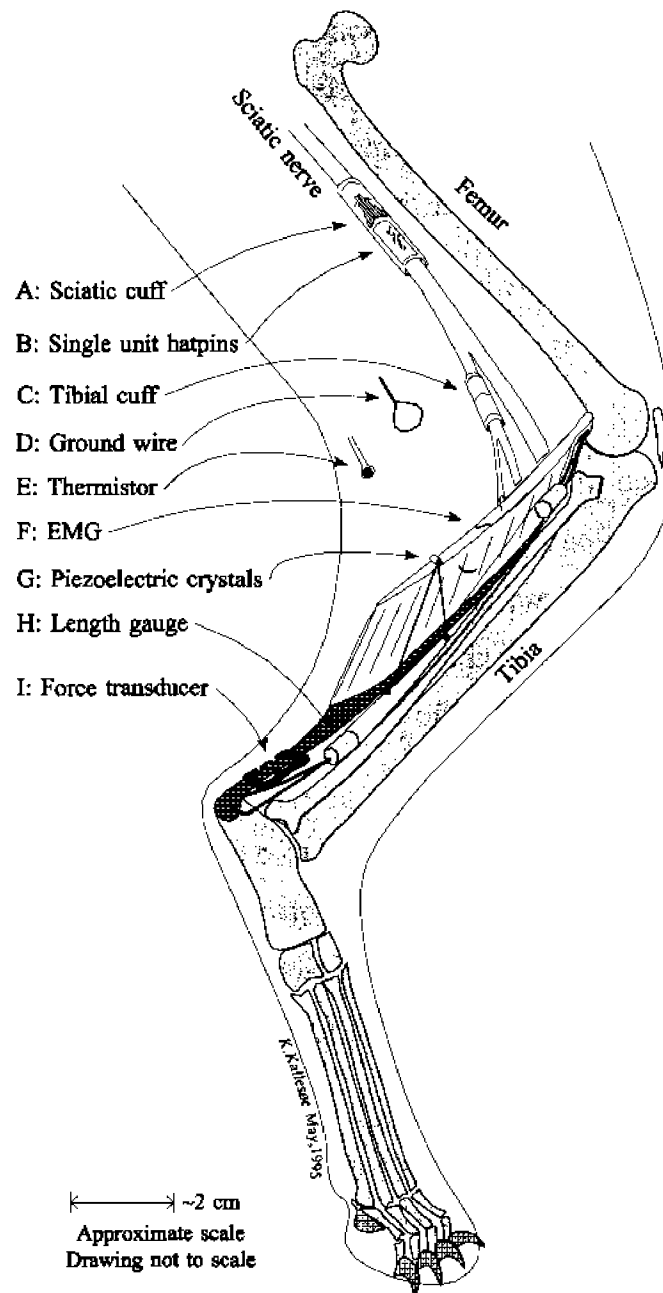


Figure II.1: Typical devices implanted in a cat's left hindlimb. (A): A 28-30 mm long nerve cuff encompassed the sciatic nerve. The cuff included a stainless steel shield to cover the single unit window. (B): 8-16 single unit intraneural hatpin or finewire electrodes were implanted in the MG nerve inside the sciatic cuff window. (C): A 10 or 15 mm long tibial nerve cuff was implanted distal to the bifurcation of sciatic into its main branches. (D): Ground wire. (E): Thermistor to compensate for temperature drift during recordings (Stegeman and De Weerd 1982b, Dioszeghy and Stålberg 1992). (F): 3-4 sets of bipolar buried EMG electrodes in the MG muscle, possibly with additional sets in the soleus, lateral gastrocnemius and tibialis anterior muscle. (G): 3 double piezoelectric crystals were attached to the superficial and the deep aponeurotic planes of the MG. (H): A length gauge was attached near the origin and insertion of the MG muscle. (I): A force transducer was attached on the MG tendon.

The recording setup included the implantation of nerve cuff devices with recording electrodes attached circumferentially to the inside of silicone tubes. A longitudinal opening in the tube allowed the installation of the cuff around the nerve. This opening had previously been sealed and locked using surgical sutures attached to the outside of the tube (e.g. Hoffer 1990).

As part of this thesis, an innovative nerve cuff closing mechanism was developed (Kallesøe et al. 1996). The mechanism improved the handling and performance of the existing nerve cuff design (Strange et al. 1996).

One cuff was implanted on the sciatic nerve, 2-3 cm proximal to the bifurcation point of the tibial and common peroneal nerves (A in Figure II.1). A second cuff was implanted on the tibial branch, approximately 1 cm distal to the bifurcation point (C in Figure II.1). Each cuff had a tripolar set of recording electrodes attached to the inside surface. The three electrodes in the tibial cuff were evenly spaced along the length of the cuff, whereas the sciatic nerve cuff was asymmetrical (see next section).

*Intraneural Single Unit Electrode:* The proximal portion of the sciatic nerve cuff (A in Figure II.1) was designed with a similar electrode configuration as the tibial cuff, except that the internal electrodes were limited to approximately  $\frac{1}{4}$  of the inner cuff circumference. This enhanced the recording of activity in the MG nerve branch, which was in close proximity to the electrodes.

In the distal section, the cuff wall was partially removed, opening a "window" access to the encompassed nerve section. The window allowed delicate intraneural single unit electrodes to be inserted into the MG fascicle. The external surface of the cuff provided an attachment platform for the lead-out cables of these electrodes.

To prevent dislocation of the sciatic cuff, the cuff was anchored to the epineurium with 3 or 4 sutures (8-0 mono-filament nylon). This procedure required the alignment of the window of the cuff directly over the MG nerve branch.

Recordings from individual axons were required in order to characterize the functional behavior of proprioceptors in the MG muscle. Recordings were performed with intraneural

electrodes inserted in the MG nerve fascicle of the sciatic nerve. These intraneural electrodes were typically very small and fragile, requiring mechanical support to stabilize their location.

The intraneural electrodes inserted through the window were either finewire, "hatpin" or silicon probes (Kallesøe et al. 1994). To protect them from surrounding tissue movement, a stainless steel cover was attached to the sciatic cuff which also served as a reference recording electrode. Given its fairly large size (approximately 25 x 16 mm) this was considered an indifferent reference electrode with potential equal to the average potential of a large volume around and inside the sciatic nerve cuff.

*Additional instrumentation:* Other devices that were used in the present thesis research were developed earlier (described in Hoffer 1990) and were manufactured and implanted according to the general protocols of the lab. These devices included:

- piezoelectric crystals for measurement of muscle fiber movements, aponeurosis deformation and muscle belly thickness (G in Figure II.1)
- a tendon force transducer to measure muscle force through the tendon (I in Figure II.1)
- intramuscular EMG electrodes to record muscle activity (F in Figure II.1)
- a thermistor in close proximity of the nerve cuffs, to provide a local measurement of tissue temperature (D in Figure II.1), and
- a ground wire to serve as reference electrode for the electrical recordings (E in Figure II.1).

The design and theory of operation of these transducers were reviewed by Hoffer (1990).

### **Surgical approach**

Implantation of the full set of hindlimb electrodes and transducers typically required 2 surgical sessions separated by 2 to 3 weeks. Each surgical session was performed with the cat deeply anaesthetized using Halothane mixed with oxygen. The cat was administered pre-surgical sedatives to facilitate intubation, as well as post-operative analgesics to minimize recovery discomfort. The combination of medication mixtures varied throughout the years, but a typical combination was an intramuscular premedication of Ketamine/Acepromazine/Atropine

( $5 \text{ mg}\cdot\text{kg}^{-1}$  /  $0.05 \text{ mg}\cdot\text{kg}^{-1}$  /  $0.02 \text{ mg}\cdot\text{kg}^{-1}$  ), followed by intravenous Ketamine/Valium ( $5 \text{ mg}\cdot\text{kg}^{-1}$  /  $0.2 \text{ mg}\cdot\text{kg}^{-1}$ ). During the surgical procedure, life signs were monitored (pupillary dilation, expired %  $\text{CO}_2$ , respiration rate and heart rate). Post-operative analgesics used were either Morphine ( $0.1\text{-}0.25 \text{ mg}\cdot\text{kg}^{-1}$ ), Torbugesic ( $0.2 \text{ mg}\cdot\text{kg}^{-1}$ ) or Temgesic ( $0.01 \text{ mg}\cdot\text{kg}^{-1}$ ) and were maintained for a minimum of 24 hours. Derapen or Cefadrops antibiotics were given for seven days following the surgery.

All procedures were in accordance with guidelines of the Canadian Council for Animal Care and were approved initially by the University of Calgary and later by the Simon Fraser University Animal Care Committee.

*1<sup>st</sup> Surgical Session:* Immediately prior to the hindlimb surgery, two minor procedures were performed. During the first procedure, two printed circuit (PC) boards were attached externally, allowing all cables exiting the body to be terminated in standard 40 pin 3M connectors. The PC boards were mechanically connected in a "V" shaped structure, resembling a "saddle" or "backpack" riding externally on the spine. To attach this backpack, two braided #5 Mersilene sutures were passed subfacially between the L1-L2 and L4-L5 vertebra with a large curved needle.

The second procedure consisted of installation of a permanent intravenous catheter in one of the jugular veins. This was done through a 4-5 cm longitudinal incision along the jugular area, slightly off the center in the frontal plane (0.5-1 cm). A silicone catheter (DowCorning 205: ID 1.0 mm, OD 2.1 mm) was inserted in the vein, and tunneled subcutaneously along and around the sternum to the backpack connector. The catheter was routed transcutaneously to a stainless steel tube attached to the backpack PC boards. To prevent coagulation, the catheter was filled with a 1-5% heparin saline solution and the tube was capped. This jugular vein implant was discontinued approximately half way through the series of thesis experiments, due to limited benefits compared to the maintenance required.

The hindlimb surgery required a midline incision slightly medial to the cleft between medial gastrocnemius muscle (MG) and the lateral gastrocnemius muscle (LG) that provided access to the popliteal fossa and the MG muscle. The popliteal fat pad was removed and the

incision was extended caudally past the calcaneus bone. The superficial and deep surfaces of the MG muscle were dissected free to allow for installation of 3 or 4 sets of intramuscular EMG electrodes. Three sets of double piezoelectric crystals were sutured to the MG aponeurotic planes. A length gauge was installed along the medial side of the MG and attached with two 2-0 sutures, one passed through the calcaneus bone of the heel and the other through the sesamoid bone at the proximal MG tendon, posterior to the knee joint. An E-shaped force transducer was attached to the MG portion of the triceps surae tendon. Finally, a ground wire and a thermistor were sutured subcutaneously, approximately in the location of the removed popliteal fat pad.

All leadout wires included large strain-relief loops and were routed subcutaneously to the back where they emerged transcutaneously and were connected to the backpack.

Total surgical time was typically 10-12 hours.

*2<sup>nd</sup> Surgical Session:* A minimum of one week after the 1<sup>st</sup> surgical session, a second surgery was performed. The midline incision from the 1<sup>st</sup> surgical session was extended proximally to gain access to the sciatic and tibial nerves. A 1.5-2.0 cm section of the tibial nerve and 3.5-4.0 cm section of the sciatic nerve were gently dissected free to accommodate the sciatic and tibial nerve cuffs. The MG fascicle was identified by visual inspection and by electrical micro-stimulation (in the 100-200  $\mu$ A range) on the surface of the sciatic nerve. The previously implanted MG EMG electrodes were used to monitor the electrical recruitment of single motor units. The tibial nerve cuff was installed below the branching point of the common peroneal nerve. The sciatic nerve cuff was aligned so that the window in the cuff gave access to the MG fascicle. Up to four very fine sutures (8-0) were sewn through the edge of the cuff window to mechanically anchor the cuff to the epineurium. Working inside the window, each single unit electrode was inserted intraneurally. Motor units in the MG muscle were recruited by constant current stimulation through each inserted electrode. The proximity of the electrode to MG motor axons was estimated from the required microstimulation current. The threshold for exciting axons of MG motor units had empirically been found to be as low as 0.5  $\mu$ A. Electrodes with constant current microstimulation levels higher than 20  $\mu$ A were typically repositioned. Electrodes were

occasionally monitored continuously throughout the insertion procedure, to identify spontaneously firing axons.

The electrodes were typically anchored to the epineurium either using a 8-0 suture or cyanoacrylate. A cuff shield was attached around the sciatic cuff to prevent possible damage of the intraneural electrodes due to movement of surrounding tissue. The stainless-steel cuff shield was also used as the local reference electrode. Leadout cables of all devices were routed subcutaneously in gentle curves and loops, allowing for full range of limb and back movement and were connected to the backpack.

Total surgical time was typically 10-12 hours.

### **Recording procedures**

During the time span of a chronic experiment, usually several weeks, frequent recording sessions were conducted. The most crucial ones of these were the *Single Unit Recording* sessions, where any units were identified and, when possible, recorded during walking. These sessions were repeated in successful implants on a nearly daily basis. Besides these sessions, other recording sessions were performed for the purposes of calibration and verification of device functionality.

*Pre-Surgical Recording:* Prior to the 1<sup>st</sup> surgery, the normal locomotion and postural behavior of each cat was documented. Physical measurements of body weight and femur and tibia length were recorded. The normal walking pattern was recorded on video tape for later comparison with post-implant walking patterns, to detect any abnormalities.

*1<sup>st</sup> Surgical Recording:* During the 1<sup>st</sup> surgery, internal anatomical data was collected: dimensions of the MG muscle, estimation of sciatic and tibial nerve diameter, and location of device attachment sites on the MG muscle and tendon.

*Inter-Surgical Recording:* After recovery from the first surgery (typically 2-4 days), one or two recording sessions were performed, both to test functionality of the implanted devices and to accustom the cat to the recording cable and recording procedures. Each device was checked for successful performance and electrical leakage. Any faulty devices were replaced in the second surgical session.

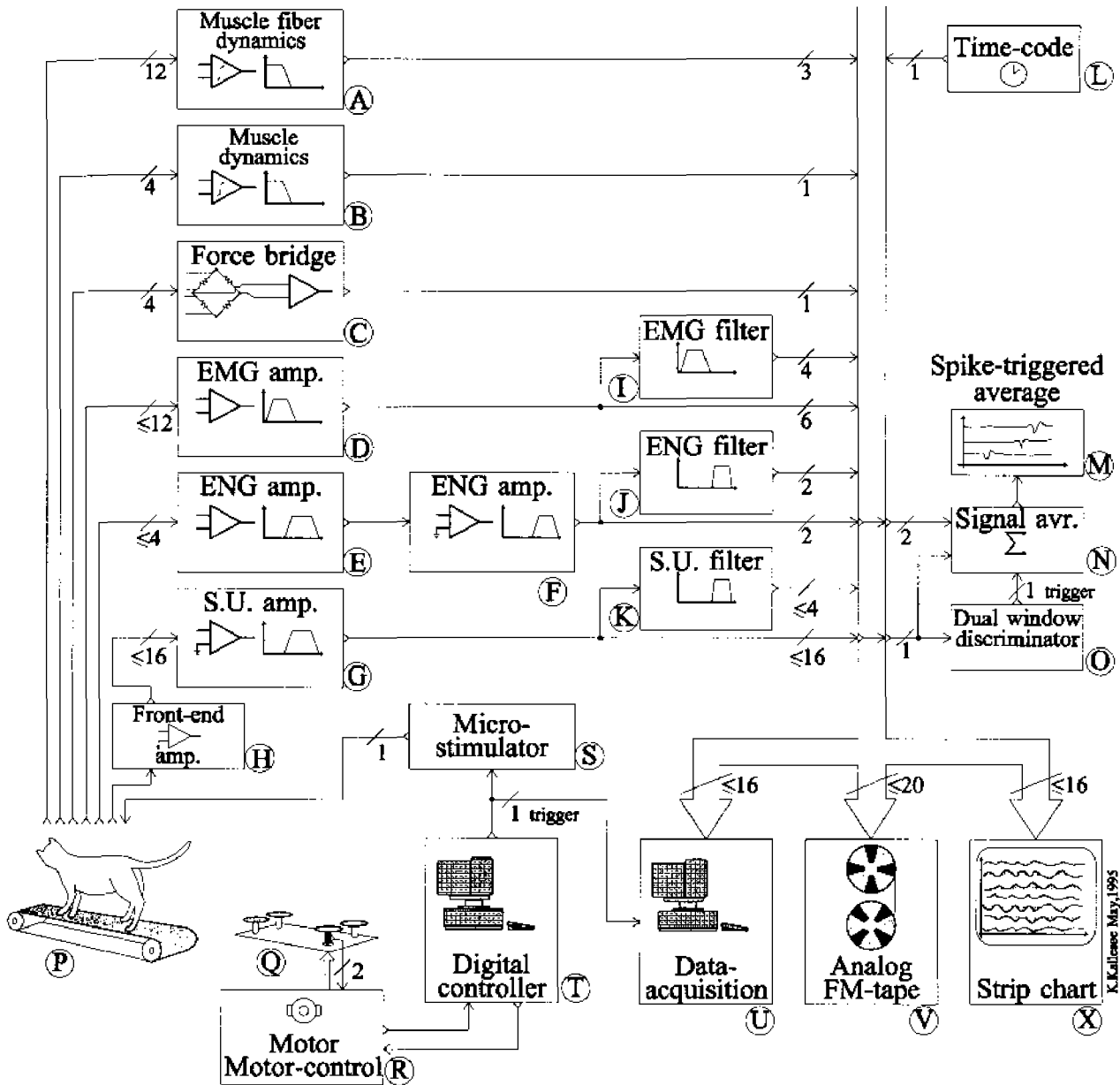


Figure II.2: Recording setup. An complete recording setup included: (A) Three muscle belly dimensions (fiber length, aponeurosis deformation and transverse belly thickness), (B) MG muscle length, (C) tendon force, (D) up to six EMGs (gain  $10^3$ , bandpass: 50-1 kHz), (E,F) two ENGs (E: gain  $10^2$ , High pass: 65 Hz, F: gain  $10^3$ , bandpass: 1 kHz-10 kHz), (L) time code. Several of these channels were filtered separately (I,J). In addition to these channels, up to 16 single unit signals (G), prebuffered and amplified (H), could be recorded and possibly filtered (K). Data were stored on hard disk (U), FM tape (V), and/or displayed on-line on a strip chart recorder (X). Single unit data were filtered on-line through a dual window discriminator (O), triggering a signal average (N), creating a spike triggered average of the two nerve cuff signals and the single unit signal (M). The cat would perform either treadmill walking (P:  $0.3-2.0 \text{ m}\cdot\text{s}^{-1}$ ) or pedestal standing (Q). The pedestal was mechanically controlled by a PMI motor (R) and a digital computer (T). Finally, a constant current microstimulator was used to stimulate either microelectrodes or intramuscular electrodes (S).

Figure II.2 (continued): Instrumentation: (A,B): Sonomicrometer, Triton Technology Inc. (C): Force bridge module, BAK Electronics Inc. (D,F,G): AC amplifier module, BAK Electronics Inc. (E): Low noise AC amplifier, QT-5B, Leaf Electronics Ltd. (H): MC33248P FET-operational amplifier. (I): Ten band frequency equalizer, Realistic. (J,K): 24dB/oct. filter, Ithaco 4302. (L): Time code generator, Datum model 9300. (M,N): Signal averager, Nicolet 12/70, Nicolet Analytic Instruments. (O): Dual window discriminator module, BAK Electronics Inc. (P,Q): Custom designed mechanical equipment. (R): PMI Switching servo amplifier, servo disc DC motor, PMI. (S): Custom designed micro stimulator. (T): 286-AT computer, later replaced by 386-AT computer. (U): 486-PC computer. (V): Tape recorder, Honeywell model 96. (X): Strip chart recorder, Gould, later replaced by strip chart recorder installed in 386-AT computer, Codas.

*2<sup>nd</sup> Surgical Recording:* As described in the *Surgical approach* section, microstimulation through each of the intraneural electrodes indicated the proximity to efferent axons. The excitation threshold for each electrode was found by monitoring the evoked single motor unit potentials in the MG muscle. Occasionally, the electrodes were monitored during insertion to detect spontaneous activity.

During this installation, the integrity of micro electrode insulation was tested by comparing the measurements of electrode impedance with and without saline surrounding it. Recording lower impedances during temporary saline submersion would indicate a leakage pathway along the electrode cabling.

Finally, anatomical measurements were made of the distance between the implanted sciatic and tibial nerve cuffs. This was done either directly, using a ruler, or indirectly by running a suture along the curvature of the nerve and then measuring its length. The length was used to calculate the propagation velocity of recorded single unit spikes.

*Post-Surgical Recording:* Immediately following the 2<sup>nd</sup> surgical session all electrodes were checked during light anesthesia for both spontaneous activity and reflex evoked activity. The reflex activity was evoked by repeatedly flexing the ankle joint which stretched the MG muscle and elicited a stretch reflex in the muscle.

*Daily Recordings:* After recovery from the 2<sup>nd</sup> surgical session (typically 2-4 days) a regular recording schedule was initiated. On a nearly daily basis, the survival of the intraneural electrodes was monitored and electrodes were scanned for neural activity. In each session, basic electrical parameters of the individual electrode were recorded. This included 1) measuring impedance (at 1 kHz), 2) estimation of proximity to efferent axons by monitoring single motor unit action potentials evoked by microstimulation through the



intra-neural electrodes, and 3) scanning each electrode for neural activity correlated with walking patterns. In the case where the daily recording indicated that neural activity was being recorded by an electrode, one or two more elaborate recording sessions were performed.

*Unit Classification:* The awake recording procedure served to characterize the detected single unit neural activity. The activity was classified in terms of axonal propagation direction (afferent-efferent) and propagation speed (e.g., spindle Group I:  $72-120 \text{ m}\cdot\text{s}^{-1}$ , spindle group II:  $20-72 \text{ m}\cdot\text{s}^{-1}$ . Mathews 1972). The classification was based on the spike triggered averaging of the ENG from the sciatic and tibial nerve cuffs, using a trigger derived from a filtered version of the neural signal recorded by the intra-neural electrode (as described by Loeb et al. 1985a). In the case where afferent activity was detected, a further classification of the signal source (GTO or spindle) was attempted based on a twitch response test. This included electrically stimulating the MG muscle through the intramuscular electrodes, eliciting a muscle twitch and brief rise in the tendon force. Correlation of the timing of this force-twitch with the firing sequence of unitary action potentials could reveal whether the source was a GTO or a spindle. If the unit was mainly firing on the rising flank of the twitch, it was classified as a force sensitive GTO. If there was no or very little activity during the contraction, and an increase in the firing rate immediately after the twitch, it was classified as a length-change sensitive spindle unit. Finally, the approximate receptor location was to be determined by correlating the frequency of spike trains with local transcutaneous muscle vibration.

*Unit Recordings during Treadmill Walking:* The treadmill recording procedures served to characterize the functional behaviors of detected units during locomotion. The characterization was done by off-line signal analysis. The recording included a minimum of 11 channels (Figure II.2): 3-4 MG intramuscular EMG electrodes, the sciatic nerve cuff ENG electrode, the tibial nerve cuff ENG electrode, the MG tendon force transducer, the MG muscle length gauge, and piezoelectric crystals (measuring MG fiber length, aponeurosis deformation and muscle belly thickness). Added to these channels were one or more single unit channels. All channels were recorded during standing/sitting, walking at a range of speeds ( $0.3-2.0 \text{ m}\cdot\text{s}^{-1}$ ) and walking uphill and downhill ( $\pm 10\%$ ).

*Unit Recordings during Pedestal Performance:* The pedestal recording procedures served to characterize the functional behavior of detected units during posture. The recording setup was similar to the setup used for treadmill recording, and differed only in the active perturbation of the postural task. The perturbation was either in the form of short duration electrical stimulation of intramuscular EMG electrodes or in the form of mechanical displacement of the pedestal supporting the left hindlimb (as described by Sinkjær and Hoffer 1987).

*Final Acute Recording:* Final recordings under anesthesia were performed to calibrate the tendon force bridge by detaching the calcaneous bone from the ankle and applying known tension forces. Post-mortem device locations on the MG muscle and tendon were recorded to verify that the devices did not migrate during the implantation period. Any abnormalities regarding implanted devices were noted.

### III. MUSCLE LENGTH GAUGE

A very important feature of any transducer system is its ability to record a specific event without disturbing the system being measured. In the case of measuring a bio-mechanical parameter, such as the length of a muscle, it is important that the mechanical transducer does not load or cause restrictions to the normal performance of the muscle.

#### **Conventional resistive length gauge**

Traditionally, direct measurement of muscle length changes have been made with extensible resistive transducers (reviewed in Prochazka 1984, Loeb and Gans 1986, and Hoffer 1990), where continuous changes in the electrical resistance of a fluid column in flexible tubing reflect changes in the tube length. These gauges have several disadvantages:

1. the stiffness of the extensible tube places a mechanical load on the biomechanical system
2. the output drifts when changes in resistance, unrelated to changes in length, occur, (this is seen when the temperature or the osmotic pressure of the fluid column changes).
3. calibration procedures are indirect and subject to measurement error.

Measurement of length changes in the millimeter range has been made with extensible length resistive transducers. A continuous change in the electrical resistance of a fluid column, confined by extensible tubing, can be recorded as the tube is changing length. The fluid is typically a homogeneous conductive medium, such as saline or mercury, exhibiting an inverse correlation between end-to-end electrical resistance and the cross-sectional area of the column. This area theoretically approaches an inverse quadratic correlation with length changes of the gauge, but for the dimensions of typical length gauges (~1 mm inner diameter, 0.3 mm wall-thickness) this correlation can be approximated as linear (Prochazka 1984).

The gauge is calibrated at several different length settings by correlating independently measured length of the gauge with the electrical resistance of the fluid column. The accuracy of the length measurement is limited by the device used (typically a ruler or a caliper).

## Objective

The objective of redesigning an implantable length gauge was to explore the possibility of using piezoelectric electric crystals as a transducer. This would potentially provide more accurate measurements, as well as easier calibration.

## The use of piezoelectric transducers

An ideal length transducer should be based on non-mechanically linked sensor technology to avoid loading the system being measured. Ultrasound is one such technology. It has been proven as an excellent signal for a variety of biomedical transducers in medical diagnostic and treatment systems (Webster 1978 pp.399-414, 600-605). These systems allow for fairly accurate estimate of dynamic dimensions of organs *in-vivo* (e.g. blood flow, soft tissue imaging, fetal monitoring etc.). Depending on the application, different transmission techniques can be used. In sonomicrometry, the ultrasound is pulsed through a conductive medium. By pulsing ("pinging") a piezoelectric crystal and measuring the time delay until a nearby similar crystal starts resonating, the transmission time can be recorded. In a medium with constant ultrasound propagation velocity, the measured propagation time is proportional to the distance between the crystals. This technique is used in both clinical and research cardiology (van Trigt III et al. 1981, Ratcliffe et al. 1995), and has been adapted in neuromuscular research for measurement of length dynamics of skeletal muscle fibers (Hoffer et al. 1989, Hoffer 1990, Caputi et al. 1992). Multidimensional recordings of muscle tissue using several sets of crystals opened a new avenue for discussion of *in vivo* muscle performance (Qi et al. 1994, Ratcliffe et al. 1995).

An attractive aspect of using an ultrasound based transducer is the potential elimination of transducer induced mechanical loading of the measured system. Combining this with fairly accurate resolution (possibly less than 1 mm) and, in some cases such as ultrasound imaging, a non-invasive interface, this transducer technology is superior to many other types of sensors. However, as with any system, transducer limitations exist. Ultrasound waves diverge and energy absorption in the tissue reduces the signal power (Goldman and Hueter 1956).

As described by Webster (1978), details of the attenuation is divided between a near and far-field region. In the near-field region, the wave front emitted from a circular piezoelectric disc,

is mostly contained within a cylindrical outline. The extent of the near-field depends on the disc diameter ( $D$ ) and the wavelength ( $\lambda$ ) of the ultrasound.

$$d_{nf} = \frac{D^2}{4\lambda} \tag{III.1}$$

The signal intensity within the near-field region is, however, not uniform. It consists of multiple maxima and minima due to the interference pattern.

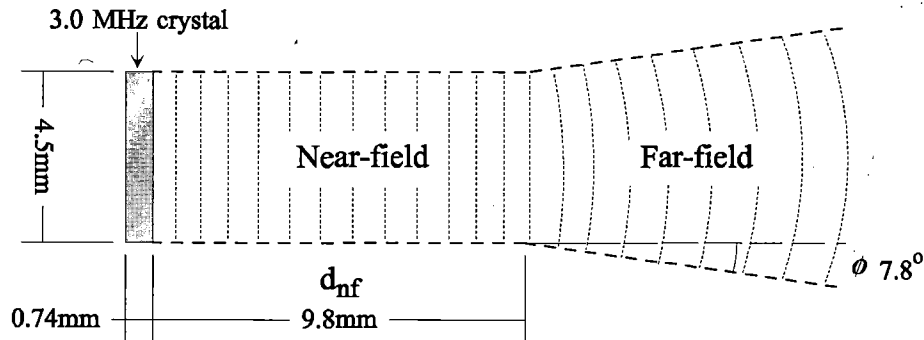


Figure III.1: Predicted ultrasound wave front pattern generated by a 3.0 MHz piezoelectric crystal (4.5 mm diameter, disc shaped shown in cross-section). The near field extends approximately 1.0 cm into the medium, and the divergence angle of the far field is approximately  $8^\circ$ . (Numbers are based on ultrasound conduction velocity of  $1540 \text{ m}\cdot\text{s}^{-1}$ ).

Beyond the near-field region, the wave front starts to diverge in the far-field area. Assuming a homogeneous and isotropic conduction medium, the signal intensity now drops off proportionally to the square of the distance from the emitting surface. The angle of the divergence ( $\phi$ ) again depends on the wavelength ( $\lambda$ ) and the disc diameter ( $D$ ).

$$\sin \phi = \frac{1.2\lambda}{D} \tag{III.2}$$

In addition, the power of a constant cross-section ultrasound wavefront decays exponentially with respect to the transmission distance, due to heat loss in the medium. This further attenuates the signal and increases the requirements of the amplifier for successful pickup of the transmitted signal. In a similar manner, the signal amplitude will be severely attenuated if the receiving crystal is located outside the far field of the transmitting crystal, as seen when the transmitting and receiving crystals are not aligned.

The limitations described above were based on the assumption of a homogeneous and isotropic conduction environment. This is seldom the case for *in vivo* environments, especially when crystals are encapsulated in electrically insulating material (like epoxy). These materials may act as ultrasound lenses and, depending on their shape, either disperse or focus the beam. This can potentially be used to enhance the performance of the transducer, but it requires well controlled manufacturing procedures.

### **Piezoelectric ultrasound based muscle length gauge**

Transmitting ultrasound from origin to insertion of a whole muscle would be the most desirable way of measuring the total length of the muscle. The *in vivo* transmission distance is, however, limited, as seen above, partly due to the inherently dissipative nature of an inhomogeneous preparation and partly due to unavoidable misalignment of the crystals when limb segments are displaced. To avoid these problems two techniques can be used. First, the crystals can be brought closer together and second, a transmission pathway can be defined between the crystals. These two approaches have been explored in the present thesis work.

#### *Initial gauge design: Piezoelectric Type 1*

The initial design of an ultrasound muscle length gauge consisted of a set of piezoelectric crystals mounted very close together ( $<5$  mm.). Two piezoelectric crystals were attached on the outside of the saline-filled silicone tubing of a conventional length gauge (Figure III.2). As the silicone tube was stretched, the gap between the crystals increased. This design was a first step approach, using the conventional gauge as a reference and also allowing testing of a new transducer type. Unfortunately, the design did not eliminate the extensible tube attached from origin to insertion of the muscle. An important benefit of using ultrasound was thus not harvested, namely the mechanical isolation of the two crystals. The gauge obviously preserved the low stiffness characteristic ( $\sim 0.03 \text{ N}\cdot\text{mm}^{-1}$ ) of the conventional gauge and benefited from the use of a direct piezoelectric calibration technique.

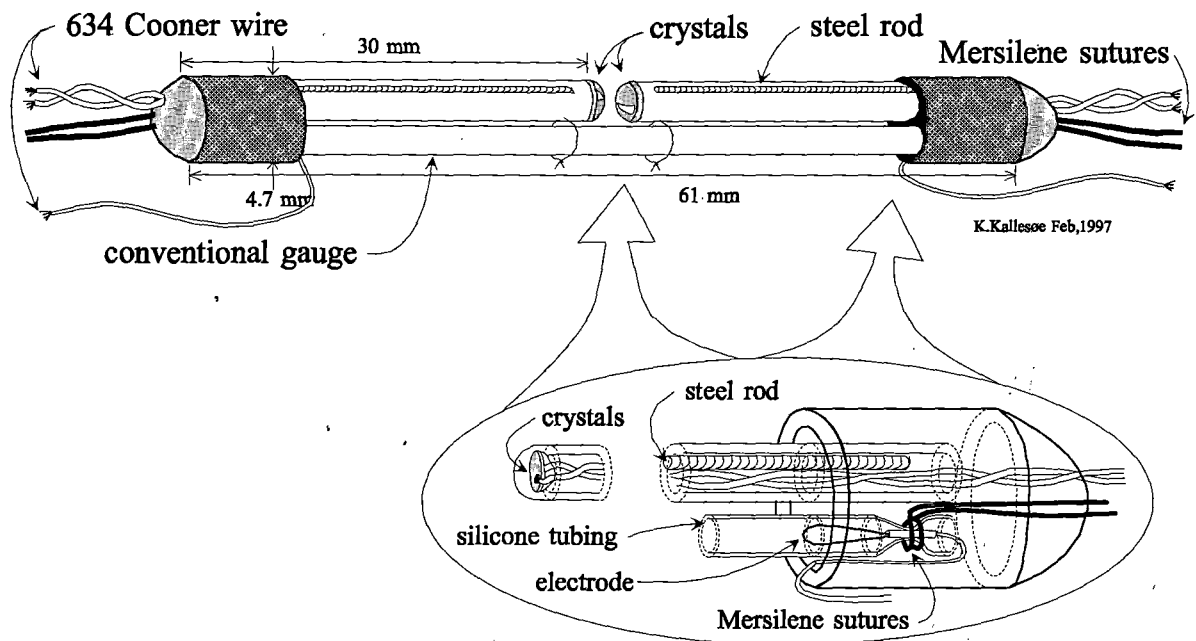


Figure III.2: Piezoelectric length gauge, Type 1. A conventional resistive length gauge served as mounting platform for two silicone tubes with piezoelectric crystals facing the center of the gauge. The mechanical interface to the environment was defined by Mersilene suture (#2) embedded in silicone adhesive and epoxy at each end of the gauge. Two sets of cables exit from the gauge, one from the conventional gauge and one from the piezoelectric gauge (Figure modified from Weytjens et al. 1992).

It was expected that an implanted gauge would be encapsulated by connective tissue, and concerns were raised about tissue buildup between the two crystals. This would potentially cause misalignment of the crystals, deteriorating the signal quality. It could also invalidate minimum length measurements, if tissue buildup had prevented crystals from returning to their original minimum-distance position. This scenario would limit the operating length range by increasing the minimum distance between the crystals. For these reasons, this gauge design was used only in short term experiments (<1-2 weeks). It was apparent that a different design technique was required to maintain successful long-term implants.

This initial length gauge design was pioneered by Weytjens (Weytjens et al. 1992).

#### *Improved gauge design: Piezoelectric Type 2*

In an improved gauge design, originally suggested by Caputi, the crystals were mounted further apart (40-60 mm) and a conductive pathway was defined between them. This pathway was created by installing the crystals inside a thin-walled silicone tube (Figure III.3). This tubing had fairly large diameter (~4.5 mm), with two disc-shaped piezoelectric crystals placed

The stiffness of a tube depended on the material characteristics of the wall. Preliminary results showed that when using commercial 0.127 mm (0.005") DowCorning 500-1 silicone sheeting as wall material for the Type 2 gauge, tube stiffness was  $\sim 0.05 \text{ N}\cdot\text{mm}^{-1}$ . This was approximately twice that of a conventional gauge.

### Application of piezoelectric length gauges

The *in vivo* performance of the piezoelectric gauges was evaluated by comparing their signal outputs to that of a conventional resistive gauge. Since no two muscles behave identically, it was necessary to include two gauges in the same implant, one being a conventional gauge and one an ultrasound based gauge. This allowed for direct comparisons with previous technology.

When testing the first length gauge design - Type 1 - there was no need for implanting a traditional resistive gauge as a reference, since the mounting platform gauge served as the "previous technology" reference. As described by Weytjens et al. (1992), this design was used exclusively for short-term chronic hindlimb experiments in 5 cats ( $\sim 1$ -2 weeks).

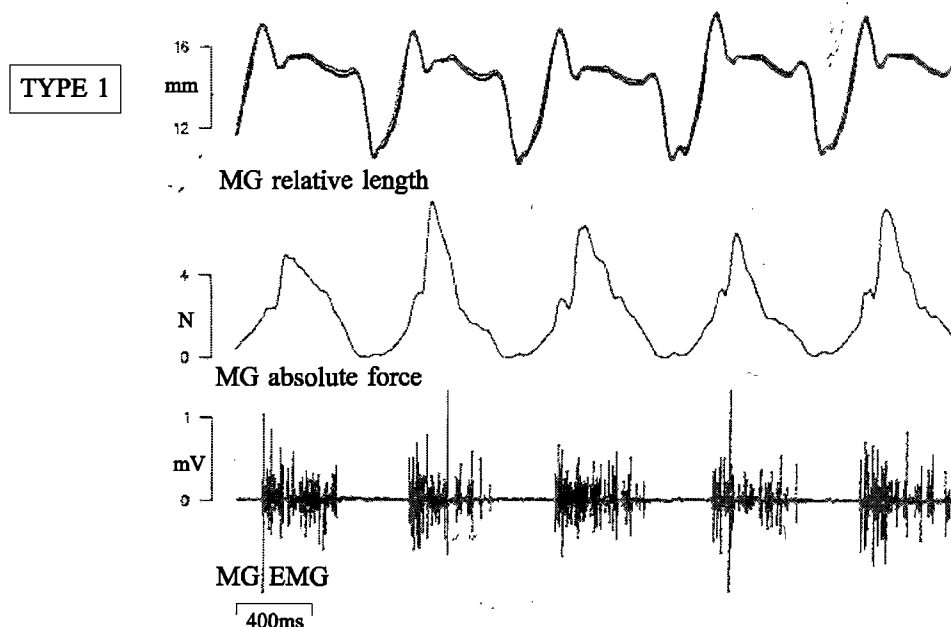


Figure III.5: Chronic measurements using piezoelectric-gauge Type 1, and a conventional resistive gauge. The recordings were made from the cat medial gastrocnemius muscle (MG) during treadmill walking ( $0.5 \text{ m}\cdot\text{s}^{-1}$ ). Top section shows two superimposed muscle length gauge traces (thin trace: conventional, thick trace: piezoelectric), middle section shows MG tendon-force, bottom trace shows MG EMG activity. (Figure adapted from Weytjens et al. 1992).



The piezoelectrically based gauge was found to produce a muscle length signal almost identical to the traditional gauge. This was based on visual inspection of the output from the two gauges, as shown in Figure III.5.

The gauge exhibited low stiffness characteristics ( $\sim 0.03 \text{ N}\cdot\text{mm}^{-1}$ ) and at the same time benefited from the use of piezoelectric based transducer technology (transducer linearity and ease of calibration).

The second gauge design - Type 2 - was initially tested in 5 chronic experiments (up to 3 months). In the first of these, an additional gauge of the traditional design was implanted alongside the new design. This was done to compare the performance of the new design to traditional technology. The maximum difference between the signal recorded from the two gauges was approximately 1.5% of the absolute length measured (Figure III.6).

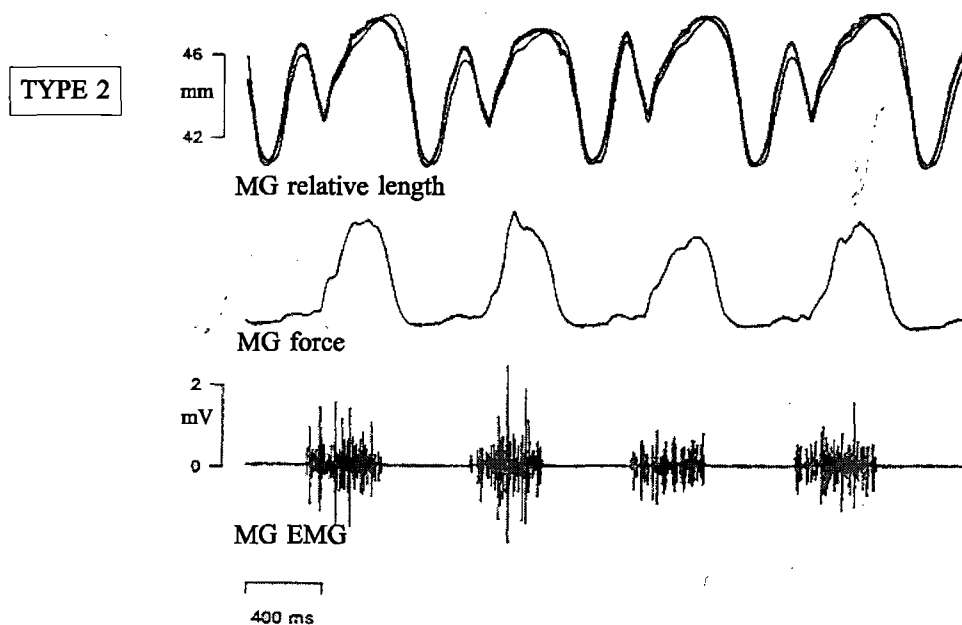


Figure III.6: Chronic measurements using piezoelectric gauge Type 2, and a conventional resistive gauge. The recordings were made from the cat medial gastrocnemius muscle (MG) during treadmill walking ( $0.5 \text{ m}\cdot\text{s}^{-1}$ ). Top section shows two superimposed muscle length gauge traces (thin trace: conventional, thick trace: piezoelectric), middle section shows MG tendon force, bottom trace shows MG EMG activity. (Figure adapted from Weytjens et al. 1992).

At postmortem, it was found, that the Type 2 design effectively eliminated connective tissue growing between the crystals. The design, furthermore, assured alignment of the crystals when the tubing stretched. The gauge was mounted with a slight pre-stretch to eliminate signal drop

out at minimal muscle length. It was, however, noted that a gauge stiffness of  $\sim 0.05 \text{ N}\cdot\text{mm}^{-1}$  was potentially loading the limb, although no changes in the cat's walking pattern were observed.

## Discussion

In summary, when measuring the total length of a muscle using the ultrasound technology described above, the crystals would ideally be attached to the origin and insertion of the muscle of interest. However, due to the signal attenuation during transmission, the distance over which a signal can be detected reliably, is limited. This distance depends on the size and shape of the crystals, on the signal frequency and on the transmission pathway. The pathway is dependent upon the inhomogeneous and anisotropic nature of an *in vivo* preparation and the potential misalignment of the crystals. To alleviate these problems, new length transducers were designed (Weytjens et al. 1992).

A number of failures still exist in these gauge designs, but several of them can be relatively easily avoided.

1. For the Type 2 gauge, obstruction of the ultrasound propagation pathway can occur when the tube is compressed, bent or collapsed, or when air-bubbles are present in the tube. The surface interface between air and saline will effectively reflect and scatter ultrasound waves, dramatically reducing the transfer of energy. To avoid this situation, proper handling and installation of the length gauge is important.

First of all, the gauge is filled with hypertonic saline to osmotically maintain inflation of the tubing. This saline solution should be thoroughly "out-gassed" to avoid the formation of air-bubbles during the exposure to high temperature sterilization ( $>100 \text{ }^\circ\text{C}$ .) The gauge should be kept moist at all times to avoid the loss of fluid through the silicone membrane. Secondly, defining an appropriate pathway across surrounding muscle tissue, tendon sheet and bone is essential during the surgical installation procedure. The flat surface crystals have anisotropic transmitting characteristics with the strongest signal amplitude being in the perpendicular direction to the crystal surface. To maximize the transmitted signal, the gauge should thus be installed in as straight a line as possible. Use of other shapes of

crystal can allow for focusing or scattering the beam, potentially enhancing the transfer of energy.

2. For all gauge designs, it was noted that any elastic tube has inherent nonlinear stiffness characteristics (Figure III.4). This introduces a small, but undesirable nonlinear mechanical loading of the limb. This problem can be minimized by the use of very compliant tubing materials, or by eliminating the tube altogether. Eliminating the tube, however, requires improvements in both ultrasound emission and detection techniques.
3. Leakage of hypertonic saline in the Type 2 design was observed in one implant. This was due to either poorly assembled tubing or abrasive action of surrounding material (like Cooner wires). With proper manufacturing technique and use of a double shell tubing this failure can be avoided (see *Future directions* below).
4. Both Type 1 and 2 gauge designs were typically installed using Mersilene sutures to anchor them to internal structures, typically bones. This anchor has been found to detach either due to degeneration of the anchoring tissue or due to non secure locking of the suture. The risk of this failure can be minimized by carefully selecting and preparing the anchor tissue, the suture material and the surgical knot.

#### *Future directions*

From the preliminary experiments described above with the Type 2 gauge, it became apparent that the stiffness of the gauge should be reduced. This can be done by choosing more compliant tubing material. For bio-compatibility reasons, silicone has been the material of choice for a number of implantable devices. Unfortunately, sheeting is usually only available in 0.127 mm (0.005") or thicker. An alternate rubber material, Latex, exhibits better elongation properties and is, in its natural form, found to be biocompatible (Park and Roderic 1992). The use of 0.097 mm (0.0038") latex as the tubing wall material reduced the Type 2 gauge stiffness to approximately 0.01-0.02 N·mm<sup>-1</sup> (Figure III.7).

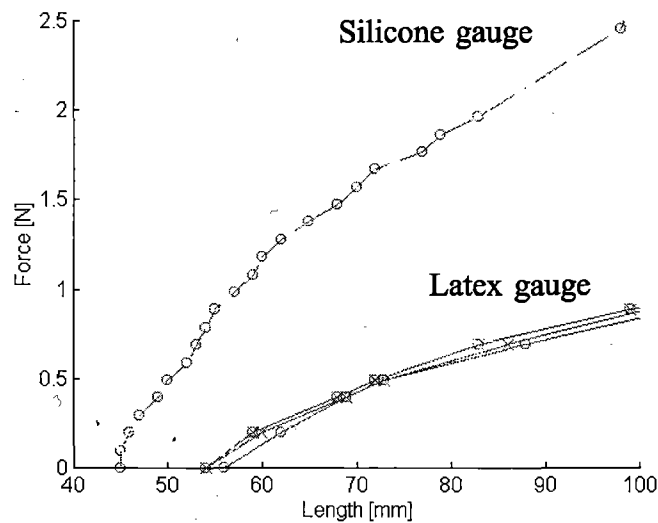


Figure III.7: Stiffness characteristics of a Latex based piezoelectric length gauge compared to the silicone based Type 2 gauge.

Latex is not as durable as silicone, so the thin-walled latex-tubing design requires external abrasion protection. This was achieved by installing an outer silicone shell around the gauge that prevented direct contact between the Latex and body tissue. The stiffness of this outer shell was not critical, as long as it was mechanically disengaged from the stretching latex tube. One way of achieving this was to oversize the length of the outer shell by 40-50% of the length of the inner shell. Besides the mechanical protective advantages of this outer shell, a potential improvement in the transfer of ultrasound is expected due to entrapped air between the sheet layers. This air will effectively reduce the loss of ultrasonic energy, until it is eventually absorbed through the membranes.

However, installing a long silicone tube around the shorter latex tube, forces the outer silicone tube to "wrinkle", possibly squeezing the latex tube and thereby constricting the ultrasound pathway. To avoid that, the silicone tube can be of the same resting length as the inner latex tube, but cut in the middle to form two "guidance" tubes around the latex (Figure III.8.) These guidance tubes separated during gauge stretching.

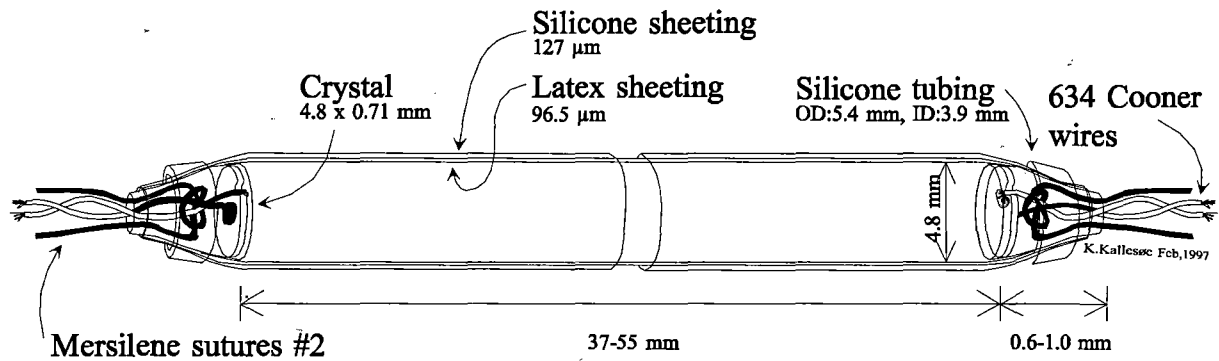


Figure III.8: Final Type 2 length gauge design, including the double layer shell.

The improved Type 2 gauge was used in several series of experiments (Qi et al. 1994, Eng et al. 1995a, Eng et al. 1995b, Eng et al. 1996.)

In conclusion, the gauge was still fairly bulky (~5mm in diameter) and displaced a considerable amount of tissue when implanted in the cat hindlimb. Reduction in size is desirable but will require more powerful crystals transmitting more ultrasound energy per  $\text{mm}^2$ . Such improvement would potentially eliminate the need for guidance tubes altogether. Until this is the case, the ultrasound length gauge may be considered more of an alternative to, rather than an improvement of the conventional resistive gauges.

## IV. NERVE CUFF RECORDING ELECTRODE

Tripolar nerve cuff recording electrodes have recently evolved into versatile devices used in several areas of neuromuscular research (reviewed by Hoffer 1990), but have clinically only been implemented on a modest experimental basis to date (Haugland 1994, Haugland et al. 1995). This has in part been due to inherent problems of the existing nerve cuff design, including:

- secure closing and sealing of the cuff opening
- mismatch of mechanical properties between the cuff structure and the surrounding nervous and connective tissues
- concerns with long-term survival of either transducer or nerve, or both
- damage caused by, and to, leadout wires.

### **Objective**

The objective was to improve the traditional design of a peripheral nerve cuff, with special emphasis on the closing mechanism and the mechanical compliance of the cuff wall.

### **Theory of operation**

A nerve cuff electrode is a device creating a restricted conductive pathway around the extracellular space of a group of axons. This group is typically a total nerve, including several fascicles, and the recording - the electroneurogram (ENG) - reflects neural activity in this group of axons. The extracellular current flow around these axons is restricted by the dielectric properties of the cuff wall, defining a resistive pathway along which a potential drop is detectable. The specific configuration of the recording electrodes is crucial for the interpretation of the recorded extracellular potentials. As reviewed by Stein (1980), biphasic and triphasic signals can be recorded from configurations of 2 and 3 electrodes, representing the 1<sup>st</sup> and 2<sup>nd</sup> derivative of the source potential, the transmembrane voltage drop (Figure IV.1).

Typically, a differential tripolar electrode configuration is used, with an electrode at either end of the cuff tube, and a central recording electrode. The two end electrodes are shorted together

and an ENG is recorded by differential amplification between this short and the center electrode (reviewed by Hoffer 1990). This recording configuration reduces the pickup of "noise" potentials from nearby contracting muscle tissue.

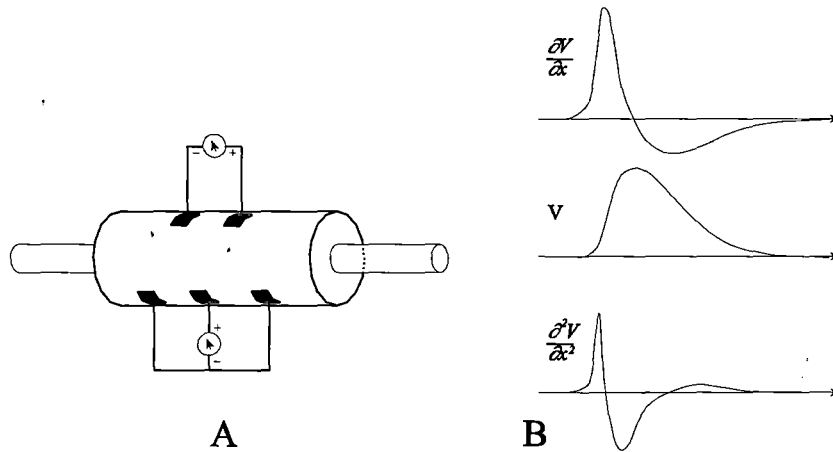


Figure IV.1: Extracellular recording methods from peripheral nerves. A) Methods for recording biphasic and triphasic potentials from an axon in a restricted extracellular space (adapted from Stein 1980). B) The 1<sup>st</sup> and 2<sup>nd</sup> derivative of the transmembrane potential recorded from single axons. (Adapted from Lorente de No 1947).

In this recording configuration, it remains imperative to minimize the leakage current flow from the center recording electrode to the external ground potential. This was discussed by Brunner and Koch (1990), who described a simplified model for the center recording electrode and its preamplification stage (Figure IV.2).

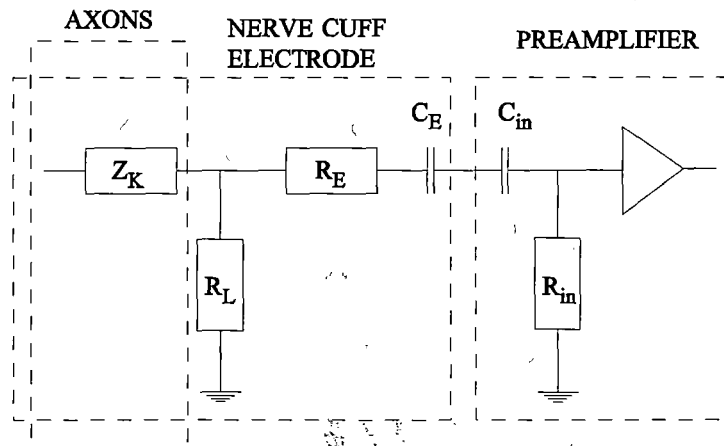


Figure IV.2: Electrical model of the center recording electrode of the nerve cuff. The output impedance of the nerve is  $Z_K$ , the leakage resistance  $R_L$ , the electrode resistance and capacitance are  $R_E$  and  $C_E$ , and the preamplifier input resistance and capacitance are  $R_{in}$  and  $C_{in}$ . (Adapted from Brunner and Koch 1990).

This model describes an all important leakage resistance,  $R_L$ , from the recording electrode to a ground potential. This leakage resistance is comprised of a leakage pathway along the inside of the cuff towards either end, and a leakage pathway through the slit opening of the wall. The resistance along the inside of the cuff wall depends upon the tightness of the cuff fit, the characteristics of the tissue between the nerve and the cuff wall, and the length of the cuff. The resistance through the opening of the wall depends on the effectiveness of the cuff seal.

The signal amplitude recorded by the center electrode depends upon the voltage division across the leakage resistance and the nervous tissue impedance,  $Z_K$ . The latter impedance is determined by the neural tissue exclusively, and has been approximated by Brunner and Koch (1990) as a purely resistive component. The recording conditions can be optimized by maximizing the leakage resistance in the nerve cuff design. This is the rationale for the present redesign of the cuff closing mechanism.

### Existing recording nerve cuff designs

Existing recording nerve cuffs are typically designed with two components: 1) a flexible tubular cuff made from a dielectric material, typically silicone, with an opening and closing feature to allow the cuff to be installed around a nerve, and 2) a set of electrodes located on the inside surface of the cuff wall.

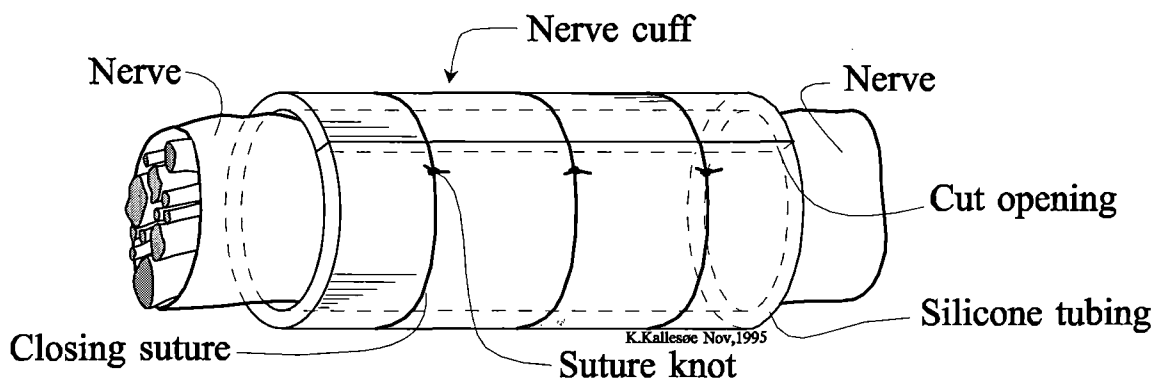


Figure IV.3: Traditional nerve cuff with suture closing. Inside electrodes are not shown for clarity, see Figure IV.5 for more details on electrodes. (Adapted from Kallesøe et al. 1996).

Traditionally, the closing has been made using sutures around the exterior of the cuff (Figure IV.3) and the internal electrodes have been made from stainless steel wires, sewn into the cuff



wall (Figure IV.5). This design has two critical elements: 1) the *closing* mechanism of the cuff, and 2) the mechanical characteristics of the *cuff wall* material.

*Existing cuff closing techniques:*

Closing a nerve cuff with suture material has the advantage of using standard surgical techniques to close and seal the cuff. However, several drawbacks have been identified:

1. Collapsed cuff: A longitudinal opening in a tube may collapse, when the two edges are pushed together. If wet edges slip past one another, the lumen of the cuff is reduced (Figure IV.4), and the enclosed nerve is likely to suffer compression damage (Stein 1980).

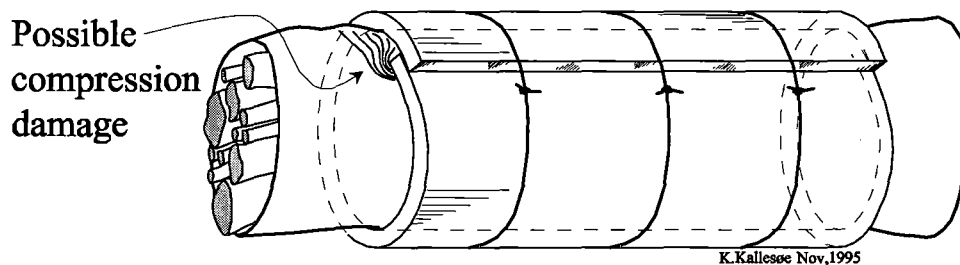


Figure IV.4: Possible failure points in the traditional suture closed cuff. The cuff collapses when closing sutures are tied too tight, or when the cuff is compressed by external forces. (Adapted from Kallesøe et al. 1996).

2. Suture material failure: If the sutures or the suture knots give way, the seal of the cuff opening is compromised and the quality of the recorded signal declines. To minimize the likelihood of this happening, braided sutures have been used. Knots made from this material are less likely to slip, compared to monofilament suture knots. It does however, have the undesirable property of providing an excellent substrate for connective tissue to adhere to. This can potentially rotate and displace the nerve cuff, possibly creating kinks and damage to the nerve.
3. Complex suture installation procedures: The number of sutures needed to seal a cuff is related to the length of the cuff, - the longer the cuff, the more sutures. To create an effective seal, it is desirable to maximize the number of sutures. However, from a surgeon's point of view, fewer sutures and knots mean shorter installation time. Choosing the number of sutures on a particular cuff design, is thus a tradeoff between installation complexity and quality of electric seal. Finally, the suture closing method is inherently a

one-time-only installation. Once the suture knots are trimmed, there is no chance to re-tie the knots should it become necessary to open the cuff.

4. Cleaning procedures: Braided suture material is very difficult to clean if it has been contaminated during the cuff construction. Although non-absorbable sutures typically are sterilized well, it is difficult to eliminate particles embedded in the braiding.

These issues were addressed in a new cuff closing technique where the suture materials were eliminated altogether.

*Existing cuff wall design:*

The wall of a nerve cuff is typically made of a silicone tubing, forcing the finished cuff into a cylindrical shape. This gives stability in the mounting of the internal electrodes, but it also exposes the nerve to several potentially damaging factors:

5. Typically, commercially available silicone tubing material is fairly non flexible, forcing the nerve to conform to the shape of the cuff. When using fixed volume nerve cuffs, post surgical edema and swelling dictates the use of cuffs with an internal diameter larger than the nerve diameter (typically by a minimum of 20%). When the stiff cuff is mounted on the soft nerve, it is crucial that the cuff stays aligned with the natural path of the nerve. This is very difficult, when lead-out wires or connective tissue are likely to twist the cuff slightly, creating a "sharp corner" at one or both ends of the cuff. Such compression points are likely to damage the nerve.
6. Complicated electrode installation: The electrode configuration of a typical nerve cuff is a set of wires, hand sewn to the inside of the cuff wall. This is a laborious manufacturing method with variable results. The wires are prone to misalignment, splaying, or even strand breakage, and unbalanced inter-electrode distance (Figure IV.5). The production quality is an important issue for larger scale nerve cuff production, but within the present thesis context, the focus is on the design, not the manufacturing techniques.

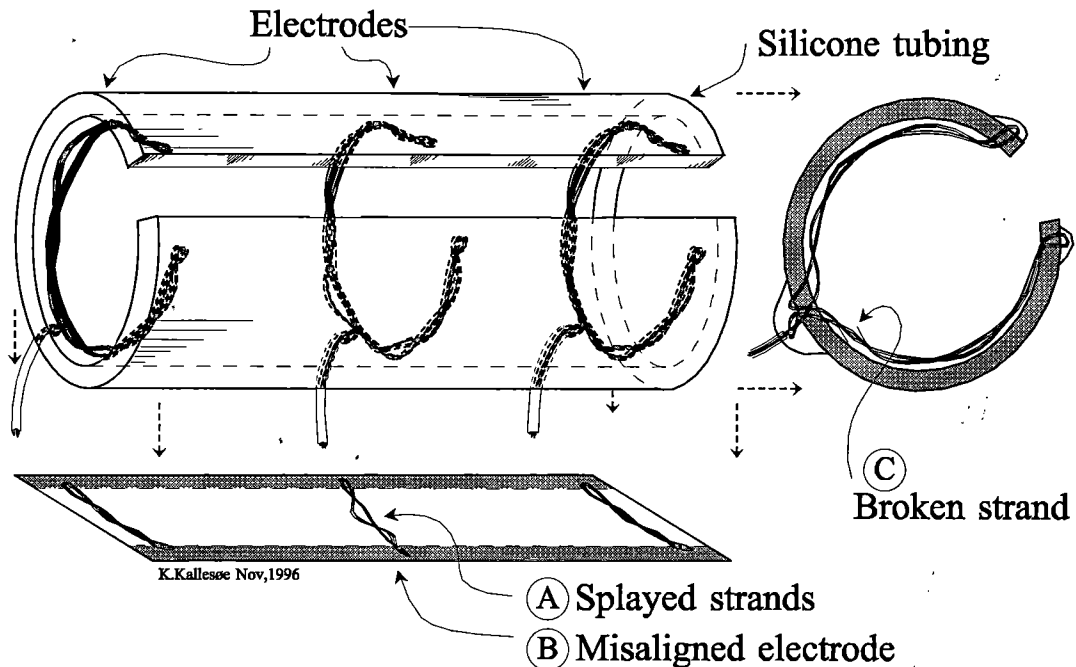


Figure IV.5: Possible failure points in the traditional sewn wire electrodes. (A) Splayed strands occur when the twisting of the stainless steel strands is not tight enough. This decreases the temporal resolution of the recorded signal. (B) Misaligned electrodes occur, when the electrode sewing is not precise enough. This distorts the shape of the recorded signal. (C) During sewing of the electrode, individual strands may catch the needle or other strands and break. A broken sharp single strand can be a potential hazard for the nerve.

7. Wire electrodes are very stiff: The relatively stiff twisted wire electrodes need to be molded along the curvature of the cuff wall, otherwise the strands will work their way, like a “cheese-slicer” through the nerve tissue. Shaping the electrodes to a snug fit is very difficult, and small gaps between the electrode and a cuff wall will inevitably allow connective tissue to grow around and embed the electrodes. This complicates any future removal of the cuff, increasing the risk of damaging the nerve during such procedures.

The issue of cuff wall flexibility can be addressed by the use of alternate materials. Using thin silicone or Teflon sheeting instead of silicone tubing, increases the mechanical flexibility of the assembly. However, a more flexible cuff wall design requires redesign of both the wire electrodes and the cuff closing mechanism. The stiffness of present electrodes will cause a pronounced deformation of a thin sheet cuff wall. It is thus important to design highly flexible electrodes, which offer a minimal exposed surface for connective tissue growth, and at the same time maintain a large exposed conductive surface area.

## New nerve cuff designs

To address the above described issues, two new design features were introduced in the cuff design:

1. The mechanical properties of the cuff closing mechanism were improved by replacing the suture closing technique with an interlocking "zipper" device. The challenge was to design a closing mechanism, that was easy enough to close (and open) and at the same time adequately locking and sealing the opening of the cuff in a safe and permanent manner.
2. The mechanical properties of the cuff wall were improved by replacing the relatively stiff silicone tubing with thinner and more compliant silicone sheeting. The challenge was to design and install electrodes that were as flexible as the compliant silicone sheeting, and at the same time had the same electrical properties, as the traditional hand sewn electrodes.

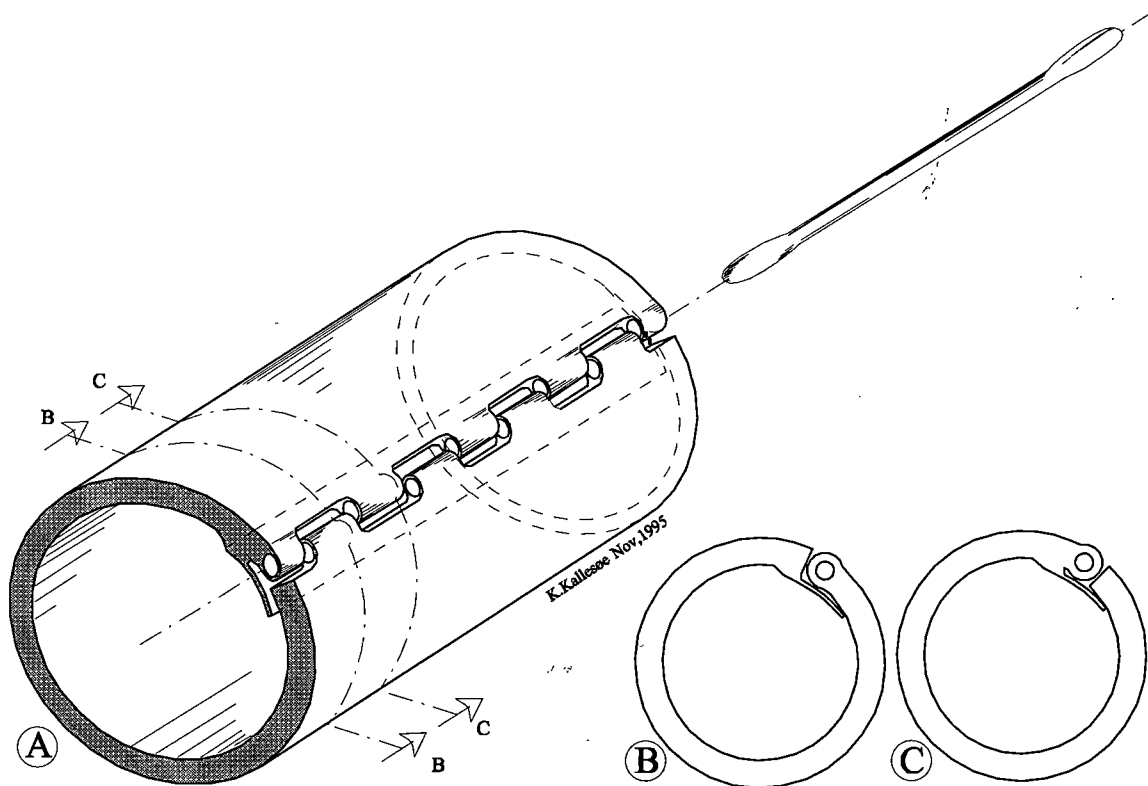


Figure IV.6: Nerve cuff closing method. (A) New closing method. Small tubes (OD: 0.6 mm, ID: 0.3 mm) glued in an interdigitated pattern along the edges of the longitudinal opening of the cuff, allowed for the insertion of a locking device. This device was either a stainless steel rod, a suture or a Teflon coated stainless steel wire. (B-C) Cross section of cuff wall, showing an inside flap sealing the opening. (Adapted from Kallesøe et al. 1996).

*New cuff closing technique:*

The basic idea behind the new closing mechanism was to move the element that provides the mechanical locking of the cuff opening, from the traditional external location on the outer surface of the cuff wall to an internal location in the opening gap (Figure IV.6). This allowed the locking mechanism to "pull" the edges together, similar to a traditional clothing zipper.

The new "zipper" of the cuff was designed from a set of small "closing" tubes, glued along the edges of the longitudinal opening in the cuff wall. The tubes were glued in an interdigitated pattern, like the teeth of a closed zipper (Figure IV.6A). By inserting a rod or suture through them, when these were interdigitated, a secure lock was formed. The cuff could be unlocked again by removing the locking rod or suture. This technique provided a mechanically secure closure although, not necessarily a good electrical seal. To obtain this, a flap of silicone sheeting was attached on the inside of the cuff along one of the longitudinal edges. An electrical seal of the opening was created when internal tissue pushed the flap against the inside of the cuff wall (Figure IV.6B-C). This seal was important for the functionality of the cuff and had previously been attempted in the suture-closed cuffs, by mounting the flap on the outside of the cuff. This approach was less effective, since it was not held tightly against the entire length of the opening. Connective tissue was therefore growing through the suture-closed opening.

When installing a traditional suture-closed nerve cuff, the sutures were used to pull open the cuff, allowing the nerve to slip in. These sutures were typically evenly distributed along the length of the cuff, providing an even pull and opening of the cuff. Without the sutures, a slightly different installation technique was needed.

Two stainless steel rods, each with a suture running through them, were inserted through the closing tubes along each edge of the cuff. The stiff rods provided an even pull along the whole length of the cuff, when the sutures were pulled (Figure IV.7).

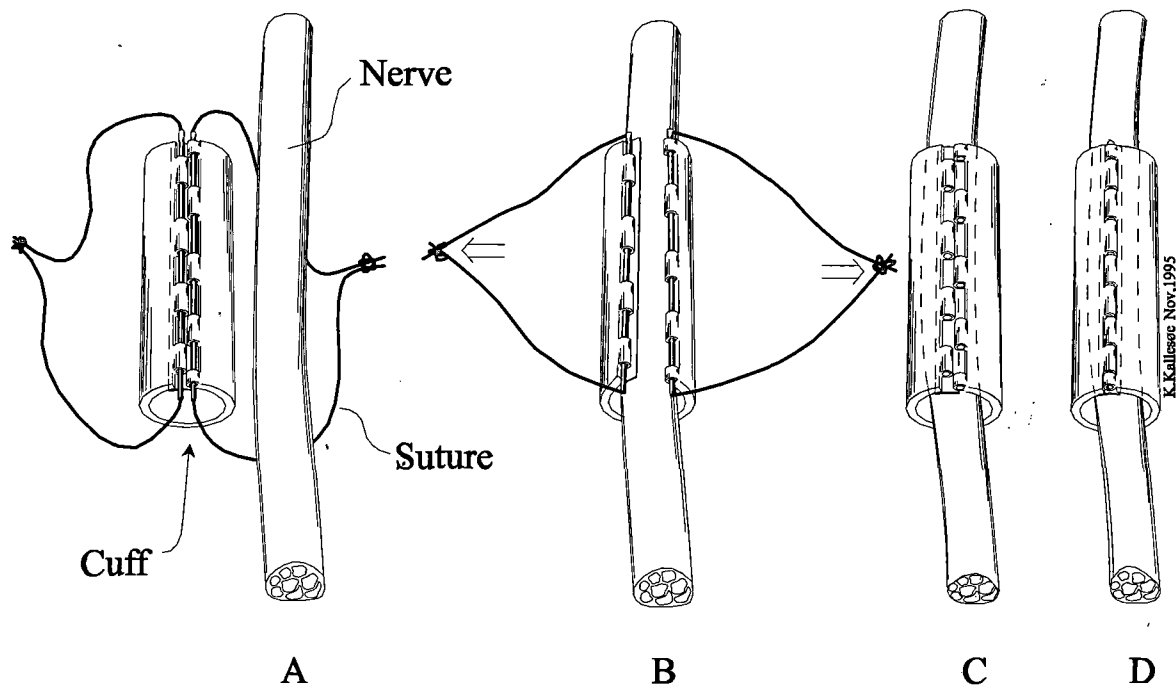


Figure IV.7: Nerve cuff installation. (A) Two stainless steel tubes (OD: 0.40 mm (0.0160"), ID: 0.19 mm (0.0075")) were inserted through the cuff opening tubes, each with a 4-0 suture passed through. (B) The cuff was pulled open, using the sutures. The steel rod ensured an even opening. (C) The opening steel rods were removed, and (D) a locking device was inserted through the closing tubes. Different locking devices were tested, such as stainless steel rod, braided suture or Teflon coated Cooner wire, all of which securely locked the cuff. (Adapted from Kallesøe et al. 1996).

#### *New cuff wall design:*

When designing a device that necessarily needs to be in intimate contact with a delicate neural structure, it is important to consider the mechanical, electrical and chemical interactions. In order to preserve the integrity of the target nerve, all of these components should be transparent, i.e. the presence of the device should pose no additional load, mechanically, electrically or chemically to the nerve. Specifically, the mechanical characteristics of the cuff wall, should ideally be comparable to those of the encompassed neural tissue. Traditional silicone tubing cuff is a fairly stiff structure, creating a sharp mechanical discontinuity at each end of the cuff. The neural tissue may thus suffer compression or bending damage at these points. Similarly, even if thin sheeting is used (e.g. Walter et al. 1995), the ends are not necessarily flexible enough to safely accommodate movements of the nerve. In fact, some sheeting materials, like Teflon and Mylar, are rather sharp at the edges, and should, for this

reason, either be treated specially along the edges or avoided altogether. Silicone sheeting, however, is a very flexible material, especially when casted from Silastic<sup>®</sup> medical adhesive. Large sheets are commercially available in thickness down to 0.127 mm (0.005"), and they can, on smaller scale (10 x 10 cm), be made as thin as 0.051-0.076 mm (0.002"-0.003").

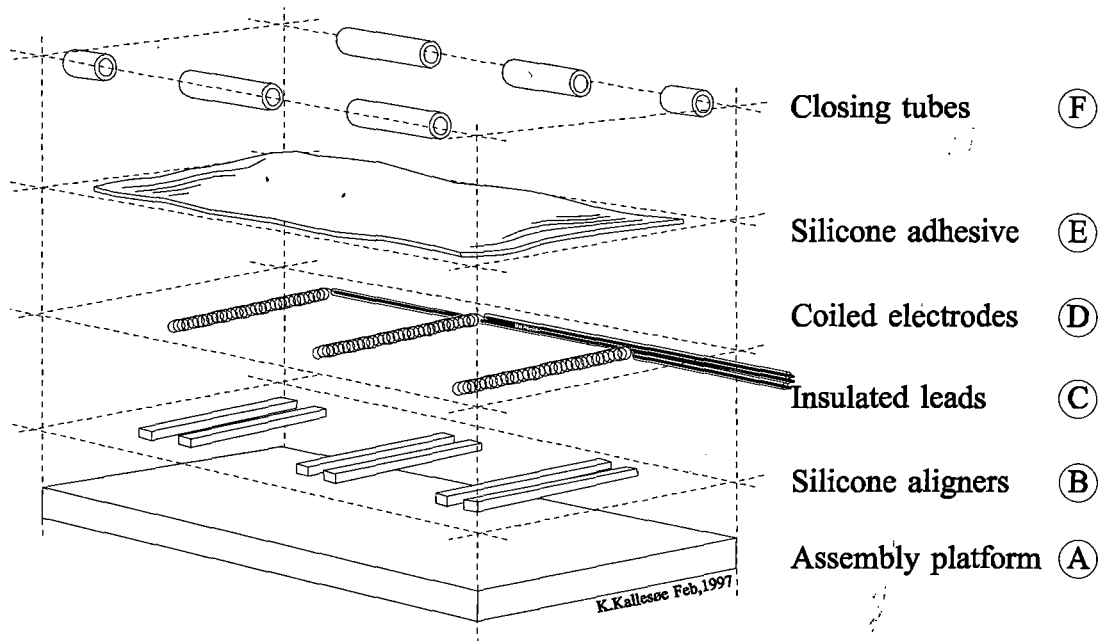


Figure IV.8: Casting a nerve cuff using Silastic<sup>®</sup> medical adhesive. (A) The assembly platform is coated with a non-stick material, like Saran Wrap, to allow the finished cuff to be removed. (B) Silicone aligners protect the electrodes from becoming totally embedded in the silicone adhesive. (C) Insulated leadout cables, typically Teflon coated 631 Cooner wire, exit longitudinally. (D) Deinsulated electrode sections are formed in coiled spirals. (E) Silastic<sup>®</sup> medical adhesive covers the total assembly. (F) Closing tubes are embedded along the edge of the silicone adhesive.

Thin silastic sheeting was, in a fairly simple manner, casted from silicone medical adhesive (Figure IV.8). First, an assembly platform was covered with a non-stick material to prevent the finished cast from adhering to the platform. Next, a spacer was attached to along the edges of the platform, defining the thickness of the final sheet. This spacer could be as simple as a piece of tape. Finally silicone adhesive was poured into the "mold" and excess material was scraped away. Different silicone adhesives exhibited unique mechanical characteristics. DowCorning 732, DowCorning 734 and DowCorning Medical Adhesive 891 have all been used for their non-viscous properties.

A cuff wall based on thin silicone sheeting was more flexible than silicone tubing and was thus more likely to conform to the natural shape of the nerve. For the same reason, however, it also required more flexible electrodes. One possible way of achieving this, was with the use of foil electrodes, rather than wires. This has most recently been explored by Haugland (1996), with promising results. However, a metal foil layer, like platinum, may be extremely flexible in one direction (up and down bending), but fairly fragile in other directions (stretching and sideways bending). Furthermore, metal foils are likely to create mechanical stress points in a 3-dimensional structure like a circumneural electrode. These points are exposed to relatively large amounts of deformation, during repeated opening and closing of the cuff, and thus make them prime targets for potential electrode failure. Despite these potential pitfalls, the number of failing electrodes are very limited (personal communication with Haugland 1996).

An alternative to the foil based electrode, was the wire electrode reshaped into a tight spiral or coil-like structure. In this form, the stiff wire becomes very compliant in all directions. The idea of using a coiled electrode in a thin sheet cuff wall design, has been reported elsewhere (Grandjean and Lee 1991) and it was included in the casting of the cuff wall by embedding the electrode in the Silastic<sup>®</sup> medical adhesive material (Figure IV.8). Several benefits were obtained in this process:

1. It allowed for more precise positioning of the electrodes with respect to one another, and it also limited the possibilities of splay in the individual electrodes.
2. It allowed each electrode to be partially embedded in the silicone, along most of the inner circumference of the cuff. This reduced the possibility of connective tissue growth between the electrode and the wall (Figure IV.9).
3. It allowed a greater wire length to be exposed to the surface of the nerve (in the order of 5 times longer than the existing hand-sewn electrode). This reduced the electrical impedance of the electrochemical interface between electrode and extraneural tissue. Potentials generated by sources far from the electrode were, because of the lower impedance, not generating as large a "noise" potential. This improved the cuff's ability to detect small signal neural activity.



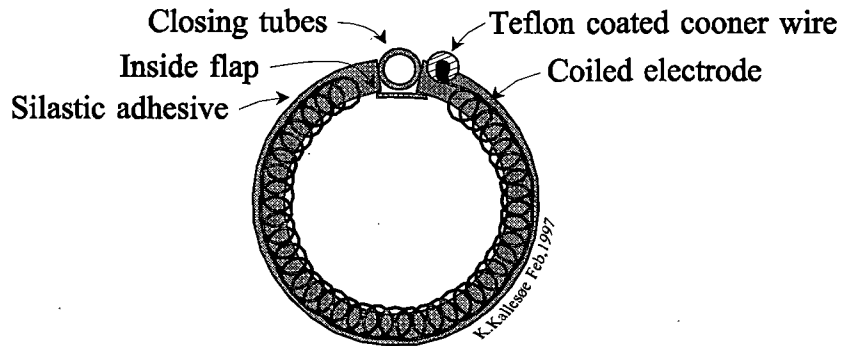


Figure IV.9: Cross-section of a spiral electrode cast in a silicone cuff wall. The electrode is located in a circumferential groove in the cuff wall, and is not completely embedded in the wall material as might be interpreted from this figure. Only the outer circumference of the spiral loop is in contact with the silicone adhesive.

Combining the new closing technique with the new cuff wall and electrode design, resulted in a finished cuff design with a compliant wall and a set of very flexible electrodes. Furthermore, the cuff and the electrodes retained their original shape in the event of external compression flattening the cuff. This is a significant improvement on the early thin sheet cuff with stiffer electrodes, which deformed the cuff shape when bent or squeezed.

## Application of new designs

### *New closing method*

Cuffs with the new closing mechanism were used both, in the recording setup described in Chapter II, and in a cuff evaluation setup, testing the long term performance of the devices in the peripheral nerves of the cat forelimb (Strange et al. in revision). This recording setup was significantly different from the setup described in Chapter II, and will thus be briefly summarized. In total, 16 nerves were implanted with suture closing cuffs, and 12 nerves were implanted with zipper closing cuffs. The implant periods were 101-300 days, in a total of 14 cats. In each forelimb, two sets of nerve cuffs were implanted on the median and ulnar nerve, one above and one below the elbow joint on each nerve. (Other devices, such as EMG electrodes, thermistors and occasionally patch ENG electrodes were implanted as well). Compound action potentials were evoked under anesthesia by electrical stimulation through one cuff (above the elbow), and recorded from the companion distal cuff. The stimulation was constant current, with a balanced charge of 50  $\mu$ s initial pulse width and 500  $\mu$ s secondary pulse width. The stimulation was supramaximal below 2 mA.

The objective of the test was to verify the survival of both nerves and the implanted nerve cuffs. This was done by recording the following:

1. The excitability of the nerve was monitored by recording the stimulus current amplitude needed to elicit an action potential. A damaged nerve, with scar tissue forming around remaining axons, will exhibit an increased excitability threshold. This was a measure of the functional survival of the nerve at the stimulating site.
2. The number of axons conducting action potentials through the recording nerve cuff was monitored by recording the amplitude of the compound action potential (CAP) elicited by supramaximal stimulation. A decrease in the maximal amplitude is seen when either the number of axons contributing to the CAP decreases, or when the recording cuff fails to maintain an isolated center electrode. This measurement reflected the combination of the functional survival of the nerve at the recording site and the integrity of the cuff seal.
3. The survival of the nerve between the two cuffs was monitored by recording the conduction latency between the nerve cuffs. An increase in the latency is to be expected if the larger, faster conducting axons are damaged. This is seen in mild compression damage where larger axons are affected more than the smaller axons. Since, tripolar nerve cuffs record primarily from these larger axons (Hoffer et al. 1981), mild compression damage will increase the latency and decrease the amplitude of a compound action potential. The measurement indicated the functional survival of the nerve between the cuffs.
4. The survival of the cuff seal and of the leadout cables was monitored by recording the electrical impedance of all electrodes. A decrease in electrical impedance, is detectable when the integrity of the insulation of the electrodes and leadout cables is compromised. This is seen when a cuff seal fails, when electrodes are pulled out of the cuff wall, or when the insulation of the leadout cables is broken, exposing the conducting wire. This is a measure of the functional survival of the transducer systems.

Two series of six-month-long implants were performed, comparing the viability and stability of the new closing method with respect to the traditional suture closing. Each series involved periodic monitoring of the above mentioned features: evoked compound action potentials,

latency and electrode impedance. Force majeure factors, such as the cat pulling out leads, were eliminated from the analysis.

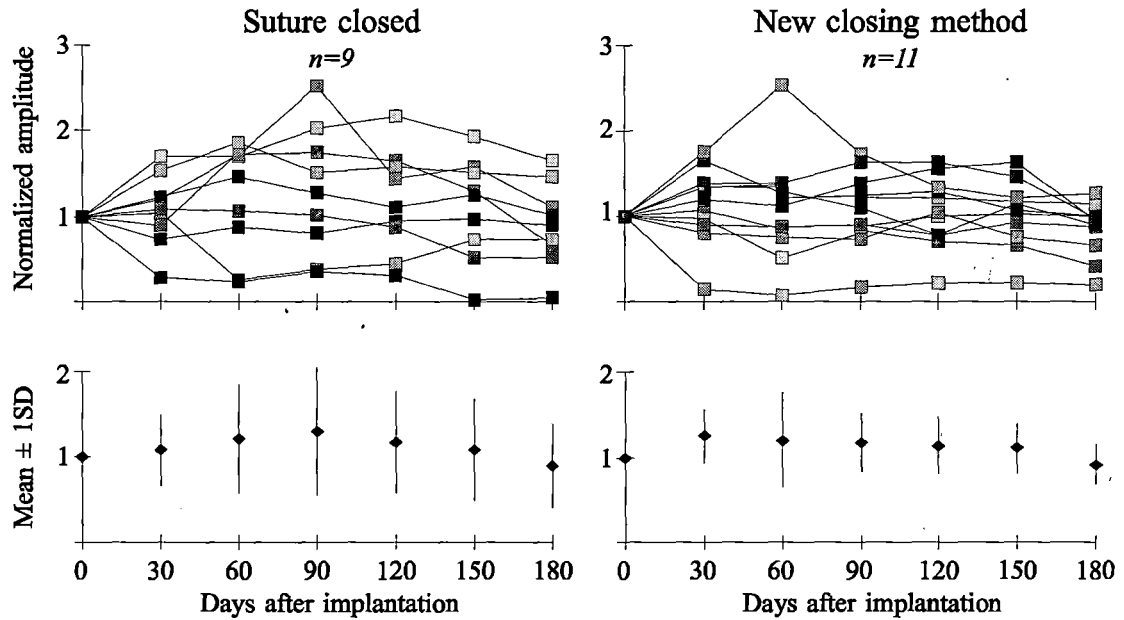


Figure IV.10: Top: Normalized peak-to-peak amplitudes of CAPs recorded from two series of implants over 180 days. Bottom: Same data showing the geometric means, where error bars represent  $\pm 1$ SD. The means were not found to be statistically different for the two experiments (T-test one sided, two samples assuming unequal variance,  $P < 0.05$ ). Similarly, the variance was found not to be significantly different (F-Test, two-Sample for Variances,  $P < 0.05$ ). Data from original recording days have been interpolated to 30 day intervals. (Adapted from Strange et al. in revision).

Figure IV.10 shows that the CAPs recorded from the suture closed cuff had a larger variability compared to the new closing method. This is most easily seen in the differences of the error bars in the bottom two graphs of the figure. The new closing techniques thus shows a more consistent seal of the cuff than that of the suture closed cuff.

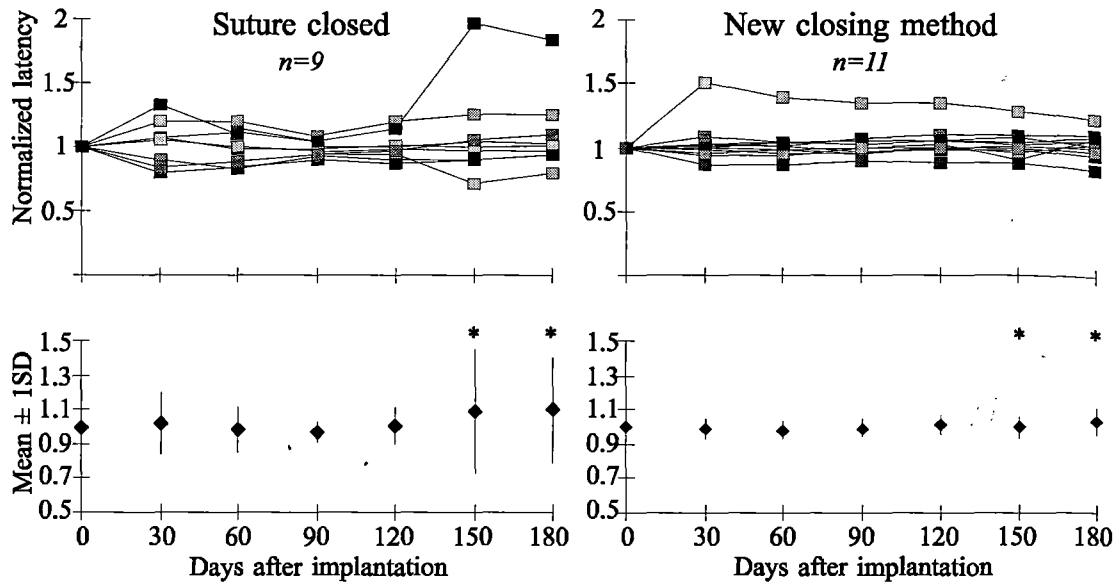


Figure IV.11: Top: Normalized conduction latencies of CAPs recorded from two series of implants over 180 days. Bottom: Same data showing the geometric means, where error bars represent  $\pm 1SD$ . The means were found not to be statistically different for the two experiments (T-test one sided, two samples assuming unequal variance,  $P < 0.05$ ). The variance on two recording days (\*) was found to be significantly different, day 150 and 180 (F-Test, two-Sample for Variances,  $P < 0.005$ ). However, as seen in the top trace of the suture closed cuffs one sample deviated notably from the general trend in the data. Given the limited number of samples ( $n=9$ ), this caused the two sample sets to be statistical significant. Data from original recording days have been interpolated to 30 day intervals. (Adapted from Strange et al. in revision).

Figure IV.11 shows that the latency of the CAPs remained relatively stable in both series of implants. Given that the CAP mainly reflects activity in larger superficial axons, this finding was indicative of very limited damage in these fibers. The smaller standard deviation of the recordings again confirmed a more consistent closure using the new closing technique.

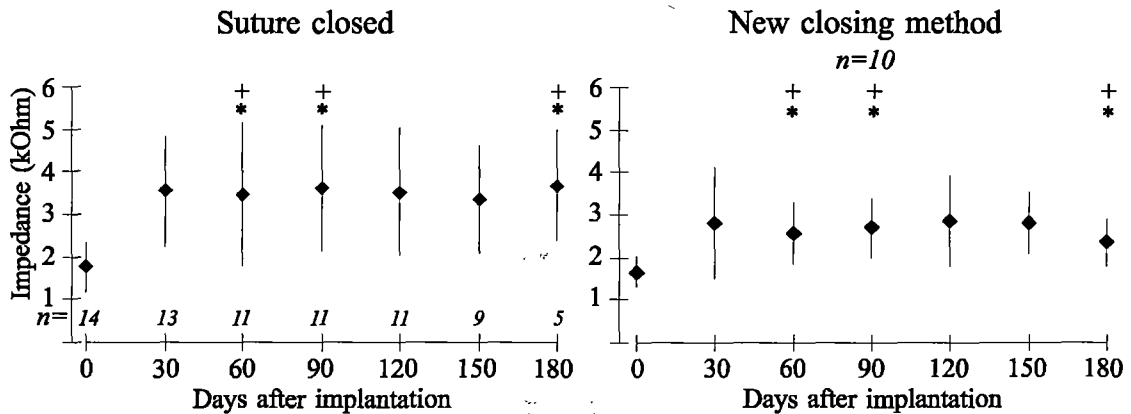


Figure IV.12: The geometric mean of the impedance of distal nerve cuff electrodes from the two series of implants over 180 days were found to be statistically different (+) (T-test one-sided, two samples assuming unequal variance,  $P < 0.05$ ). Error bars represent  $\pm 1SD$  and the variance on three recording days (\*) were found significantly different (F-Test, two-Sample for Variances,  $P < 0.05$ ). (Adapted from Strange et al. in revision).

Figure IV.12 shows that the cuffs with the new closing method had in general a more stable impedance. It is also apparent that the average impedance were in general lower for this group, compared to the suture closed cuff. This was due to a slightly larger diameter of the cuffs having the new closing methods compared to the diameter of the suture closed cuffs.

The results overall show that for a long term implants, the zipper closed cuffs had more consistent electrode impedances and CAPs.

#### *Thin wall cuff*

Results from the design of thin wall cuffs are very preliminary. A limited number of prototypes (8) were successfully assembled, of which only one was implanted. The initial results from this implant show an electrical performance equivalent to that of a traditional cuff (based on CAP amplitude and electrode impedance). Obviously, the limited number of implants, precludes the possibility of determining the significance of the improvements. However, when removing the cuff at postmortem (26 days), it was observed that connective tissue did not grow into the spiral electrodes. The cuff was removed from the nerve with minimal visible disruption of the tissue.

### **Discussion**

The overall design goal of a recording nerve cuff is to establish an electrochemical interface to peripheral nerves by placing electrodes on the surface of the nerve without causing harm. Several mechanical flaws were identified in existing cuff designs and possible solutions to these were documented. The nerve cuff design is far from being ready to be used in large clinical trials, mainly because of leadout wires, mechanical incompatibility of cuff wall and neural tissue and lack of selectivity in the recording or stimulating interfaces. The design features described here address some of these important issues for future designs of both recording and stimulating nerve cuffs.

The new cuff closing technique where designed to improve on the functionality of existing recording nerve cuffs in terms of easier manufacturing and implantation techniques. The long term recording stability and nerve survival was not found to differ from the previous suture closed cuffs and the cuffs were found to provide a more consistent seal around the nerve (Strange et al. in revision). In addition, the new technique differs from other designs,

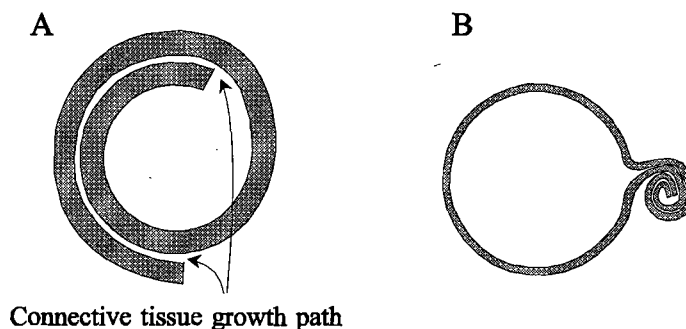


Figure IV.13: Self sizing nerve cuff designs. A) Cross section of existing self-sizing stimulation nerve cuff, and the potential pathway for connective tissue growth. B) An alternative self-sizing nerve cuff, with self locking opening, minimizing the risk of connective tissue growing through the opening.

The curling action can, however, be moved away from the nerve, possibly gaining several advantages. Prototypes have been manufactured, consisting of two self curling sections on a thin sheet of silicon (Figure IV.13B). The nerve is encompassed by a non-curling section of the sheet, and the closing is generated by the two curled sections. The closing curl, however, does not curl around the nerve, but rather around itself. The advantages gained here are:

- 1) Expansions in the nerve volume no longer need to overcome the shear friction of the wall material. The cuff lumen is expanded by unwrapping the external spiral from the inside of the cuff.
- 2) Connective tissue is less likely to grow through the opening, since the pathway from inside to outside is tightly coiled.

This externally spiraling nerve cuff design concept has been used in construction of "large" scale nerve cuffs (4-5 mm in diameter). As with any mechanical design, several aspects of the construction of "small" scale cuffs (less than 2 mm in diameter) still remain to be addressed. These designs have yet to be implanted.

Another future direction in cuff design is in making more selective recordings with additional electrodes in the cuff as seen in preliminary studies by Lichtenberg and De Luca (1979), Struijk et al. (1996), Christensen et al. (1997). These authors replaced the circumneural electrodes with the multiple electrodes distributed around the inside circumference, similar to multi contact stimulation nerve cuffs (Rozman et al. 1994). That opened the possibility of recording selectively from local compartments (fascicles) of the nerve, potentially increasing

the versatility and clinical application areas of the nerve cuff. As described by Brunner and Kock (1990), multichannel cuff electrodes suffer from leakage control between the recording sites. As a simple solution, they suggest "tightening the cuff wall between the electrodes to provide a seal ...". This "tightening" could be incorporated in the cuff wall design, providing additional electrode isolation. Another approach to create this intimate contact between the nerve surface and cuff wall was suggested by Lynch in 1991. Here, strips of adhesive were envisioned between multiple electrodes in the full length of the cuff. However, this approach does not allow for expansion of the nerve volume and is thus likely to create compression damage.

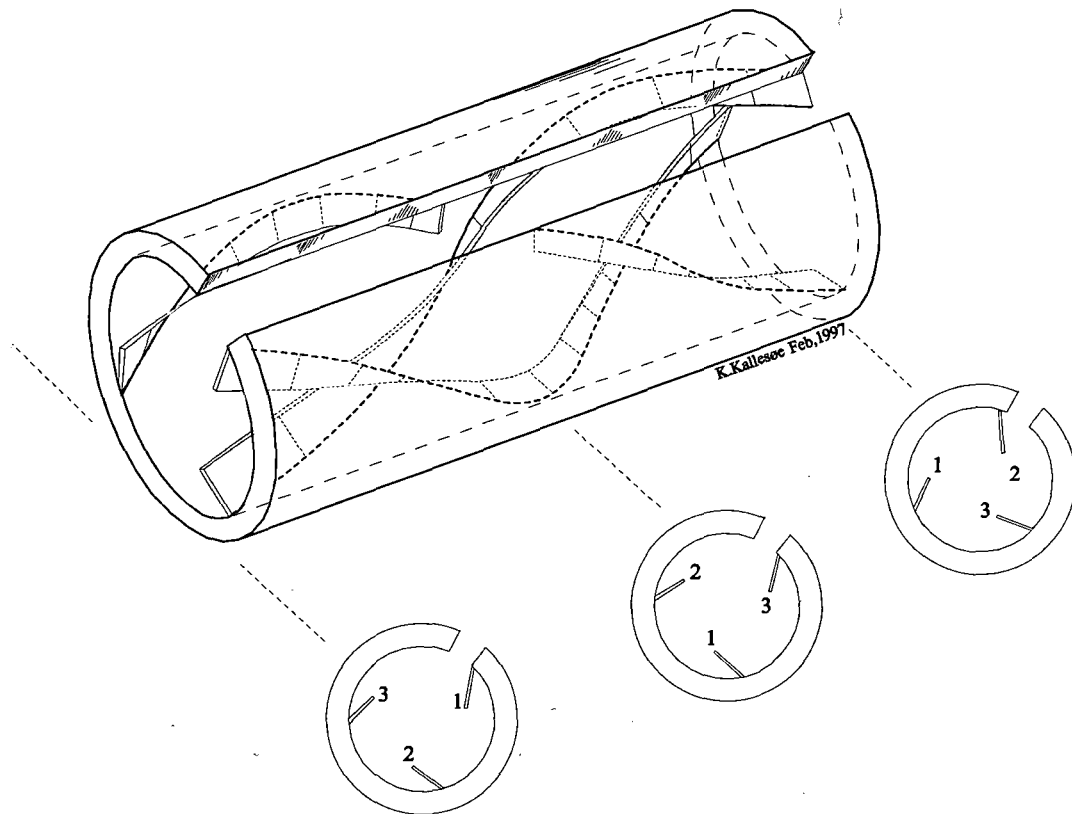


Figure IV.14: The "gun barrel" cuff design. Thin flaps of silicon sheeting are embedded in the cuff wall during flat casting procedures. The flaps run in straight lines when the cuff is completely opened and laid flat. The flaps accommodate changes in nerve volume and increase the electrical isolation of recording electrodes (not shown). The mechanical support of the nerve is obtained by lifting the flaps from the cuff wall, allowing them to be easily pressed down. The flaps may loop once or more around the inner circumference, depending on the length of the cuff and the mechanical support needed. The more loops, the more supporting contact surface. Looping less than one total circumference is also a possibility, but it requires more flaps to maintain the mechanical support of the nerve. The key point is, that the flaps will not run in parallel with any multiple electrode arrangement.

Other important issues in the design of nerve cuffs still remain to be addressed, such as: development of active circuitry on or near the cuff, to optimize recording conditions and minimize, or possibly eliminate leadout cables by the use of telemetry; development of a biocompatible electrochemical interface between an ion conducting fluid medium and the electron conducting electrodes; refinement of electrode configurations with multiple recording points, to optimize selectivity in recording and stimulation. These features may improve the design to the point where the nerve cuff is ready for a large scale clinical use.



## V. FINE WIRE AND HATPIN SINGLE UNIT ELECTRODE

A long-term goal in neuromuscular research has been to characterize the functional behavior of neuromuscular control systems. This has been attempted by correlating afferent discharge patterns of individual proprioceptors with the mechanical dynamics of muscle fibers and tendon elements (Prochazka et al. 1977, Elek et al. 1990). Also, recording of efferent discharge has been of interest, to possibly yield more insight as to the function of fusimotor axons (Prochazka and Wand 1981, Hulliger and Prochazka 1983). These recordings have, however, typically been made in reduced or anesthetized preparations. Documentation of the behavior of these systems during awake voluntary movements, has been characterized as a formidable task (Lemon 1984, Rothwell 1994). Special peripheral single unit (PSU) electrodes have been designed for this purpose (Hoffer 1990).

In brief, an extracellular interface to a peripheral axon is achieved by introducing an electrode either inside (intra-neural interface) or in close proximity to a nerve (extra-neural interface). The design of such an electrode for use in the peripheral nervous system (PNS) was initially based on electrode designs used in the CNS (Geddes 1972, Snodderly 1973, Burns et al. 1974, Lemon 1984). Several issues were addressed in adapting single unit recording technology to the PNS:

- 1) PNS electrodes need to float with the moving tissue, rather than being rigidly linked to a long-shafted electrode shank as in typical CNS recordings;
- 2) Electrodes inserted in moving tissue require some sort of anchoring system. Many electrode designs offer very limited mechanical support for maintenance of their position inside the tissue;
- 3) The current sources in the peripheral nerve, the nodes of Ranvier, deliver very small amounts of current, ~3-5 nA (Marks and Loeb 1976).

Furthermore, the size of an intra-neural electrode should be as small as possible to minimize damage to neighboring axons. Also, the cabling should be extremely flexible to avoid movement of the electrode inside the fascicle.

This "floating fine wire electrode" concept was pioneered in the CNS of conscious, freely moving cats by Burns et al. (1974), and consisted essentially of a fine gauge wire. The diameter of the insulated wire was comparable to an individual axon diameter (20-25  $\mu\text{m}$ , including the myelin), and the cut end formed the electrochemical interface to the neural tissue. A similar electrode design was used by Prochazka et al. (1976) and by Loeb et al. (1977) in the spinal roots of freely walking cats. Since then, the electrode design has successfully been used for recording neural activity in mammalian dorsal root and ganglia (Prochazka et al. 1976, Prochazka and Wand 1981, Hoffer et al. 1987a,b, Gorassini et al. 1993).

Interfacing to more peripheral nerves has proven more challenging (Schoenberg and Kendell 1993). This could be in part due to technical challenges in designing electrodes and to post-implant physiological changes in the nerve. The latter was addressed by Schoonhoven and De Weerd (1984), who discussed the influence of extraneural electrode dimensions and location on a simulated CAP. This was based on a volume conductor model of a nerve encapsulated in fat and muscle tissue. The simulation showed that high amplitude and high frequency signals are to be expected during near nerve recordings. It is thus important to locate recording electrodes in close proximity of the axon of interest, and to be able to handle high frequency signals.

Schoonhoven and De Weerd (1984) furthermore showed, that single fiber action potentials (SFAP) were significantly influenced in amplitude and shape by the presence of a near nerve recording electrode. Once again, the specific location of the electrode, in relation to the nerve is thus important for the interpretation of the recording.

Some success has been reported using fine wire electrodes for longer term stimulation purposes (Yoshida and Horch 1993, Bowman and Erickson 1985). Again, the importance of the electrode location was seen in studies of the performance of stimulating electrodes (Veltink et al. 1989a). It was found that intraneural electrodes excited neurons independent of the size of the neuron i.e. they were equally likely to excite, both, large and small diameter neurons. In contrast, the same authors confirmed that, extraneural electrodes exhibit a selective recruitment order, with larger diameter fibers being excited first. Intrafascicular electrodes should thus be

capable of creating an extracellular interface to individual axons of, both, small and large fiber diameters within a peripheral nerve fascicle.

The fine wire electrode design was refined further in a "thumb-tack" or "hatpin" electrode design (Salcman and Bak 1973, 1976), in which a short and stiff insulated needle at the end of a fine flexible wire served as the interface site. A limited amount of the insulation on the tip of the needle was removed to expose the conducting surface. The connecting flexible fine wire created a very compliant mechanical linkage to external leadout wires, allowing the electrode to float relatively unrestricted in the neural tissue. These hatpin electrodes were successfully used in chronic recordings from cat motoneurons in lumbar ventral root (Hoffer et al. 1987a), and in the dorsal root (Loeb et al. 1985a,b,c). Limited success was reported when using the same electrodes for recording purposes in more peripheral nerves (Hoffer and Weytjens 1990).

### **Objective**

The objective of the single unit fine wire electrode design developed here, was to create an interface to single axons in the peripheral nervous system based on existing micro-electrode techniques. The electrodes should be capable of recording stable unitary axon potentials for use in characterizing proprioceptive feedback in unrestrained conscious animals.

### **Electrode fabrication and implantation**

The design of peripheral single unit (PSU) recording electrodes originates in similar single unit (SU) electrodes used in the central nervous system (Burns et al. 1974). The main differences in the requirements of this design are a mechanically more mobile peripheral environment, and an expectation of smaller electrical signal amplitudes. The expected electrical potential on the surface of a single axon has been estimated as 5-50 nV (Schoonhoven and De Weerd 1984, Buchtal et al. 1984, Schoonhoven et al. 1986a).

*Hatpin Electrode:* The hatpin electrode used in this thesis was based on the design used by Hoffer and Weytjens (1990). In this design, a short sharp needle tip was attached to the end of a fine flexible wire (Figure V.1). This allowed the assembly to "float" with the movements of the tissue and included the properties of a stiff, penetrating needle electrode, similar to Salcman and Bak's (1976) electrode. The connection between needle and fine wire was

insulated by an epoxy encapsulation, creating a rounded ball at the end of the tungsten "pin". The pin was made from 50  $\mu\text{m}$  or 75  $\mu\text{m}$  tungsten wire, etched to a sharp needle point (1-2  $\mu\text{m}$ ). This etching was done by slowly ( $\sim 5 \cdot 10^1 \mu\text{m} \cdot \text{s}^{-1}$ ) lifting the electrode out of a 15-20 M  $\text{KNO}_2$  solution while applying an AC voltage (3-5 V) across the tungsten and the solution. The speed and the voltage applied, determined the shape of the electrode. A long, very sharp but fragile tip was created with high speed and low voltage settings. In contrast, a short, dull and robust tip, was the result of quick lifting and high voltage setting. (See Snodderly 1973 for detailed description of electrode etching and assembly.)

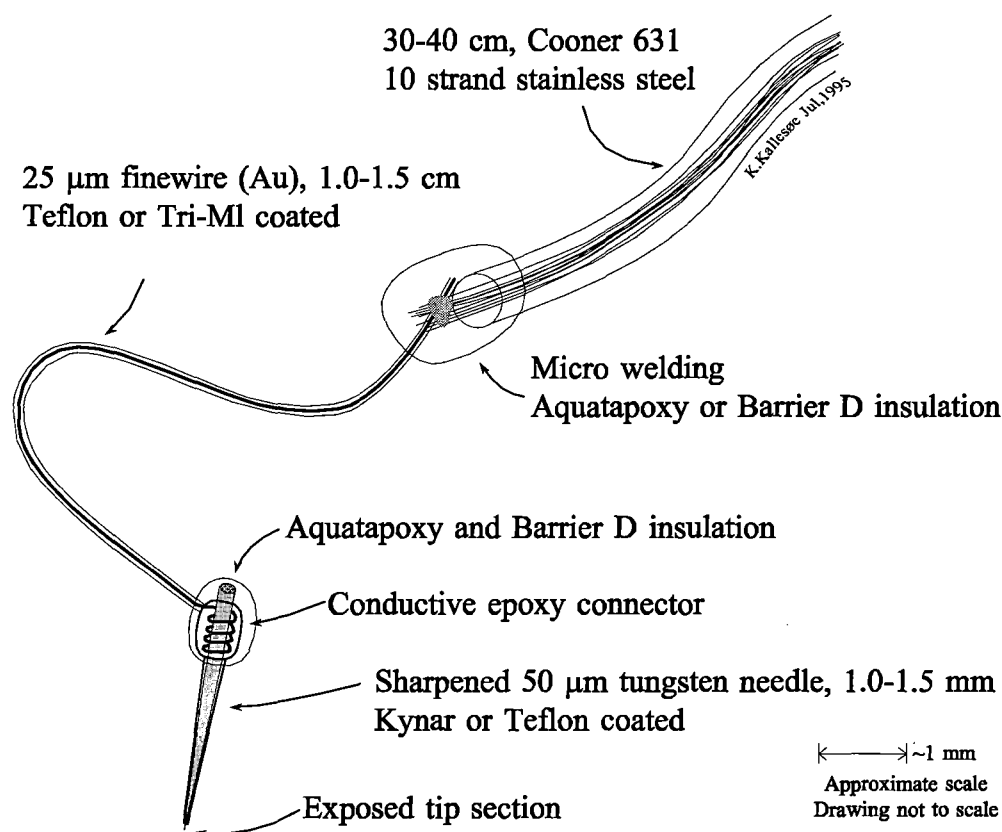


Figure V.1: The hatpin design. Stainless steel strands of a quadruple Teflon coated 631 Cooner wire was micro-welded to a Tri-ML coated 25  $\mu\text{m}$  gold wire, 1.5-2.0 cm in length. The distal end of the gold was wrapped around a sharpened 50  $\mu\text{m}$  or 75  $\mu\text{m}$  tungsten electrode. Prior to assembling the electrode, a coating of either Kynar or heat-shrinkable Teflon was applied to the tip section. A limited area of this insulation was removed, resulting in a electrode tip impedance of 200 k 300 k  $\Omega$  (at 1 kHz). The electrical connection between gold and tungsten was established with silver based conductive epoxy. This junction was insulated with Aquatapoxy and Barrier D. Failures occurred if the insulation of the assembly was compromised, or if mechanical stress broke the continuity of the conductor.

The bare etched electrode was then insulated with a thin dielectric layer (2-3  $\mu\text{m}$ ). The choice of this dielectric material was found to be crucial for the performance of the electrode. Several types of insulation materials have been reported in the literature, e.g. vinyl lacquer (Snodderly 1973), Parylene (Schmidt 1983) or enamel (Hoffer 1990). In the present thesis research an epoxy ("Kynar"), was initially used. This epoxy was applied by dip coating the tip and curing it pointing upwards, to avoid drop formation on the tip. Even a minor unevenness in the thickness of the epoxy would cause mechanical weaknesses and cracks in the insulation.

As an alternative, attempts were made with Teflon as a coating material. Pure Teflon has a relative high melting point, making non-pure mixture a more attractive alternative. A non-pure heat shrinkable Teflon from Small Parts inc. (Florida) was used to deposit a 2-3  $\mu\text{m}$  insulating layer along the tip section. Unfortunately, this material became porous and thereby conductive after a couple of days of submersion in saline. This approach was therefore abandoned.

Regardless of the coating material used, a hole was needed in the insulation to create a conductive pathway. This was done either mechanically, by running the tip across a very fine abrasive surface, or by an electrostatic high voltage spark, arcing from the tip. Mechanical damage to the tip was obviously less likely to occur in the latter of the two procedures. The spark was created with a high voltage "zapping" device designed by D. Viberg (engineering support in Dr. Hoffer's lab). A hole in the insulation material lowered the tip impedance from the  $\text{M}\Omega$  range to 200 k-300 k  $\Omega$  at 1 kHz.

The finished electrode tip was attached to a fine wire, by wrapping it around the shank of the tungsten electrode. Both of these had to be deinsulated to facilitate conduction across the junction. The TriMI coating on the gold fine wire was removed with heat, and the Kynar or Teflon on the tungsten by mechanical abrasion. To assure a stable contact, additional conductive epoxy was applied between the gold and tungsten. The total junction was encapsulated in a water resistant epoxy ("Aquatapoxy" from American Chemical Corp., St. Louis, MO).

In order for the hatpin electrodes to remain anchored to the peripheral nerve, they needed a mounting platform to carry the load of the leadout cables. Such a platform was created by modifying a traditional nerve cuff (Figure V.2). A distal section of the cuff wall was removed

to provide access to the surface of the nerve. The SU electrodes were inserted through a window and the flexible gold fine wire allowed the electrodes to float with the nerve, when it moved relative to the cuff. The leadout cables were glued to the outside with silicone adhesive through an array of silicone guide tubes. To provide mechanical and electrical protection of the implanted hatpins, the window and parts of the nerve cuff were covered with a stainless steel cover. Results from the initial design of this cuff were reported by Hoffer and Weytjens (1990).

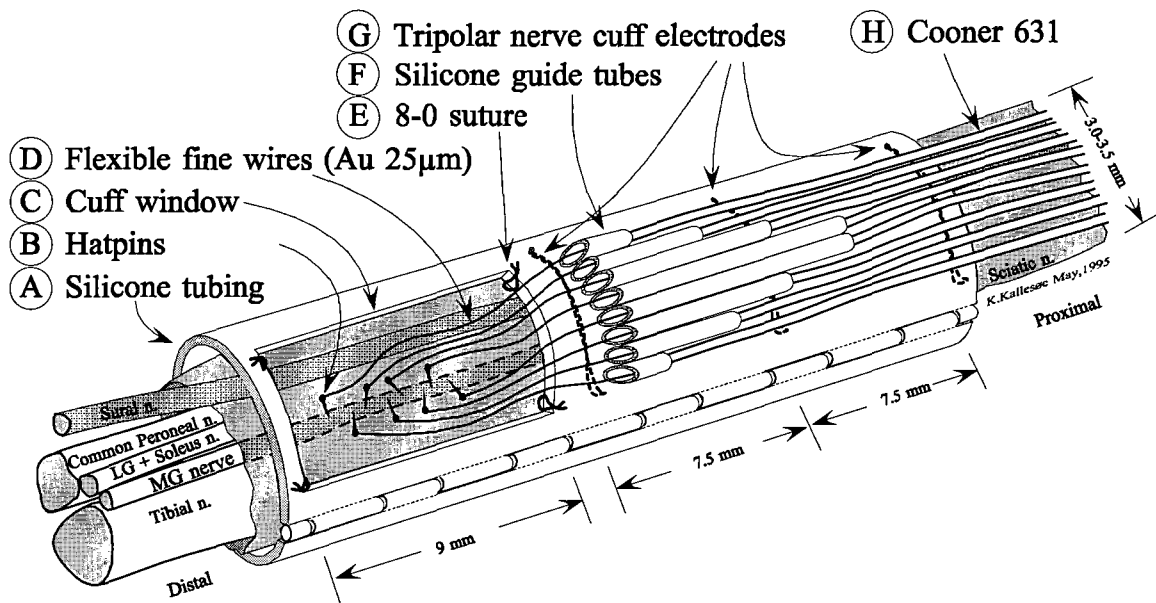


Figure V.2: Sciatic nerve cuff with hatpin electrodes attached to the external cuff surface. In the distal section of a silicone tube (A) (Sil-Med 31005, ID: 4.0 mm, OD: 5.5 mm) a "window" (C) was cut out providing access to the sciatic nerve. The window allowed flexible fine wires (D) to access the surface of the nerve. Internural hatpin electrodes (B) were inserted in the MG fascicle. The cuff was sutured to the epineurium with three or four 8-0 suture stitches (E), to fix the location of the MG fascicle with respect to the window. The proximal section had a set of tripolar electrodes (G) attached in the inside of the tube. An array of small diameter silicone tubes (F) (Dow Corning 602-155, ID: 0.6 mm, OD: 1.2 mm) on the external surface of the cuff provided a mechanical anchor for the exiting wires (H) (Cooner 631). A stainless steel cuff cover (not shown) protected the cuff and provided an electrical reference for single unit recordings.

In using the hatpin design, it was found that the limited anchoring surface may have prevented long term intraneural stabilization of the electrode. It was also found, that the insulation of the tip was very likely to fail, preventing recording of neural signals. It was thus decided to attempt using a simpler finewire electrode.

*Simple fine wire electrode:* Fine wire electrodes had previously been used in the mammalian spinal roots (Prochazka et al. 1976, Loeb et al. 1977) and an electrode design very similar to these was adapted for the present thesis work (Figure V.3). Electrodes were fabricated from a flexible cut wire with a thin dielectric coating of Teflon, enamel or epoxy paint. The wire material was either stainless steel, platinum-iridium or gold. Material properties and dimensions of the fine wire determined the flexibility of the electrode assembly. This flexibility allowed the electrode, once inserted, to "float" with the moving tissue. Typically a diameter of 20-25  $\mu\text{m}$  was used, with a total length of up to several centimeters, depending on the application. Each fine wire was attached to multistranded stainless steel leadout cables (Cooner 631) (Figure V.3). These were connected to external amplifiers (see Chapter II for the recording setup).

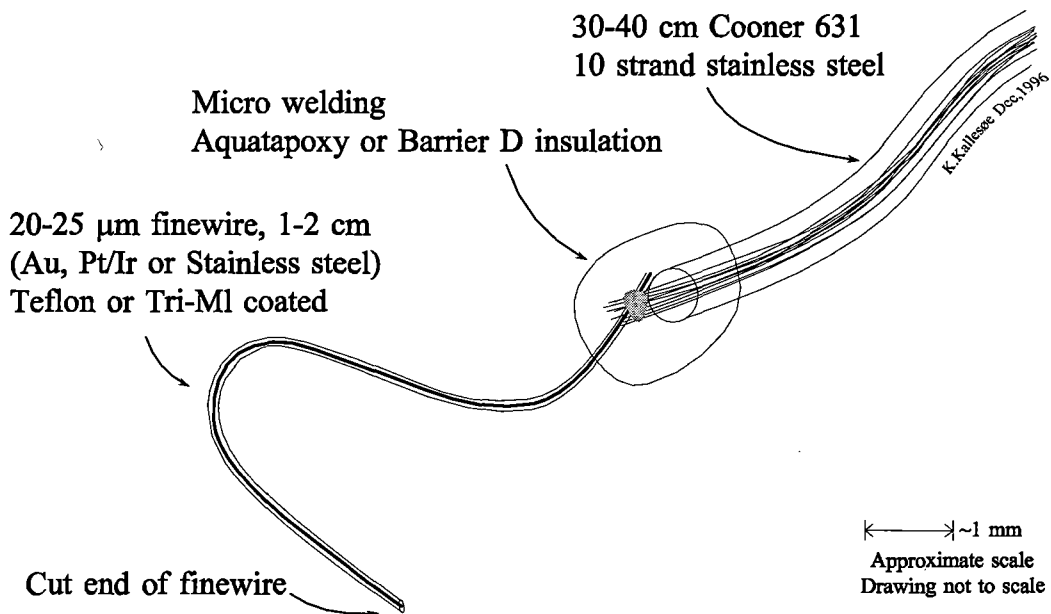


Figure V.3: The simple fine wire design. Stainless steel strands of a quadruple Teflon coated 631 Cooner wire were micro-welded to a Tri-ML coated 25 $\mu\text{m}$  stainless steel, Pt-Ir or gold wire, 1.5-2.0 cm in length. Failure of the assembly occurred, if the insulation of the assembly was compromised, or if mechanical stress broke the continuity of the conductor.

The cut end of the electrode formed the electrochemical interface with the neural tissue. The surface area of a cut circular wire was in the range of  $1.2 \cdot 10^3$  to  $1.9 \cdot 10^3 \mu\text{m}^2$ , depending on the cutting angle. This area determined the electrode impedance (100 k-300 k  $\Omega$  at 1 kHz) and it was manipulated by cutting the tip at an oblique angle. This produced a sharper electrode,

easing the tissue penetration. The ability to penetrate was found to be an all important factor, when attempting to insert electrodes through tough dura or epineurium.

It was found, that a soft and flexible electrode was likely to bend, compromising the integrity of the insulation material or the continuity of the conducting metal. A new electrode design was therefore tested, based on similar design used for myographic single unit recordings (Andreassen and Rosenfalck 1978).

*Needle-Threaded Fine wire Electrode:* This design again included a tungsten needle attached at the end of a flexible fine wire, either gold or stainless steel (Figure V.4). The needle, however, did not serve as electrode but rather was designed to penetrate and create a path through neural tissue in advance of the fine wire. After this initial pass, the needle was removed and the cut end of the fine wire was pulled back into the nerve close to axons. This implantation technique greatly improved the length of flexible cable that was "woven" through connective tissue before reaching the axons of interest. Although this anchored the electrode better than both the traditional fine wire and the hatpin electrodes, the design still had the possible failure mode of the electrode "slipping" out of neural tissue.

A slightly different version of the needle threaded electrode was developed, to prevent the installed fine wire from slipping out of the nerve. The recording point was moved from the tip to a small hole, located 5-10 mm from the tip needle. The hole was created by arching a high voltage spark through the insulation material. Moving the recording point eliminated the need to pull the cut end of the wire back into neural tissue. The needle was again used to thread the fine wire, to create a mechanical anchor, as described above. With the recording point inside neural tissue, the wire could now be moved slightly back *and* forth through the neural tissue, effectively optimizing the location of hole.

The final installation step was to insulate the cut end of the fine wire. This was done by passing the needle through the soft silicone cuff wall, and then breaking it off from the fine wire. That terminated the wire end inside the silicone cuff wall, and thus provided electrical insulation.



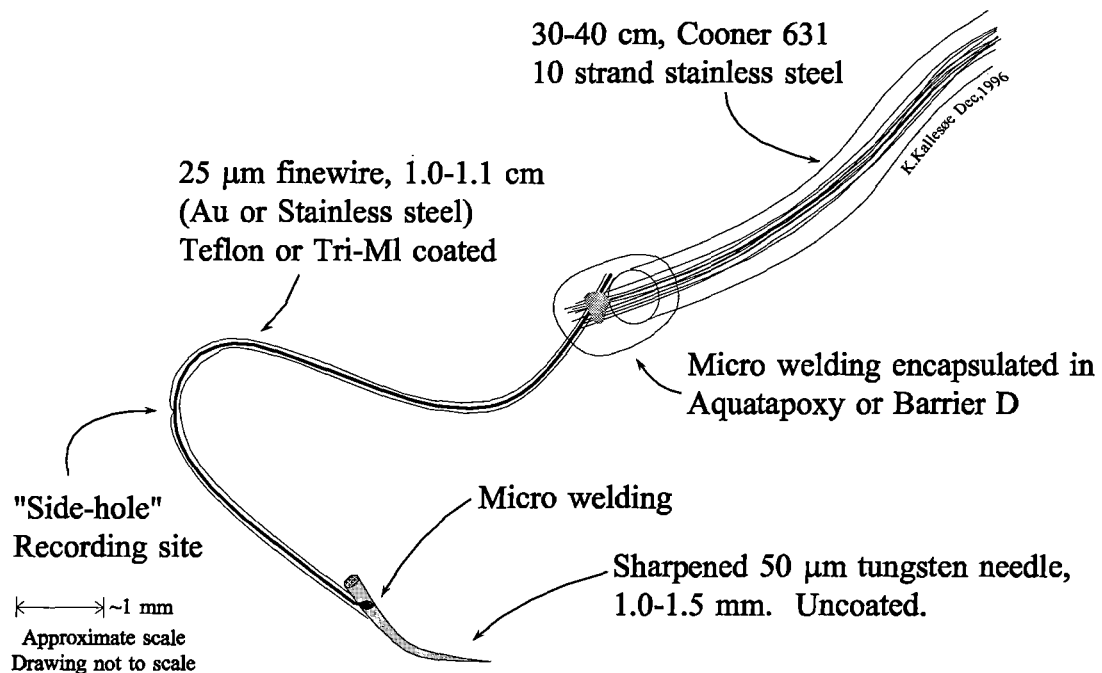


Figure V.4: The revised fine wire design. Similar assembly as described in Figure V.3. A 1.0-1.5 mm tungsten needle was micro-welded to the end of a fine wire. The needle was uncoated and served only to thread the fine wire through connective/neural tissue. The needle was removed after the fine wire was installed. The conductor of the fine wire was either exposed at the tip, by cutting of the needle, or through a single "side hole" made 5-10 mm from the cut end. The later exposure was made with a high voltage spark.

A similar intraneural recording electrode was designed by Horch and coworkers (Lefurge et al. 1991, Goodall et al. 1991, Goodall and Horch 1993, Mirfakhraei and Horch 1994, Yoshida and Horch 1996). The latter electrode did not have a "side hole", but rather a fairly large exposure of the conductor along a  $\sim 1$  mm section of the fine wire. This lowered the electrical impedance of the electrode significantly, and changed the nature of the recorded signal from a single unit to a multiunit recording.

### Results of 1<sup>st</sup> and 2<sup>nd</sup> series of implants

The studies with hatpin and fine wire electrodes were initially divided into two experimental series, all including most of the general setup described in Chapter II. The 1<sup>st</sup> series used hatpins, with a total of 80 electrodes implanted in 9 hindlimbs. The 2<sup>nd</sup> series used a simpler fine wire electrode, with a total of 31 wires implanted in 4 hindlimbs. A 3<sup>rd</sup> series, used a different hatpin style electrode, based on the initial results from the first two series. This 3<sup>rd</sup> series is described later in the section *Hatpin micro-electrode based on commercial electrode tips*.

Exp.	ID	Duration [days]	Implants	Single unit recording notes	Microstimulation levels	
					lowest	no. of sites <20 $\mu$ A
1	D-Sep90	4	12 hatpins 35mm sciatic cuff	Nerve damage - ankle yield	2.5	10
	E-Nov90 (left)	22	12 hatpins 32mm sciatic cuff		4.8	0
	E-Dec90 (right)	12	8 hatpins 28mm sciatic cuff		-	0
	F-Feb91	78	8 hatpins 25mm sciatic cuff	3 sites recorded ( $\sim$ 15 $\mu$ V)	2.7	7
	G-Mar91	10	8 hatpins 26mm sciatic cuff	4 sites recorded ( $\sim$ 12-35 $\mu$ V)	1.0	5
	H-Apr91	15	8 hatpins 27mm sciatic cuff		60	0
	I-May91	10	8 hatpins 26mm sciatic cuff	Damaged by cyanoacrylate	9.4	4
	J-Jun91	43	8 hatpins 27mm sciatic cuff	8 sites recorded units (15-35 $\mu$ V)	2.9	8
	K-Jul91	25	8 hatpins 25mm sciatic cuff	7 sites audible activity, 1 recorded (40 $\mu$ V)	3.5	5
2	J-Oct91	40	8 fine wires 27mm sciatic cuff	2 sites recorded (15-20 $\mu$ V) up to 9 days	5.0	2
	Lab move					
	L-Jun92 (left)	195	8 fine wires 30.5mm sciatic cuff		-	0
	L-Dec92 (right)	35	7 fine wires	1 site recorded (15 $\mu$ V)	10.5	6
	M-Jan93	14	8 fine wires	Sciatic cuff slipped	8.0	4

Table V.1: Hatpin and fine wire experimental series (1 and 2).

*1<sup>st</sup> series: Hatpin implants.* Hatpin containing nerve cuffs typically included 8 electrodes (Table V.1), out of which 7 or all 8 were successfully implanted in the nerve. The 8 hatpins installed in the cuff were selected from a manufactured batch of typically 16-20 hatpins, all of which were soak tested in saline. This test included submersion of the electrode in saline from 2-3 days up to 2-3 weeks. Electric impedance was measured periodically to verify the integrity of the electrode insulation. A drop in the impedance would be indicative of a leakage in the assembly, and the electrode would either be repaired, or discarded.

The surgical manipulations to install the cuff around the nerve and the manipulations of individual electrode would occasionally cause breakage of an electrode. The remaining electrodes were inserted intraneurally, and their proximity to efferent axons was determined by micro stimulation (see Chapter II for surgical installation and recording procedures). At the time of implant, excellent low microstimulation levels (less than 20  $\mu$ A) were found in 39

electrodes. These low levels tended to rise somewhat by the end of the surgery (~2 h). However, the initial post-surgical stimulation, again performed under anesthesia, for a typical cuff would yield 2-3 electrodes at less than 20  $\mu\text{A}$ . When recording from these electrodes, they would also show low amplitude afferent signals (less than 15-20  $\mu\text{V}_{\text{PP}}$ ) when stretching the MG muscle and loading its tendon. Occasionally, a single recording could be made from a 35-40  $\mu\text{V}_{\text{PP}}$  unit.

When awake recordings were performed on the first, or second day after the surgery, the majority of the electrodes typically showed near background noise activity (10-15  $\mu\text{V}_{\text{PP}}$ ) and no correlation with any movement of the implanted limb. Of the 1<sup>st</sup> series implants, only 16 electrodes were capable of recording activity, that could be classified as neural in origin (see Chapter II for classification procedures). The signals from these were marginal in amplitude (less than 20  $\mu\text{V}_{\text{PP}}$ ) and no reliable spike train could be recorded. The signals remained detectable for a maximum of 2-3 days after implantation, which is barely enough time for the cat to recover.

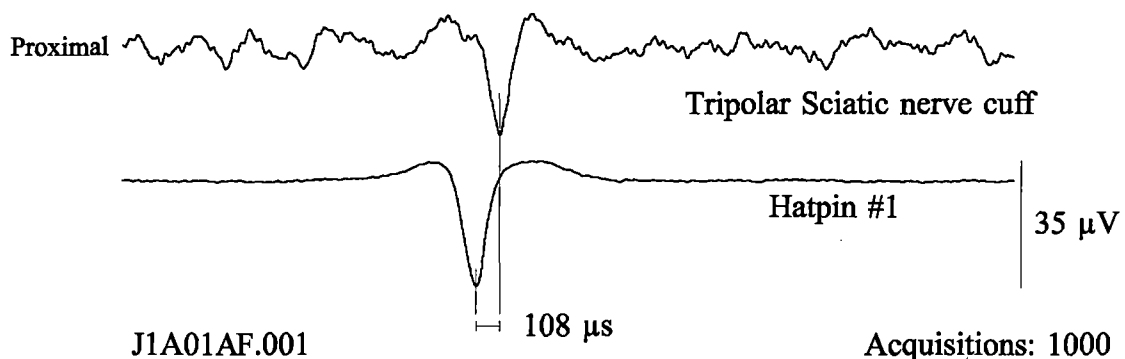


Figure V.5: An example of a spike triggered average of a 1<sup>st</sup> series implant hatpin. Top trace is from the tripolar sciatic nerve cuff. The bottom trace is a single unit record, defined in shape by the filter settings of a dual window discriminator. The filtered unit signal provided the trigger for averaging of the sciatic nerve cuff signal. The fact, that a peak was present in this top trace indicates a filter setting selecting a neural signal. The later occurrence of the sciatic peak indicates, that an afferent fiber was responsible for the single unit signal. Background noise was canceled by averaging if it was uncorrelated with the single unit signal.

*2<sup>nd</sup> series: Fine wire implant.* The assembly of the fine wire nerve cuffs was identical to hatpin nerve cuffs, except of course for the installation of 8 fine wires instead of hatpins. As in the manufacturing of hatpins, an overproduction of fine wires was necessary to insure a selection of high quality electrodes. However, due to the simpler design of the fine wire, on

average only 10-12 electrodes were assembled for every 8 fine wires installed in the nerve cuff.

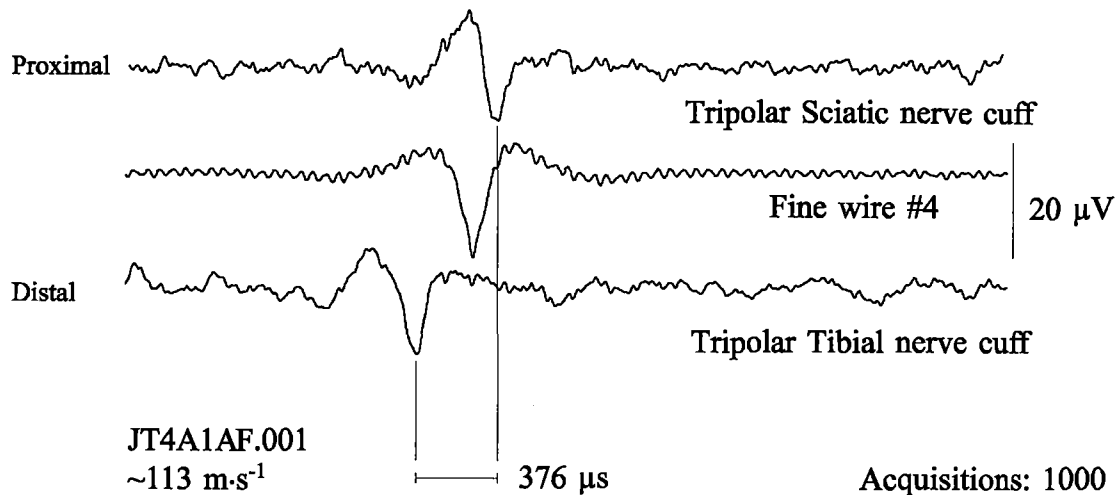


Figure V.6: Spike triggered averaging of 2<sup>nd</sup> series implant. The conduction direction and velocity was determined by the combined recording of ENG activity in the fine wire electrode (middle trace), the tibial nerve cuff (bottom trace) and the sciatic nerve cuff (top trace). Based on the propagation time and direction, this unit was classified as group Ia or Ib afferent.

The minimum microstimulation levels required to recruit motor units at the time of implant were typically very low (less than 5  $\mu\text{A}$ ) in 3-5 electrodes, with the remaining electrodes showing acceptable levels (less than 20  $\mu\text{A}$ ). From this 2<sup>nd</sup> series of implants, one unit was detected at maximum amplitude of 40  $\mu\text{V}_{\text{PP}}$ , making it distinguishable from the background noise, but still not producing a reliable spike train. The period for which this unit was detectable was limited to less than 72 hours post surgical.

### Discussion of 1<sup>st</sup> and 2<sup>nd</sup> series of implants

*1<sup>st</sup> series: Hatpin implant.* Several technical failure modes were identified in the hatpin design, all of which manifested themselves by the failure in establishing stable intraneural interfaces.

Electrical failures occurred when the integrity of the electrode insulation was disrupted. Insulation damage could be caused by manipulations during the implantation, by the actual insertion or by inherent properties of the insulation material. The latter was seen in uneven coats of Kynar epoxy or in the porous heat-shrinkable Teflon. All types of leakage decreased

the impedance of the electrode assembly, effectively shunting the recorded signal. This was assumed to occur over time in a majority of all the hatpin implants.

Mechanical failure occasionally occurred if handling procedures caused a break in the fine wire and created a permanent or intermittent loss of the electrical connection. Mechanical breakage was detected by an increase in the impedance of the electrode assembly. Mechanical failure may also have happened on a macroscopic scale (mm - cm) if the complete wire assembly, cuff included, was pulled. This was the case, when there was too small a strain relief loop between the cuff assembly and the external backpack connector.

Physiological failure modes were likely caused by movement of the hatpin. Tissue reaction was expected to happen on a microscopic scale (less than 1  $\mu\text{m}$ ) and cause a buildup of connective tissue between the recording surface and the neural tissue. This forced the electrode and axons apart, degrading the quality of the recorded signal.

Regardless of whether a failure was caused by microscopic or macroscopic movements, dislocation of the electrode tip from the intraneural compartment would not be detectable by changes in assembly impedance but by an inability to record and stimulate.

*2<sup>nd</sup> series: Fine wire implant.* A possible electrical failure mode was identified in the insulation of the fine wire. The integrity of the wire insulation may have been compromised by prolonged storage (5-10 years), of the raw wire materials used. The breakdown may have been accelerated by the manipulation and insertion procedures. The compliant fine wire electrode bends more easily than the stiffer tungsten used in hatpins, and is thus more likely to be exposed to excessive bending. This could create cracks in the insulation, decreasing the electrode assembly impedance, as was observed over time in a majority of fine wire electrodes.

As described above, a possible mechanical failure mode was too little cable slack between the cuff and the backpack. This was unintentionally created by routing the exiting subcutaneous Cooner wires along the shortest possible route from the nerve cuff to the backpack location. When the cat flexed its spine the sciatic cuff was likely to slide up along the sciatic nerve. In an attempt to prevent such movement of the cuff, up to four 8-0 stitches were used to attach the sciatic cuff to the epineurium. Furthermore, once the potential problem of too little slack had been identified, routing of the cuff leadout wires was changed to a distal direction. This

provided an additional strain relief loop. The indirect routing pathway was adopted in the later half of all implants. It minimized not only the mechanical load on the cuff, but also increased the electrical load of the axons by adding about 50% more cable resistance and capacitance.

As with the hatpin implants, mechanical failure occurred when the electrode tip was dislocated from the intraneural compartment. This was characterized by an inability to record and stimulate axons, with little or no change in assembly impedance.

A new physiological failure mode was potentially created by the implantation technique use for the some of the fine wire electrodes. Given the flexibility and sharpness of the fine wires, these were typically not able to penetrate the epineurium. To facilitate the penetration, an alternate insertion approach was adopted, using an electrode "starter". This consisted basically of a long (~5 cm) sharpened tungsten needle, mounted on a glass handle. The needle was used to nick a pilot hole in the epineurium and possibly the perineurium. This allowed the fine wire electrode to "slip" in far more easily, than having to penetrate these connective tissue layers on its own. However, with this approach there was a danger of nicking a hole too large. This potentially created herniation where axons could be squeezed out through the epineurium.

*Needle threaded fine wire electrode:* It was speculated, that passing a relatively large needle through the neural tissue was likely to cause damage to the very axon of interest. This was the argument for discontinuing the use of the needle threaded electrode.

*Recording results:*

The longevity of recordings in the 1<sup>st</sup> and 2<sup>nd</sup> series of hatpin and fine wire experiments were unexpectedly short. Although initial low levels of micro stimulation were obtained, electrical characteristics over the long term (weeks) were generally unsatisfactory. The use of simpler fine wire electrode improved the electrical characteristics, but the tip remained difficult to insert through the epineurium. Both the hatpin and the fine wire style electrode types were designed with smooth surfaces, and the mechanical stabilization of these therefore required special attention. Since the MG fascicle runs fairly superficially along the surface of the sciatic nerve, any stimulating electrode tip only needed to penetrate a fraction of a millimeter, to be able to excite an individual axon. With such a small mechanical attachment area, the electrodes were very likely to be dislocated during limb movements. Such dislocation would

explain the lack of recording from the electrode that maintained acceptable electrical characteristics but remained "silent".

*Attempted improvements:*

The technologically simplest anchoring solution would be to rely on connective tissue adhering to both the electrodes and the peripheral nerve. During the initial weeks post surgery, connective tissue typically forms a dense matrix around all implanted devices. This time frame, however, far exceeds the time period for which the limb can be immobilized to prevent movement of the implants.

Alternative mechanical anchoring methods were attempted to improve the mechanical stability of the electrodes. The anchoring surface was increased by weaving the electrode tips through neighboring epineurial tissue. This complicated the surgical insertion procedures and increased the requirements of carefully planning the routing of the fine gold wires. Other anchoring techniques had been tested for electromyographic single unit recordings, where the electrodes were designed with barbs along the tip section (Cooke et al. 1990). With the manufacturing techniques available for this thesis work, it was not found feasible to incorporate similar barbs on the smaller hatpin or fine wire electrodes.

A chemical anchoring approach to fix the location of the electrodes was attempted by adhering these to the epineurium at the time of surgery. This was done with quickly curing medical adhesives, like cyanoacrylate. A drop of this instantaneously "froze" all structures on the surface of the nerve within the reach of the glue drop. Although the desired effect of fixing the location of all electrodes was obtained, two new possible failure modes arose.

First, the electrodes were no longer floating in the nerve. They were attached to the glue and if this lifted from the nerve, so did all of the electrodes. In a similar way, if the underlying structure (individual fascicles) of the nerve moved, some or all of the electrodes were likely to be dislocated from their original target axons. Neither was desirable when attempting to maintain stable recording conditions.

A second argument against the use of cyanoacrylate, was found in visual postmortem observations of re-vascularization. Neural tissue covered by the cyanoacrylate appeared pale

white, without the normal fine vessel innervation. By visual inspection, it was found that the re-growth of vessels took place exclusively in the neighboring non-glued tissue.

### **Hatpin micro-electrode based on commercial electrode tips**

Based on the complications described above, an alternative implantation technique and electrode design were conceived. The electrical characteristics of the hatpin were improved by using commercially available microelectrodes (Microprobe Inc.), to replace the needle tip of hatpin electrode. The anchoring problem was addressed by inserting the new hatpin electrode through a thin walled cuff, into the MG branch. The cuff wall thereby provided the mechanical stabilization of the electrode.

*New Hatpin Tip:* The tungsten tip of the traditional hatpin electrode was replaced by the tip section of a long shafted single unit electrode, designed for acute interfacing to the CNS. These electrodes were available in Platinum-Iridium (20%) or tungsten versions, both coated with 3  $\mu\text{m}$  Parylene-C to insulate the conducting metal. The insulation material on the tip was removed by the vendor using an electric arc or laser. This allowed a fine control of the electrode tip impedance, according to custom specifications. The amount of material removed depended on the electro-chemical characteristics of the underlying metal and on the desired electrode impedance. For the Pt-Ir electrode, 55  $\mu\text{m}$  was exposed to give a tip impedance of 200 k-300 k  $\Omega$  at 1 kHz. Due to the capacitive properties of the tungsten based tips, these required up to 75  $\mu\text{m}$  of Parylene-C to be removed to yield the same electrical characteristics.

The tungsten tip was attached directly to the Cooner lead out cable (Figure V.7). Otherwise, remaining assembly of the hatpin was similar to that of the traditional hatpin design.



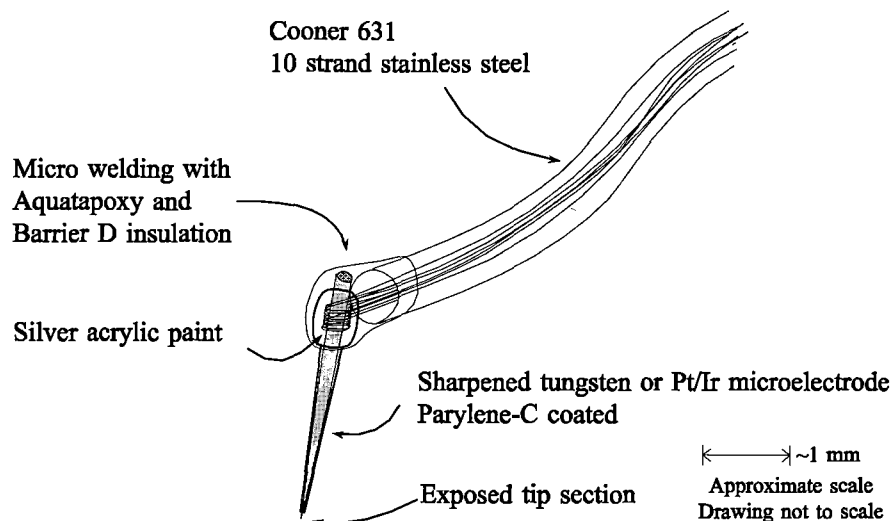


Figure V.7: New hatpin design. Stainless steel strands of a quadruple Teflon coated 631 Cooner wire were micro-welded to a commercially available tungsten or platinum-iridium electrode tip (PI200355A, WE300375A, WE300350A and WE300370 A from Micro Probe Inc., Maryland). The manufacturer precoated the tip with Parylene-C and removed a limited area of this insulation from the tip section. The electrode tip impedance was 200 k-300 k  $\Omega$  (at 1 kHz). The electrical connection between Cooner wire and tungsten/platinum-iridium was established with silver based conductive epoxy. This junction was insulated with Aquatapoxy and Barrier D. Failures occurred, if the insulation of the assembly was compromised.

*New Microelectrode Cuff:* Two new cuff designs were introduced to improve on the hatpin anchoring technique. Both were based on the hatpin penetrating a cuff wall, instead of being inserted through a window. This stabilized the electrode location with respect to the nerve cuff.

The first cuff design was a double compartment cuff, with one silicone tube for the tibial nerve and an additional tube for the MG branch (Figure V.8). Isolating the MG fascicle in a separate compartment ensured that hatpin electrodes were inserted into that particular branch. To limit the stress on the branch, care was taken to recess the MG compartment of the cuff into the main tibial compartment. Unfortunately, it also increased the complexity of the surgical installation procedure. The cuff was installed fairly distal, close to the MG nerve entry point (~5-10 mm).

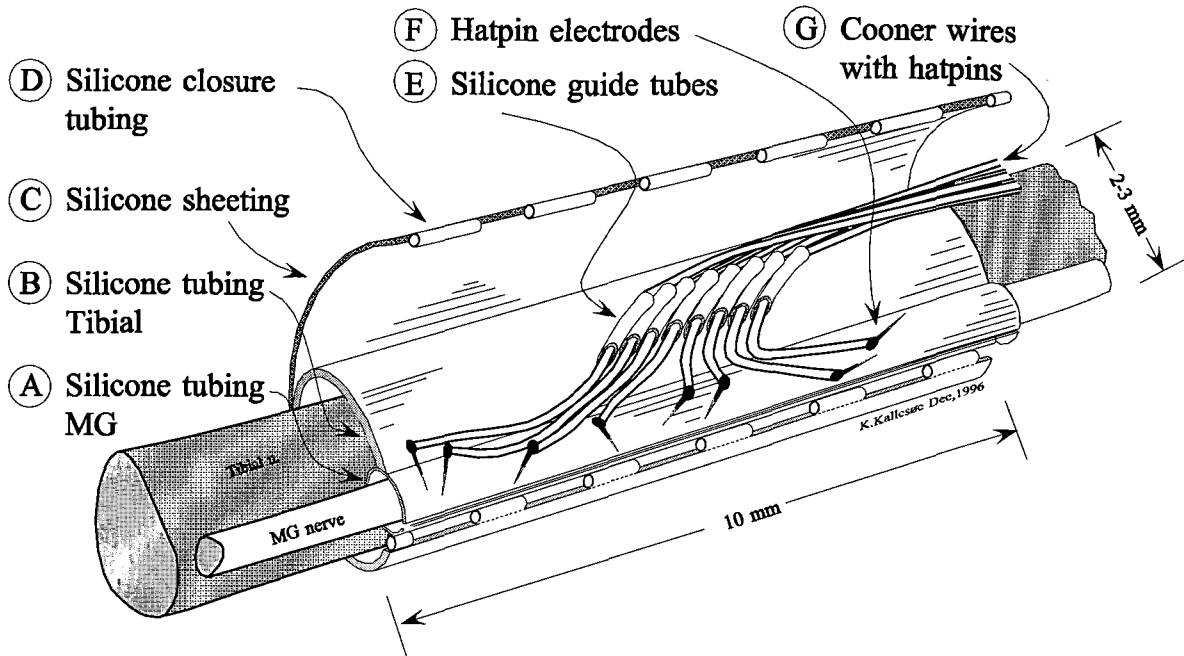


Figure V.8: A double compartment tibial cuff. The MG fascicle was placed in a separate cuff (A) (Dow Corning 602-235, ID:1.5 mm, OD:2.0 mm), recessed into the wall of the main tibial cuff (B) (Dow Corning 601-335, ID:3.4 mm, OD:4.6 mm). An array of 8 silicone guide tubes (E) (Dow Corning 602-105, ID:0.3 mm, D:0.6 mm) were attached to the external surface of the tibial cuff, allowing the lead-out wires (G) (Cooner 631) of the hatpin electrodes (F) to be secured to the cuff. The hatpin electrodes were inserted into the MG fascicle, through the silicone cuff wall (A). To prevent dislocation of the electrodes, silicone sheeting (C) (Dow Corning Silastic Q7-4840 Medical grade, thickness: 0.13 mm) was wrapped around the hatpins and locked to the main tibial cuff with silicone locking tubes (D) (Dow Corning 602-105, ID:0.3 mm, D:0.6 mm).

Hatpin electrodes were attached to the outside of the main compartment, orienting the tip section towards the MG compartment. The electrodes were inserted through the cuff wall, and thin silastic sheeting was used to close and lock both cuffs. This prevented the inserted hatpins from slipping out.

In a second cuff design, the MG fascicle was left intact with the whole nerve in a single compartment cuff. Again, the thin wall silicone sheeting allowed hatpin electrodes to be inserted through the wall and mechanically anchored to the cuff. A new feature of the cuff was a perforation pattern covering the majority of the cuff wall surface, allowing connective tissue to grow through the wall, fixing the cuff to the nerve.

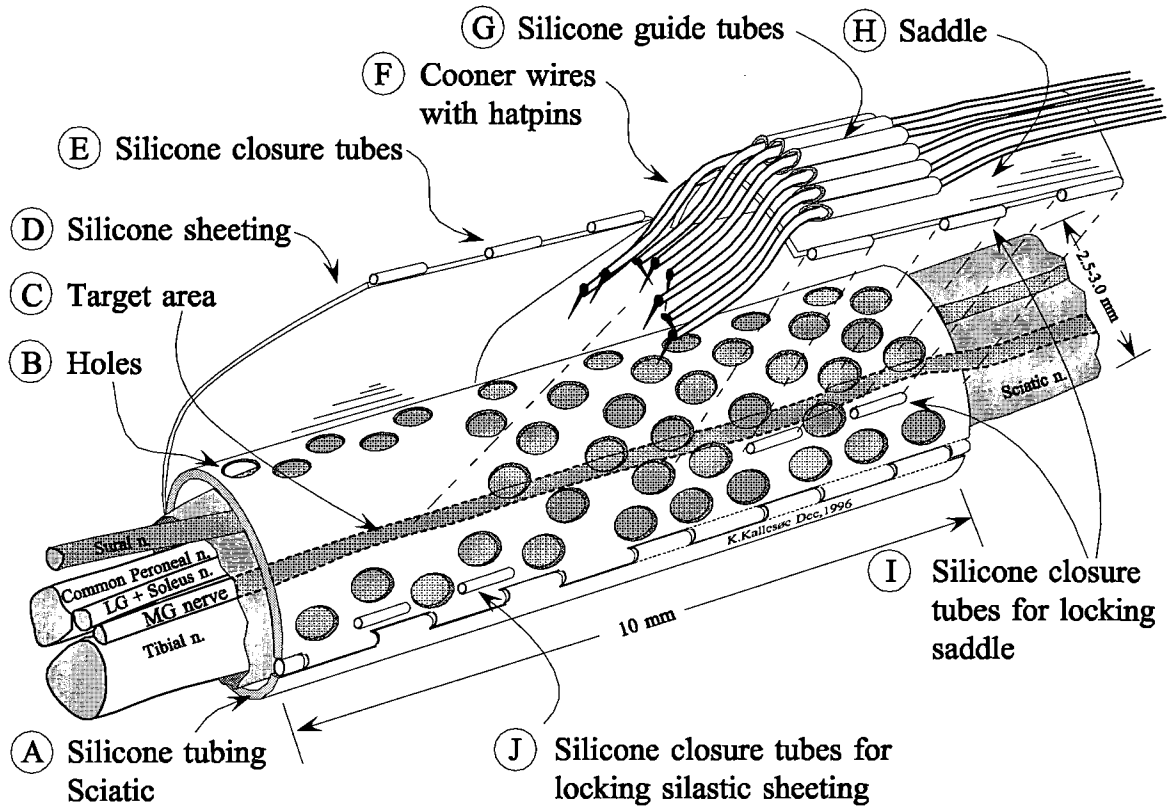


Figure V.9: Thin wall sciatic cuff (A) (Dow Corning Silastic Q7-4840 Medical grade, thickness: 0.13mm), with silicone sheathing saddle (H) attachment for the hatpin electrodes (F). Holes (B) were pre-punched out of thin sheathing cuff wall prior to implantation, to facilitate tissue adhesion. The hatpin electrodes were attached to the saddle through silicone guide tubes (E) (Dow Corning 602-105, ID:0.3 mm, OD:0.6 mm). The main cuff without the saddle, was implanted approximately 1 week prior to the implantation of the saddle and the hatpin electrodes. The saddle was attached to the cuff by interdigitated locking tubes (G) (Dow Corning 602-105, ID:0.3 mm, OD:0.6 mm). The hatpins were inserted through the cuff wall in a target area (C) above the MG fascicle. After the initial surgery, this target area was kept free of connective tissue growth by silicone sheathing (D). After insertion of the hatpins, this sheathing was used as a protective cover over the electrodes, preventing dislocation from the MG fascicle. The silicone sheathing was locked in place with interdigitated tubes (I) on the external surface of the main cuff. (Figure modified from Pugh 1996.)

To allow this fixation to take place, the cuff was implanted in a first surgical session, with a second session a week later for implantation of the hatpin electrodes. These were glued to a "saddle", attached to the main cuff. Hatpin tips were inserted through a non perforated target section of the main cuff, located above the MG fascicle. Thin silicone sheathing was used to tightly cover the hatpins, preventing dislocation from their insertion points.

The cuff was tested at a more proximal location than the first cuff design. The second design was implanted around the sciatic nerve, as described in Chapter II).

The development of the new micro electrode cuff was done in close collaboration with Simon Fraser University, Kinesiology honors student Jeff A. Pugh, who presented these developments in part in his thesis (Pugh 1996).

### Results of 3<sup>rd</sup> series of implants

*3<sup>rd</sup> series: New hatpin implant.* The new hatpin design was used in 4 chronic experiments, with a total of 32 hatpins implanted. They were found to be less fragile during surgical maneuvers, due to their more robust design compared to the traditional hatpins. The tips were found adequately sharp for penetration of the thin cuff wall. It was feasible to install the cuffs, although the silastic sheeting securing the hatpins was found hard to close. Once installed, it was very efficient in ensuring that the hatpins remained inserted in the cuff. At postmortem, all hatpins were confirmed to have remained inserted in the cuff.

Exp.	ID	Duration [days]	Implants	Single unit recording notes	Microstimulation levels	
					lowest	no. of sites ≤20 μA
3	T-Jul95	0	8 hatpins	Electrode failure. Low impedance	14.0	2
	C-Oct95	14	8 hatpins 6 tungsten, 2 Pt/Ir		1.0	1
	S-Nov95	92	8 hatpins tungsten	4 sites recorded (12-46μV)	0.7	5
	B-Jan96	50	8 hatpins	1 hatpin broke 1 site recorded	49.0	0

Table V.2: Hatpin experiments using commercial tip electrodes.

The electrode impedances were documented by Pugh (1996) as more stable than previous hatpins and fine wire electrodes. Although some initial fabrication changes were necessary, the majority of the electrodes had stable impedances above 100 k Ω for the initial 2 weeks after implantation.

As in previous single unit implants, very low micro stimulation levels (less than 5 μ A) were required at the time of implant in most implants. Unfortunately these increased consistently within the initial 24 hours post surgery.

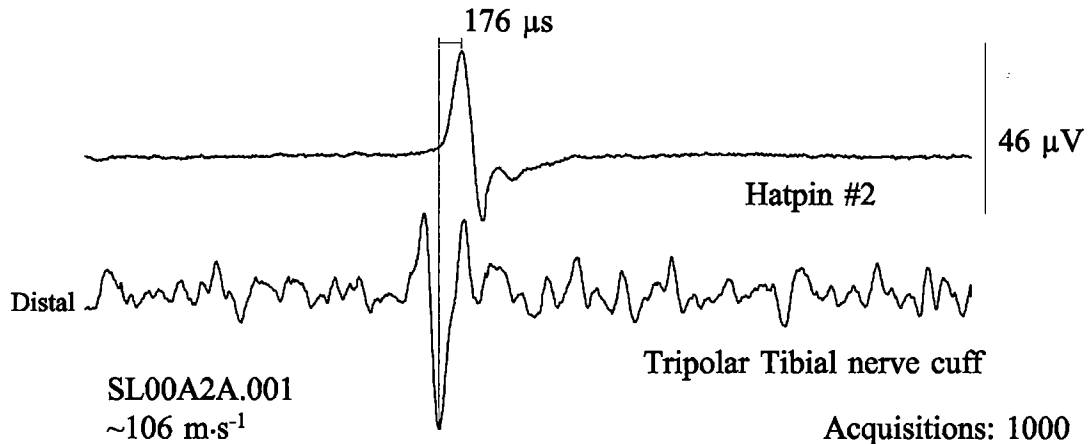


Figure V.10: Spike triggered averaging from the new hatpin style. The unit was classified as group I afferent, with a conduction velocity of 106 m·s<sup>-1</sup>.

The majority of the electrodes had no detectable signals beyond the background noise level. In 5 active electrodes, initial recordings (less than 12 hours) had neural activity very similar to recordings obtained with previous hatpin and fine wire designs. Again the longevity was very short (less than 24 hours).

### Discussion of 3<sup>rd</sup> series of implants

The stable impedance of the electrodes indicates that the integrity of the insulation was preserved. The mechanical design of the sciatic cuff ensured that the electrodes remained inserted in the cuff wall as confirmed in postmortem recordings. The question is then, whether the electrode tips remained inside the nerve, and in stable proximity to specific axons?

The increased stability of the tip impedance and more secure location of the electrodes eliminated two major technical failure modes of previous hatpin and fine wire electrodes - 1) the microscopic movement of the electrode and - 2) the possible deterioration of the electrical insulation.

The lack of recordings of neural activity could possibly be explained by local nerve damage. This was most likely to happen during surgical installation procedures of the double compartment tibial cuff (Figure V.8). This required an epineuriotomy of the MG fascicle and the tibial nerve, possibly compromising blood flow in minor vessels. As a result, the thin walled sciatic cuff was developed (Figure V.9).

In this design another possible physiological failure mode was identified. Even though the cuff was well adhered to the epineurium of the sciatic nerve, intraneural movements were observed. This became apparent when the Felix Fontana striation of individual fascicles was visually observed to slide back and forth inside the epineurium. (The Felix Fontana striations are visually apparent spiral bands seen in peripheral nerve fascicles. The bands alternate in appearance between light and dark and are approximately 1-2 mm long. They are caused by a wave-like arrangement of individual nerve fibers within the fascicle. The purpose of the arrangement is assumed to be mechanical protection against stretch injuries of the nerve.

Observations of sliding fascicles confirmed documented findings of intrafascicular movements (Millesi et al. 1995, Zachary 1993), and it made it quite apparent that an electrode fixed rigidly to the epineurium could potentially cause severe axonal damage to individually moving fascicles. Although no functional deficit was observed, local damage to individual axons could still have been present around the electrode tips. The only way to confirm that, would be in a histology analysis.

Another potential source of nerve damage could have been introduced through contamination of the Parylene-C coating (Agnew and McCreery 1990). However, this would most likely not cause such a lack of recordings as seen in the present experiments. Furthermore, other research groups have shown Parylene-C to be nontoxic in the cerebral cortex (Schmidt 1983).

### **Discussion of fine wire or hatpin single unit electrode**

A large number of fine-wire and hatpin electrodes (102) were implanted, with refinement of electrode designs and implantation techniques taking place throughout this series of the experiments. A common outcome of the implants was a very short lived interface with individual motor units, and in a limited number of cases, also afferent units. The goal of establishing a peripheral nerve interface was achieved for a few electrodes (16), but not for extended periods of time (less than 72 hours). The lack of stability of these interfaces prevented their use for neuromuscular research of proprioceptive feedback in behaving animals.

As described in the *Discussion of 1st and 2nd series of implants*, several failure modes were identified. Electrical failure modes were corrected in the new hatpin design (3<sup>rd</sup> series), but

new physiological failure modes were hypothesized. These failure modes can be summarized as excessive necrosis around the electrodes, interrupting contact between active neural tissue and the electrode interface site. The necrosis was most likely caused by a mechanical movement of the electrode, possibly transecting axons.

#### *Future directions*

In further revisions of the design of peripheral single unit electrodes several issues should be addressed:

1. From the experience of using rigidly attached hatpins (3<sup>rd</sup> series), it has become apparent, that it is crucial to have the micro-electrodes float with the axons. The appropriate next step is therefore to develop a floating micro-electrode with stable electrical characteristics. This electrode will need a special anchoring system, to allow it to maintain a stable location inside the nerve.
2. The fine wire and the hatpin were both manufactured manually. This increased the variability in the quality of the electrode production.
3. Both the fine wire design and the hatpin design exhibit a severe limitation in transmitting only one channel of information. A multiple site configuration would open the possibility of interfacing to a population of axons (BeMent et al. 1986, Veltink et al. 1989a), but would also introduce new technical difficulties. The choice of leadout wires is more critical, since the stiffness of the mechanical coupling between the probe and the external wiring is increased.

These problems are addressed further in the following chapter on electrode designs based on silicon. Silicon material and its manufacturing techniques offer the opportunity to micro-machine an electrode with very light lead-out cables, self-anchoring properties, multiple interface sites, and automated manufacturing.

## VI. SILICON BASED SINGLE UNIT ELECTRODE

It is feasible to implant fine wires in peripheral nerve and record and stimulate activity in a single axon. However, as discussed in the previous chapter, the electrode manufacturing is tedious and susceptible to variability and breakdown. In addition, the fine wire microelectrodes are restricted to providing only one channel of information per fine wire/hatpin. In neural prostheses applications, such as natural sensory feedback for FES control of limb movement, it is desirable to record neural activity from populations of natural sensors, rather than from just a single or a few sensors. Using the fine wire or hatpin technology, it is thus an undesirable necessity to implant multiple electrodes to interface to a population of neurons. This limitation has been addressed in the redesigning of a neural interface.

The replacement of the fine wire and hatpin electrodes, should meet the following general specifications:

- The interface should be robust and have reliable performance for a long time. Neural prostheses are intended to be used for years, preferably without the need for frequent calibration and other maintenance.
- Interfacing to a population of single units is a requirement for several prosthetic applications. Recordings from single axons are of interest to the field of basic neuroscience, whereas neural prostheses need a broader spectrum of information, to provide efficient motor control.
- The interface should exert minimal mechanical load on surrounding tissue. The size of the interface should, therefore, be close to that of a single axon. Any connecting cables should be flexible enough to allow the interface to float with the general movements of the neural tissue.
- Any surface material used on the interface should be biocompatible, and resistant to dissolution and corrosion. This is especially important at the electrochemical interface site. The surface material should exhibit chemical reversibility during electrical stimulation cycles, as seen when using activated iridium.



The development of such an interface array was addressed early on in designing CNS electrodes, using either silicon micromachining techniques (Wise and Star 1969), or other materials such as Teflon, Mylar or Parylene sheeting as a substrate carrier (CNS electrodes: Sonn and Feist 1974, PNS electrodes: Loeb et al. 1977). The development effort was aimed at producing electrodes with very small interface sites and mechanical properties suitable for insertion in the cortex.

The use of silicon based electrodes in the CNS has so far mainly been focused on the refinement of the recording techniques, especially the electrodes (BeMent et al. 1986, Campble et al. 1991). The requirements for these electrodes differ significantly from those of the PNS electrode, and consequently the finished electrodes appear quite different. This is especially true in the case, when interfacing to a large number of neurons distributed in a volume of tissue. Electrode arrays used in the visual cortex area are designed with multiple (~100) shanks simultaneously penetrating the cortex. These electrodes resemble a fakir's bed of nails (e.g. see scanning electron micrographs in Campble et al. 1991). Despite its unique appearance, the underlying process for the manufacturing of each of the shanks is the same as for the more common single shank electrode.

Several research groups (BeMent et al. 1986, Drake et al. 1988, Carter and Houk 1993) have reported successful short term (acute) cortical recordings, with single unit spikes of 150-675  $\mu\text{V}$  or 3-10 times the amplitude of the background noise. These recordings were done with high impedance sites (1.2 M-4 M  $\Omega$ ) with surface areas of 110-368  $\mu\text{m}^2$ . Long term CNS recordings over several weeks have also been reported with similar electrode designs (UMCISC 1991, Carter and Houk 1993).

For a number of reasons, silicon has been the material of choice for several new bio-electric neural prostheses transducers. First, silicon thin film production techniques offer the precision and resolution (less than 1-2  $\mu\text{m}$ ) required to position multiple interface sites (8-10) on a probe comparable in size to the diameter of individual axons (10-20  $\mu\text{m}$ ). Secondly, the micromachining techniques also allow for the manufacturing of probes with sharp and penetrating tip sections and flexible leadout cables. Thirdly, the techniques for embedding on-board active circuitry is readily available given the use of similar silicon substrates in low voltage integrated

circuitry (BeMent et al. 1986, Tanghe et al. 1990, Najafi and Wise 1990, Hoogerwerf and Wise 1994). In addition, the space required for such circuitry is fairly limited, allowing for inclusion of complex signal processing circuitry close to the signal source. Finally, thin film production techniques allow biocompatible materials, such as gold, platinum or activated iridium, to be deposited on the electrochemical interface.

A driving force in the development of silicon based electrodes has been the possibility of producing electrodes with multiple interface sites within a very small area. That made it possible to interface to a population of axons where the activity of networks of neurons can be studied simultaneously (BeMent et al. 1986, Veltink et al. 1989a). An increased number of interfaces does, however, introduce new technical challenges. It makes the choice of leadout cables more critical, since an increase in the number of conductors will increase the stiffness of the mechanical coupling between the electrode and the external wiring. Recently, this problem has been addressed by advances in micro machining techniques, that make it feasible to produce very thin (5  $\mu\text{m}$ ) and flexible silicon multichannel leadout cables (Hetke et al. 1994).

In summary, silicon based electrodes have several advantages compared to the fine wire and hatpin electrodes:

- High density of interface sites, allowing for simultaneous recordings from a population of axons.
- The use of biocompatible metals on the electrode sites, allowing for stable electrochemical interfaces.
- Well defined shape and stiffness of probe tip, allowing for controlled insertion and anchoring of the electrode.
- Well defined shape and size of electrode sites, allowing for control of recording and impedance properties.
- Well defined shape and flexibility of leadout cable, enabling the electrode to float relatively unrestricted by movements of the neural tissue.
- Automated manufacturing process, reducing the fabrication related variability.

- Future incorporation of active circuitry on the electrode, constituting an active compact neural interface, possibly including onboard data analysis, storage and telemetry transmission.

## **Objective**

The objective of designing a new peripheral single unit electrode was to improve on both mechanical and electrical characteristics of previously used hatpin and fine wire technology. A priority in this design was to implement multiple recording sites on a single electrode, including appropriate leadout cabling. The challenge was to appropriately scale the features of the design to suit the mechanical and electrical requirements of the peripheral nervous system.

## **Designing a silicon based electrode**

The silicon based electrode used in the present thesis was developed in collaboration with the Center for Neural Communication Technology (CNCT) at University of Michigan. The center has extensive experience in designing silicon probes for the CNS, to which our local expertise in designing and using fine wire and hatpin electrodes in the PNS was added. The designs were done using a computer aided design program, specialized for silicon micro machining and micro electronic design ("CADANCE"). The probes were manufactured at the University of Michigan and the final assembly was made at SFU. The assembly steps included the development of bonding techniques to allow for a compact implantable connection to stainless steel Cooner leadout cables.

As described elsewhere (Najafi et al. 1985, BeMent et al. 1986, Najafi et al. 1990, UMCISC 1991), a silicon probe consists of a silicon substrate, supporting an array of thin-film conductors. These are insulated above and below by dielectric layers of silicon oxide. Openings in the upper dielectric layers define interface sites between the probe and the neural tissue. The sites are inlaid with conductive noble metals to form biocompatible electrochemical interface sites with relatively low electrical impedances. The probe thickness varies in different regions from (5 -15  $\mu\text{m}$ ), depending on the required stiffness and flexibility.

The thin film layers used in a sandwiched fabrication technique were grouped in the following order, from the bottom:

1. A silicone substrate, that defined the mechanical shape and flexibility of the electrode. The shape of this substrate was determined by a *Deep* and a *Shallow diffusion* mask.
2. A *dielectric layer*, that insulated the interconnecting layers from the silicon substrate.
3. A *conductive layer*, defining interconnections between electrode sites and bonding areas.
4. A *dielectric layer*, that insulated the underlying conductive interconnections from surrounding tissue and fluids. Holes were cut out for exposure of conductive surface areas, that provide the electrochemical interface sites.

Each layer was defined by a thin film mask. The total silicon probe design thus consisted of a series of mask drawings, each determining various parameters of the final electrode assembly.

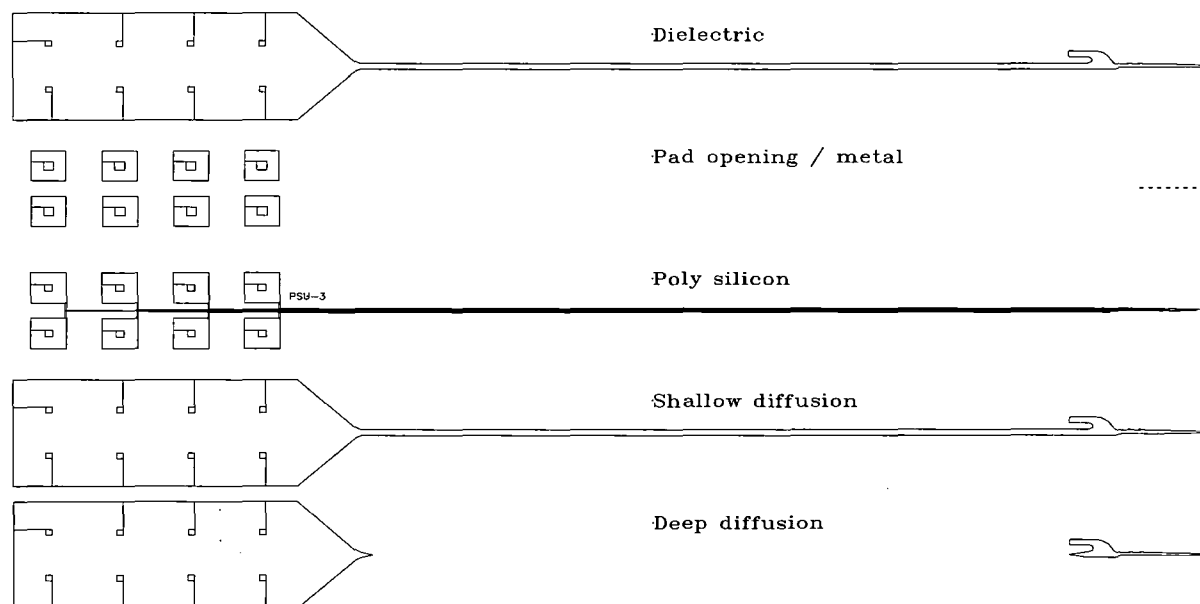


Figure VI.1: Thin film masks for a silicon probe design. Each defines a specific characteristic of the final sandwiched design (not shown). Some masks were used for several processing steps, assuring optimal alignment of the mask and substrate wafer. (See text for details on each mask.)

*Substrate formation / diffusion masks:* The basic shape of the probe was defined by doping a silicon wafer with boron in patterns defined by *diffusion masks*. Silicon that was not exposed to the boron, was later removed by an etch-stop technique EDP - ethylene diamine-pyrocatechol. This process is known to stop etching when the boron concentration in the silicon exceeds  $5 \cdot 10^{19} \text{ cm}^{-3}$  (Najafi 1985). The diffusion depth of the boron was determined by the duration of the exposure. A “deep” diffusion, penetrating  $15 \mu\text{m}$  into the silicon, required

15 hours of exposure at 1175°C. A more “shallow” diffusion to 2.5  $\mu\text{m}$  required only 30 minutes of exposure. Flexible sections of the probe were thus defined by a *shallow diffusion* mask, and more rigid structures by a *deep diffusion* mask.

*Dielectric mask:* The doped silicon wafer was conductive and a dielectric layer was necessary for electrical isolation of conductive traces. A dielectric layer was formed by a low-pressure chemical-vapor-deposition of silicon dioxide (400 nm), silicon nitride (200 nm), and silicon dioxide thin film (400 nm). The outline of this layer was defined by a *dielectric mask*, which was typically very similar to the deep diffusion mask. The dielectric mask was used both for defining a lower dielectric layer between the silicon wafer and conducting polysilicon traces, and for defining an upper dielectric layer on the surface of the conductive traces.

*Conductor / polysilicon mask:* Conductive polysilicon traces were deposited according to a *polysilicon mask*. A strict set of design rules defined the minimum distances from individual conductive traces to other conductors and to the edges of the probe design (typically ranging from 3 to 10  $\mu\text{m}$ ). For electrical isolation purposes, the polysilicon traces were formed on a lower dielectric layer (see above) and covered by an upper dielectric layer.

*Metal pad opening mask:* A *metal opening* mask defined areas where the upper dielectric film was opened, exposing the polysilicon traces. The polysilicon traces connected the individual electro-chemical interface sites with larger bonding pad areas. These were gold plated, to allow stainless steel Cooner wires to be attached with conductive epoxy. At the electro-chemical interface site, iridium was generally used as surface metal (150-300 nm). This noble metal adhered fairly poorly to most other materials and it was thus necessary to prime the polysilicon conductors with titanium (30-40 nm). Titanium, as a very reactive metal, adhered well to both silicon and iridium.

*Contact mask:* In the Fall of 1995, an additional mask was added to the complete silicon probe design. This mask was a *contact mask*, defining a layer of contact points between the surface metal and the polysilicon traces. It had been found by the Michigan group (CNCT) that the larger metal surface areas (larger than 3  $\mu\text{m}$  x 3  $\mu\text{m}$ ) had an increased likelihood of lifting off from the remaining probe structure. To minimize this risk, a contact layer was introduced,

requiring all larger metal surfaces to have an underlying patchwork of  $3\mu\text{m}$  squares, spaced  $3\mu\text{m}$  apart.

These six masks described above, defined the total design of a silicon based probe. Some of the masks were used several times, assuring the alignment of each process. With present manufacturing technology a production accuracy of  $1\mu\text{m}$  or better was achieved (Drake et al. 1988).

At the university of Michigan, a variety of recording and stimulation electrode designs are available. Designs are continuously modified and added to this collection, making it possible to specify and produce unique electrode designs. However, their typical 6 month turn-around time from design submission to final manufacturing, made it desirable to use designs already in production.

### Initial experiments with silicon based “Schmidt probe”

The majority of probes produced at the university of Michigan have been targeted for use as CNS interfaces. One of these was selected for interfacing to peripheral nerves - the “Schmidt probe” (Schmidt et al. 1993). This probe was designed with three main characteristics: a tip section with 6 iridium coated interface sites, a flexible ribbon cable, and a bonding platform, allowing for bonding of single stainless steel strands from Cooner 631 leadout wires.

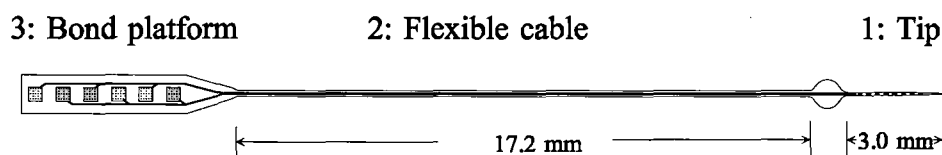


Figure VI.2: “Schmidt 2” probe layout. (1): A 3 mm tip section with 6 recording sites (not clearly visible at this magnification). Recording sites were  $13 \times 38\mu\text{m}$  large and spaced  $200\mu\text{m}$  apart. The tip section was  $50\mu\text{m}$  wide and  $15\mu\text{m}$  thick. A circular section at the proximal end of the tip served as forceps handling platform ( $550\mu\text{m}$  in diameter). (2): A flexible cable connected the tip section with a bonding platform. 6 conductive traces (not visible here) ran along the  $5\mu\text{m}$  thick flexible cable. (3): A  $15\mu\text{m}$  thick bonding platform with 6 gold sites facilitated the connection of gold or stainless steel wire. (Sketch modified from CNCT design catalog).

The “Schmidt” probes were used in initial test experiments, to fine-tune the dimensions of a new peripheral nervous system silicon probe. Although the quality of the supplied “Schmidt” probes was quite variable, attempts were made to verify the feasibility of establishing a silicon based neural interface to single axons in the peripheral nervous system.

*Approach:* The general setup, surgical procedures and recording procedures described in Chapter II were limited to the minimum instrumentation needed to confirm a functional interface. This included 1 or 2 nerve cuffs (sciatic and tibial), 3 or 4 EMG electrodes, a ground wire and finally 1 or 2 silicon probes. The implant location of the instrumentation was identical to the general setup (Figure VI.3)

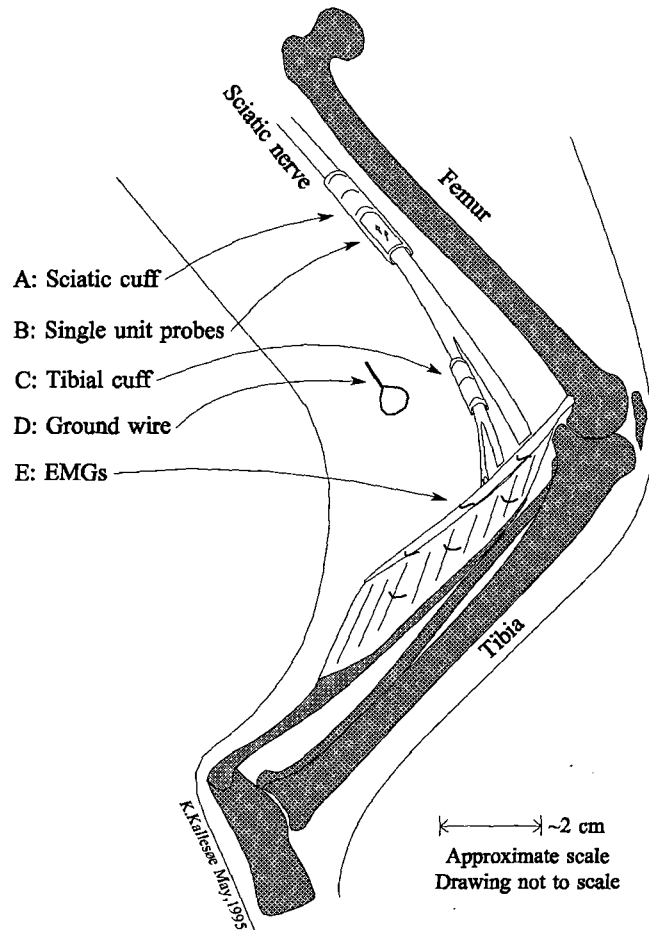


Figure VI.3: Minimal instrumentation of intact left cat hindlimb. (A): A 28-30 mm long nerve cuff encompassed the sciatic nerve. The cuff included a stainless steel shield to cover the single unit window. (B): 1-2 single unit intraneural silicon probes were implanted in the MG nerve inside the sciatic cuff window. (C): A 10 or 15 mm tibial nerve cuff was implanted distal to the bifurcation of sciatic nerve into its main branches. (D): A ground wire. (E): 3-4 sets of bipolar buried EMG electrodes implanted in the MG muscle.

A special implantation technique was adopted to facilitate tip penetration of the epineurium. A sharp tungsten needle preceded the silicon probe tip, effectively nicking a hole in the epi- and endoneurium. Once the needle was inserted, a gentle lift allowed the silicon probe to slide in behind. Once the probe was inserted, the tungsten needle was carefully removed.

This insertion procedure intuitively reduced the risk of probe breakage which had been high during pre-surgical penetration test.

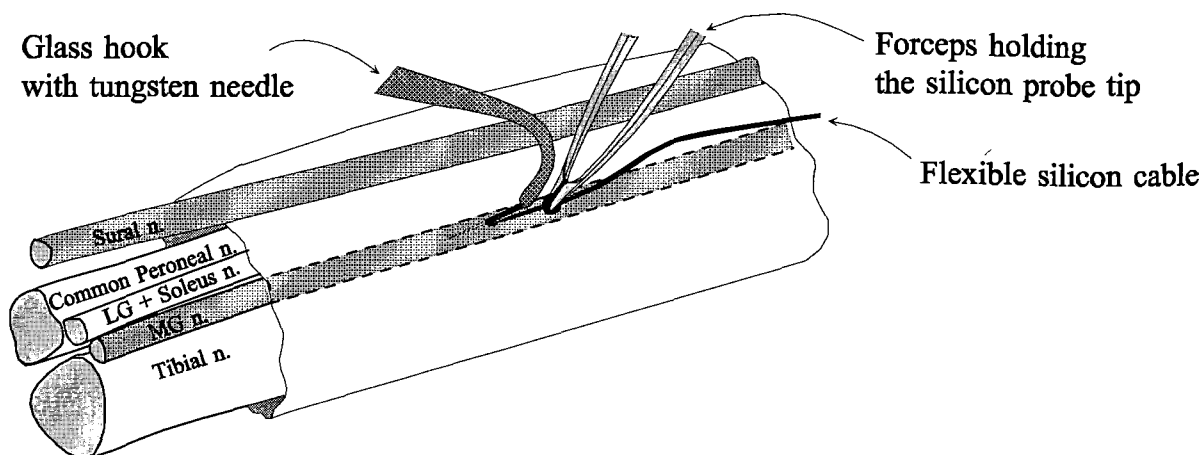


Figure VI.4: Surgical insertion technique. The probe was gently held with forceps while a sharpened tungsten needle mounted on a glass hook was used to penetrate the epineurium. The tip of the probe was inserted along the tungsten needle.

This insertion technique carried a risk of acutely damaging local axons. Long-term axonal damage was also possible if axons were constricted by a herniation through the open perineurial tissue.

*Results:* An acute implant showed promising low microstimulation levels. Two chronic implants were performed, bringing the total number of available interface sites to 24.

Exp.	ID	Duration [days]	Implants	Single unit recording notes	Microstimulation levels	
					lowest	no. of sites <20 $\mu$ A
4	U-Jun93	0	6 sites on one "Schmidt" probe	Acute experiment	2.5	4
	D-Jul93	22	6 sites on one "Schmidt" probe	2 sites recorded (10-15 $\mu$ V)	1.6	4
	C-Sep93	6	12 sites on two "Schmidt" probes	no recordings	2.3	9

Table VI.1: Initial silicon probe experiments using the "Schmidt" probes.

In one of the chronic implants, low amplitude neural activity was detected during the initial 36-48 hours. Although the signal to noise ratio of the signal was very low (1.1:1), not allowing for clear discrimination of unitary action potentials, it was possible to set a window



discriminator to accept one or more action potentials that rendered spike-triggered averages appropriate for Group I sensory afferents (Figure VI.5).

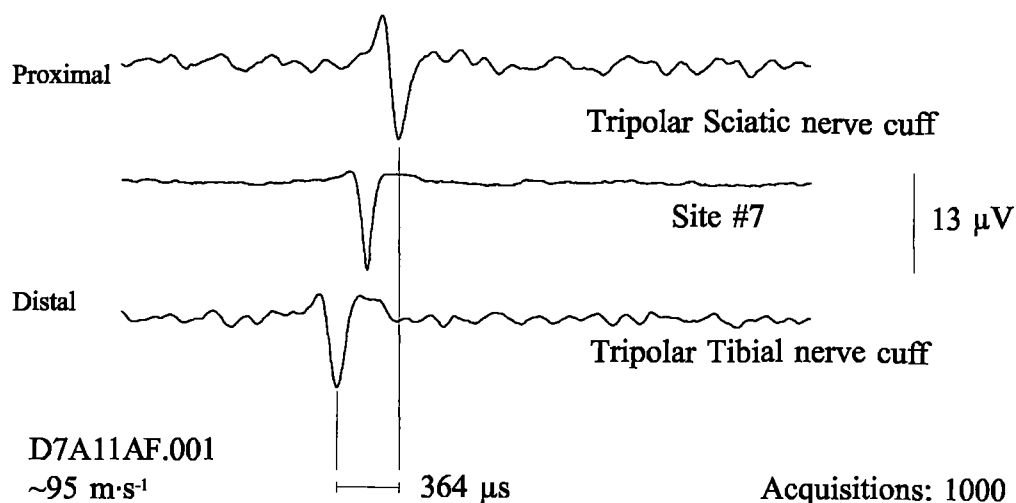


Figure VI.5: An example of a spike triggered average from a “Schmidt” probe implant. The top trace is from the tripolar sciatic nerve cuff, middle trace is from the single unit recording site (#7), and bottom trace is from the tripolar tibial cuff. The single unit wave form was defined in shape by the filter settings of a dual window discriminator. The filtered unit signal provided a trigger for averaging of the sciatic and the tibial nerve cuff signals. The fact that a peak is present in both of these traces, indicate that the filter was detecting a signal of neural origin. Given the later timing of the sciatic peak, and the earlier timing of the tibial peak, it was concluded that one or more afferent fiber(s) was/were responsible for the averaged signal. The conduction velocity ( $95 \text{ m}\cdot\text{s}^{-1}$ ) was from the distance between cuff recording electrodes (34.5 mm) and the time delay between main peak occurrences (364  $\mu\text{s}$ ).

*Conclusion:* The “Schmidt” probe was originally designed to establish an interface in the central nervous system and the dimensions of the probe were therefore *not* ideal for the purpose of peripheral recordings. It was difficult to adapt the relatively long (23.5 mm) “Schmidt” probe assemblies in the 25-28 mm sciatic nerve cuff. Furthermore, the probe length (3.0 mm) and the lack of a sharp penetrating tip increased the likelihood of breaking the tip.

Despite these obstacles, related to the probe’s size, 3 were successfully implanted. The poor neural activity recordings were attributed to several factors. First of all, it was unclear whether the tip section maintained a stable position inside the epineurium. Attempts were made to attach the flexible silicon cable to the epineurium with 8-0 sutures. Postmortem examinations were done to visually confirm the location of the probes. The accuracy of this estimation was very much affected by the intense growth of connective tissue inside and around the implants.

It could thus only be concluded that the electrode tips had remained intact and in the general vicinity of their original insertion location.

A second reason for the limited success in recordings of neural signals was attributed to defects in the surface material of the electrode sites of the silicon probe. Each recording site had a layer of iridium sputtered on the surface to create an electrochemical interface of either pure iridium or iridium oxide. The metal deposition technique used at CNCT prepared the silicon surface by etching the substrate thoroughly prior to the deposition. This procedure turned out to be flawed, causing poor adhesion of the iridium. This severely affected all production batches, manifesting itself in the lift-off of the iridium. The damaged sites exhibited poor electrical conduction, as well as inability to form iridium oxide. CNCT became aware of the problem, and identified the flawed procedures in mid 1994 (reported at the Neural Prosthesis Workshop, Bethesda Oct. 1994 and in NIH Progress report #9, Feb. 1995 (UMCISC 1995)).

### **1<sup>st</sup> Silicon design: PSU-0 probes**

The mechanical incompatibility between the "Schmidt" probes and the PNS implantation techniques encouraged the development of a new electrode design, specifically to interface to Peripheral Single Units (PSU). This was done in collaboration with CNCT and University of British Columbia engineering student Ignacio Valenzuela.

The general layout of the PSU-0 probe was similar to that of the "Schmidt" probe with three sections: 1) penetrating tip attached to a forceps handling platform, 2) flexible cable and 3) a bonding platform (Figure VI.6). The CAD layout of the design was made to 1 thousands of a  $\mu\text{m}$  accuracy and several new mechanical improvements were introduced:

- The shaft section of the tip was made shorter than in the "Schmidt" probe, to reduce the risk of breakage during the penetration of connective tissue. The interface sites were thus spaced closer together (44  $\mu\text{m}$  apart).
- The tip was made sharper by offsetting the deep and the shallow boron diffusion mask by 40  $\mu\text{m}$ . A sharp (5  $\mu\text{m}$ ) layer protruded from the thicker (15  $\mu\text{m}$ ) substrate.

- Miniature barbs were added at the root of the penetrating shaft. This was designed to stabilize the inserted probe by catching epi- or perineural tissue.
- The flexible cable was shortened to 10 mm to fit within the length of the sciatic cuff.
- Each bonding pad area was made larger ( $490\ \mu\text{m} \times 490\ \mu\text{m}$ ) to facilitate the connections to the 10 strands of a Cooner 631 stainless steel leadout cable. The "Schmidt" probes had been bonded to only one strand.

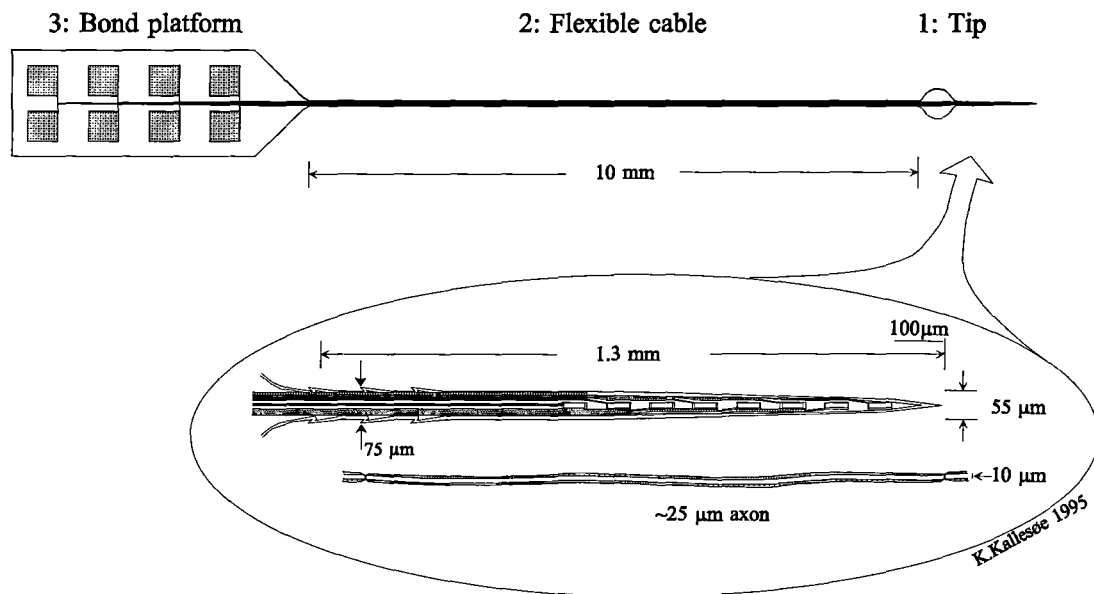


Figure VI.6: Layout of the Peripheral Single Unit design PSU-0. Section (1): A  $15\ \mu\text{m}$  thick tip section shaft supporting 8 iridium coated interface sites ( $10\ \mu\text{m} \times 44\ \mu\text{m}$ , spaced  $44\ \mu\text{m}$  apart). The maximum width of the shaft was  $56\ \mu\text{m}$ . At the proximal end of the shaft section, 3 barbs on each side facilitated anchoring to epineural tissue. The tip-section was connected to a flexible ribbon cable through a circular enlarged forceps-handling section. (In the insert: A portion of a large myelinated axon, including two nodes of Ranvier, is shown schematically for dimensional comparison). Section (2): A flexible  $5\ \mu\text{m}$  thick ribbon cable provide a compliant linkage between the tip section and bonding platform section. Section (3): A  $15\ \mu\text{m}$  thick bonding platform with 8 gold plated bond sites, allowed larger Cooner leadout wires to be connected to the probe.

*Results:* A total of eight PSU-0 probes were used in four chronic experiments. As with the "Schmidt" probe implants, the general setup was reduced. Two sets of tripolar circumneural electrodes within the sciatic and tibial cuffs, implanted above and below the intrafascicular electrodes, served to resolve the direction and velocity of conduction of each recorded axon using spike-triggered averaging (Figure VI.3).

Sequential recruitment of single motor units (SMUs) using intrafascicular microstimulation was monitored through intramuscular recording electrodes implanted in three regions of the MG muscle. Other procedures followed the general description in Chapter II: Experimental Design, Surgical Approach and Recording Procedures.

Exp.	ID	Duration [days]	Implants	Single unit recording notes	Microstimulation levels	
					lowest	no. of sites $\leq 20 \mu\text{A}$
5	B-Apr94	24	16 sites on two PSU-0 probes	1 probe broke during surgery; no recordings	-	0
	C-May94 (left)	255	16 sites on two PSU-0 probes	1 probe broke during surgery; no recordings	5.8	7
	C-June94 (right)	220	16 sites on two PSU-0 probes	no recordings	2.8	4
	R-Jul94	197	16 sites on two PSU-0 probes	8 sites recorded (5-20 $\mu\text{Vpp}$ )	20.0	1

Table VI.2: Silicon probe experiments using PSU-0 probes.

Two probes in the same implant (C-June 94) remained stable throughout the initial 72 hours. At the time of implant, the minimum current required to recruit the lowest-threshold motor units, using single biphasic charge-balanced stimuli, was as low as  $2.8 \mu\text{A}$ . This indicates that the electrode surfaces were in close proximity to efferent axons. Despite this encouraging result, recording neural activity remained impossible.

In a fourth PSU-0 implant (R-Jul94), unitary potentials were recorded from multiple sites during limb movements. These recordings provided a trigger for a spike-triggered averaging of the neural activity recorded from the tibial and sciatic nerve cuffs. The single unit signal was filtered with a dual window discriminator, defining the shape of accepted single unit potentials. By changing the single unit window discrimination settings, two simultaneously active muscle afferents could be detected in some interface sites (Figure VI.7). These multiple units would typically have different signal amplitudes, reflecting differences in axon size and in conduction pathways between site and axons. In a similar fashion, the same single axon could simultaneously be recorded from multiple sites (Figure VI.8).

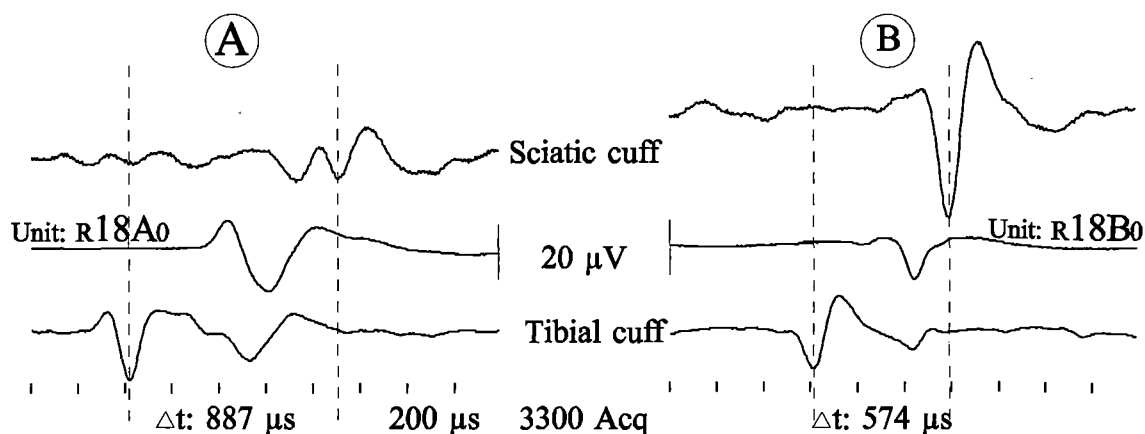


Figure VI.7: Spike-triggered averaging of two MG afferent neurons simultaneously recorded from electrode site #18. Note that although unit A (top) had a larger unitary potential ( $25.9 \mu\text{V}$ ) than unit B (bottom) ( $15.5 \mu\text{V}$ ), the estimated axonal conduction velocity was  $46 \pm 1 \text{ m}\cdot\text{s}^{-1}$  for unit A (Group II range) and  $71 \pm 2 \text{ m}\cdot\text{s}^{-1}$  for unit B (Group I range). This indicates that unit A originated from a smaller axon in closer proximity than unit B. (Modified from Kallesøe et al. 1994).

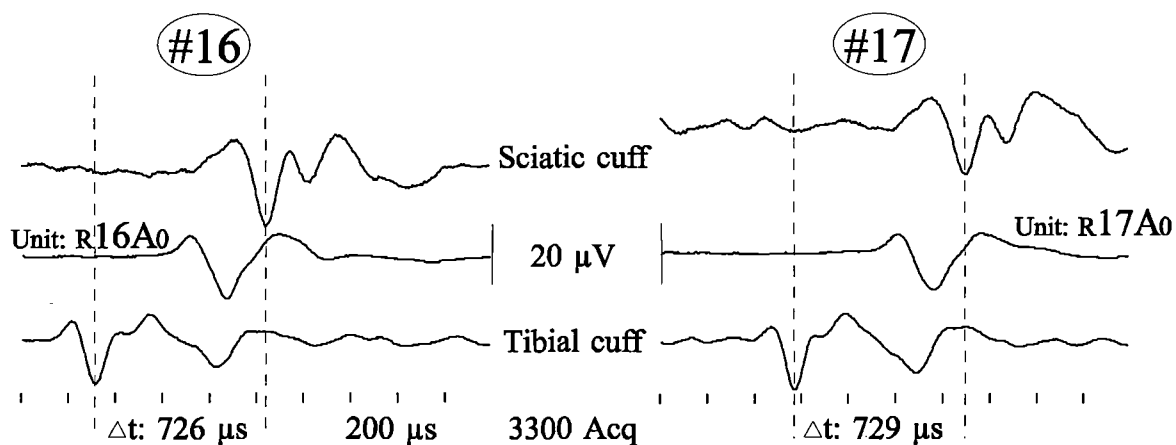


Figure VI.8: Spike-triggered averaging of a MG afferent neuron simultaneously recorded from two neighboring electrode sites, #16 and #17. The cuff spike shapes and propagation latencies recorded from both sites were similar. Estimated axonal propagation velocity:  $56 \pm 1 \text{ m}\cdot\text{s}^{-1}$  (Group II range). (Modified from Kallesøe et al. 1994).

During treadmill locomotion, simultaneous recordings were made from 8 intraneural electrode sites in one animal. Unitary profiles from identified MG muscle afferents were discriminated using the above described spike-triggered averaging technique (Figure VI.9).

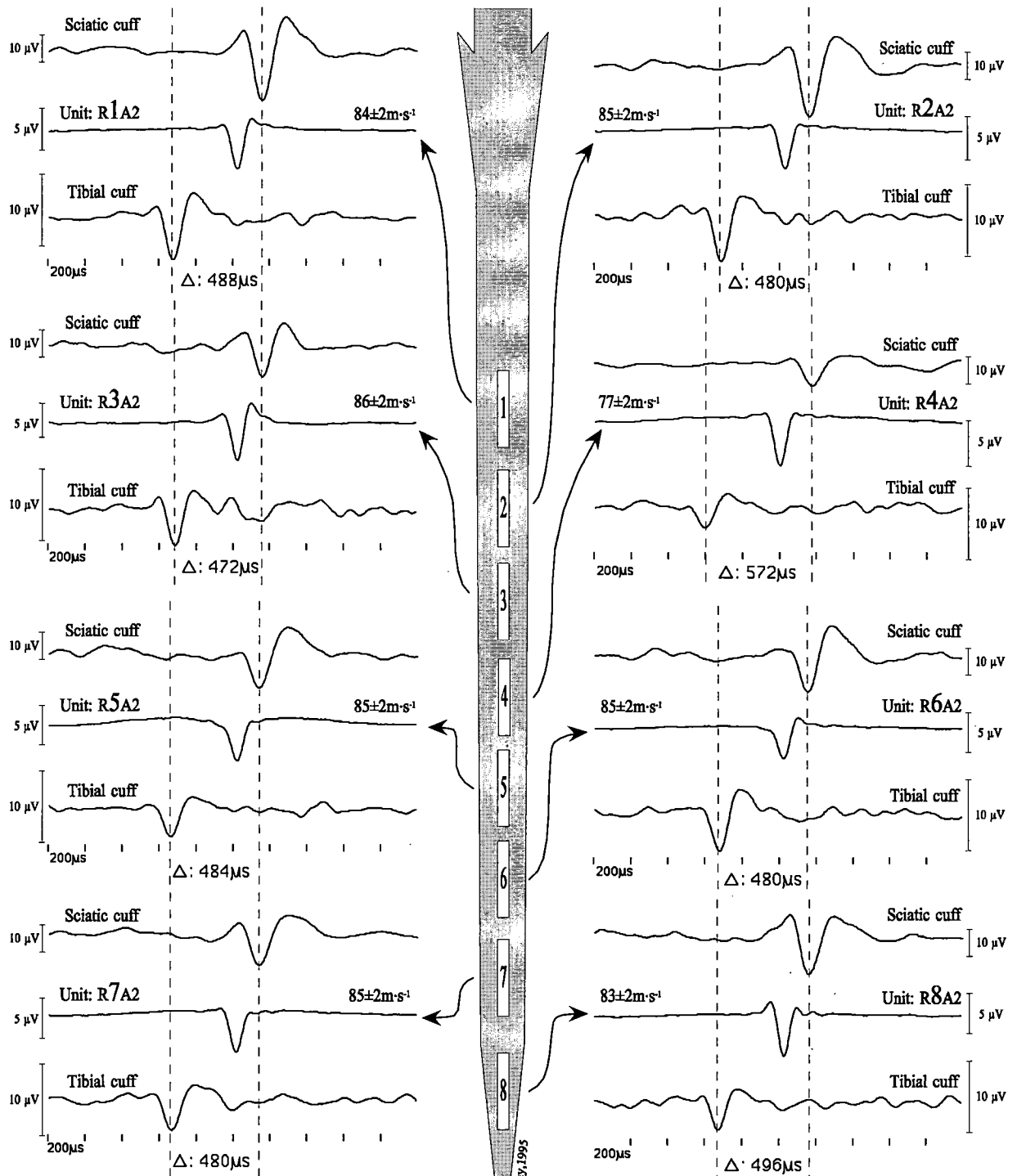


Figure VI.9: Spike triggered average of several MG interface sites on one silicon electrode. The recording axons were probably recorded by more than one site (e.g. site # 1,2,3) whereas different axons were clearly recorded by other sites (e.g. site #4). The axonal conduction velocities ranged from  $46 \pm 2 \text{ m}\cdot\text{s}^{-1}$  to  $86 \pm 2 \text{ m}\cdot\text{s}^{-1}$ . (Modified from Kallesøe et al. 1994).

afferent neurons recorded simultaneously from 8 was performed during treadmill walking.

Some axons were probably recorded by more than one site (e.g. site # 1,2,3) whereas different axons were clearly recorded by other sites (e.g. site #4).

The axonal conduction velocities ranged from  $46 \pm 2 \text{ m}\cdot\text{s}^{-1}$  to  $86 \pm 2 \text{ m}\cdot\text{s}^{-1}$ .

Simultaneous recording from several sites along the probe shank allowed for detection of activity in a population of axons in the vicinity of the probe. Given the longitudinal insertion direction along the axon fibers, it is likely that some electrode site may have recorded potentials from the same axons. This appears to be the case in several of the recording sites shown in Figure VI.9, although one site (#4) seems to have both a different unit shape and conduction velocity. The fact that all units were of afferent origin could be attributed to a possible modality segregation within the fascicle (Roberts and Elardo 1986, Hallin et al. 1991).

The activity patterns of several neurons were recorded simultaneously from one probe during rhythmic limb movements under light anesthesia (Figure VI.10). It was noted, that each neuron showed distinct bursts of activity, often correlated with the EMG recording from the MG muscle. Discrimination of the units was however, not always secure, as seen in the occasional abnormally even firing frequencies (more than 200 Hz).

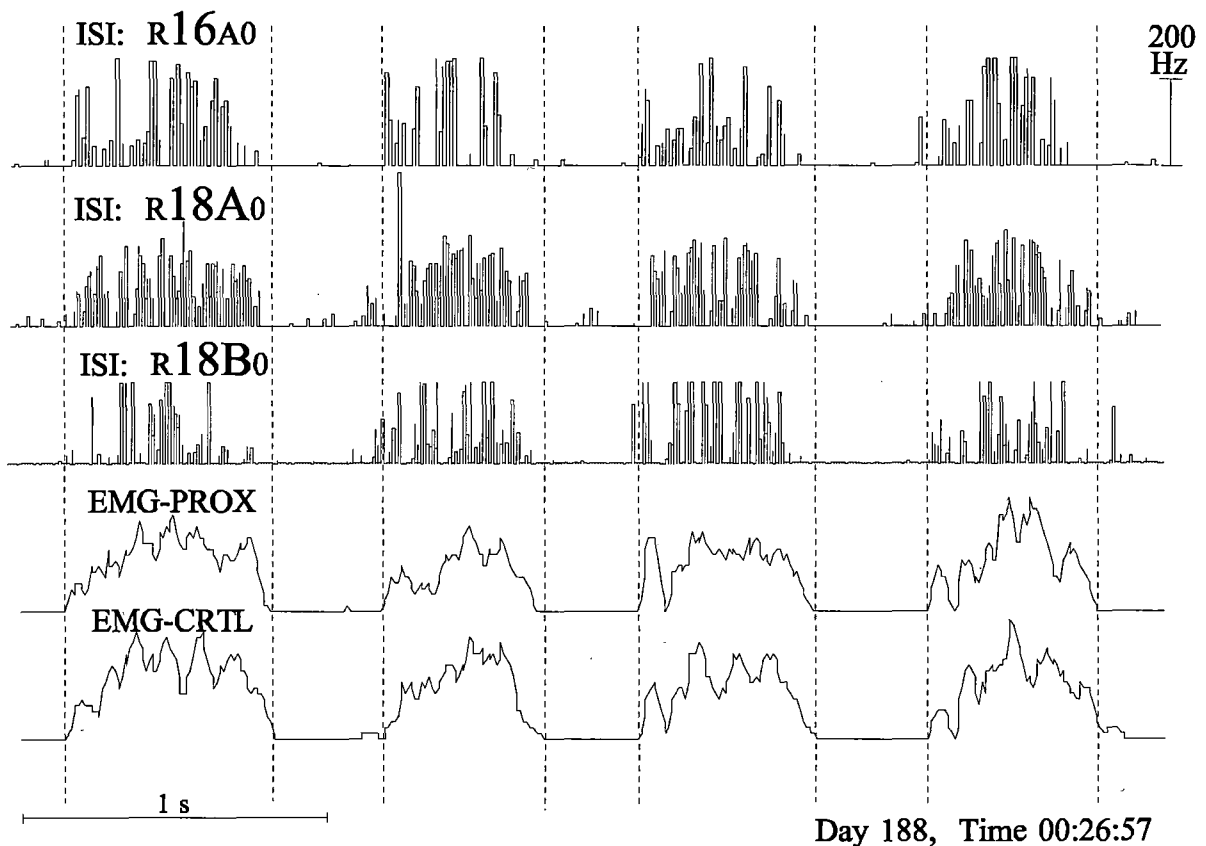


Figure VI.10: Activity of 3 simultaneously recorded MG afferents during rhythmic limb movements. The interspike interval (ISI) of three units (3 top traces) are shown in comparison to the EMG activity of the central and proximal regions of the MG muscle (2 bottom traces) (Kallesøe et al 1994).

*Conclusion:* It was concluded, that silicon multicontact electrodes were suitable for recording and micro-stimulating identified single axons in peripheral nerves of conscious animals, for short periods of time (1-2 days). It was noted, however, that the longevity (less than 72 hours) of the implants was unacceptably short, and that the signal-to-noise ratio was poor. Postmortem examination of the implants showed instances of mechanical breakage of the flexible cable leading from the bond platform, possibly explaining the short longevity of the implants.

The disappointing performance of the electrodes raised further concerns regarding the integrity of the probe insulation and the survival of the iridium surface.

### **Iridium activation**

Iridium was chosen by the Michigan group (CNCT) because of the ability to form a biocompatible oxide ( $\text{IrO}_2$ ) on the metal surface. This activation increased the charge capacity (Robblee et al. 1983), a desirable feature for stimulation applications, and reduced the site impedance by increasing the surface area.

Activated iridium can be applied by several methods (Agnew and McCreery 1990). A relatively simple method is Anodically formed Iridium Oxide Film (AIROF) where the oxide forms on the metal surface through electric activation in a saline solution. This was achieved using cyclic voltammetry (Bockris 1980, Gileadi et al. 1975), where a 3-electrode scheme allowed for a controlled current to be passed through the interface site (Monk et al. 1995).



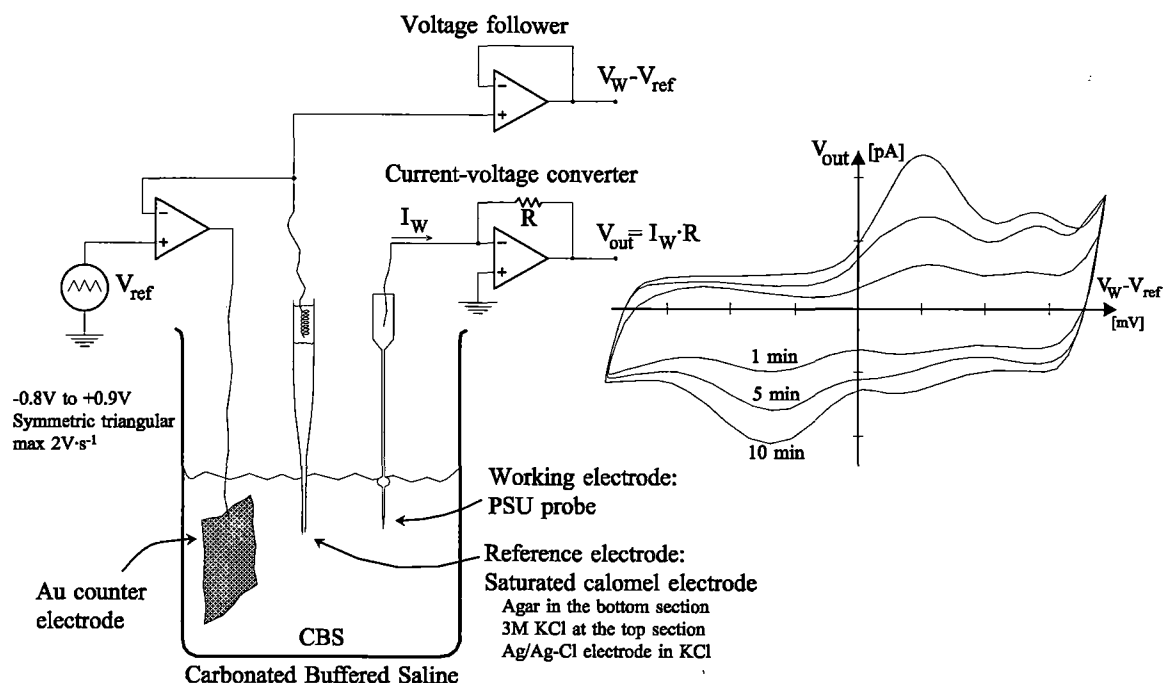


Figure VI.11: Setup for cyclic voltammetry. The Cyclic Voltammogram (CV) displayed at the right, represents a typical oscilloscope display. (Adapted from UMCISC 1995).

The AIROF process has been described elsewhere (Weiland 1997), and is only summarized here.

The current flow through the working electrode to ground was monitored while the potential of a large counter electrode was cycled with a triangular wave form ( $-0.8 \text{ V}$  to  $+0.9 \text{ V}$ ). During the anodic sweep of the cycle, an inner oxide layer ( $\text{IrO}_2$ ) was formed from pure iridium on the metal surface. As the potential increased, the oxide layer changed to a hydrous outer layer ( $\text{Ir}(\text{OH})_3$ ) and limited the formation to a monolayer (Pickup 1987, Weiland 1997). The inner layer was again reduced to iridium on the cathodic sweep, leaving the outer layer as a porous oxide. It was because of this porosity, that the metal surface remained in contact with the solution, and allowed for additional oxide layers to be formed on successive sweeps. When the oxidation process had formed a sufficiently thick outer layer of oxide, it was left in either an anodic or a cathodic state, depending on where the sweep cycle was stopped. The oxide allowed for a transfer of charge via a valence change reaction of the oxide, and a charge density of up to  $100 \text{ mC} \cdot \text{cm}^{-2}$  could be obtained (Weiland 1997). The porous oxide layer increased the surface area of the electrode, thus decreasing the resistance and increasing the

capacitance of the site. To verify the formation of the oxide, electrical characteristics of the sites were documented, both by cyclic voltamograms, and by an impedance test of the tip section exclusively. Typical preoxidative tip impedances of a  $400 \mu\text{m}^2$  iridium surface were  $500 \text{ k}\Omega \angle -65^\circ$  at a 1 kHz test signal. This was reduced to approximately  $200 \text{ k}\Omega - 300 \text{ k}\Omega \angle -35^\circ$  after 10-20 minutes of oxidation. For a parallel RC model of the site, this is equivalent to  $1.2 \text{ M}\Omega$ ,  $288 \text{ pF}$  reduced to  $244 \text{ k}\Omega - 366 \text{ k}\Omega$ ,  $456 \text{ pF} - 304 \text{ pF}$ . The capacitive component could be increased further by additional oxidation. This was tested in a few electrodes with long-term (19h) oxidation test where a site capacitance in the  $300 \text{ nF}$  range was reached. (These highly capacitive sites were not tested *in vivo*).

Further studies on whether iridium is a suitable electrode material, are warranted given the conflicting information present in the literature. Under static potentials, Anderson (1989) claimed that pure iridium is a stable material, whereas under dynamic conditions Bernstein (1977) reported it to be very corrosive. The exact oxidation reactions of the iridium also remain controversial, as reported by Monk et al. (1995), and questions remain, as to whether it is important to stop the oxidation cycle anodically, or cathodically (Heetderks W, personal communication 1995). This decision determines, if the oxide remains clear or black, similar to the switching appearing in a liquid crystal display. Finally, the methods for maintaining the oxide are not clear. Sterilization of electrodes using autoclaving at temperatures above  $100^\circ\text{C}$  may not be desirable, given reports of oxide destruction at these temperatures (Monk et al. 1995). Once implanted, it still remains unknown, what the optimal maintenance procedures are for the oxide. Similarly, ad hoc techniques have been used for possible *in vivo* re-oxidizing of individual sites.

## **2<sup>nd</sup> Silicon design: PSU-3 and PSU-4 probes**

Implanting the "PSU-0" probes revealed several mechanical design shortcomings:

- The flexible cable had limited rotational flexibility, i.e. the cable prefers to remain flat and is thus likely to twist the tip section, to return to this condition.
- The epineurium barbs were too small to catch a significant amount of tissue.

- Insertion of the flat dagger-like probe was assumed to cause minimal nerve damage, when inserted along the axons. The round platform on the tip section used for forceps handling of the PSU-0 probe, hindered the possibility of inserting the probe at a shallow angle.
- During insertion, the flat dagger-like tip of the probe was oriented so as to minimize nerve damage due to transection of axons. Insertions of the probe was done along the axons with the plane of the substrate perpendicular to the surface of the nerve (Figure VI.12). This allowed the probe to slide in between axons. Given the fact that the MG fascicle is located superficial in the sciatic nerve, a shallow insertion angle was required. However, the round platform on the tip section used for forceps handling of the tip, hindered the possibility of inserting the probe at the required shallow angle.

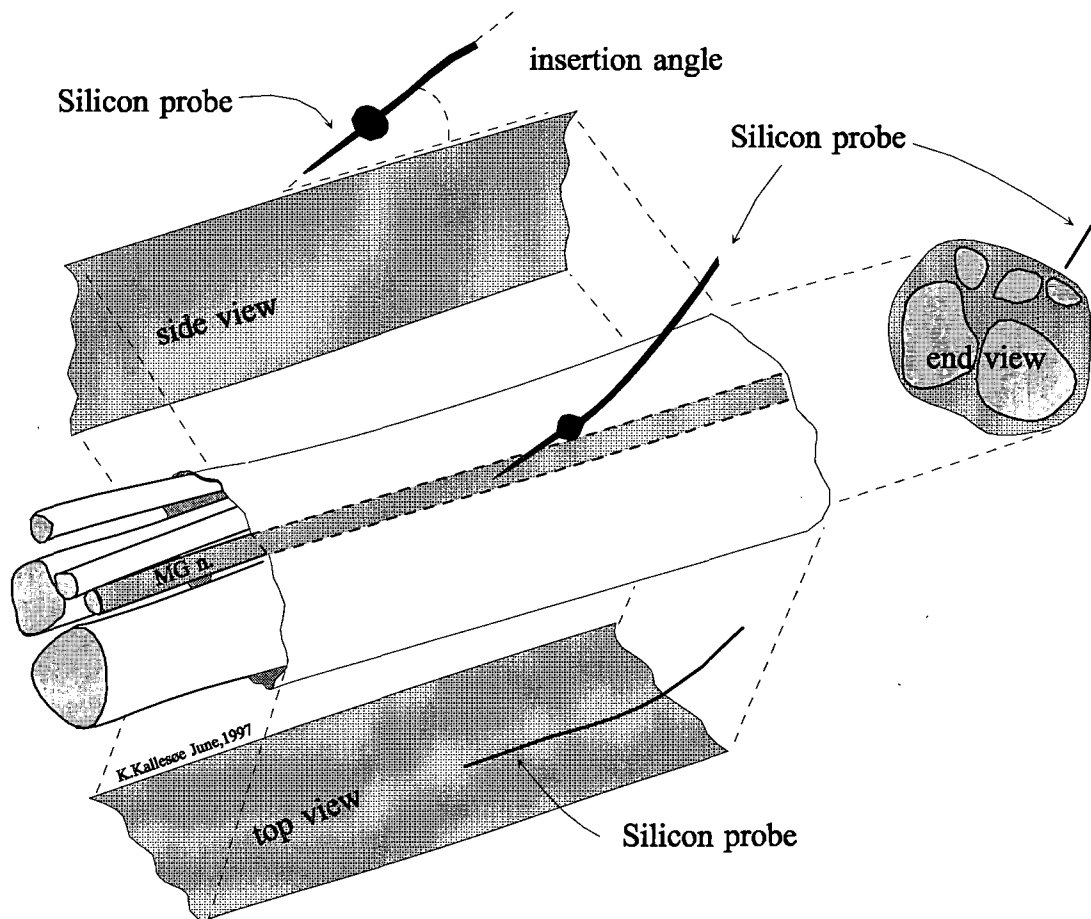


Figure VI.12: Probe insertion technique. Because the MG fascicle is located superficially in the sciatic nerve, a shallow insertion angle was required. A steeper insertion angle would have meant that only the tip would have penetrated the tissue and the probe would not have been anchored properly.

- The bonding of Cooner wire to the PSU-0 design did not allow for easy and compact bonding.
- The flexible cable was found to be very fragile when manipulated during pre-implantation procedures.

*Design modifications:* The PSU-0 design was modified in two stages. The first step was to increase the rotational flexibility of the thin flexible cable by introducing longitudinal slots between paired conducting polysilicon traces. This idea originated from CNCT, University of Michigan (Hetke J, personal communication 1994), who had used a similar design technique to enable two dimensional structures to curl. These slots changed the original PSU-0 single flexible cable form a width of 100  $\mu\text{m}$  with 8 conductors, to 4 cables 10  $\mu\text{m}$  apart each 35  $\mu\text{m}$  wide with 2 conductors. Since the exact flexibility and fragility of this design was unknown, two designs were submitted - one with and one without slotted cabling (PSU-1 and PSU-2).

A second redesign of the PSU-0 probe included:

- 1) larger barbs (20  $\mu\text{m}$ ) on the shank of the probe;
- 2) a hole in each bonding platform to improve Cooner wire attachment;
- 3) the forceps handling platform was reshaped into a hook. This allowed for an 8-0 suture to be used for tying the probe to the epineurium;
- 4) removing half of the circular forceps handling platform allowed the probe to be inserted at a shallower insertion angle (Figure VI.12).

These changes were included before PSU-1 and PSU-2 were in production and the new designs were thus named PSU-3 and PSU-4 (Figure VI.13). They successfully went into production in late 1994.

A new Cooner wire bonding technique was implemented in the PSU-3 / PSU-4 design. The previous technique used in both the "Schmidt" probe and in the PSU-0 design, was to connect stainless steel strands to the top surface of the bonding platform with conductive epoxy. This required delicate assembly procedures, where the bare ends of 8 Cooner wires were held in place above the bond site, while conductive epoxy immobilized and electrically connected the

wire strands. Aligning all 8 connecting wires simultaneously was a tedious and time consuming assembly technique.

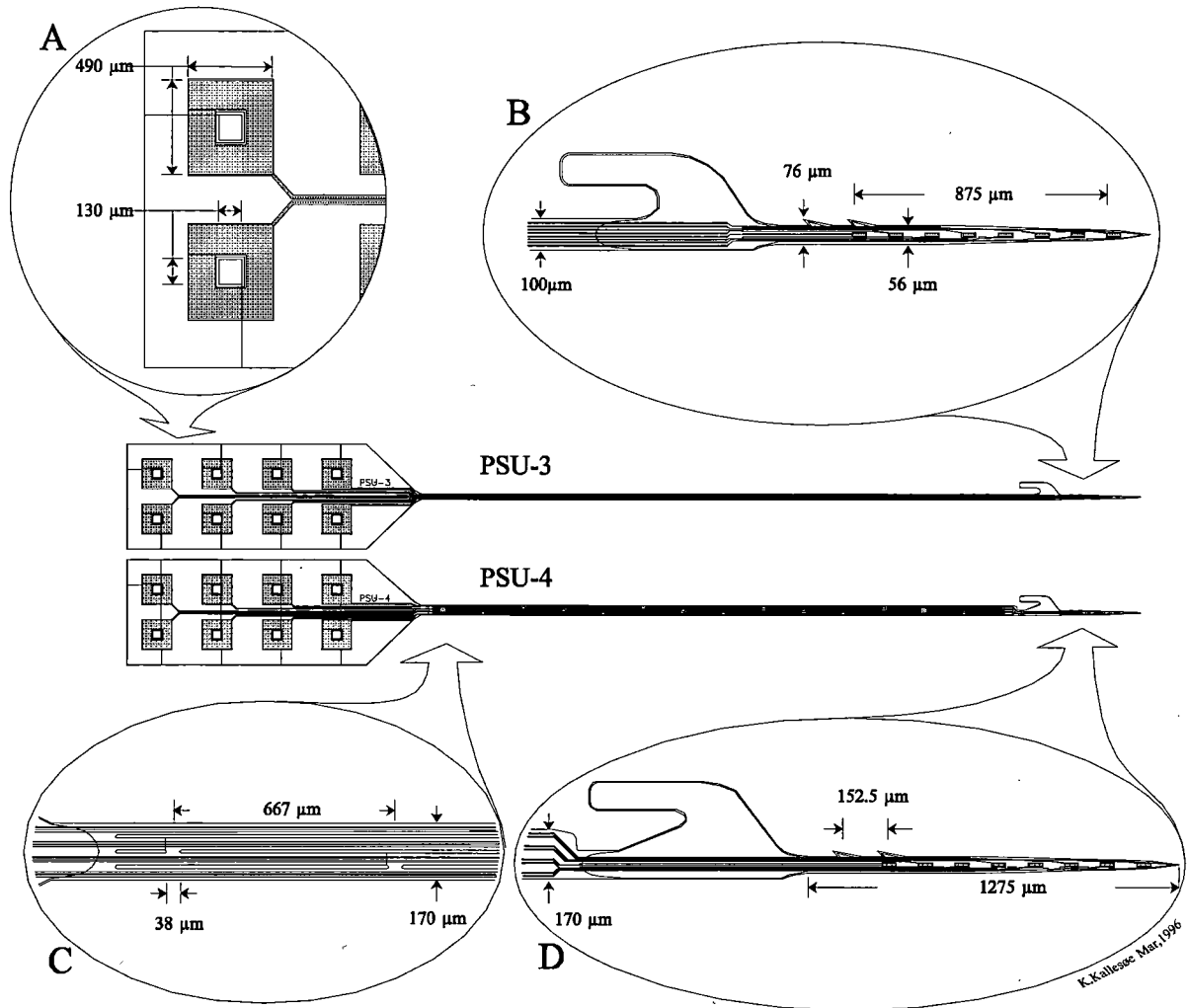


Figure VI.13: Details of the PSU-3 and PSU-4 designs. (A) Center holes were added to each bonding pad site. This allowed connecting Cooner wires to pass through all mask layers. (B & D) The tip sections were given a hook shape to anchor the probe with an 8-0 suture. (C) The main difference between the PSU-3 and PSU-4 design was the slotted flexible cable of PSU-4. The cable was divided into 4 minor cable strands, 10  $\mu\text{m}$  apart, each carrying 2 conductors. To support the cable structure, small bridges were left between the strands at 2 mm intervals. The bridges were 38  $\mu\text{m}$  in length and distributed asymmetrically along the total length of the flexible cable.

The bonding technique was simplified by the implementation of a hole in the center of each individual bond site. Cooner wire strands were fed through the hole from the bottom surface,

bent around and connected on the top surface. The wires were aligned by the holes and fixed to the bottom surface of the bond platform with insulating epoxy (Aquatapoxy).

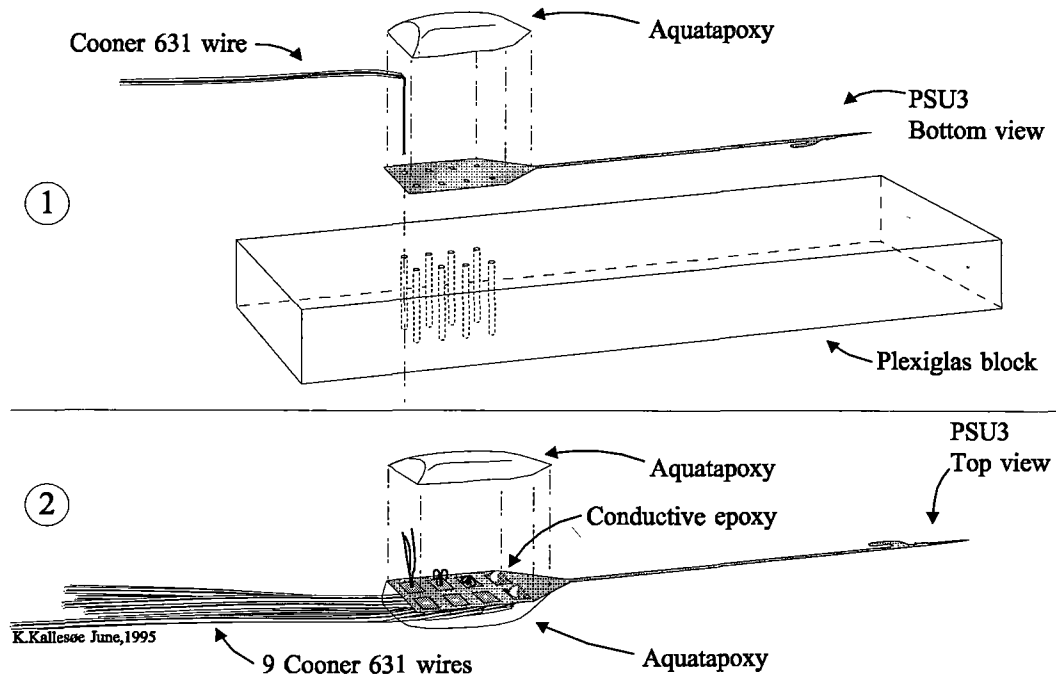


Figure VI.14: The assembly technique of PSU-3-4-5-6 designs. (1) The probe was initially positioned with the bottom plane facing up, on a block of Plexiglas with holes drilled 1mm apart to match the hole pattern in the bonding platform. The deinsulated end of each 631 Cooner wire was passed through the probe and Plexiglas holes. The end of the wire was bent on the bottom side of the Plexiglas to prevent the wire from slipping back out. A thin encapsulation of Aquatapoxy was used to fix the location of all 8 wires. A ninth wire was embedded in the Aquatapoxy to detect any leakage in this area. (2) A piece of adhesive tape attached to the Plexiglas prior to the first step of the assembly, allowed the probe to be lifted from the Plexiglas. Any excess Aquatapoxy that otherwise would have fixed the probe to the Plexiglas, was easily removed from the tape. The assembly was flipped over and the bare Cooner wire strands were trimmed down to approximately 1mm. These ends were spread out on the gold bonding pad sites and conductive epoxy was used to connect all strands to the gold. All connections were embedded in Aquatapoxy.

*Results:* In total, six probes, three PSU-3 and three PSU-4, were implanted chronically, with a total of 48 possible interface sites. Two of the probes (one PSU-3, one PSU-4) were implanted in an acute experiment. The slotted flexible cable of the PSU-4 design exhibited good handling properties, both during assembly and during implantation. It allowed the tip to be rotated over a wider range than the PSU-3 design, but it still had a tendency to regain its original orientation after insertion in soft tissue. Furthermore, the individual cable strands were very fragile and were found to break.

Exp.	ID	Duration [days]	Implants	Single unit recording notes	Microstimulation levels	
					lowest	no. of sites <20 $\mu$ A
6	T-Jun95	25	16 sites on a PSU-3 and a PSU-4 probe	Stimulation possible for 12 days;	22.0	0
	S-Feb96	5	16 sites on a PSU-3 and a PSU-4 probe	3 sites recorded 1.5x background noise	7.0	8
	B-Feb96	0	16 sites on a PSU-3 and a PSU-4 probe	1 site recorded (~20 $\mu$ V)	12	1

Table VI.3: Silicon probe experiments using the PSU-3 and PSU-4 probes.

All implanted PSU-3 and PSU-4 probes showed signs of failing electrical insulation, which rendered them unusable as recording electrodes. This was seen as a very low shunt electrode impedance (less than 5 k $\Omega$  at 1 kHz), indicating a very large conductive surface area. However, in one of the probes it was possible to selectively stimulate MG motor units, indicating a mechanically intact probe in close proximity to axons in the MG nerve branch. This stimulation interface was maintained for 12 days. Fluctuation (80-390  $\mu$ A) in the stimulation recruitment thresholds, most likely reflected movement of the electrode with respect to the excitable neural tissue. At postmortem examination, both probes showed mechanical breakage of the flexible cable close to the bonding platform. This was apparently caused by connective tissue growth. To minimize the risk of cable breakage, later probes were coated with a low viscosity Silastic adhesive (DowCorning 734).

Experiment S-Feb96 had promising initial results with micro stimulation and some recordings. Unfortunately, these disappeared after the use of a vector impedance meter (HP4800A) possibly passing destructive amounts of current through the electrode.

The B-Feb96 experiment served to test the use of shorter lead-out cables. This was done in an acute preparation, where the Cooner cable was reduced from the typical 40-50 cm to only 10 cm. No indications of improved recording conditions were found.

*Conclusion:* The mechanical characteristics of PSU-0 were improved and successfully tested in the PSU-3 and PSU-4 design. Several advantages were gained:

- 1) The flexible cable had an improved rotational flexibility, although it still had some tendency to regain its preferred flat orientation.
- 2) The epineurium barbs were increased in size from 10  $\mu\text{m}$  in the PSU-0 design to 20  $\mu\text{m}$  in the PSU-3 / PSU-4 designs. This improved the fixation of the probe to the extent, that it was no longer possible to remove it without severe tearing of the epineurium.
- 3) The change in the shape of the forceps handling platform successfully allowed the probe to be implanted at a more shallow angle. Although this position was maintained throughout the surgical procedure, it was unclear whether the probe remained there post-surgically.
- 4) The holes added to the bonding pads allowed for an easier assembly technique, but introduced a new problem: the conductive silicon substrate was inadvertently also connected to the Cooner wires bonded through the holes in the substrate (Figure VI.14; further description follows below).
- 5) The flexible cable was successfully coated with silicone without the creation of severe stress-points due to uneven coating.

Using a hole through the substrate as described above (4), turned out to have an inherent major flaw. The substrate is conductive and the de-insulated Cooner wire passing through the substrate holes could possibly make a connection to the silicon (Figure VI.15).

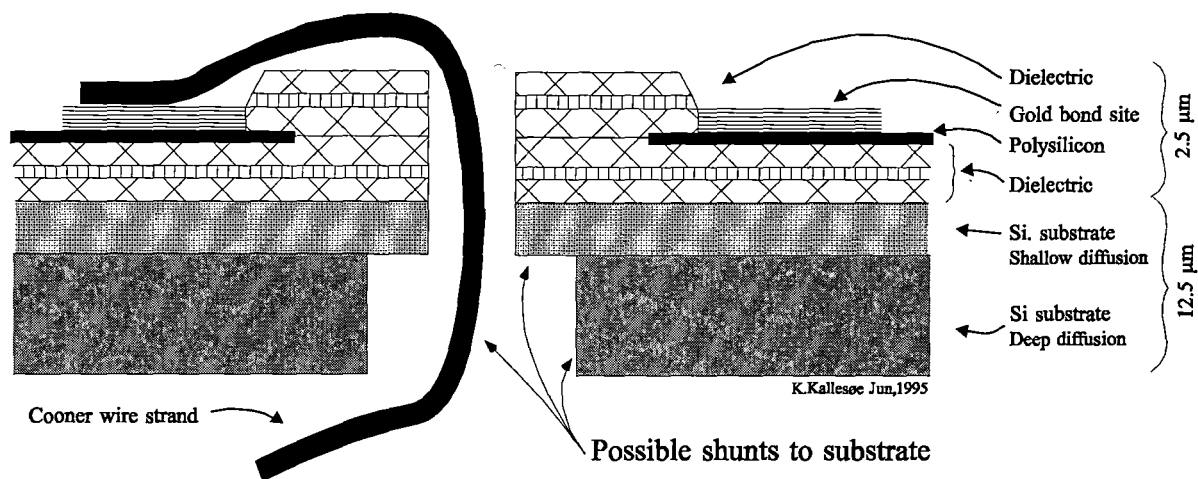


Figure VI.15: Unwanted electrical connections to the Si-substrate were formed on the bottom side of the bonding platform. Another potential point of current leakage was at the location, where the hard Aquatapoxy cured on the surface of a thin dielectric layer, possibly cracking it during thermal expansions and contractions.



The entire boron diffused substrate then acted as a very large leakage pathway, potentially shunting signals from nearby axons. This could attenuate the recorded signal amplitude. However, microstimulation of neighboring axons was still possible, as seen in the T-June'95 implant (Table VI.3).

To eliminate this unwanted shunt, an extra assembly step was introduced after the T-June'95 implant. The extra step involved applying a thin insulation coat of 5-minute epoxy to the Cooner wires prior to insertion through the bond hole. The Cooner wires were then fixed with Aquatapox to the bottom surface of the bonding platform as described above (Figure VI.13), and the 5-min epoxy insulation extending through the hole was carefully stripped. This allowed the strands of the deinsulated the Cooner wire to be glued with conductive epoxy to the bond pads with minimal risk of shorting to the substrate. The assembly technique was more cumbersome than intended with the original design of the bond pad holes, but it greatly increased the assembly yield.

### **3<sup>rd</sup> Silicon design: PSU-5 and PSU-6 probes**

Once the problem with Cooner wire shorting out to the substrate had been identified in the PSU-3 / PSU-4 designs, changes were introduced to bonding pad design.

*Method:* The risk of creating a short to the bonding pad, was reduced by passing the Teflon insulation of the Cooner wire through the hole in the bonding pad. This required a larger hole size to accommodate the insulated Cooner wire (Figure VI.15). The holes of PSU-3 and PSU-4 designs were changed from a square (130  $\mu\text{m}$  x 130  $\mu\text{m}$ ) to a round ( $\text{\O}$ : 350  $\mu\text{m}$ ) shape. The round shape was chosen to minimized the gap around the Cooner wire and thus limiting the amount of epoxy that could leak through.

In addition to the bonding pad changes, CNCT increased some of the safety margins in their set of general silicon micromachining rules. The minimum dimension of any design feature on the masks was set to a conservative 3  $\mu\text{m}$ . This required a complete redesign of each mask layer for the PSU-5 / PSU-6 designs.

Furthermore, CNCT required an additional *contact mask* to correct problems with poor adhesion of the metal layers. This mask defined the contact area between metal layers and the conducting polysilicon, and consisted of  $3\ \mu\text{m} \times 3\ \mu\text{m}$  squares spaced  $3\ \mu\text{m}$  apart.

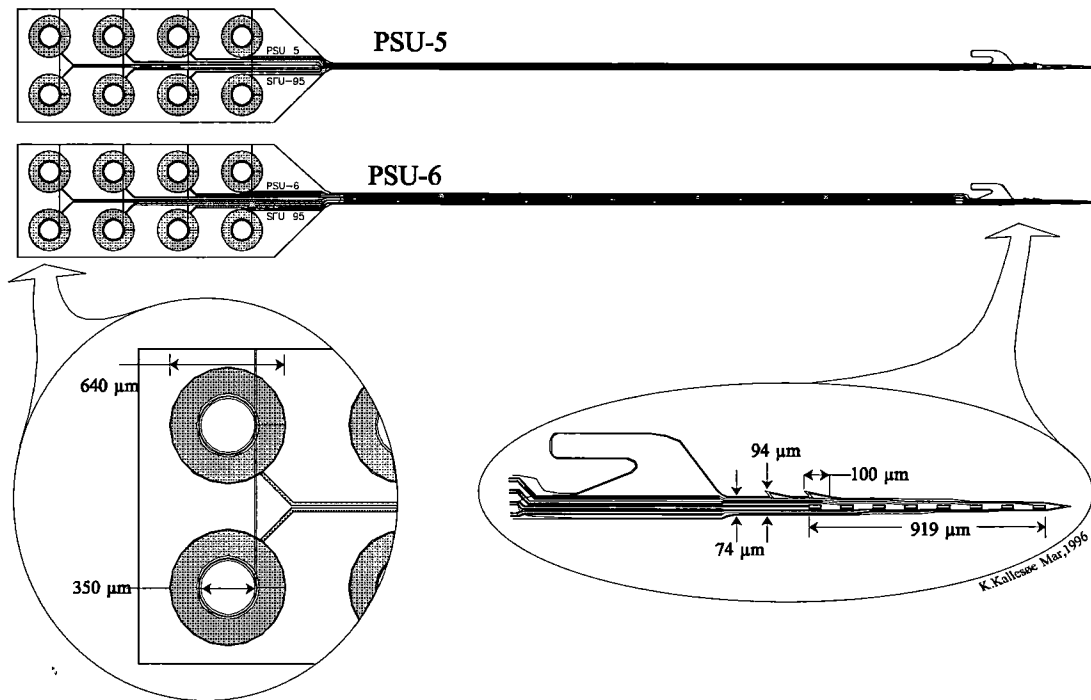


Figure VI.16: The bonding pad sites were redesigned on the PSU-5 and PSU-6 probes. The sites and the holes were made round to accommodate the Cooner wires. Both designs were redrawn to a new set of more conservative design rules. Significant changes included the rerouting of polysilicon traces close to the edge in the tip section and the addition of a contact layer (not visible at this magnification).

**Results:** The complete revision of the PSU-5 and PSU-6 drawings allowed for a rerouting of all conductive traces. This eliminated some of the marginal features of earlier PSU designs.

The completed drawings were submitted to CNCT in late 1995 and an initial fabrication batch was returned in early 1996. Four probes were implanted in June of 1996.

Exp.	ID	Duration [days]	Implants	Single unit recording notes	Microstimulation levels	
					lowest	no. of sites $\leq 20\ \mu\text{A}$
7	S-Jun96	5	16 sites on a PSU-5 and a PSU-6 probe	1 probe broke; 1 recording 1.2 x backgr. noise	43	0
	S-Jun96 (acute)	0	16 sites on a PSU-5 and a PSU-6 probe	Acute no recordings	25	0

Table VI.4: Silicon probe experiments using the PSU-5 and PSU-6 probes.

In a chronic experiment (S-Jun96), one PSU-5 and one PSU-6 probe were installed in a sciatic nerve, but only one probe remained intact at the time of insertion. Similar to previous implants, low microstimulation levels were seen at the time of implantation, but only weak neural signals were detectable in the following 48 hours.

After the initial recording problems, the chronic probe of S-Jun96 was repositioned one week later in an acute experiment. This was done by using collagenate to remove the connective tissue build up (50 mg in 3 ml saline solution). The probe was repositioned several times in the MG fascicle without noticeable improvements in its ability to recorded signals or stimulate SMU's.

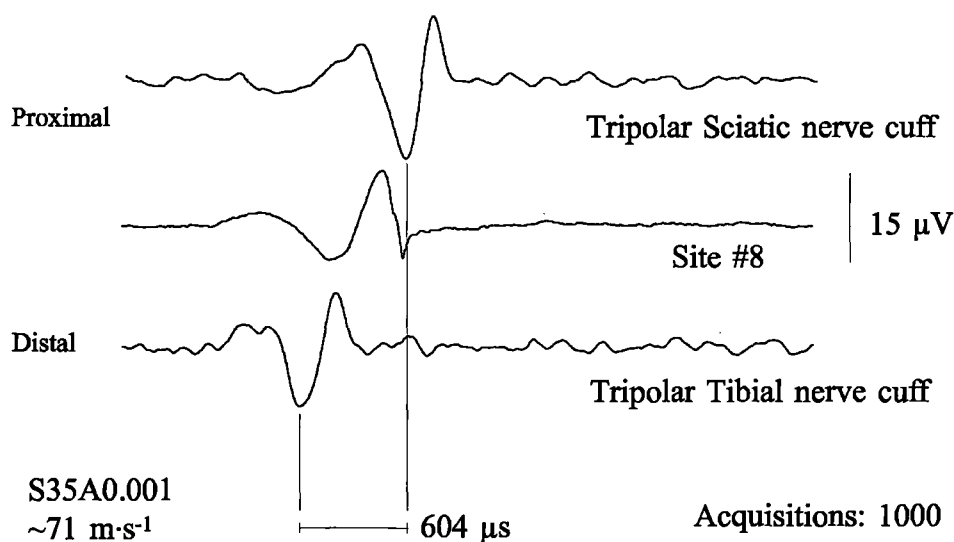


Figure VI.17: Spike-triggered averaging of an MG afferent neuron recorded from electrode site number 8 on a PSU-6 probe (S-June96). Estimated axonal conduction velocity:  $71 \pm 1 \text{ m}\cdot\text{s}^{-1}$  (Group I range).

*Conclusion:* Design changes to the bond platform provided an easier and safer connection of the Cooner wires. It did not, however, totally eliminate the possibility of a short circuit connection to the substrate, which was found in several of the presurgical assemblies.

The iridium oxide formation showed more stable characteristics from site to site, compared with earlier silicon probes. This was attributed to the new contact layer and the improved manufacturing procedures at the CNCT.

## Discussion

The objective of designing a new peripheral single unit electrode was to improve on both the mechanical and electrical characteristics of previously used technology (hatpins and fine wires). This was attempted through the use of leading edge technology - silicon micromachining. Several innovative design features were created and submitted for production.

A total of 22 silicon probes were implanted, with 168 potential interface sites. Typically 6-8 sites on each probe showed close proximity to motoneurons at the time of implant, but only 1 or 2 sites on each probe had detectable neural activity within the initial 24 hours post surgery.

In the introduction of this chapter, a number of mechanical and electrical requirements of a successful PSU interface were outlined:

- Interface robustness: The developed PSU probes all proved to be fairly fragile, having a very limited mechanical lifetime, typically less than 2 weeks. This is obviously not acceptable for the design of neural prostheses systems. Future research is needed to improve this. Based on experience with similar "floating" silicon probes in the cortex (Drake et al. 1988), considerably longer survival times (i.e. many weeks) should be possible but longevity will depend on the extent of movement in each implant site.
- Interfacing to single or small groups of peripheral axons was successfully accomplished (Figure VI.9) with as many as 8 recording sites simultaneously. The quality of this multi-axonal interface was, unfortunately, limited by the electrical and mechanical characteristics of the probes.
- Each probe was connected with a very flexible silicon cable. To improve on rotational flexibility new design features of a slotted cable were introduced.
- Interface sites were covered with iridium or iridium oxide, exhibiting minimal chemical dissolution. To monitor neural damage caused by mechanical or chemical properties of the implanted electrode would require histology sampling of the tissue. This was not done systematically.

It was shown that it is feasible to use silicon base probes to micro-stimulate and record single peripheral axons in animals. The results and experience with the silicon probe design remained preliminary, and it is expected that future implants may yield larger and more robust unitary potentials.

It should be emphasized here, that the present state of the silicon technique exhibits severe limitations and weaknesses. Perhaps the largest limitation is the fact that thin and delicate structures of silicon are fragile. The delicate dimensions produce a cable with a great deal of lateral flexibility but very limited ability to accommodate longitudinal length changes. Despite this drawback, some success has been reported in the use of silicon probes in the CNS (BeMent et al. 1986, Drake et al. 1988), although the use of this technology has been hampered by technical problems in the manufacturing procedures (UMCISC 1995).

The next step in the silicon probe design is to address the questions of why the probes failed to maintain the initial interface to peripheral single axons and why recorded signal amplitudes were so small compared to CNS recordings. Looking at the differences between the CNS and PNS interfaces may yield some answers.

First of all, given the presence of contractile muscle tissue around a PNS interface, it is more likely that the electrode is disturbed mechanically in this peripheral location, compared to more protected CNS locations. This could account for broken flexible cables and dislocated electrode tips.

Secondly, CNS electrodes are inserted in tissue with a high density of cell bodies surrounded by current conducting clefts between other support cells such as glia cells (Peters et al. 1970). The average cell body density of the CNS varies tremendously, with  $4.6 \cdot 10^{-6}$  cells per  $\mu\text{m}^3$  in the oculomotor nucleus (monkey) and more densely in the cortex with  $1.56 \cdot 10^{-5}$  cells per  $\mu\text{m}^3$  (Robinson 1968). These densities are 2.5 to 8 times larger than the nodal density of the PNS ( $1.8 \cdot 10^{-6}$  cells per  $\mu\text{m}^3$  in the peroneal nerve of the rat; Rutten and Meier 1991) making it more likely for a CNS electrode to be inserted in close proximity of neural current sources.

A technical difference between the CNS and PNS setup was in the surface characteristics of the recording site. Given the greater likelihood of CNS electrodes to be close to an intense

extracellular field, smaller surface areas have been used ( $20\text{-}80\ \mu\text{m}^2$ ; BeMent et al. 1986) compared to PNS electrodes ( $400\text{-}500\ \mu\text{m}^2$ ). The resistance of CNS electrodes ( $1\ \text{M} - 20\ \text{M}\Omega$ ) is thus 1-2 orders of magnitude larger than for PNS electrodes ( $100\ \text{k} - 300\ \text{k}\ \Omega$ ). A smaller area increases the volume from which the electrode will detect electric fields and makes it more likely to record from smaller and more distant current sources. A drawback of a high resistive surface, is the increased pickup of unwanted noise. Therefore, the surface area of the PSU electrodes were made larger than that of the CNS electrodes.

The capacitance of CNS electrodes is smaller ( $\sim 100\ \text{pF}$ ) compared to PNS electrodes ( $\sim 300\ \text{pF}$ ). The smaller capacitance has the advantage of limiting the electrical load of the current source. A disadvantage is that it requires the parasitic capacitance of the leadout cables to be small to avoid significant attenuation. This is generally not a problem for CNS preparations, where amplification circuitry is mounted close to the electrode tip. In a chronic PNS setup, however, longer lead out cables are required. This places a constraint on the selection of cable type and length. The parasitic capacitance can be reduced by the use of neutralized input capacitance amplifiers (Amatniek 1958). This technique, is also called negative capacitance coupling of the front end amplifier, was tested in a few of the PSU implants. The general result was discouraging with highly unstable output signals and large noise artifacts.

The preliminary use of silicon based PNS electrodes presented here opens a new set of questions regarding the design and implantation techniques:

- 1) The probe design included a conductive substrate that could potentially connect the surrounding tissue around the inserted probe to the extraneural space. Could this grounding back plane cause a reduction in the recorded signal amplitude ?
- 2) The amplitudes of recorded signals were unacceptably small. Could this be attributed to the location of the recording sites with respect to the axons, or to the electrical characteristics of the electrode ?
- 3) To what extent would movement of the recording sites with respect to individual nodes of Ranvier affect the recorded signal amplitude ?

- 4) What was the reason for the poor longevity of the implants ?

*Future directions:* A recommended future direction will be to include integrated active electronics on the probe, close to the recording sites (Ji et al. 1990). This could potentially reduce signal loss due to poor electrical characteristics of the recording site. It could also lead to the desirable implementation of a telemetry link to the probe, which would completely eliminate the need for a flexible cable and therefore reduce the mechanical load on the probe.

## VII. SIMULATION OF SINGLE AXON RECORDING INTERFACES

Thus far, the design parameters for fine wire, hatpin and silicon based electrodes have generally been empirically determined. To understand and possibly improve these designs, further theoretical work on the characteristics of intraneural electric dynamics was needed.

### Objectives

A model of an intraneural single unit electrode was designed to clarify the recording dynamics of such electrodes. The purpose of the model was to address the performance shortfall of existing electrode designs and possibly outline improvements for future electrode designs. In addition, a model of the neural environment was designed to expose the electrode model to the electric field around a single axon.

The following questions regarding the intraneural electrode design were addressed:

- Is the conduction of action potentials along individual fibers significantly changed by the insertion of an intraneural electrode ?
- Is the design with combination of intraneural electrode tip and extraneural reference electrode efficient for single unit recordings ? This is especially interesting for the silicon probe design, where a very long conducting silicon substrate close to the recording site may affect its ability to record unitary action potentials.
- To what extent will movement of an electrode with respect to a node of Ranvier influence the recorded neural activity ?

Models of the electric field in and around peripheral nerves have been derived to simulate either stimulation or recording of neural activity (e.g. Lorente de N6 1947, Patlak 1955, Rosenfalck 1969, Stein 1980, Heringa et al. 1989, Schoonhoven and Stegeman 1991). As with any model, many of these required severe simplifications of the system being modeled and were typically constructed to address very specific questions regarding the behavior of the system. These simplifications included assumptions like cylindrical symmetry around the longitudinal axis of an axon, and an isotropic and homogeneous conductive medium. This



limited the models' applicability to real neural signals. When attempting to describe a more realistic environment with a conductive medium surrounded by other axons, multiple fascicles, electrical conducting vascularization and insulating support tissue, formulating an analytical solution became a truly formidable task.

### **Analytical modeling**

#### *Models of potentials generated by single fibers:*

The electrical characteristics of active nerve fibers have been modeled mainly in two different ways. In the first approach, an electrostatic analogy was used for solving the differential field equations for a single active fiber in a homogeneous, isotropic and infinite environment (Lorente de N6 1947). This laid the foundation for what has been termed in biophysics "the volume conductor theory". The theory describes the laws governing the stationary behavior of currents in a conductive isotropic medium. The approach suffered from the major disadvantage of not handling boundary conditions inside or around the conducting environment (Barker et al. 1979).

A second approach included an analytic solution to the field equations (Poisson equation) for a single nerve fiber (e.g. Plonsey 1969, Rosenfalck 1969, Marks and Loeb 1976, Ganapathy and Clark 1987, Plonsey and Bar 1988, Malmivuo and Plonsey 1995). A major complication in these models was, again, the description of boundary conditions. These conditions were analytically addressed with Green's theorem but the solutions typically resulted in fairly complex mathematics, even for a relatively simple conducting medium (Weinberg 1942, Geselowitz 1967). The analytical modeling approach has, nevertheless, been very instrumental in interpreting a variety of bio-potentials, both from single axons and from single muscle fibers. In this way, microelectrode recordings were shown to reflect the transmembrane current flow rather than the intracellular potentials (Rosenfalck 1969, Andreassen and Rosenfalck 1981, Nandedkar and St6lberg 1983).

As referenced above, several variations on the modeling approaches have been reported, some of which differ significantly in the estimate of the potential near a single fiber (Schoonhoven et al. 1986b). Two factors have proven important: the description of the field source (voltage source vs. current source, distributed vs. localized) and the boundary condition (unbounded or

bounded). It was concluded by Heringa et al. (1989), that the field source was best modeled by a distributed current source along the length of the axon. The shape of the electric field was, furthermore, found to be significantly dependent upon the boundary conditions around the model. The authors recommended modeling any finite volume conductor system to the full level of complexity of the configuration actually involved.

*Models of potentials generated by multiple fibers:*

Models of a single fiber action potential (SFAP) have been used to predict recordings of compound action potentials (CAP) from whole nerves. This was done through the so called "forward model" using a linear summation of multiple SFAP's (Stegeman et al. 1979, Schoonhoven et al. 1986a, Wijesinghe et al. 1991a). This forward approach was complemented by an "inverse model", where recorded CAPs were used to estimate the size distribution of axons in a nerve (Milner et al. 1981, Stegeman and De Weerd 1982a). The same modeling approach was also used to determine the distribution of propagation velocities of axons in a peripheral nerve (Schoonhoven et al. 1988, Stegeman et al. 1988, Wijesinghe et al. 1991c). This inverse modeling has important clinical implications as a neurological diagnostic tool and has, therefore, been validated by correlation with nerve biopsy and CAP recordings from human sural nerves (Schoonhoven et al. 1987).

The location of a recording electrode relative to a potential source has been found to influence the recording of an action potential (Schoonhoven and De Weerd 1984a, Stephanova et al. 1989, Gootzen et al. 1993). Not surprisingly, maximum signal amplitude is obtained by positioning the recording electrode in close proximity to the source. On the other hand, the boundary potential created by anisotropic impedance properties of surrounding tissues cannot be controlled. Dramatic boundaries like skin to air have been shown to confine and enhance the recorded potentials. This is seen even when the electrode-to-source distance is increased when the recording point is moved from the fiber towards the skin (Schoonhoven and De Weerd 1984, Benamou et al. 1990). The authors concluded that reflections from the skin interface were the cause of the signal enhancement.

*Models of electrical stimulation:*

Although the techniques for electrically inducing nerve and muscle fiber excitation are significantly different from those for recording from these fibers, an important body of modeling literature exists on the subject of fiber stimulation and excitation. Some of these modeling techniques have been adapted for recording models.

McNeal (1976) presented a groundbreaking paper on computing the excitation threshold of a myelinated nerve fiber. This was done for stimulation pulses of finite duration, delivered by electrodes that were not in direct contact with the nerve. The model confirmed that increasing the extraneural electrical stimulation amplitude selectively excites larger diameter fibers before the smaller diameter fibers. This size selectivity was confirmed by Veltink et al. (1988a,b, 1989a,b), who used numerical simulations and experimental recordings to compare intraneural and extraneural stimulation.

Following McNeal's publication, a number of other authors addressed the intrafascicular stimulation of single axons (Altman 1988, Rattay 1989, Plonsey and Bar 1995). The original single fiber concept was expanded to bundles of variable diameter axons (Roth and Altman 1992) and generalization of stimulating electrode configurations and their location (Meier et al. 1992). Plonsey and Bar (1995) examined the transmembrane potential in an unmyelinated nerve fiber exposed to an electric field generated by a point current source at various distances (up to several centimeters). They noted that an excitable transmembrane potential can only be generated when either the electric field is nonuniform or when internal boundaries of different conductivity create a potential drop in the field.

These models are of importance in the design and implementation of intrafascicular stimulation electrodes. A related area is epidural FES of the spinal cord that may provide pain relief, alleviation of motor deficits and bladder voidance. Coburn and Sin (1985) and Coburn (1985) used a large 3-dimensional finite element analysis of the human spinal cord to simulate epidural electrical stimulation. This allowed them to test various electrode configurations important for the design of future neural prostheses. Furthermore, Struijk et al. (1992) used both a volume conductor model and a finite difference model to address the issue of electrode location with respect to nerve fiber collateral branching in the dorsal column. Their

conclusion, that branching fibers have lower excitation and blocking thresholds than unbranching fibers, is important in selecting stimulation sites for epidural FES systems.

### **Discrete numerical solution to analytical models**

Analytical models typically assume rotational symmetry along the fiber length (Lorente de Nó 1947, Patlak 1955, Rosenfalck 1969) which makes these models fairly inflexible when trying to simulate a more complex conduction medium. Such a medium includes tissue anisotropies and inhomogeneities, electrode surfaces, other axons and anatomically correctly shaped fascicles and whole nerves. The presence of inhomogeneous tissue creates internal boundaries which have been addressed by directly solving the partial differential Poisson field equations (excellent reviews of fundamental bioelectric field theory have been given by Plonsey and Bar 1988, Malmivuo and Plonsey 1995).

Generally two techniques have been used for approximating the exact analytic solution - finite element analysis (FEA) and the finite difference method (FDM). Both methods are based upon dividing the conductive medium into a computational grid of smaller sections within which the field propagation is assumed to be linear. The two methods differ in their definition of the grid geometry. The FDM is restricted to a fixed grid size, whereas FEA allows the size of each section to depend on the complexity of the conductive medium in a specific local region. For both methods, the calculation of the potential at each grid point is based upon the potentials at all neighboring grid points. An iterative procedure is used to propagate a potential through the computational grid according to the conductivity between points. Such iterative methods are referred to as relaxation of the field equations (van Rotterdam 1973, Barker et al. 1979).

The finite difference method typically divides the conducting medium into equally sized and shaped segments independent of any inhomogeneities of the medium (for an exception see Klee and Plonsey 1972). The advantage of the finite difference method is that it is more intuitive in its implementation than finite element analysis. However, it is likely to be computationally inefficient when having a detailed structure in large areas with relatively insignificant changes in conductivity. The finite element analysis compensates for this, by allowing each segment to have variable size. Regions with little change in conductivity will thus have larger segments. This reduces the number of iterations required to relax the system,

but it makes the choice of segmentation less intuitive and complicates the implementation method.

Either of the numerical approaches, FEA or FDM, allow the conducting environment to include boundaries, inhomogeneities and anisotropy. Both methods have been used for small scale 2- and 3-dimensional modeling of bioelectric fields, and as accessible computer power continues to increase, both methods are expected to be applied to larger scale models (4-dimensional).

In this thesis the finite difference method was chosen because of its intuitive implementation.

*Finite difference method:*

The finite difference method is based on an evenly spaced computational grid structure with each grid point connected to its immediate neighboring points through conductive elements. Each connecting element is assigned an impedance according to the tissue characteristics of a specific region and each grid point represents the electrical potential of a particular point in the environment. The potential at each point is calculated from a linear average of the potentials at the surrounding nodes. The electric field of the total environment can be determined by an iterative calculation of the potentials at all points of the grid-structure.

The technique described above was used by Veltink et al. (1989b) to evaluate the effect of the shape and location of a stimulating electrode in a peripheral nerve. The authors devised a numerical model of peripheral nerve sections (rat and human) by compartmentalizing intra- and extraneural volumes into equal sized wedge shaped volume elements. Each element consisted of an equilateral triangle cross-section with a side length of 20  $\mu\text{m}$  in rat or 90  $\mu\text{m}$  in human and a length (thickness) of 170  $\mu\text{m}$  in rat or 210  $\mu\text{m}$  in human. The electric potentials at the corners of each element were calculated according to the electrical resistive properties of the interconnecting tissue. These properties were made anisotropic by using three conductivity parameters according to the direction of conduction pathways within the element. Each element was assigned one of six attributes: fascicle, perineurium, epineurium, extraneural fat, blood vessel or surrounding tissue at larger distances from the nerve. Using these elements, a multi-compartment model was constructed which represented a peripheral nerve with its anisotropic and inhomogeneous properties. As described above, Veltink and coworkers

compared intraneural vs. extraneural stimulation and found that intraneural stimulation was less selective in recruiting different size axons than extraneural stimulation. This was assumed to be caused by the intraneural electrodes being in closer proximity to smaller axons than the extraneural electrode.

The finite difference method was used for calculating bio-potential fields in whole body segments (Klee and Plonsey 1972, Cunningham et al. 1986). It involved solving the 2-dimensional Poisson equation for several conductive media, represented by orthogonal conductive matrices with up to 65x100 points. The points were distributed in a "stick figure" human upper body shape, with square sections for the head, neck, torso, arms and hands. Each point was assigned a potential and current was allowed to flow between the points according to the conductivity of the medium and the constraints of the boundaries. A few points (4-8 altogether) were given generator characteristics of either a potential source or a sink. The current flow between and around these points and the potential field created was estimated by repeated recalculations of the potentials at each grid point. Multiple iterations ( $10^4$ ) were required before the solution relaxed. This relaxed solution described a stationary potential field and the calculations were repeated for other current source configurations. The final field solution was used to model the 'stationary' potential field distribution throughout whole body segments (Cunningham et al. 1986). The source of the field was assumed to be somatosensory propagation from a finger conducting through wrist, arm, shoulder, chest, neck and head. The authors were specifically trying to model changes in this 'stationary' potential ('far-field') due to the influence of different boundary conditions, such as narrow wrist and neck sections.

### **Formalism**

Given the complexity of an analytical model addressing the above questions, a numerical finite difference method was selected. It was used to model a single unit interface between an individual axon in a conductive environment of extracellular fluid including neighboring axons and a recording electrode. The model was restricted to two spatial dimensions and one time dimension.

***DEFINITION OF THE CONDUCTIVE UNIVERSE***

The conductive universe was scaled to model the space surrounding a given length of an individual axon. Dimensions of the universe were based upon the expected dimensions of the electric field around the central axon. The minimum length was therefore determined by the spatial extent of an action potential in a large myelinated axon - approximately 10 mm. In a similar manner, the width was determined by the inter axonal space surrounding the axons which is less than 10  $\mu\text{m}$  for myelinated mammalian peripheral nerve. Given the three-dimensional structure of a peripheral axon bundle, electric fields were expected to be distributed beyond the minimal inter axonal space. The width of the universe was therefore chosen to be 20  $\mu\text{m}$  on either side of a modeled axon (10  $\mu\text{m}$  in diameter, plus 5-6  $\mu\text{m}$  myelination). The conductive universe had a total dimension of 10 mm by 50  $\mu\text{m}$ .

The universe was designed with three different internal elements, as illustrated in Figure VII.1:

1. A myelinated axon was running the full length of the universe, positioned centrally with respect to the width of the universe. In special cases simulating the enclosure of the central axon, other axons were positioned at both of the long edges of the universe.
2. Current generating sources distributed discretely along the length of the myelinated axon simulated nodes of Ranvier. Given an anatomical inter-nodal spacing of approximately 1mm for large myelinated axons, 10 source points along each membrane were included.
3. An electrode interface region included a conductive surface material and insulating dielectric material.

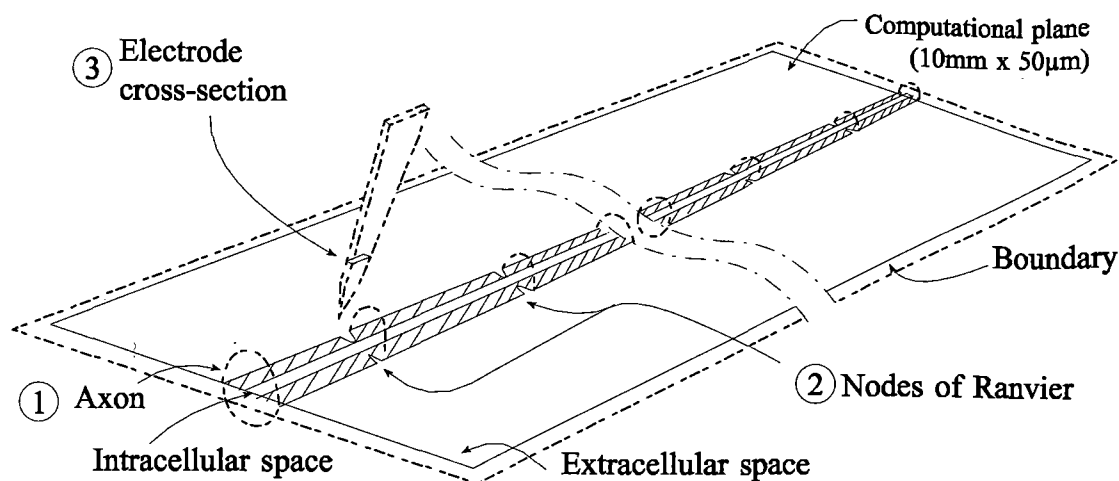


Figure VII.1: Sketch of the conductive universe. Three elements were included: 1) A myelinated axon, 2) current generating sources and 3) an electrode interface. The total universe was enclosed by a boundary region.

In addition to these 3 elements, an all important edge region also had to be modeled. This boundary region, along the edges of the universe, characterized the numerical horizon of the universe. Two possible boundary conditions were tested, either restricting the potential build up inside the universe - "grounded boundary" - or allowing it to accumulate freely - "floating boundary" - (see *Boundary specifications* below).

In the discrete implementation of the above universe, evenly spaced potential nodes distributed throughout the model were connected with conductive elements between neighboring nodes (Figure VII.2.A). Potentials were allowed to propagate through the connecting elements according to their conductivity characteristics. These characteristics were determined by the tissue properties of a particular local section of the modeled environment. Connecting elements representing insulating material, like the myelin sheet, were thus assigned low conductivity characteristics, while elements representing intra- or extracellular fluid were highly conductive. Values for the electrical parameters of the physiological components in the modeled environment were based on values reported in previous literature (Tasaki 1955, Schwan and Calvin 1956, 1957, Geddes and Baker 1967, Marks and Loeb 1976, McNeal 1976, Andreassen and Rosenfalck 1981, Veltink et al. 1988b, Veltink et al. 1989b, Rattay 1989, Wijesinghe et al. 1991b, Meier et al. 1992, Roth and Altman 1992, Frijns and ten Kate 1994, Goodall et al. 1995)



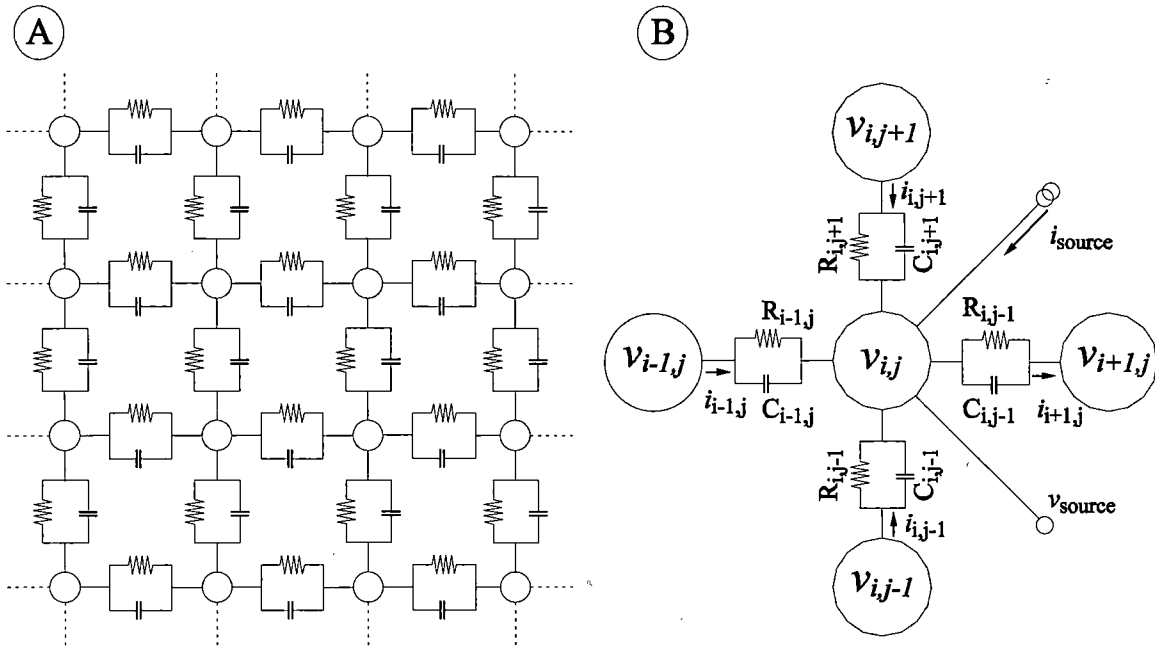


Figure VII.2: Electric grid-point model of the “conductive universe”. (A) Each point in the grid was attached to four neighboring nodes through conductive elements. (B) The conductive elements consisted of a resistive and a capacitive component. A few selected points had an additional constant current source ( $i_{source}$ ) or constant voltage source ( $v_{source}$ ) attached to simulate nodes of Ranvier or ground electrodes.

The spatial resolution of the model was determined by the grid size of the discrete implementation. To be able to describe a potential distribution around a single node of Ranvier a resolution of approximately  $1\ \mu\text{m}$  was required. This fine resolution dictated a discrete universe dimension of  $10^4$  by 50 grid-points to model a 1 mm by  $50\ \mu\text{m}$  environment.

Each grid-point represented the numerical value for the electric potential at that point. Transfer of charge between neighboring nodes was done through resistive elements, except in the areas where capacitive conduction was necessary. These elements were implemented in a grid-structure of parallel resistive (R) and capacitive (C) elements (Figure VII.2). Throughout the grid, most of the capacitive elements were set to zero capacitance due to the non-capacitive nature of extra- and intracellular tissue and fluid. The discrete implementation of axon, current sources and electrode interface was done exclusively with these parallel RC elements.

### AXON MODEL

In the 2-dimensional environment, a single axon was modeled as two parallel myelin barriers as if the neuron had been split longitudinally. This created an intracellular conductive section

between the barriers, flanked by insulating myelination and surrounded by extracellular conductive fluid. Up to three axons were included in the modeled universe, always with one located along the central longitudinal axis. Two other axons were occasionally included at the edge of the conductive environment to simulate neighboring axons.

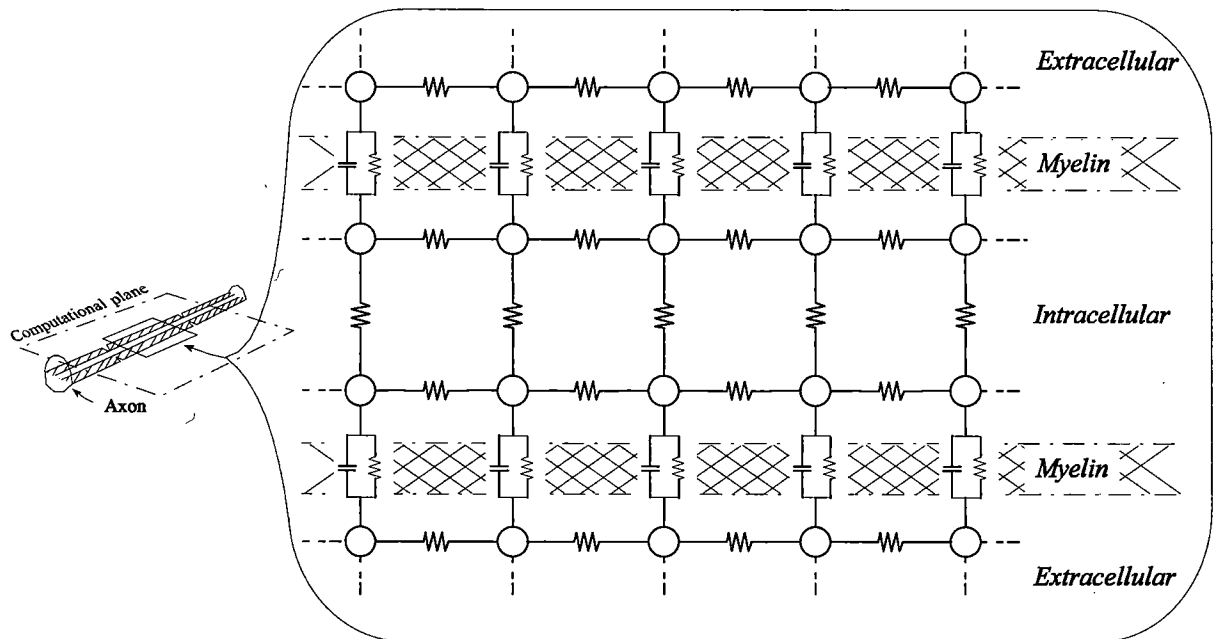


Figure VII.3: Discrete axon model. The myelin separation between intra and extracellular potentials was modeled as mainly a capacitive conductor ( $C_m = 1.4 \text{ nF} \cdot \mu\text{m}^{-1}$ ,  $\sigma_m = 3 \cdot 10^{-6} \Omega^{-1} \text{m}^{-1}$ ). The intra- and extracellular fluids were assigned purely resistive properties ( $\sigma_i = 1.1 \Omega^{-1} \text{m}^{-1}$ ,  $\sigma_e = 0.33 \Omega^{-1} \text{m}^{-1}$ ).

Although real axons do not run straight through a fascicle (Zachary 1993), modeled axons are generally represented by straight lines in the computational universe (see Xiao 1995 for an exception). This assumption creates a symmetric electric field pattern on either side of the axon, provided that no electrode or other inhomogeneous structures are present.

The inside diameter of each axon was set to  $10 \mu\text{m}$ , with a  $5 \mu\text{m}$  myelin wall on either side. At  $1 \text{mm}$  longitudinal intervals, nodes of Ranvier were introduced into the myelin wall by constricting the sheathing thickness to  $1 \mu\text{m}$ . Both the intra and extracellular fluids were assigned high conductivity properties whereas the myelin sheet was assigned low conductivity. Capacitive properties were distributed mainly in the myelin along the length of the axon.

*NEURAL CURRENT SOURCE MODEL*

The nodes of Ranvier were modeled as constant current generators located every 1 mm along the myelin barrier. The model of each node was split in two, one for each of the two myelin barriers (Figure VII.4).

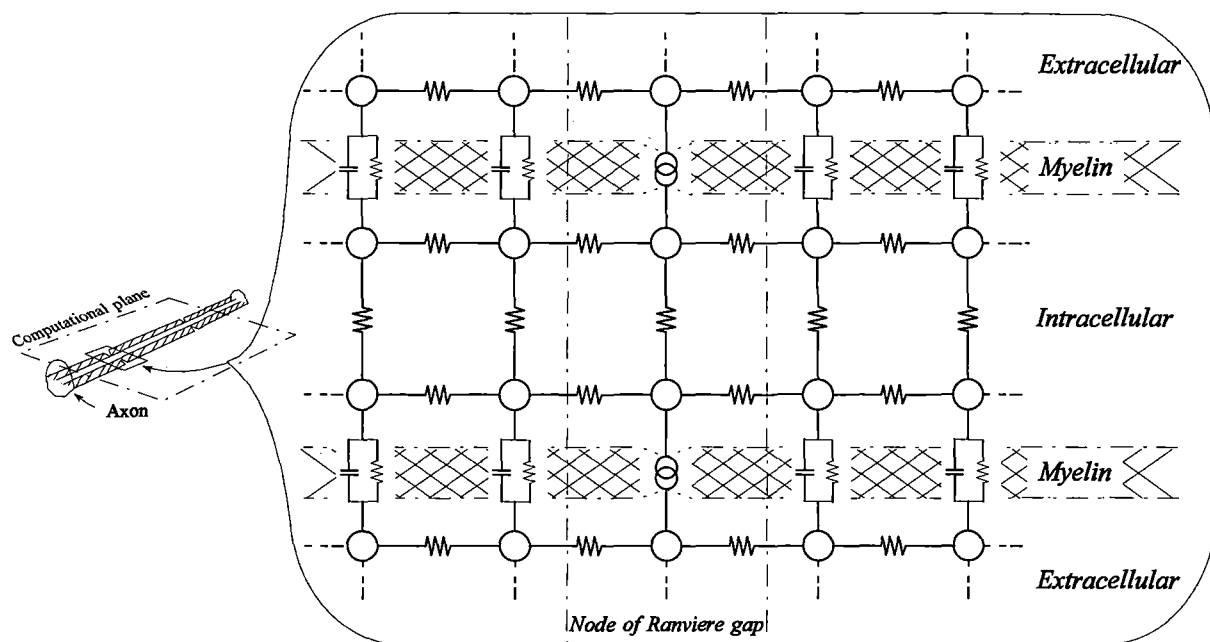


Figure VII.4: Discrete implementation of nodes of Ranvier. Each node of Ranvier was modeled as current "pumps" across the myelin barriers (two pumps shown in figure). Each pump consisted of two current generators, one on either side of the myelin. The generators were linked so that one was a source and the other an equal and opposite sink.

Cross-barrier charge transfer was simulated by positioning a generator on either side of each barrier. These generators were linked internally so that one acted as a source on one side of the barrier and the other as an equal amplitude sink on the other side. This created an intracellular potential relative to the extracellular environment.

The total model of each node of Ranvier thus consisted of four generators, two positioned immediately adjacent to the myelin membranes on the intracellular side and, two on either extracellular side. The combination of several nodes of Ranvier created a set of distributed current generators. Each of these was assigned amplitude values according to the second derivative of the transmembrane potential as derived by Lorente de N6 (1947) (Figure VII.5).

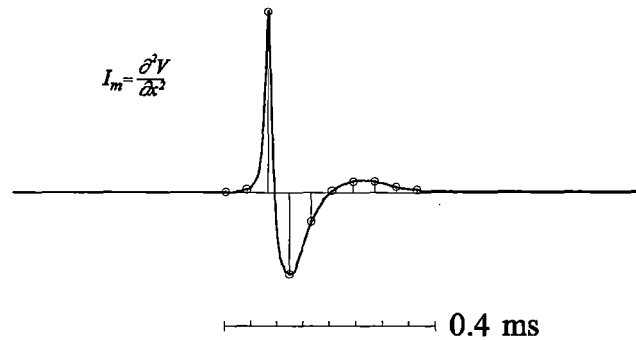


Figure VII.5: Transmembrane current flow based upon the second derivative of the transmembrane potential (adapted from Lorente de N6 1947). The original data was recorded from a bullfrog sciatic nerve at an unspecified temperature. Its duration was changed from 2.1ms to 0.4 ms to match characteristics of mammalian nerve fibers at 37 °C. This was in accordance with methods used by Barker et al. (1979) and Heringa et al. (1982). The amplitude was scaled to 6 nA<sub>pp</sub> (Marks and Loeb 1976).

Distributing the current generators along the length of the axon creates a "stationary" action potential, i.e. a potential field frozen in time. A propagating action potential was simulated by shifting the stationary transmembrane current profile along the longitudinal axis of the axon. In this manner, all current generators were assigned amplitude values according to their location along the profile sketched above (Figure VII.5)

The shift was done in discrete time steps, creating a series of "frames" of the electric field generated during the propagation of an action potential. The calculation of this electric field in each frame was dependent upon both, the present location of the current generators and on the potentials present in the previous time frame. The connection to the previous time frame was established through the existence of capacitive elements in the modeled environment.

### **BOUNDARY SPECIFICATIONS**

The extent of the electrical field around an axon is naturally limited by internal boundaries, such as the non-conducting myelin of neighboring axons, epi-, endo- and perineurial tissue and ultimately the skin-to-air interfaces. Furthermore, by the nature of attenuation in the surrounding tissue, the field strength is rapidly reduced as the distance to the source is increased. The region of significant electrical field strength around a peripheral axon is thus very limited, and the dimensions of the discrete conductive universe was chosen accordingly (see above section on *Definition of the conductive universe*).

However, a finite discrete universe is limited in its spatial extent and minute computational errors are bound to occur at the boundary edges. These errors accumulate easily, especially when using iterative solution methods, and the computational artifact produced can generate very significant errors in the derived electric field. It was thus necessary to select boundary conditions very carefully. Several options were available, as described by Panescu et al. (1994):

1. The outer perimeter potentials can be set to zero, effectively creating a "grounded" boundary with current flowing freely across it. Fixing the boundary potential at zero is a special case of the *Dirichlet boundary condition*, where potentials along the boundary are specified as a function of time. A system of discrete partial differential equations with Dirichlet boundary conditions is solvable, but it does not mimic the "infinite" universe very well.
2. The outer perimeter potentials can be set to match the potentials of the inner perimeter. With equal potentials on either side of the boundary, no current was flowing across the edge. This kind of a boundary potential is "floating" according to the fields generated by any current sources inside the bounded domain. The condition is termed the *Neumann condition*, which formally states that the potential gradient perpendicular to the boundary is set to zero. The solution to discrete partial differential equations with the Neumann boundary condition is not as trivial as for the Dirichlet condition, given that there are fewer equations than unknowns. To compensate for this an additional system constraint is required, that specifies that the net current flow across the boundary is zero (i.e. the total amplitude of all current sources is equal to the amplitude of all current sinks present within the boundary).

There are other possible boundary conditions (Press et al. 1988, Mascagni 1989, Saad 1996) most of which are aimed at mimicking an infinite computational universe under certain restrictive conditions. Within the scope of this thesis only the above two mentioned boundary conditions were examined.

### Solution method

In the 2-dimensional model, each computational grid point was connected to its four neighboring points through resistive and capacitive elements (Figure VII.2A). According to the superposition principle, the charge arriving at each point is the algebraic sum of the contributions of all the neighboring points. In addition, Kirchhoff's law of conservation of charge is applied to any given point so that the steady state conditions at that point do not result in any net change in charge, i.e. current flowing into the point equals the current leaving the point.

$$i_{total} = \frac{dQ_{total}}{dt} = 0 \quad (VII.1)$$

$$i_{total} = i_{i,j+1} + i_{i,j-1} + i_{i-1,j} + i_{i+1,j} + i_{source} \quad (VII.2)$$

where  $i_{i,j+1}$ ,  $i_{i,j-1}$ ,  $i_{i-1,j}$  and  $i_{i+1,j}$  denote the current flow through conductive pathways between the center point ( $i,j$ ) and its neighboring points (Figure VII.2B). In addition,  $i_{source}$  denotes the current supplied from any external sources (both constant current and constant voltage sources). These external current sources were set to zero for the majority of the points in the grid.

The current flow between two points was split into a resistive and a capacitive flow.

$$i_{total} = i_{R,i,j+1} + i_{R,i,j-1} + i_{R,i-1,j} + i_{R,i+1,j} + i_{C,i,j+1} + i_{C,i,j-1} + i_{C,i-1,j} + i_{C,i+1,j} + i_{source} \quad (VII.3)$$

The current flow through a resistive element is proportional to the voltage difference across the element:  $I_R^t = g(V_{point1}^{t-\Delta t} - V_{point2}^{t-\Delta t})$ , where  $g$  is the conductance per unit length of the interconnecting element between the two points. The superscript notation,  $t-\Delta t$ , refers to a time index, where  $\Delta t$  is the size of the discrete time step between two consecutive time frames. Assuming that the potential across the resistive element propagates instantaneously, the only parameter needed to calculate the resistive current flow at time  $t$  is the potential drop across the element at time  $t-\Delta t$ . The use of time notation has little implication for the resistive elements but it has been introduced for consistency with the description of the capacitive current flow.

The current flow through a capacitive element is proportional to the change in voltage across the element over time,  $I_C = C \frac{dV_C}{dt} \approx C \frac{V_C^t - V_C^{t-\Delta t}}{t - (t - \Delta t)}$ . Here C is the capacitance per unit length

of an interconnecting element between points across which a potential  $V_C$  changes during the time step  $\Delta t$ . The potential drop across the capacitor is given as the difference between the potentials on either side of it:  $V_C^t = V_{point1}^t - V_{point2}^t$ , (similar for  $V_C^{t-\Delta t}$ ). Current flow through a

capacitive element is thereby given as:  $I_C^t = C \left( \frac{V_{point1}^t - V_{point2}^t}{\Delta t} - \frac{V_{point1}^{t-\Delta t} - V_{point2}^{t-\Delta t}}{\Delta t} \right)$ .

Inserting  $I_R^t$  and  $I_C^t$  in equation VII.3 gives:

$$\begin{aligned}
 0 = & g_{i,j+1} \frac{v_{i,j+1}^{t-\Delta t} - v_{i,j}^{t-\Delta t}}{\Delta j} + g_{i,j-1} \frac{v_{i,j-1}^{t-\Delta t} - v_{i,j}^{t-\Delta t}}{\Delta j} + g_{i-1,j} \frac{v_{i-1,j}^{t-\Delta t} - v_{i,j}^{t-\Delta t}}{\Delta i} + g_{i+1,j} \frac{v_{i+1,j}^{t-\Delta t} - v_{i,j}^{t-\Delta t}}{\Delta i} \\
 & + C_{i,j+1} \left( \frac{v_{i,j+1}^t - v_{i,j}^t}{\Delta t} - \frac{v_{i,j+1}^{t-\Delta t} - v_{i,j}^{t-\Delta t}}{\Delta t} \right) + C_{i,j-1} \left( \frac{v_{i,j-1}^t - v_{i,j}^t}{\Delta t} - \frac{v_{i,j-1}^{t-\Delta t} - v_{i,j}^{t-\Delta t}}{\Delta t} \right) \\
 & + C_{i-1,j} \left( \frac{v_{i+1,j}^t - v_{i,j}^t}{\Delta t} - \frac{v_{i+1,j}^{t-\Delta t} - v_{i,j}^{t-\Delta t}}{\Delta t} \right) + C_{i+1,j} \left( \frac{v_{i+1,j}^t - v_{i,j}^t}{\Delta t} - \frac{v_{i+1,j}^{t-\Delta t} - v_{i,j}^{t-\Delta t}}{\Delta t} \right) + i_{source}^t
 \end{aligned} \tag{VII.4}$$

This equation is discrete in one time dimension with an interval step of  $\Delta t$ , and discrete in two space dimensions with interval steps of  $\Delta i$  and  $\Delta j$ . The two latter dimensions are given by the mesh structure of the model and are per definition set to be equal and at unity. These are therefore eliminated from the equation.

The variable of interest in equation VII.4 is the new potential  $v^t$  at point  $i,j$ . To solve for this variable, equation VII.4 is rearranged as follows:

$$\begin{aligned}
 0 = & (g_{i,j+1} + \frac{C_{i,j+1}}{\Delta t}) v_{i,j+1}^{t-\Delta t} + (g_{i,j-1} + \frac{C_{i,j-1}}{\Delta t}) v_{i,j-1}^{t-\Delta t} + (g_{i-1,j} + \frac{C_{i-1,j}}{\Delta t}) v_{i-1,j}^{t-\Delta t} + (g_{i+1,j} + \frac{C_{i+1,j}}{\Delta t}) v_{i+1,j}^{t-\Delta t} \\
 & - \left( \frac{C_{i,j+1} + C_{i,j-1} + C_{i-1,j} + C_{i+1,j}}{\Delta t} + g_{i,j+1} + g_{i,j-1} + g_{i-1,j} + g_{i+1,j} \right) v_{i,j}^{t-\Delta t} \\
 & - \frac{C_{i,j+1}}{\Delta t} v_{i,j+1}^t - \frac{C_{i,j-1}}{\Delta t} v_{i,j-1}^t - \frac{C_{i-1,j}}{\Delta t} v_{i-1,j}^t - \frac{C_{i+1,j}}{\Delta t} v_{i+1,j}^t \\
 & + \frac{C_{i,j+1} + C_{i,j-1} + C_{i-1,j} + C_{i+1,j}}{\Delta t} v_{i,j}^t + i_{source}^t
 \end{aligned} \tag{VII.5}$$

It is seen that the future potential  $v^t$  in a given point  $(i,j)$ , is dependent upon the future potential of its four neighboring points,  $v^t$  at points  $(i,j+1)$ ,  $(i,j-1)$ ,  $(i+1,j)$  and  $(i-1,j)$ , and on past potentials,  $v^{t-\Delta t}$  at points  $(i,j)$ ,  $(i,j+1)$ ,  $(i,j-1)$ ,  $(i-1,j)$  and  $(i+1,j)$ . When isolating for  $v^t$  at point  $(i,j)$ , an equation of 5 unknowns appear, assuming that the initial potential field condition,  $v^{t-\Delta t}$ , is known for all points.

The potential at each point of the computational grid can thus be derived from equation VII.5 when all equations from all grid points are combined. This creates a system of  $n \times m$  interconnected equations for a computational environment of  $n \times m$  grid points. Specifying a Dirichlet boundary condition, a total of  $n \times m$  unknowns make the system solvable. For a Neumann boundary condition, however, a total of  $n \times m + 2(n+m)$  unknowns exist, where the additional  $2(n+m)$  unknowns originate from deriving the boundary potentials from the potentials along the circumference points of the universe. This Neumann system is solvable under the condition of no net current flow across the boundary.

The total system of equations can be represented as matrices, with the independent variable matrices  $v^{t-\Delta t}$ ,  $v^t$  and  $i_{source}^t$ , and with two system matrices, **A** and **B**, containing all coefficients of the equations.

$$0 = \overline{\overline{\mathbf{A}}} \cdot \overline{\overline{v^t}} + \overline{\overline{\mathbf{B}}} \cdot \overline{\overline{v^{t-\Delta t}}} + \overline{\overline{i_{source}^t}} \quad (\text{VII.6})$$

Each row in the system matrices **A** and **B** contain the coefficients linking one grid point to its neighbors. Based on the equation for the system (eq.VII.5), it is seen that a maximum of 5 non-zero entries exist in each row of the system matrices. This underlines the fact, that only the four neighboring grid points and the grid point itself affect the future value of a specific grid point.

Solving a system of equations for a  $n \times m$  universe requires that each row of the system matrices contains  $n \times m$  elements, i.e., entries for all grid points. The total size of the system matrices is thus  $(n \times m)^2$  elements. For the  $10^4$  by 50 grid structure sketched above, this comes to a total of  $250 \cdot 10^9$  elements ! Fortunately, the majority of these elements are zero so sparse matrix solution methods can be utilized (Saad 1996).



When organizing the column vectors of  $v^{t-\Delta t}$ ,  $v^t$  and  $i_{source}^t$  in a *natural* order, a unique pattern arises in the **B** system matrix. A natural order is obtained by sequencing all elements according to their location in the grid structure. The first element is a corner point and points are added to the sequence row by row. The resulting system matrix is similar to that found when solving a second order elliptic equation like *Poisson's* or *Laplace's* equations and the sparse system matrix is generally termed "tridiagonal with fringes" (Press et al. 1988).

Equation VII.6 is a discrete representation of a partial differential equation and it can be solved either through a direct method or through an iterative approach. The direct method was tested and found not to converge for the specific scaling of matrices **A** and **B** used here. An iterative method, *Quasi-Minimal Residual Method*, was instead selected. This method attempts to solve the system of linear equations by iterating from an initial guess which by default is an all zero vector. (see Saad 1996 for further details on effective methods for solving partial differential equations with sparse matrices).

Given that the discrete iterative method was used to approximate an exact solution, it was found important to specify which criteria indicated a satisfactory solution. These criteria were summarized by Mascagni (1989):

*Consistency:* A numerical solution method is considered consistent when it solves a discrete problem that is consistent with a desired continuous problem. For the finite difference methods this is tested by applying the exact solution to the difference equations. In this case only a small approximation error should occur. This definition is very similar to that of convergence except it is only valid for a single solution point, not necessarily everywhere in the time-space universe.

*Stability:* A method is considered stable if the solution remains bounded as grid dimensions go to zero. There may be several levels of stability depending on other grid parameters.

*Convergence:* A solution is converging if an error between the numerical solution and the exact solution can be made as small as desired (i.e. numerical and exact solution differ by a term that goes to zero as  $\Delta t$ ,  $\Delta j$  and  $\Delta i$  go to zero). Convergence is the most strict requirement for partial differential equation solution methods. It demands that the numerical and exact

solution differ by an arbitrarily small amount at every point in space and time. The finite difference method for a linear partial differential equation is convergent if and only if it is both consistent and stable (Lax equivalence theorem).

### IMPLEMENTATION

The model was coded in a general matrix manipulation program ('Matlab' from Mathworks Inc.) to provide a relatively fast and very flexible implementation. In this environment all variables were stored as matrices and all numerical manipulations were done using matrix operators.

The implementation was tested for a series of simple conditions where the field distribution was either known or easily predicted. Three major components were tested: 1) combinations of current sources and sinks, 2) resistive elements and 3) capacitive elements.

#### *Test of monopole source:*

The field strength of the potential generated by a single source in a purely resistive homogeneous and isotropic environment is inversely proportional to the distance from the source generator (Plonsey and Barr 1988). This was tested for both the floating and the grounded boundary environment (Figure VII.6).

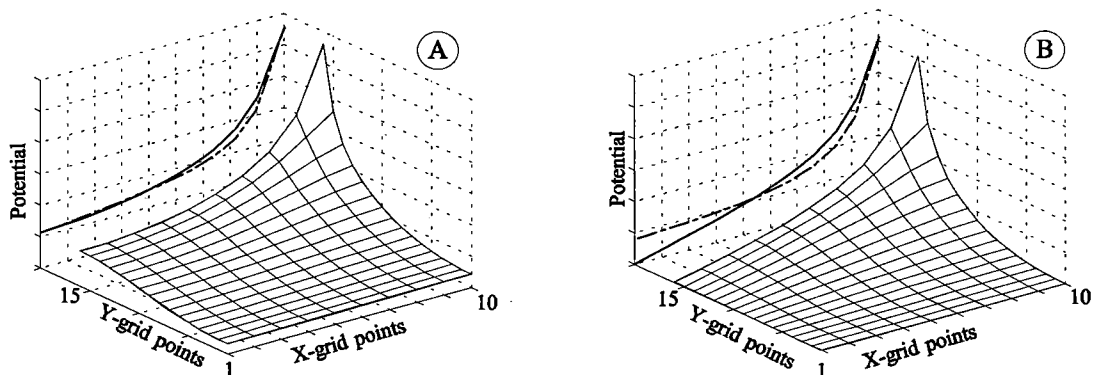


Figure VII.6: Test of monopole source. A single source was positioned in a homogenous, isotropic environment with either floating boundaries (A) or grounded boundaries (B). The source was located at grid point (10,16) of a 31 by 31 grid point mesh (only  $\frac{1}{4}$  of the total mesh is shown). The left rear wall of each plot shows a projection of the centerline profile of the potential distribution. The inverse of the distance to the source is shown for comparison (dash-dotted line).

between the generators is expected to be highly influenced by the characteristics of the resistive barrier. This was tested by increasing the resistance between the source and sink in the above model (*Test of double source*). The "resistive barrier" ran perpendicular to the intense inter-generator current flow (Figure VII.8).

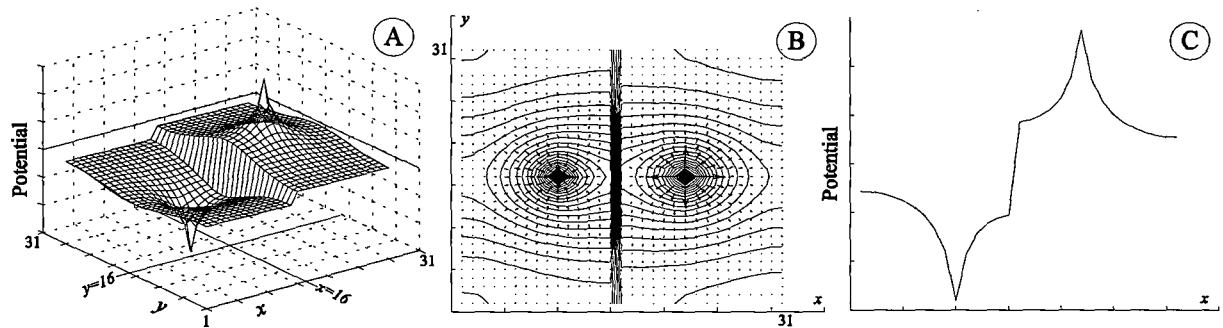


Figure VII.8: Test of resistive barrier. (A) An insulating "barrier" was inserted between a source (21,16) and a sink (10,16). The barrier separated grid points at the center of the universe ( $x=15$  and  $x=16$ ) along the full length of the  $y$ -axis and the barrier was assigned a fraction of the conductivity of the surrounding environment ( $50 \cdot 10^{-9} \Omega^{-1} \text{m}^{-1}$  and  $0.5 \Omega^{-1} \text{m}^{-1}$  respectively). (B) The barrier was anisotropic, obstructing current flow in the  $x$ -direction only. Given the uneven distribution of resistance, the total environment became inhomogeneous. (C) The potential along the center line of the environment ( $y=16$ ) showed a relatively large drop across the barrier.

The barrier divided the environment in two sections, one containing a current source and the other a current sink. Given that the barrier was somewhat conductive, the potential distribution and generator configuration in the two sections still affected one another (Figure VII.8.A-B). As expected, the potential change across the barrier was more pronounced than in the lower resistance surrounding environment (Figure VII.8.C)

#### *Test of leaky resistive barrier:*

Current flowing along a myelinated axon will cross the myelin sheet at the least resistive regions (Nodes of Ranvier). These crossings become hot-spots with a high current density in their vicinity. This was tested by weakening the barrier described above at two discrete points. The resistance of these points was set to that of the surrounding environment. The barrier was thus capable of conducting current in the  $x$ -direction through these "channels" (Figure VII.9).

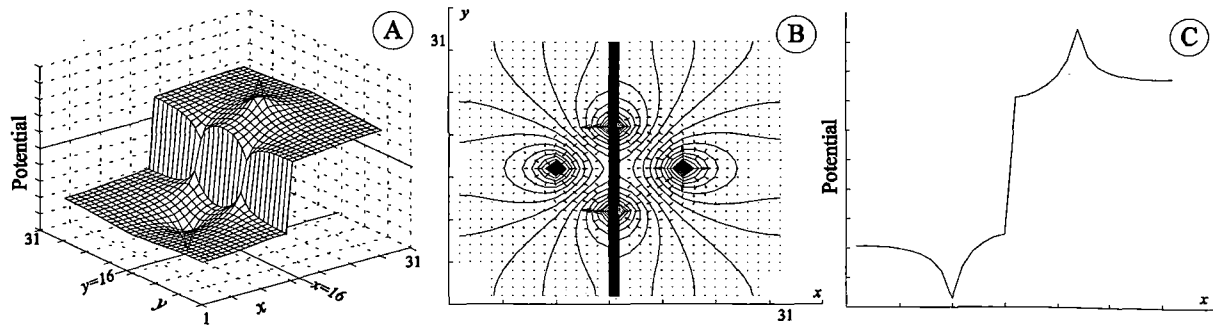


Figure VII.9: Test of leaky resistive barrier. (A) A "leaky" resistive barrier was inserted between a source and a sink. Two points along the barrier were assigned conductance equal to that of the surrounding environment ( $0.5 \Omega^{-1}\text{m}^{-1}$ ). (B) The barrier was anisotropic, obstructing current flow in the  $x$ -direction only. Given the uneven distribution of resistance, the total environment became inhomogeneous. (C) As seen above (Figure VII.8.C), the potential drop at the center line of the environment ( $y=16$ ) showed a large potential drop across the barrier.

The leaky barrier allowed current to flow from the higher source potential region to the lower sink region (Figure VII.9.A). This created anticipated high current density around the leakage points (Figure VII.9.B) while the centerline potential (Figure VII.9.C) remained relatively unchanged from the non-leaking simulation.

#### *Test of charging capacitive barrier:*

The axon membrane and its myelination act as electrical insulators between the conductive intra- and extracellular environments. This gives the axon capacitive properties distributed along the length of the axon. Local regions, such as the nodes of Ranvier, can have a relatively high capacitance given the very limited charge separation distance (few nm across a cell membrane).

To model this capacitance, elements with charge accumulating properties were included as inter-point conductors. These capacitive elements were tested by inserting a capacitive "barrier" between two current generators (Figure VII.10.A) in a similar fashion as the resistive barrier was inserted above. The capacitors were initially completely discharged.

The simulation confirmed that the capacitive elements were charged maximally for the potential difference across them (Figure VII.11.A). This created a predicted current flow through the elements (Figure VII.11.B), shaping the potential field very similarly to that of non-obstructed double source test (Figure VII.7.B). As anticipated, the potential drop across the charged capacitive elements was not affected by the fully charged barrier (Figure VII.11.C).

*Test of discharging capacitive elements:*

A charged axon membrane acts as a current limited source generator when discharged. Given the relatively small surface area of the axon and its myelination, only a very limited total amount of charge can be delivered. The discharge occurs when the forced potential field is reduced below the level of the voltage drop across the charged capacitor. This was tested by removing the current source and sink and recalculating the potential field of the above model (*Test of charging capacitive barrier*).

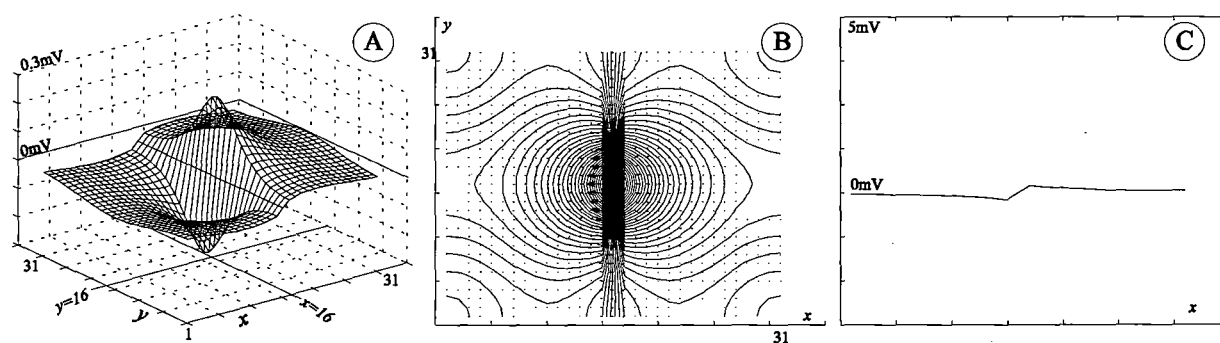


Figure VII.12: Test of discharging capacitive elements. (A) The capacitive elements (located as above) divided the environment in two sections. The potential field in these sections were generated by the charged capacitors, and the patterns in the two sections were mirrored and had opposite polarity. (Note the change in scale compared to the above "charging" plots, Figure VII.10 and Figure VII.11). (B) The charged elements created a current flow pattern as if a single source and sink had been present in very close proximity around the center point of the environment. (C) The potential drop along the center line showed a discharge amplitude related to the maximum charge accumulated in the capacitors (shown for comparison on the same scale as the previous capacitor test plots, Figure VII.10 and Figure VII.11).

It was anticipated that the discharge of the capacitive elements would create a current source and sink at either end of the capacitor. The simulation confirmed this (Figure VII.12.A-B) and showed a small amplitude potential drop across the capacitors (Figure VII.12.C).

Similar to the charging procedures seen above (*Test of charging capacitive barrier*), discharging the capacitive elements required repeated recalculations of the potential field.

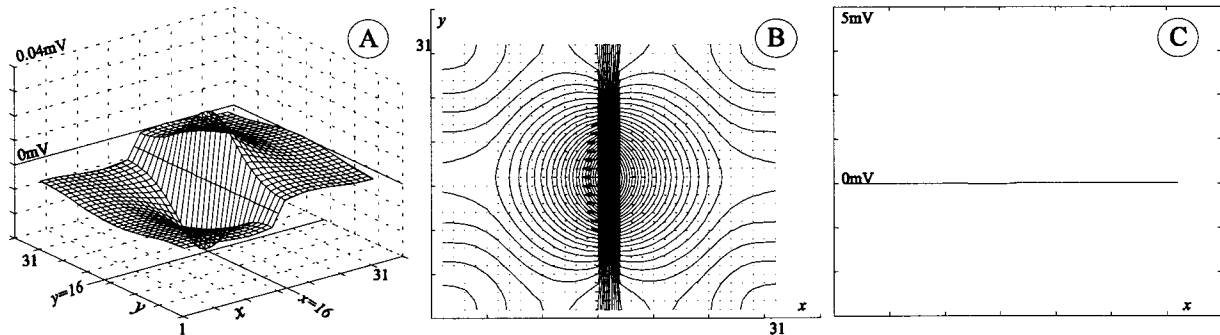


Figure VII.13: Continued test of discharging capacitive elements. (A) Capacitive elements in the center of the environment (located as above) were nearly completely discharged. (Note the change in scale compared to Figure VII.12). (B) The charged elements created a current flow pattern as if a single source and sink generator had been present in very close proximity around the center point of the environment. (C) The potential drop along the center line showed a minimal discharge amplitude (shown for comparison on the same scale as the previous capacitor test plots).

With continued recalculation of the potential field, without the presence of external current generators, the voltage drop across the capacitors eventually diminished (Figure VII.13.C). This confirmed that the capacitive elements were being discharged. The timing of this depended on the capacitor size, amount of charge accumulated and the impedance of the environment into which it is discharged.

To finalize the tests on the capacitive elements the potential at a single point next to the capacitors anode was plotted (Figure VII.14).

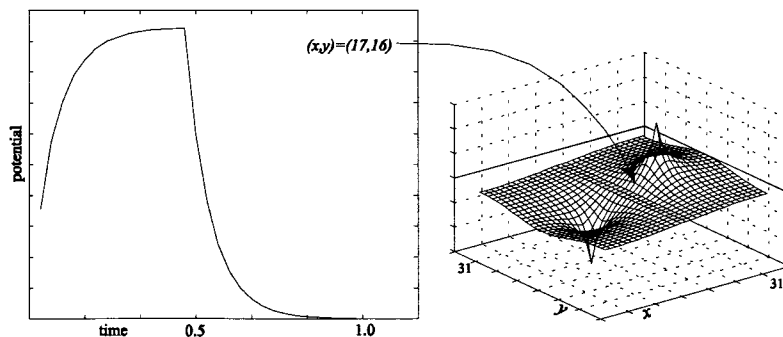


Figure VII.14: Potential characteristics of a single point in the computational grid. Initially the external current generators created a source and a sink on either side of the point as described in *Test of charging capacitive barrier*. The external source was removed at time=0.5, and the environment was left to relax. The capacitive elements discharged during this second half of the simulation as described in *Test of discharging capacitive elements*. A total of 60 iterations was performed.

This test revealed the typical characteristics of a capacitive element being charged and then discharged.

### THE INTERFACE SITE, ITS CABELING AND PREAMPLIFICATION

The recording site of an extracellular microelectrode with a metal surface has in general been modeled as a circuit of parallel resistive ( $R_E$ ) and capacitive ( $C_E$ ) elements serially connected to a resistive component ( $R_{elect}$ ) (Figure VII.15) (Robinson 1968, Geddes 1972). A resistive component ( $R_S$ ) is added because of tissue resistance between the recording site and the biological source. Furthermore, the impedance of leadout cables ( $R_{Cooner}$ ,  $R_{Co.Shunt}$ ,  $C_{Co.Shunt}$ ) and front end amplifier ( $Z_{in}$ ) loads the recording electrode.

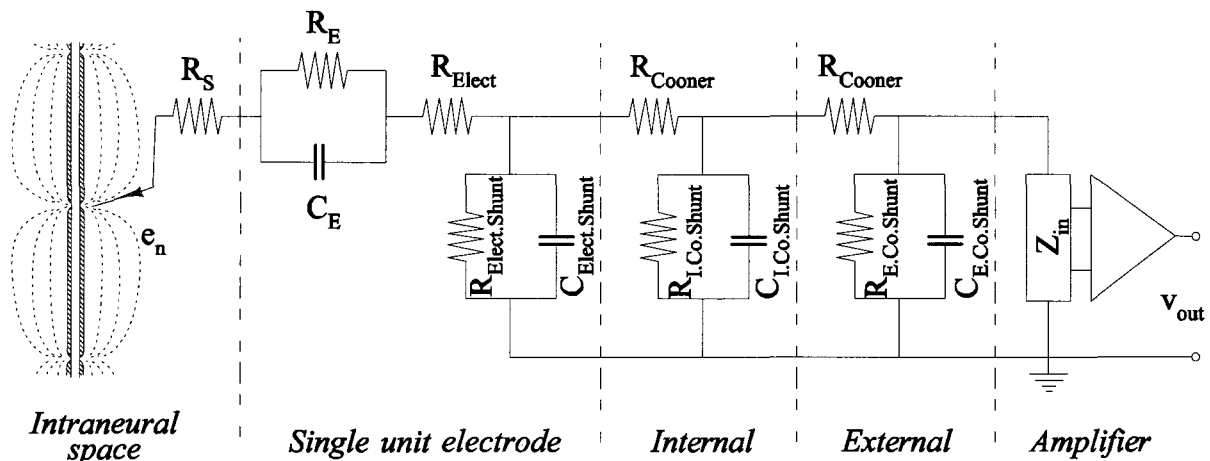


Figure VII.15: The equivalent circuit of a metal microelectrode, lead-out cables and front end amplifier. The electrical field,  $e_n$  generated by nodes of Ranvier along a peripheral nerve, propagates through an extracellular medium with a distributed spreading resistance  $R_S$ .  $R_E$  and  $C_E$  represent the impedance of the electrochemical interface between metal surface and extracellular fluid.  $R_{Elect}$  represent the resistance through the electrode conductors be it fine wire or polysilicon.  $R_{Elect,Shunt}$  and  $C_{Elect,Shunt}$  represent the shunt impedance from the microelectrode conductor to the extracellular fluid.  $R_{cooner}$  represents the resistance of the Cooner lead wire.  $R_{I,Co,Shunt}$  and  $C_{I,Co,Shunt}$  are the shunt resistance and capacitance of the Cooner lead wire running along internal pathways, i.e. surrounded by conductive saline fluid.  $R_{E,Co,Shunt}$  and  $C_{E,Co,Shunt}$  are the shunt resistance and capacitance of the Cooner lead wire running external with air around the cable.  $Z_{in}$  is the amplifier input impedance.

To adapt this model to a finite difference environment certain simplifications were needed.

$R_S$

The resistance of the extracellular medium depends on the size of the exposed electrode surface and on the electrical characteristics of the conductive medium around the electrode. In

the PNS, a highly anisotropic medium, electric fields are generated by a predominantly longitudinal neural current flow. The shape of this flow is determined by the insulating myelin sheet of neighboring axons and support tissue (epi-, endo- and perineurium). In the CNS, current flow is, in a similar manner, defined by the insulating glia cells. Robinson (1968) estimated that the majority (92%) of the extracellular current flow was concentrated in the capillary space between these cells (Figure VII.16).

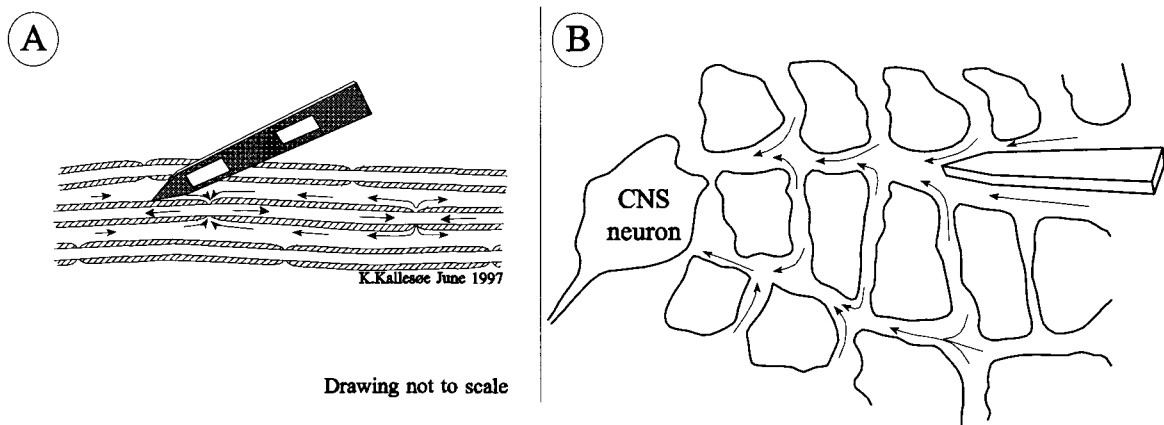


Figure VII.16: Assumed extracellular current pathways in neural tissue. (A) extracellular current flow in the myelinated PNS (solid arrows) is restricted by the myelination of neighboring axons. The tissue as a whole therefore exhibits anisotropic conduction properties:  $\sim 0.5 \Omega^{-1}\text{m}^{-1}$  in the longitudinal direction,  $\sim 0.08 \Omega^{-1}\text{m}^{-1}$  in the transverse direction (Clark and Plonsey 1968, Marks and Loeb 1976). (B) The extracellular current pathways in CNS structures are determined by micro clefts between glia cells (fibrous astrocytes sketched here. Adapted from BeMent et al. 1986).

The estimate of the conductive pathway resistance in the medium was based upon the electric characteristics of the extracellular fluid (Robinson 1968). A minimum value of this estimate was found by assuming that the total electrode surface was shaped as a sphere with radius  $r_e$ , located in an infinite homogeneous medium of resistivity  $\rho$ :

$$R_S = \int_{r_e}^{\infty} dR_S = \int_{r_e}^{\infty} \rho \frac{1}{4\pi r^2} dr = \frac{\rho}{4\pi r_e} \quad (\text{VII.7})$$

For an electrode with a surface area of approximately  $400 \mu\text{m}^2$ , ( $r_e \approx 8 \mu\text{m}$ ), and a resistivity of the extracellular fluid of  $\rho = 2 \Omega\text{m}$ , the distributed medium resistance is  $20 \text{k}\Omega$ . This is considered negligible in comparison to the electric properties of typical high impedance electrochemical interface sites ( $R_E \gg 20 \text{k}\Omega$ ).



The spreading resistance plays an important role in determining the dynamics of the electric field around multiple current generators (nodes of Ranvier). In the numerical modeling presented here, the distributed extracellular resistance was included as resistive elements between computational nodes (see preceding section on the topography of the conductive universe).

#### $R_E$ and $C_E$

When a metal surface is immersed in an electrolyte solution, chemical surface reactions create an immediate chemical transfer of charge on both sides of the electrochemical interface. The charge buildup creates an opposite directed electric gradient and the interface site establishes an equilibrium potential. The electrochemistry behind this goes beyond the scope of the thesis (further details on iridium oxide surfaces are found in Trasatti 1980). Basically, the charge transferred across the interface is trapped on either side of the site and forms a so called electric double layer (Robinson 1968, Geddes 1972, Albery 1975). This electric layer effectively constitutes an electrolyte capacitor.

The impedance of an oxidized  $400 \mu\text{m}^2$  iridium site measured, with a vector impedance meter, was found to be in the order of  $R_E = 300 \text{ k}\Omega - 400 \text{ k}\Omega$  and  $C_E = 250 \text{ pF} - 300 \text{ pF}$ , at 1 kHz.

#### $R_{\text{Elect}}$

The resistive value of a specific conductor depends on the width, the length and the thickness of the polysilicon ( $R = 10 \Omega \cdot \text{Length/Width}$ ). The conductive polysilicon traces on the probe designs had an internal sheet resistance of  $10 \Omega$  per square (The "per square" unit assumes a standard sheet thickness, i.e. a  $2 \mu\text{m}$  wide conductor running a length of 3 mm would have  $3 \text{ mm} / 2 \mu\text{m} = 1500$  squares, with an impedance of  $15 \text{ k}\Omega$ ). A conservative estimate of the present PSU design shows that this resistance ( $\sim 28 \text{ k}\Omega$ ) was fairly insignificant compared to that of the electrochemical interface ( $300 \text{ k} - 400 \text{ k}\Omega$ ). This value was found as the sum of the resistance along the entire probe, including: conductors on the tip section: approximately  $5 \text{ k}\Omega$  for  $2 \mu\text{m}$  wide by 1 mm long; conductors on the flexible cable plus the forceps handling platform: approximately  $21 \text{ k}\Omega$  for  $5 \mu\text{m}$  wide by 10.5 mm long; and conductors on the bonding platform: approximately  $2.5 \text{ k}\Omega$  for  $20 \mu\text{m}$  wide by 5 mm long. These resistive values

could be lowered by an order of a magnitude if the polysilicon would be replaced by aluminum or gold conductors.

$R_{\text{Elect.Shunt}}$  and  $C_{\text{Elect.Shunt}}$

Given the insulating properties of the dielectric layer, the shunt impedance was dominated by the parasitic capacitance (i.e.  $R_{\text{Elect.Shunt}} \approx \infty \Omega$ ). This shunt capacitance from the polysilicon conductors through the upper and lower dielectric layer was given as the product of the layers effective dielectric constant and the area of the conductor,

$$C_{\text{Elect.Shunt}} = 2 \cdot 4.025 \cdot 10^{-9} \text{ F cm}^{-2} \cdot \text{Area}$$

The effective dielectric constant is dependent upon the thickness of the dielectric and the factor 2 is included to account for both the upper and the lower parasitic capacitance. Given the dimensions above for the PSU silicon probe designs, a shunt capacitance ( $C_{\text{Elect.Shunt}}$ ) of 4.4 pF was computed.

$R_{\text{cooner}}$

The Cooner lead wire had an internal series resistance of  $150 \Omega \cdot \text{m}^{-1}$ . For each recording site approximately 30-50 cm of wire was used to bring the recorded signal from the sciatic cuff to an external amplifier connected to the cat's backpack connector. A conservative estimate of the total Cooner wire resistance for one channel was set at  $75 \Omega$ , which was negligible compared to both the internal resistance of the polysilicon and especially the electrochemical interface.

$R_{\text{I.Co.Shunt}}$  and  $C_{\text{I.Co.Shunt}}$ ,  $R_{\text{E.Co.Shunt}}$  and  $C_{\text{E.Co.Shunt}}$

Given the insulating properties of Teflon coating along any length of Cooner wire, shunt impedance was predominantly determined by a parasitic capacitance (i.e.  $R_{\text{I.Co.Shunt}} \approx \infty \Omega$  and  $R_{\text{E.Co.Shunt}} \approx \infty \Omega$ ). The capacitance depended on the conductivity of the medium surrounding the wire insulation. In the present setup any extraneural fluid was considered as ground. For the Cooner wire length outside the skin, from the subcutaneous exit hole to the backpack PC board, the shunt capacitance was negligible due to the low conductivity of air ( $C_{\text{E.Co.Shunt}} = 0\text{F}$ ). The parasitic capacitance of Cooner wire running inside the body was expressed as the capacitance of a coaxial cylinder of length  $l$ ,

$$C_{Cooner} = \frac{2 \pi \epsilon l}{\ln\left(\frac{r_1}{r_2}\right)}; \quad \epsilon = \epsilon_0 \epsilon_r; \quad \epsilon_0 = 8.854 \cdot 10^{-12} \text{ C}^2 \text{ N}^{-1} \text{ m}^{-2} \quad (\text{VII.8})$$

where  $r_1$  and  $r_2$  were the inner and the outer radii of the Teflon insulation and  $\epsilon_r$  was the relative permittivity of Teflon ( $\epsilon_r \cong 2.0-2.2$  at 1 MHz). Cooner 631 wire with four layers of Teflon coating was used for all single unit electrodes. The total diameter of the coating was 279  $\mu\text{m}$  ( $r_2$ ) with an inner diameter of 102  $\mu\text{m}$  ( $r_1$ ). This gave a theoretical parasitic leakage capacitance of 122  $\text{pF} \cdot \text{m}^{-1}$  ( $C_{I.Co.Shunt}$ ), a value confirmed over a large range of frequencies using a vector impedance meter (Table VII.1).

	Frequency [Hz]										
	159	500	1 k	1.59 k	5 k	10 k	15.9 k	50 k	100 k	159 k	500 k
Z [ $\Omega$ ]	8.00M	2.55M	1.27M	0.80M	0.26M	0.13M	80.0 k	25.5 k	12.7 k	8.0 k	2.6 k
$\angle$ [ $^\circ$ ]	-90	-90	-90	-90	-90	-90	-90	-90	-90	-90	-90
C [pF]	125	125	125	125	125	125	125	125	125	125	125

Table VII.1: Measurement of the shunt capacitance from a 1m Cooner 631 wire submerged in saline. An HP4800A vector impedance meter was used to measure the real component and the phase angle of an impedance load at selected test frequencies.

As mentioned above, each single unit recording electrode site was attached to approximately 30-50 cm of Cooner 631 lead wire, most of which was running internally. A conservative estimate of this Cooner wire capacitance was set at 60 pF.

$Z_{in}$ : Each input channel was attached to a front-end amplifier with a high input impedance ( $R_{in}=10^{12} \Omega$ ,  $C_{in}=5 \text{ pF}$ ).

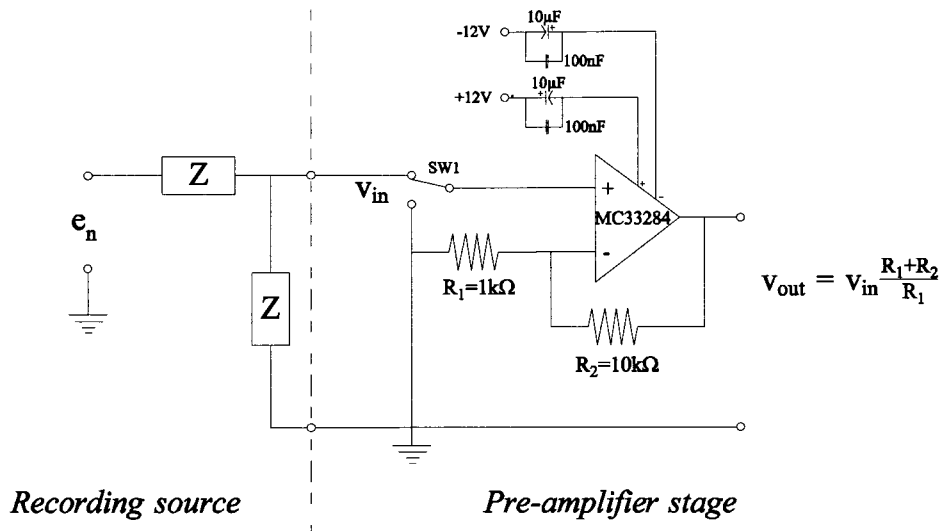


Figure VII.17: Preamplifier stage. An 8-channel preamplifier stage was incorporated onto a flexible ribbon cable connected to the backpack. The stage was based on two quadruple channel MC33284 JFET input operational amplifiers. Each channel was arranged in a non-inverting configuration with a gain factor of 11 (20.8db). Individual switches (SW1) allowed separate grounding of each input channel. The amplifiers were supplied from  $\pm 12$ V batteries, decoupled through noise reduction capacitors.

The input resistance of the preamplifier stage was negligible compared to the shunt impedance of the Cooner wire.

#### *Simplified circuitry of the interface site, its cabling and pre-amplification*

The above simplifications were used to reduce the electrode-cabling-amplifier model of Figure VII.15, to a circuit with essentially two components: 1) An electrochemical interface impedance consisting of a resistive and a capacitive component, and 2) a parasitic shunt capacitance (Figure VII.18). The shunt capacitance originated from a distributed arrangement of leakage along the silicon probe, along the Cooner wires and through the amplifier stage.

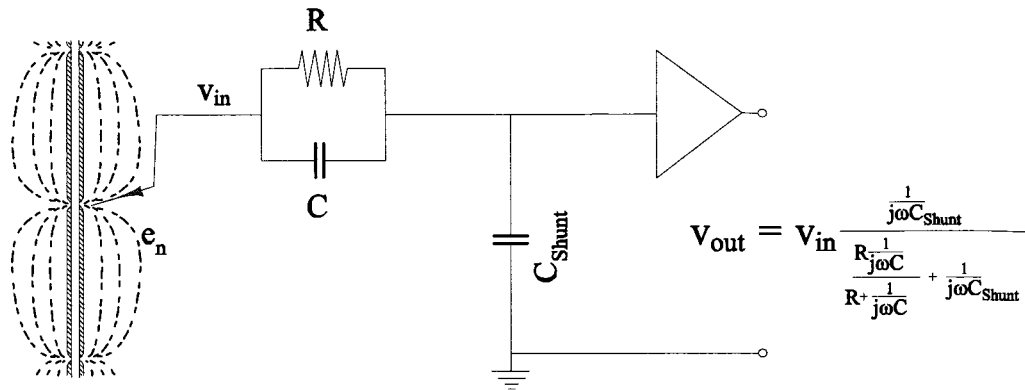


Figure VII.18: Simplified equivalent circuitry.  $R = R_S + R_E + R_{Elect} + R_{cooner} \approx R_E \approx 375 \text{ k}\Omega$ ;  $C = C_E \approx 275 \text{ pF}$ ;  $C_{Shunt} = C_{SiShunt} + C_{E.Co.Shunt} + C_{I.Co.Shunt} + C_{in} \approx 65 \text{ pF}$ .

Given the values derived above, a total attenuation factor of 0.930 was found (-0.6db) at 1 kHz (-1.8 db at 10 kHz). If the Cooner wire had not been contributing shunt capacitance ( $C_{shunt} \approx 5 \text{ pF}$ ), an attenuation factor of 0.995 would have been in effect (-0.05 db). Had there been approximately double the length of Cooner wire inside the body ( $\sim 70 \text{ cm}$ ), the attenuation would have been -0.88db, again at 1kHz.

#### *Finite difference implementation of the interface site, its cabling and pre-amplification*

The silicon based interface site was implemented in the finite difference model across 4 elements: 1) The electrochemical interface site, 2) The iridium conductor, 3) The capacitive shunt along conductors, 4) The silicon substrate (Figure VII.19).

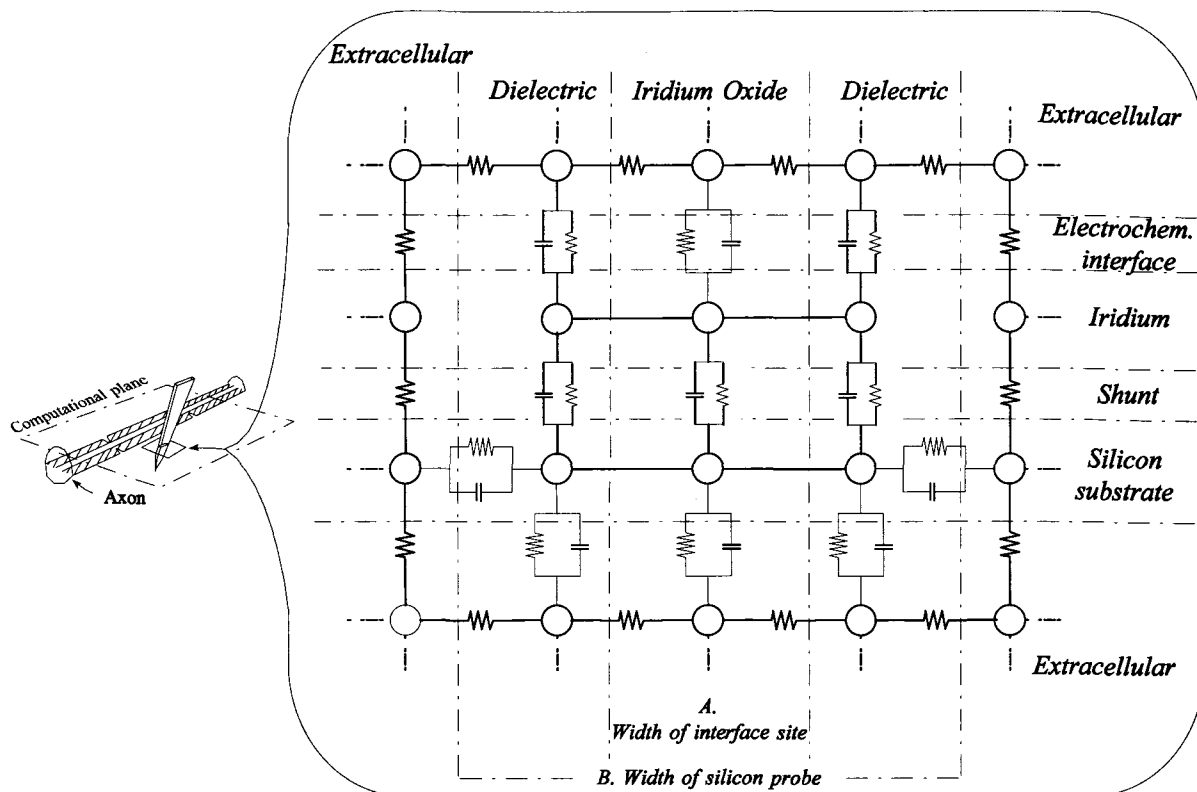


Figure VII.19: The finite difference implementation of the recording interface site, its cabling and pre-amplification. The mesh represents a cross section of the silicon probe as shown in the insert.

1. *Electrochemical interface layer.* The iridium oxide connected the iridium layer to the extracellular space through the above derived interface impedance ( $R$  and  $C$ ). At the neighboring computational points, at the edge of the silicon probe, dielectric layers created a shunt capacitive connection to the iridium ( $C_{Elecet.Shunt} = 4.4$  pF).
2. *Iridium.* The points representing the potential of the iridium were interconnected with zero resistance. The edges of the probe were isolated from the extracellular space given the very thin dimensions of the conductor.
3. *Shunt.* The parasitic shunt capacitance connected the iridium to the silicon substrate with the capacitance derived above ( $C_{shunt}$ ).
4. *Silicon substrate.* The points representing the silicon substrate were interconnected with zero resistance. The impedance of the substrate connection to extracellular fluid was estimated from impedance measurements of recording sites with substrate shorts

( $\sim 5.5 \text{ k}\Omega \angle -80^\circ$ ). It was found that the silicon substrate created a highly capacitive connection to the extracellular fluid ( $R_{sub} = 35 \text{ k}\Omega$ ,  $C_{sub} = 28 \text{ nF}$ ).

The implementation sketched in Figure VII.19 depicts a probe with a recording site width of one potential point (the *Iridium Oxide* column). Depending on the scaling of the mesh, this width was adjusted by adding more *Iridium Oxide* columns.

### **Simulated action potentials**

A series of simulations were performed:

1. Stationary potential along an unmyelinated fiber in both an unbound and a bounded environment.
2. Stationary potential along a myelinated fiber
3. Dynamic potential along a myelinated fiber

Some of the simulations were done in a more coarse grid structure than was originally planned. This was done to make it feasible to perform the calculations within reasonable time (hours instead of days for each simulation run). A typical grid structure was chosen as 50x100 grid points, giving a longitudinal resolution of 100 $\mu\text{m}$ .

#### ***STATIONARY POTENTIAL ALONG UNMYELINATED FIBER***

Initial simulations were done to derive the instantaneous, or "stationary" field generated by an action potentials. This implied that the conductive universe was assumed to be purely resistive, i.e. all capacitive components were neglected, an assumption generally made in the literature (e.g. pp. 136, Malmivuo and Plonsey 1995, Plonsey and Heppner 1967). The assumption builds on the fact that, in body tissue, electric field conduction near the speed of light creates a minimal field wave length for a 10 kHz single fiber action potential of approximately  $10^4 \text{ m}$  (Nielsen 1989). This far exceeds the space constants of any naturally occurring capacitive-resistive couplings in the environment.

For these initial simulations, the conductive universe comprised a single axon, dividing the environment into an intra and two extracellular regions. This allowed for the calculation of the

potential field generated by a single unmyelinated axon in an unbounded inhomogeneous environment. The unmyelinated axon membrane was modeled with distributed current generators along its entire length. For a single axon extending through a 100 grid point universe, a total of 400 constant current generators were included (100 pairs along each membrane section). Figure VII.20 shows the potential field and current density along such an axon.

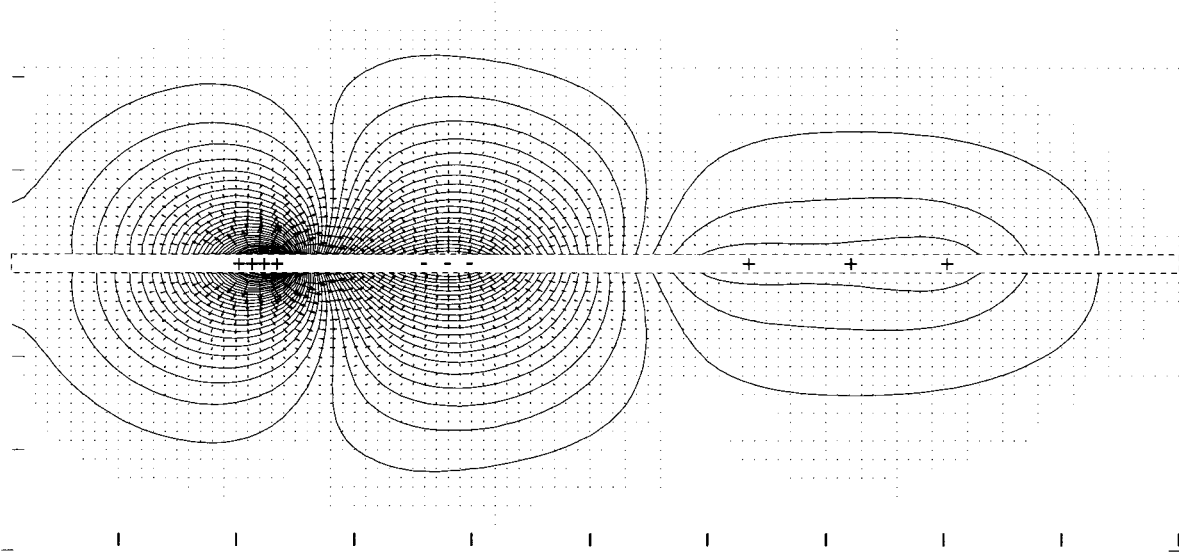


Figure VII.20: Stationary extracellular fields around an unmyelinated fiber in an unbounded environment. The stationary potential field is shown for an action potential ready to propagate from right to left. The conductive universe was assumed quasistatic, i.e. there was no capacitive effect in either the tissue or the conductive fluid. 400 constant current generators were distributed along the length of the two membranes. Each pair of generators was assigned output amplitudes according to the transmembrane current flow presented in Figure VII.5. The simulation was done with floating boundary conditions.

The potential field showed a characteristic positive frontal wave front followed by a hyperpolarizing negative section and a final and smaller positive repolarizing section. Although not identical to analytically derived potential maps, the general structure of the field was in accordance with maps presented in the literature (pp. 2826, Heringa et al. 1989). The current density map showed an intense current flow from the frontal positive section back to the hyperpolarized mid section. In addition, a weaker forward directed current originated from the repolarizing rear section flowing towards the hyperpolarized mid section.



It was expected that the potential field would be strongest close to the membrane and would diminish rapidly with increasing distance from the axon. This was verified by plotting the potential amplitudes along sections parallel to the axon (Figure VII.21).

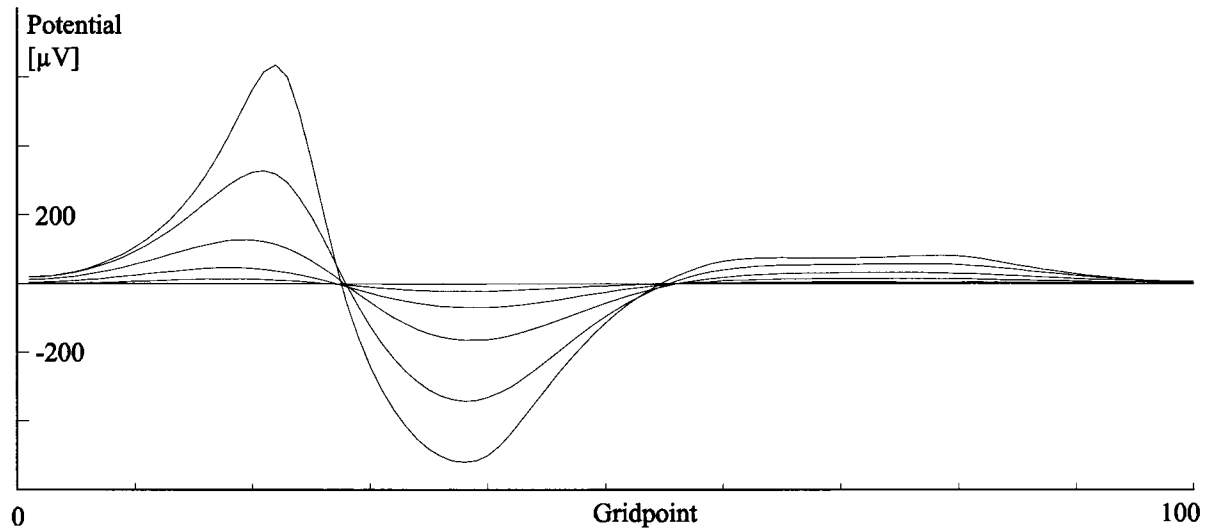


Figure VII.21: Extracellular potentials along an unmyelinated axon in an unbounded environment. Six longitudinal sections parallel to the axon gave a "time portrait" of the extracellular potential at various distances from the axon membrane (same data as used for Figure VII.20). The potentials were sampled at  $5\mu\text{m}$  intervals starting at  $5\mu\text{m}$  from the axon membrane. The largest potential amplitudes were found closest to the membrane.

A realistic model of a single axon inside a fascicle should include the boundaries created by neighboring axon membranes and their myelin sheaths. The presence of these intrafascicular boundaries creates an inhomogeneous conductive environment, potentially distorting the generated field. Two extremes of this environment were simulated, - one with an infinite unbounded environment (seen above) and one with a bounded environment. The bounded environment was simulated by aligning two neighboring fibers along the central axon (Figure VII.22).

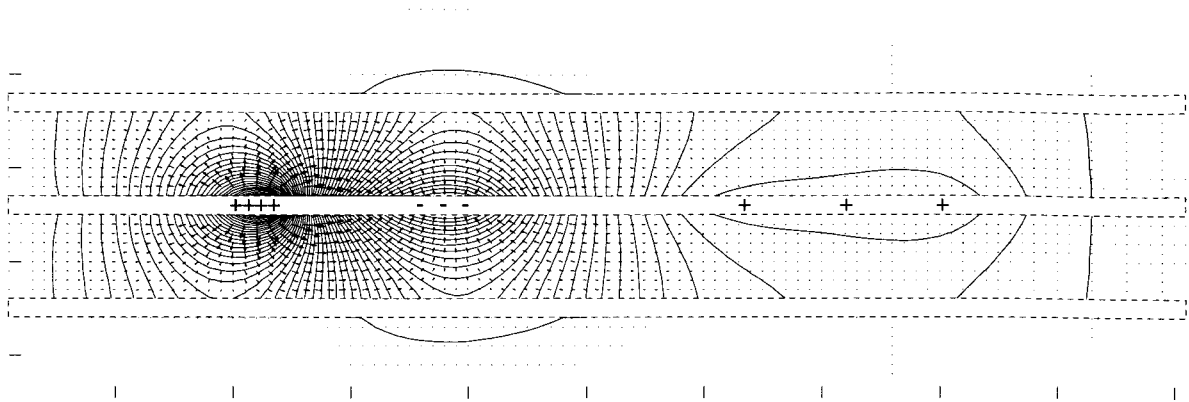


Figure VII.22: Stationary extracellular fields around an unmyelinated fiber in a bounded environment. The action potential is stationary ready to propagate from right to left. The conductive universe is considered quasistatic, i.e. there is no capacitive effect in either the tissue or the conductive fluid. The field was generated with a current source configuration identical to that used in Figure VII.20.

The potential field in the bounded environment showed a distribution close to the axon similar to that seen in the unbounded situation (Figure VII.20). Further away, however, the field characteristics changed significantly. Beyond the boundaries, the field strength dropped, not surprisingly, to insignificant amplitudes. Within the boundaries, a generally higher amplitude was found due to the "confinement" of the potential field. This was verified by plotting the signal amplitude at various distances from the axon (Figure VII.23).

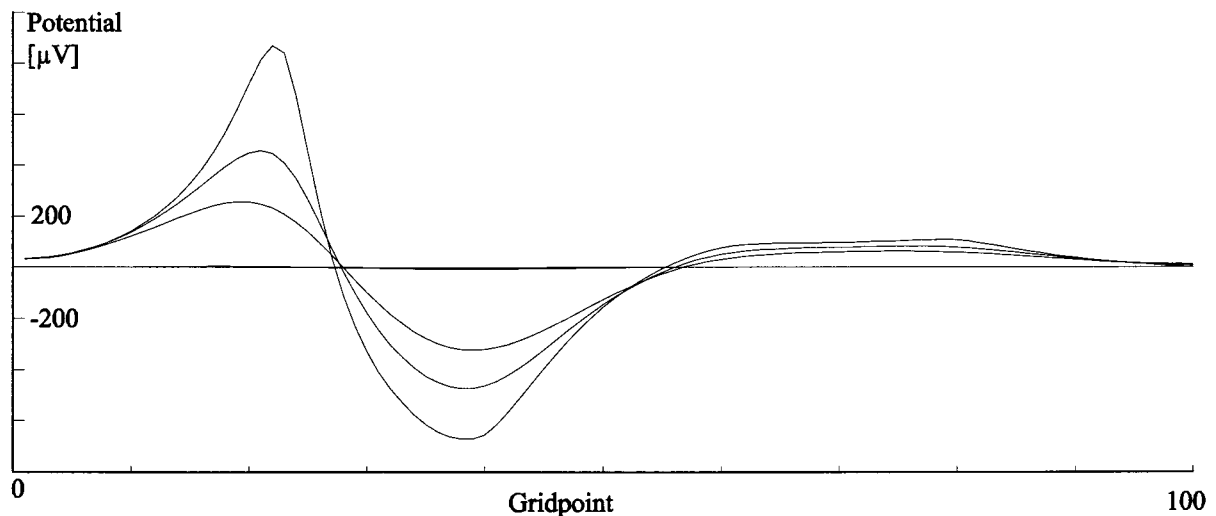


Figure VII.23: Extracellular potentials along an unmyelinated axon in a bounded environment. Four longitudinal sections parallel to the axon gave a "time portrait" of the extracellular potential at various distances from the axon membrane (same data as for Figure VII.22). The potentials were sampled at  $5\mu\text{m}$  intervals starting at  $5\mu\text{m}$  from the axon membrane. The largest potential amplitudes were found closest to the membrane.

*STATIONARY POTENTIAL ALONG MYELINATED FIBER*

Once the simulation of the potential field generated by an unmyelinated axon had been verified with analytical models, the next step was the simulation of myelinated axons. The stationary potential along a myelinated axon was simulated by distributing a limited number of constant current generators along the length of the axon membrane. These were spaced 1mm apart according to the typical anatomy of the Schwann cells and nodes of Ranvier for a  $10\mu\text{m}$  axon. The membrane sections in between the current source points were assigned conductive properties according to the electrical impedance characteristics of a myelin sheet, i.e. fairly non-conductive. As in the simulation of the unmyelinated fiber, no capacitive components were included in the simulation, given that the action potential did not propagate through the environment, hence the term stationary potential.

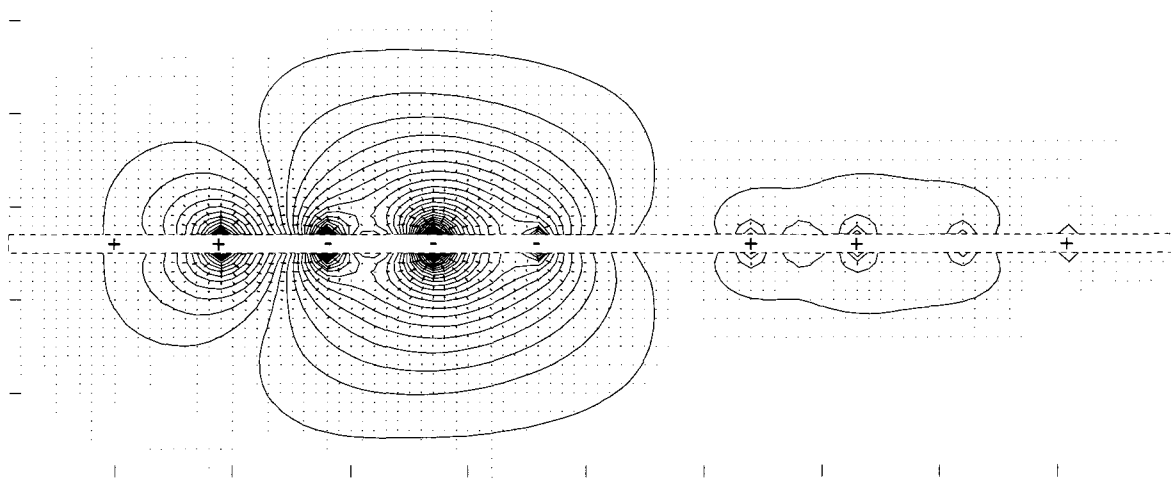


Figure VII.24: Stationary extracellular fields around a myelinated fiber in an unbounded environment. The conductive universe was assumed quasistatic. 10 simulated nodes of Ranvier were distributed along the length of the two membranes (at grid points 10,19,28,37,46,55,64,73,82 and 91).

The stationary field around a myelinated axon (Figure VII.24) shows, not surprisingly, more of a "point"-source characteristic than the unmyelinated equivalent (Figure VII.20). However, the general field pattern, especially farther away from the axon, resembled that of the pattern surrounding the unmyelinated axon. This was illustrated by plotting the potential amplitudes along sections parallel to the axon at various distances (Figure VII.25)

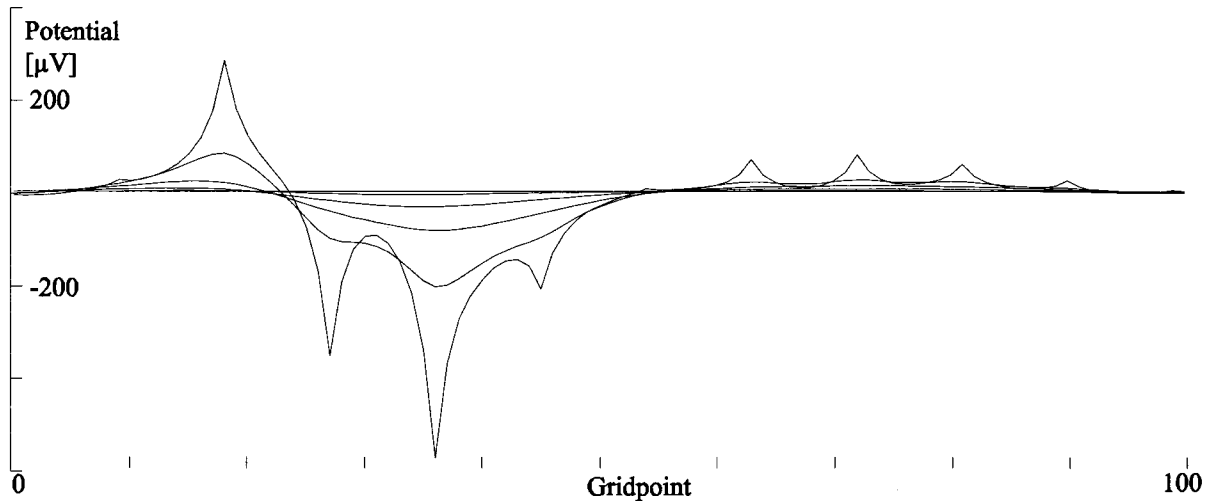


Figure VII.25: Potential amplitudes along a myelinated axon in an unbounded environment. Six longitudinal sections parallel to the axon were plotted (same data as used for Figure VII.24). The potentials were sampled at  $5 \mu\text{m}$  intervals starting at  $5 \mu\text{m}$  from the axon membrane. The largest potential amplitudes were found closest to the membrane.

#### *DYNAMIC POTENTIAL NEAR A MYELINATED FIBER*

The next step, following a simulation of a stationary potential along a myelinated axon fiber, was to estimate the field generated by a propagating potential - the "dynamic" field, which was obtained by repeated calculation of the field generated by a variable configuration of current sources. The sources were "shifted" from right to left along the axon membrane (Figure VII.26).

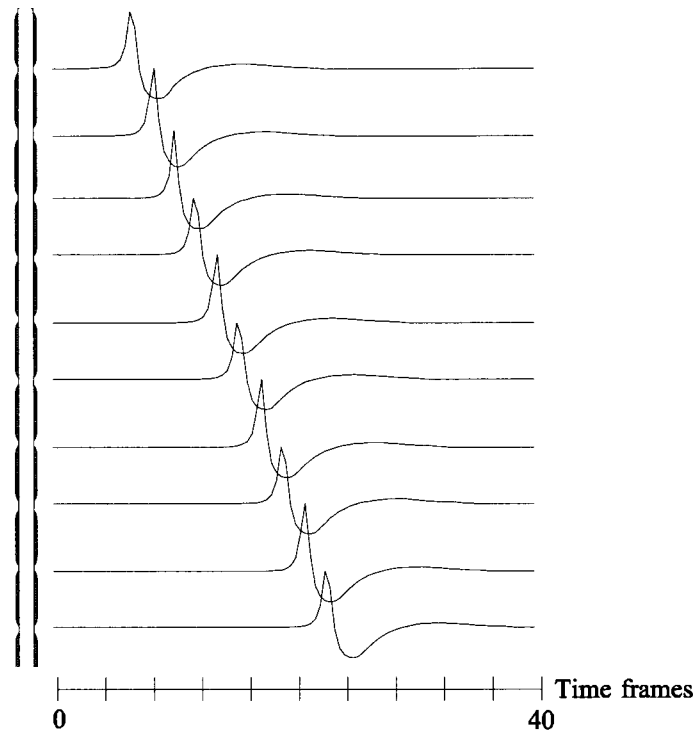


Figure VII.26: The dynamic current source configuration. The current source profile used for simulating the stationary potentials (Figure VII.5) was shifted in time to simulate the propagation of an axon potential, similar to what was done by Stegeman et al. (1987).

The dynamic potential field at any instant in time was based on both the present current source configuration and on the previous potential field distribution. In this manner, a time-history dependent potential field was derived.

For the stationary fields, the potential along the entire length of the axon was plotted as an instantaneous spatial representation of the action potential (Figure VII.20-Figure VII.25). It was necessary to use a different technique for displaying the propagating action potential, given that its dynamic field consisted of a sequence of stationary fields. The display technique was similar to inserting a recording electrode close to the axon and observing the potential at a single point as the action potential passed through the conductive universe. The electrode was either made "ideal", i.e. not disturbing the computed potential field in any way, or it was given electrode characteristic properties (Figure VII.19).

*Electrode distance from a node of Ranvier*

As the distance from an electrode to a node of Ranvier increases, it is expected that the recorded potential should decrease. This was tested by moving the recording location in two directions: perpendicular to the axon membrane at a node of Ranvier, and longitudinally along the axon while maintaining the same distance from the membrane.

Perpendicular movement of the recording site away from the membrane increased the path length between the nearest node of Ranvier and the electrode, which increased the conduction pathway impedance between them. It was, therefore, expected that the recorded potential would diminish in amplitude with increased distance (Figure VII.27).

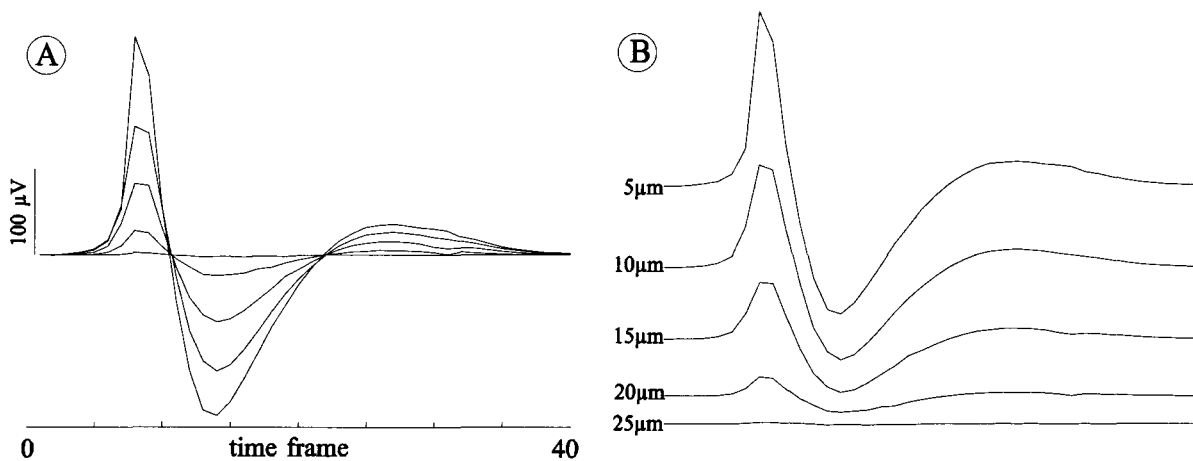


Figure VII.27: Perpendicular distance related attenuation with single point recording of a propagating action potential. A dynamic axon potential was sampled at single points at various distances from the axon (5, 10, 15 and 20  $\mu\text{m}$ ). The recording points were "ideal", i.e. they did not interfere with the field conduction and distribution throughout the environment. A total of 40 frames were computed, shifting the entire current source configuration through the conductive universe.

As expected, a triphasic signal was detected with a diminishing amplitude at increased recording distances. Compared to the peak-to-peak amplitude of an action potential recorded from the surface of the axon, a 5  $\mu\text{m}$  distance created a 7.5 dB attenuation. It is thus advantageous to minimize the distance to a node of Ranvier to record from single axons with highest possible signal amplitude, as expected. The finding also implies that a buildup of connective tissue between the electrode tip and the current generator degrades the signal amplitude, due to additional length of the conduction pathway and added tissue impedance.

Electrode movement parallel to the axon was assumed to cause changes in the recorded signal amplitude. This was tested by placing a series of "ideal" recording electrodes along the length of the axon, equidistant from the membrane, spanning from one node of Ranvier to the next (Figure VII.28).

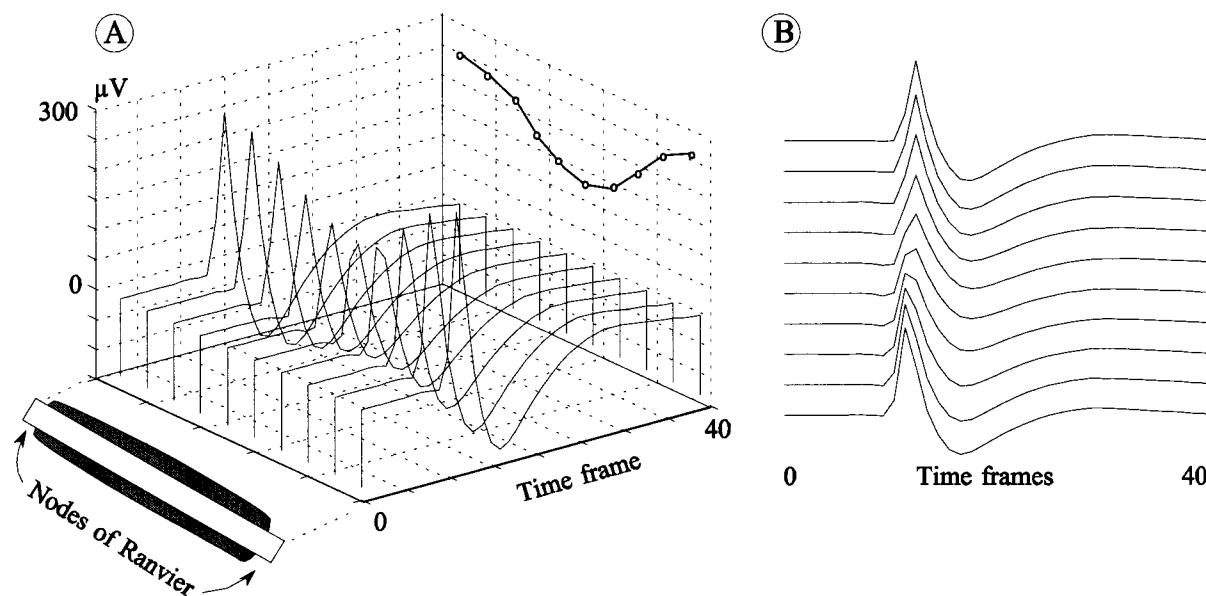


Figure VII.28: Longitudinal movement of a recording point along an axon membrane and away from a node caused attenuation in the observed potential of a propagating action potential. The potentials were recorded with an "ideal" electrode at 10 different locations between two nodes of Ranvier. All recording points were  $5\ \mu\text{m}$  from the membrane surface. The signal amplitude was found to decrease by 5.2dB ( $V_{pp}$ ) between the two nodes of Ranvier.

As expected, the potential amplitude was reduced when recording from points between the two nodes of Ranvier. This reduction was similar to that seen for perpendicular movement of the recording site.

#### *Recording electrode configuration*

In the tests described above, all recordings were done with a monopolar electrode configuration, assuming a distant indifferent reference electrode in one point the edge of the computational universe. While the monopolar recording configuration typically is the simplest *in-vivo* approach it potentially contaminates the recording with unwanted fields picked up by the reference electrode. A common way of eliminating this, is to use a differential recording

technique in which two recording sites are exposed to similar background noise. This technique was simulated by subtracting two monopolar recordings (Figure VII.29).

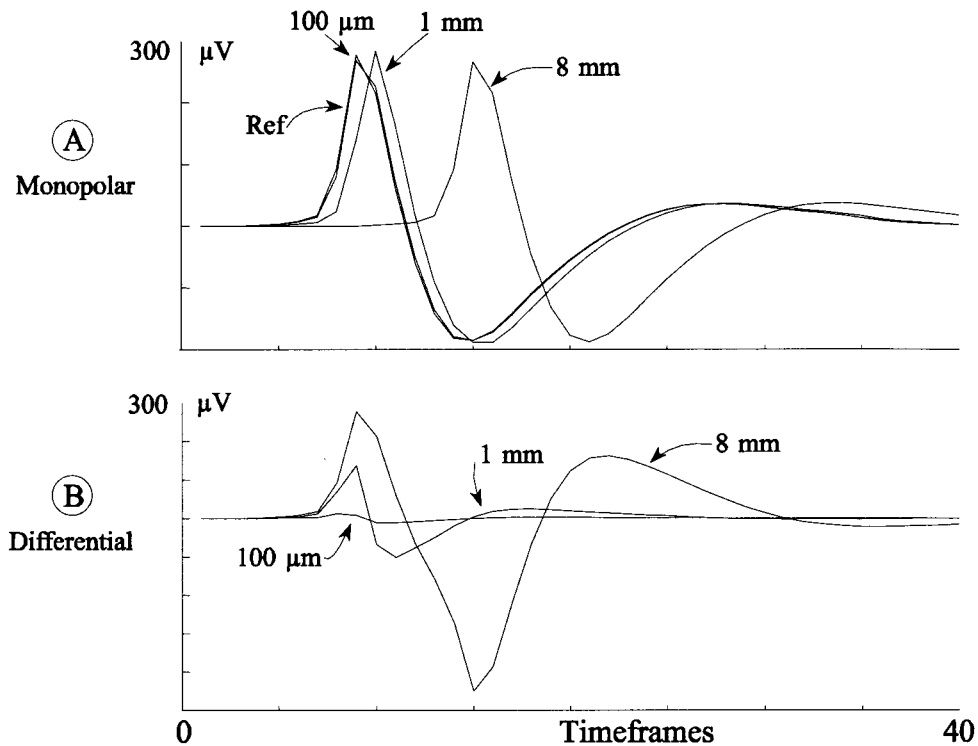


Figure VII.29: Simulated dynamic differential recording. Three monopolar recordings (A) were sampled 100  $\mu\text{m}$ , 1 mm and 8 mm from the reference recording (Ref). All recordings were done 5  $\mu\text{m}$  from the axon membrane and 40 time frames were computed to propagate the source function through the conductive universe. The differential recordings (B) show the three following traces subtracted from reference trace. The amplitude of the differential signals increased progressively as the distance between the monopolar recording points was extended.

The differential recordings showed tri-phasic characteristics, similar to recordings obtained with monopolar configurations. The duration and amplitude ratios of the phases were, however, changed. The amplitudes of the phases were more equal, and the trailing positive phase was extended. In addition, there were small negative amplitude phases (barely visible on the differential traces of Figure VII.29) which led and trailed the characteristic tri-phasic components.



*SIMULATION OF SILICON RECORDING ELECTRODE*

A silicon electrode was introduced in the conductive universe according to the model specifications derived above (Figure VII.19). The presence of the electrode caused expected local distortions of the field (Figure VII.30) (Theeuwens et al. 1993).

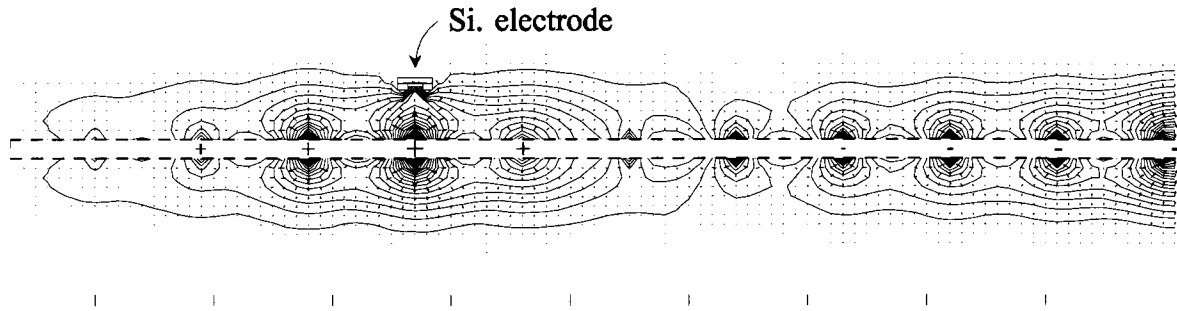


Figure VII.30: Silicon electrode in simulated dynamic action potential field. 10 simulated nodes of Ranvier were distributed along the length of the two membranes at grid points 10,19,28,37,46,55,64,73,82 and 91 (Schwan cells not shown for clarity). A silicon electrode was introduced at a  $5\ \mu\text{m}$  distance away from a node of Ranvier with the recording surface facing the membrane and the dielectric insulation layer and conductive back-plane immediately behind the site. The potential of the back-plane was clamped to ground (0 V). 40 fields, similar to the one shown, were computed to propagate the current source function from right to left through the conductive universe shown.

Field distortions were limited to the immediate surroundings of the electrode. Most notable was the change in field lines between the electrode and the membrane. In this local region, the changes were similar to what was observed when the action potential was confined by neighboring axons (Figure VII.22). The potential in the local region was found to increase in comparison to the undisturbed field distribution. This increase was attributed to the dielectric section of the silicon probe confining the field and locally restricting the flow of charge (Figure VII.31).

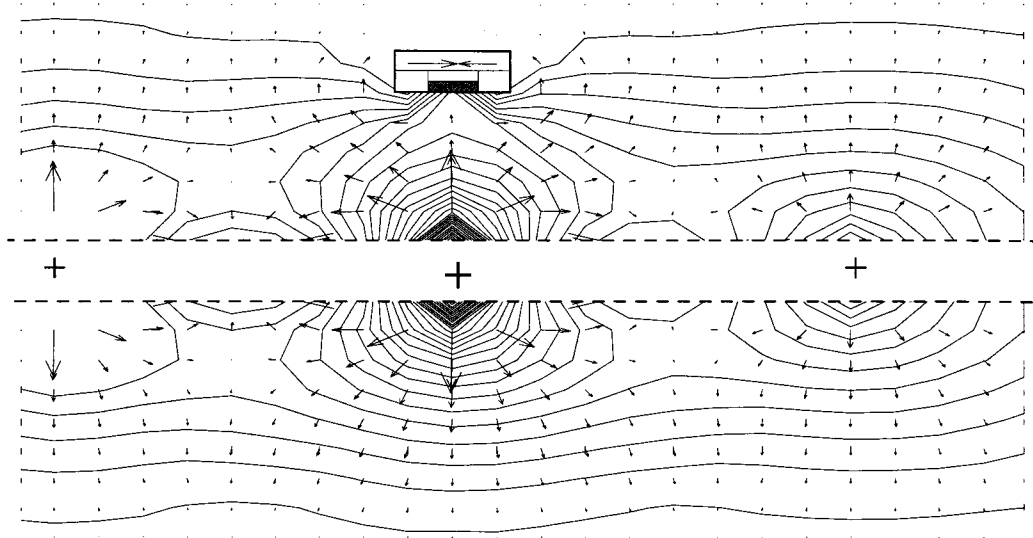


Figure VII.31: Detailed view of local field distortion caused by a silicon electrode.

*The conducting silicon substrate - the back-plane.*

The silicon substrate - the back-plane - acted as a conductor on the side facing away from the axon membrane and it was connected to extraneural space which was considered to be at a reference potential. The presence of a grounded conductive pathway along the shank of the electrode had been speculated to significantly attenuate the field strength around the electrode sites (Drake et al. 1988). In the above electrode simulations, the extraneural reference potential was set to 0 V, and its effect on the recorded signal was tested by running the simulation with and without the grounding voltage clamp (Figure VII.32).

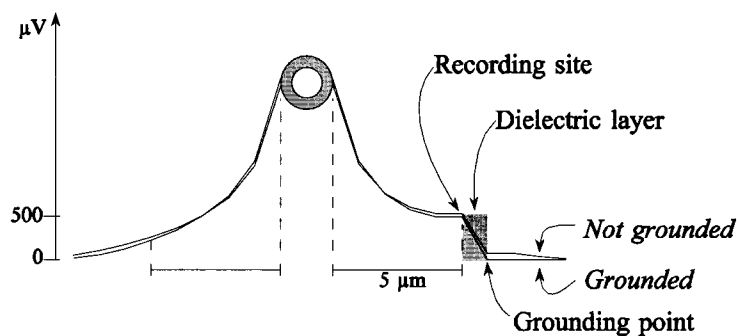


Figure VII.32: Cross sectional view of the potential drop, with and without the grounding back-plane. Cross sectional potential changes are shown as a function of distance from the axon membrane. The potential drop to the left of the axon is undisturbed by any electrode. The drop to the right shows two scenarios: Top trace is the non-grounded and bottom trace is the grounded recording condition. The sharp drop separating the recording point and the ground plane occurred across the dielectric layer of the silicon electrode. Each of the potentials shown is one of 40 computed.

As expected, the grounding reduced the potential on the side of the electrode facing away from the axon. More surprisingly though, was the limited effect on the potential observed on the side of the electrode facing the axon, where the grounding caused only a minor potential reduction at the electrode recording site. This could be explained by the dielectric layer "shielding" the recording site from the field distortions created by the nearby presence of a ground potential. As was seen in the recording without the grounding point (Figure VII.32), the potential on the back-side of the electrode was already reduced significantly, due to the dielectric shielding. Given this lowered potential, additional grounding of this region had little effect on the surroundings (Figure VII.33).

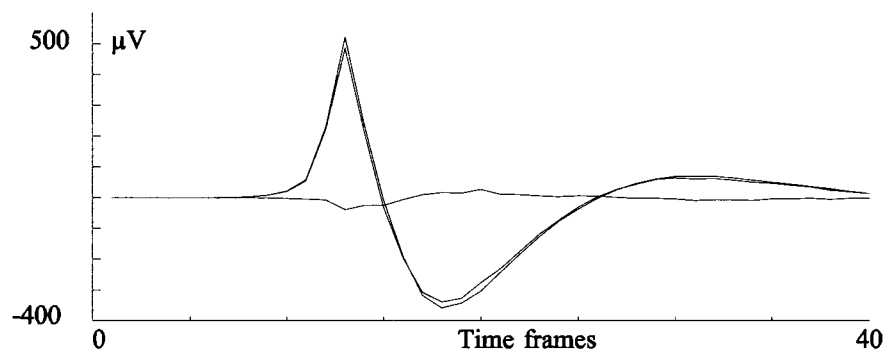


Figure VII.33: Dynamic action potentials recorded with a simulated silicon electrode. A total of 40 time frames were computed to allow the current source function to propagate through the environment. Two almost identical signals were recorded, representing electrode configurations with and without the presence of the grounding back-plane. A third trace shows the insignificant difference between the two signals.

These findings were indicative of the back-plane having very limited influence on the recording properties of the silicon electrode, when the plane is grounded to a stable constant voltage generator. Under more realistic conditions, the plane may pick up potentials originating from neighboring axons or extraneural sources, such as EMG activity. Under such circumstances, the potential originating from the back-plane, may be powerful enough to affect the characteristics of the recording.

#### *Silicon electrode recording*

As discussed above, the presence of a dielectric insulation layer supporting the recording site increased the potential observed at the electrode recording site (Figure VII.31). This significantly changed the amplitude of the recorded signal compared to a reference potential amplitude observed in the absence of the electrode (Figure VII.34).

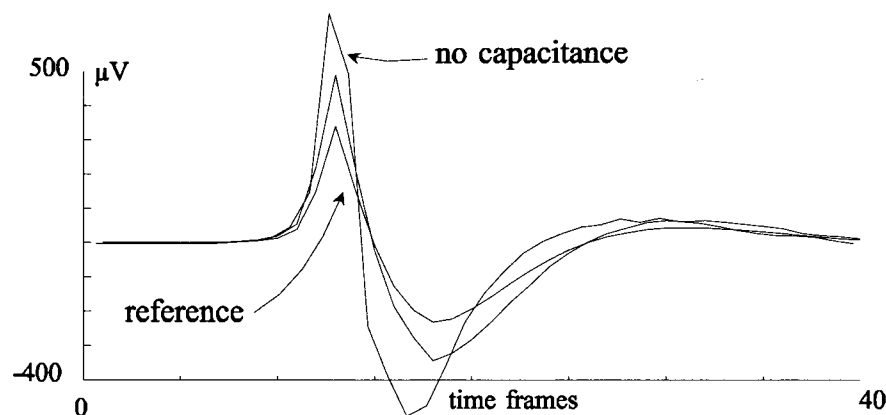


Figure VII.34: Dynamic action potentials recorded with and without the presence of a silicon electrode. Three traces are shown. Smallest amplitude is the reference trace, recorded with an ideal, non disturbing electrode. Middle trace was recorded with the simulated silicon electrode, including the grounded back plane. Largest amplitude signal was recorded from an environment without capacitive components. It was found that the dielectric layer of the silicon probe increased the amplitude of the recorded signal by 3.3 dB ( $V_{pp}$ ) at a recording distance of  $5\mu\text{m}$ .

The absolute amplitude of the recorded signal was dependent upon the amplitude of the current source configuration and on the relative size of the resistive and capacitive elements in the conductive universe. In all of the above simulations, a current source amplitude of 6 nA was used (peak to peak amplitude of Figure VII.5). As seen in the above figures, this would give a possible 800-900  $\mu\text{V}_{pp}$  recording potential, which would be a very acceptable recording amplitude, compared to a typical back ground noise of 10-15  $\mu\text{V}_{pp}$ .

The above simulated recordings (Figure VII.34) were made with a single axon located in the center of the conductive environment. A more restrictive scenario would be a test with two passive axons flanking the active central axon (similar to the unmyelinated simulation shown in Figure VII.22). As seen for the unmyelinated recordings, the potential field was more confined, compared to the field distribution in the unrestricted environment. This general confinement was very similar to what was seen in the local region around the dielectric layer of the silicon electrode (Figure VII.31). It caused a general increase in the potential field between the central source axon and each of the neighboring axons. Any additional confinement by a silicon electrode, had little or no impact on the potential recorded, given that the potentials were already raised significantly. The confined recordings, thus, looked identical to the recordings shown in Figure VII.34.

*SIMULATION OF FINE WIRE RECORDING ELECTRODE*

A final set of simulations were done to compare the above findings to simulated recordings obtained with fine wire electrodes. The model for a fine wire electrode was simplified to a single central recording point, with capacitive and resistive elements connecting in all four directions from the point. The choice of these values was based on impedance recordings from real electrodes ( $R=300\text{ k}\Omega$  to  $500\text{ k}\Omega$ ,  $\angle -72^\circ$  to  $-78^\circ$ ). It was not possible to simulate the wire insulation given the restriction of 2 spatial dimensions of the model.

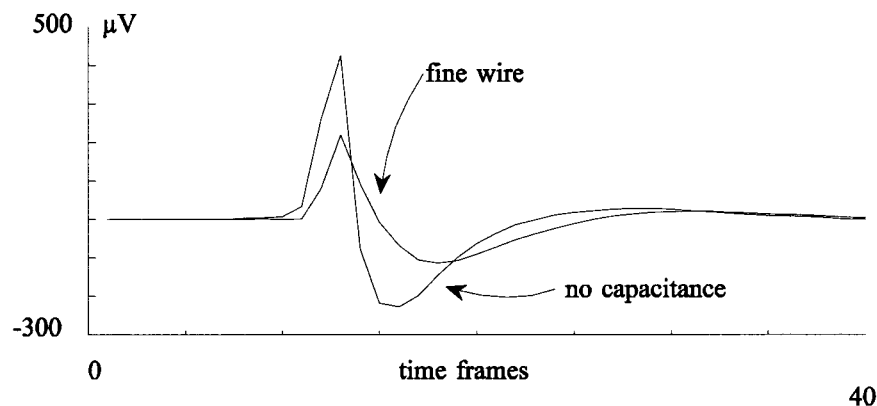


Figure VII.35: Fine wire simulation. In the “fine wire” simulation, a single recording point was surrounded by capacitive and resistive elements. All other parameters were equivalent to the ones used in the silicon electrode simulations. In the “no capacitance” simulation, all capacitive elements of both the electrode and the axon membrane were removed.

The fine wire simulations showed that a signal could be recorded with characteristics very similar to those obtained with the silicon based electrodes. The signal did, however, have a significantly smaller amplitude ( $300\text{ }\mu\text{V}_{pp}$ ) compared to the silicon recordings.

An additional simulation was performed, removing all capacitive components of the axon membrane. Comparison of this simulation with the previous fine wire simulation showed that the capacitive elements affect both the amplitude and the timing of the signal. As shown in Figure VII.35, the capacitive elements reduced the amplitude by 5.8 dB.

*Recordings in the presence of background noise*

The electric field around an axon is governed not only by the activity of the central axon, but also by potentials generated by sources other than the axon. Some of these sources may be of physiological interest, such as fields originating from neighboring axons. However, in general,

sources other than the central axon are considered background noise generators. These can be grouped as small amplitude intraneural sources, and larger amplitude extraneural sources such as nearby muscles. Each source contributes to the background noise according to its distance from a recording site and according to the amplitude and frequency characteristics of the source itself.

The background noise was simulated by a set of constant voltage generators distributed along the longitudinal edges of the conductive universe. For each time frame, all generators were assigned randomly chosen potential values, creating a background potential field equivalent in peak-to-peak amplitude to what had been found experimentally, 10-15  $\mu\text{V}_{\text{pp}}$  (Figure VII.36).

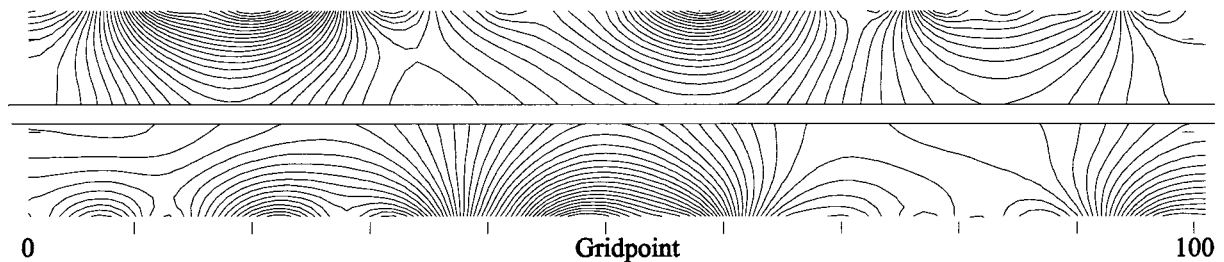


Figure VII.36: An example of back ground "noise" potential field. A set of 104 constant voltage generators were distributed parallel to the central axon. Each generator was assigned a random potential value for each time frame computed. The field strength was adjusted to yield a 10-15  $\mu\text{V}_{\text{pp}}$  amplitude at a 5  $\mu\text{m}$  distance from the axon.

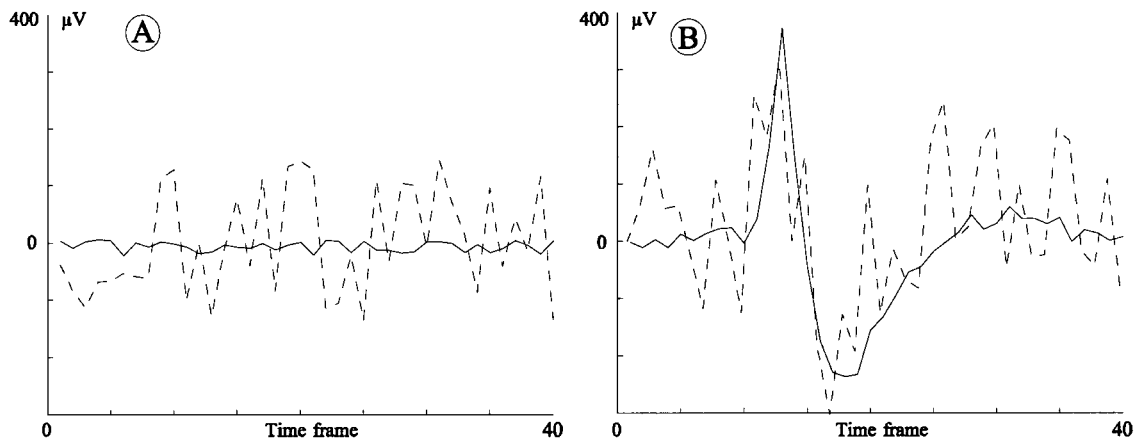


Figure VII.37: Background noise recordings. (A): The background potential field was sampled using an ideal non-disturbing electrode at a distance of 5  $\mu\text{m}$  from the axon. Two simulations were performed, one with 10-15  $\mu\text{V}_{\text{pp}}$  noise (solid line) and one with 100-150  $\mu\text{V}_{\text{pp}}$  noise (dashed line). (B): A propagating action potential was sampled in the presence of background potential with a silicon electrode 5  $\mu\text{m}$  from the axon. Both graphs (A & B) show a recording length of 40 time frames, equivalent to 5  $\mu\text{s}$  for an axon having 80  $\text{m}\cdot\text{s}^{-1}$  propagation velocity.

A second simulation showed that it was feasible to perform a silicon electrode recording of an action potential in the presence of small amplitude background noise (solid line in B, Figure VII.37). The recording showed two distinct largely unaffected phases of the traditional triphasic action potential. The trailing third phase was smaller in amplitude and was to a greater extent absorbed in the background noise.

The same simulation was performed with an increased background noise level (dashed line in B, Figure VII.37). This showed a severe effect on the recorded signal with almost all the recognizable features of the original potential absorbed in the background noise.

This confirmed, not surprisingly, that a large background noise level affects the total recording, whereas small amplitude background noise affects small amplitude signals selectively. In total, the field surrounding the electrode was determined by the action potential, the background noise and the silicon dielectric layer, and it was found that the grounded silicon substrate shielded the recording electrode from small amplitude background noise interference (Figure VII.38).

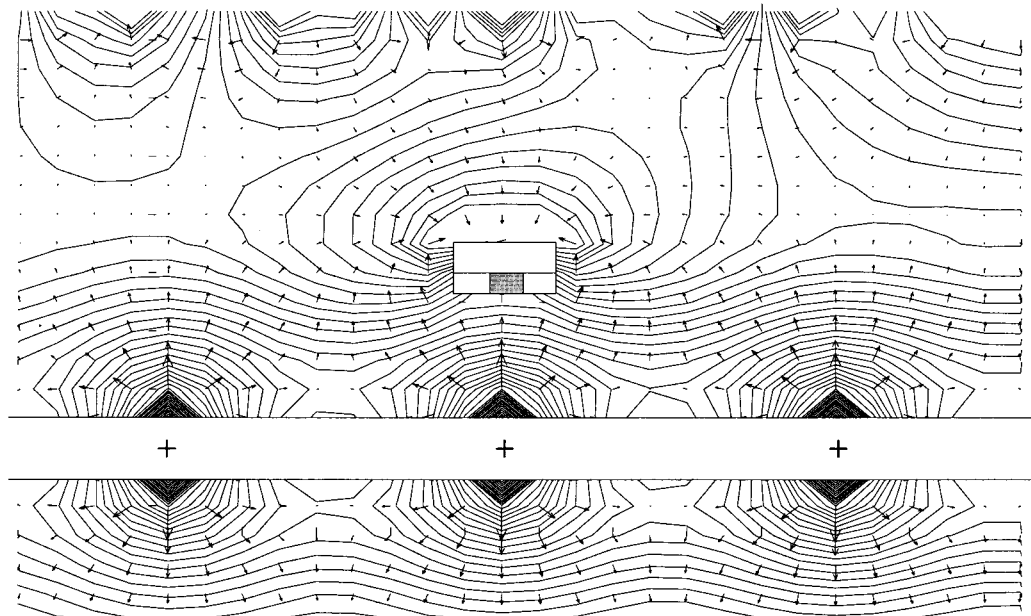


Figure VII.38: Background noise distortions around a silicon electrode. The potential field shown is from the low amplitude trailing phase of a propagating action potential in the presence of  $10\text{-}15 \mu\text{V}_{pp}$  background noise.

Noise generated by random assignment of potential values, as shown above, created a background frequency profile of several hundreds of kHz (Figure VII.37). It is unlikely that

potential fields of physiological origin will contain such high frequency components. Nevertheless, the recording simulation shows that it is feasible to obtain signals, even when the electrode and nerve environment are exposed to such high frequency components.

## **Discussion**

The objective to simulate an intrafascicular interface was to estimate the recording abilities of intraneural electrodes, when exposed to simulated axon potentials.

### *The recording instrumentation*

An electric circuit model of a silicon based single unit recording electrode was devised, including its electrochemical interface site, internal and external cabling, and the front end amplifier (Figure VII.15). With the given site impedance of the silicon electrodes, it was found that the Cooner wire shunt was negligible (less than 1dB), even at a cable length twice that used. This conclusion holds true for the relatively high impedance silicon based electrode interfaces. Electrode configurations with a lower capacitance would make it more crucial to reduce the Cooner wire shunt capacitance.

### *Electrode tip movement*

An intrafascicular interface site is susceptible to mechanical movements, due to the cabling attaching it to the extraneural environment. With respect to individual axons, electrode tip movements may be longitudinal, perpendicular or a combination of both. Displacement in either direction was shown to create changes in the recorded signal amplitude. The changes were characterized by modeling an ideal recording electrode in various locations with respect to the node of Ranvier (Figure VII.27 and Figure VII.28). As expected, the largest amplitude was observed closest to a node of Ranvier, with a 5-7 dB reduction, as the electrode was moved either longitudinally, or perpendicularly.

The distance from the node of Ranvier to the electrode could also be increased by buildup of passive tissue between them. This is expected to take place when an implanted device is encapsulated in connective tissue or when necrosis of the tissue around the electrode occurs. Not only is the conduction pathway between electrode and a node of Ranvier increased by this additional tissue, but the impedance of the tissue is also higher than the replaced extra cellular



fluid. This further increases the effective conductive pathway and distance related attenuation of the recorded signal.

#### *Recording configuration*

Using "ideal" recording electrodes, both monopolar and differential recording configurations were simulated (Figure VII.29). For the differential recording, various inter-electrode distances were tested and it was found that closely spaced electrodes (100  $\mu\text{m}$ ) caused severe attenuation of the recorded signal. It would, thus, be expected that the monopolar recording configuration would have an advantage in terms of recording the largest possible signal amplitude. However, the simulation did not include the presence of background noise, or any other potentials unrelated to the modeled single action potential event. The obvious advantage of the differential recording technique is in its ability to improve the signal-to-noise ratio of monopolar recordings.

#### *Silicon recording electrode*

A model of a silicon recording electrode was introduced in the conductive universe, including an electrochemical interface site, a dielectric layer and a conductive silicon substrate (Figure VII.19). The model was positioned in a favorable recording spot, 5  $\mu\text{m}$  from a node of Ranvier, with the recording surface facing towards the axon membrane.

When an insulating element, like the silicon electrode, was inserted, the potential field on the surface of the electrode, facing towards the axon, increased significantly. This was caused by the presence of the supporting dielectric layer, confining the field pattern and creating a low potential "shadow" on the side of the electrode facing away from the axon (Figure VII.32). This was in accordance with earlier reports on models of intracortical silicon electrodes (Drake et al. 1988) and from models of peripheral nerve electrodes (Rutten et al. 1995, Banks 1994). The shadow effect implied, that any dramatic potential changes in this region - such a grounding of the silicon substrate - did not create significant changes on the recording surface of the electrode. This was confirmed in simulations with, and without the grounding of the silicon substrate (Figure VII.33).

The insignificance of the back plane ground was unexpected. However, for *in-vivo* experiments, with real electrodes, the substrate is not necessarily clamped to a ground

potential. It will assume a variable potential equal to the average of the potentials of its surroundings, including activity in neighboring nerves and muscle fibers. Under these conditions, the recording properties of the electrode could be affected, depending on the signal strength from the surrounding "noise" sources. The limited noise simulations presented here, showed that the back ground noise has a very limited effect on the recording properties of the silicon probe. However, the characteristics of the noise generators were based on observation made with the intraneural electrodes, the very electrodes to be simulated. A more appropriate test would be to expose the recording sites to potentials generated from an independent noise model. This would be a model reflecting the physiological characteristics of multiple noise sources at various distances from the recording site, allowing for a more accurate estimate of how the recorded signal amplitudes are affected by the noise.

Given, that the dielectric layer "shields" events happening opposite the recording surface of the electrode, its orientation with respect to axons of interest, becomes important. The recording site will only be able to capture potentials on the recording surface. When comparing this limited recording volume with the larger spherical region around fine wire or hatpin electrodes, it becomes apparent that the likelihood of recording from active axons with a silicon electrode is reduced by at least 50%. However, this limitation of the silicon probes does not affect the characteristics of the recorded signal, when compared to fine wire recordings (Figure VII.35). Both signal amplitude and timing of the simulated recordings are similar, and would be very acceptable with a typical background noise amplitude of 10-12  $\mu\text{V}_{pp}$ .

Simulations of the silicon recording electrode suggest that it is possible to record potentials in the PNS of several hundreds of  $\mu\text{V}_{pp}$ , even in the presence of background noise, conducting backplane and non-optimal positioning of the recording site. This is in contrast with typical 20-30  $\mu\text{V}$  potentials found experimentally, as presented in this thesis and reported in the literature (Rutten et al. 1995, Banks 1994). From a macroscopic point of view, three possible explanations could account for this shortfall: 1) an increase in the electrical impedance of the conductive pathway between electrode sites and neural sources; 2) diversion of the neural potential field away from the recording sites through more conductive pathways; or 3) the electrode and recording equipment were not relaying the recorded signals efficiently.

In the first case the impedance of the conductive pathway between the neural source and the recording site is expected to increase in the initial days after implantation due to necrotic tissue formation around an electrode tip. This will reduce the recorded signal amplitude. In a similar manner, a relatively small increase in distance between electrode and current source was predicted to have a significant attenuating effect on the recorded signal, even in a conductive medium as simulated above (Figure VII.32).

The second possible explanation was that the neural potentials were diverted by a low impedance shunt to ground. Such a shunt is likely to form along fluid collecting on the surface of electrode shafts and leads as post surgical edema occurs. However, over time (1-2 weeks), excess fluid may gradually be replaced by connective tissue and the recording conditions should improve. The attenuating effect of a fluid layer remains to be addressed through modeling. A similar question regarding leakage inside a nerve cuff electrode was addressed by Brunner and Kock (1990), who concluded that a tighter fit between electrode and nerve surface would minimize the leakage and improve the ability to record neural potentials. It is unfortunately not as straightforward to "tighten" the tissue around an intrafascicular electrode, so additional innovations are required. Leakage caused by flexible cables or leads exiting the epi- and perineurium could be eliminated through the development of telemetry linked electrodes, which remains to be explored.

The third reason why the modeled recording potentials were so much higher than the observed potentials may have resided in the electrodes' ability to handle these signals. One, very obvious shortfall, is seen when the silicon flexible cable or the fine wire lead breaks or loses its insulation material. Both scenarios cause a loss of signal strength and a deterioration of the recorded signal. In the case of silicon cable, a breakage would leave a high impedance electrochemical interface stump, incapable of conducting any significant amounts of current. Such breakage of either conductors or their insulation may have been the reason for the lack of success with microstimulation after one week.

#### *Future directions of the model*

The numerical model presented above has answered some questions regarding intraneural single unit recordings, or lack there of, and has opened new avenues to explore. Given the

obvious facts that the silicon and fine wire electrodes yielded very limited successful recordings, and that the simulation results suggest an ability to record larger amplitude signals, neither the electrode design, nor the model development can be considered complete. Future progress on the electrode design depends partially on improvement directions, provided by the modeling effort.

What should be the next steps in the development of a numerical intraneural single unit electrode model ?

One of the most apparent limitations of the present model is its 2 dimensional configuration, compared to the environment being modeled, having 3 spatial dimensions. To address this limitation, two extreme scenarios were simulated - the unrestricted environment, with one central axon, and restricted scenario, with two axons closely flanking the central axon. Results from simulations of any other combination of neighboring distant axons would fall in between the results from the extreme simulation runs. When using a silicon based electrode, the extreme simulations showed insignificant differences in the signal recorded with or without the flanking axons. Based on this, there is little ground for investing further effort in the design of a model with 3 spatial dimensions. There are, however, two other arguments in favor of this development:

1. The silicon electrode shank is a 3-dimensional structure with its recording sites averaging the local potentials that they are exposed to. Given the extent of each interface site, this averaging effect may influence the recorded signal significantly, depending on the inhomogeneity of the field. The 2-dimensional simulation, as applied above, only allows for the averaging effect to take place in one direction. Simulating an environment with 3 spatial dimensions would allow for a more accurate computation of the recording potential across a whole recording site.
2. Many of the electrical characteristics used for simulating both physiological tissue and electrode behavior were based on 3-dimensional measurements. Converting these values to a 2-dimensional domain may have unforeseen effects. The only way to avoid this conversion error is to simulate the environment in the same dimensions as its parameter was sampled.

It is therefore recommended that future modeling effort is aimed towards designing a 4-dimensional model - three spatial dimensions and one time. Using the approach described in this chapter, there should be no mathematical or implementational limitations preventing the development of such a model. Presently, however, there are limitations in available computer power. Adding an additional dimension increases the storage and computational requirements dramatically. This restriction can be alleviated by using more efficient implementation methods, such as a compiler, instead of the Matlab interpreter, and by using a finite element analysis, instead of the finite difference method.

What questions should a future model address ?

The overall question remains *why* the current electrodes performed so marginally both for recording and microstimulation purposes. To answer this, it may be necessary to include a more accurate model of the current source of the axon membrane, addressing questions regarding how much the extracellular field can be loaded electrically without disrupting the propagation of action potentials. Or it may be necessary to include axons which are not running straight through the conductive universe, similar to the anatomical pathway of individual axons within fascicles. Real axons are aligned in a zig-zag pattern, changing direction every 1 to 2 mm and creating the visible Felic Fontana's spiral bands. A curved pathway has been shown to create significant asymmetries in the generated extracellular potential around a single axon (Xiao et al. 1995).

This sort of inhomogeneous environment can, in a fairly straightforward manner, be implemented in numerical solution methods. Once a model is capable of addressing the performance questions, action can be taken on improving the electrode design.

## VIII. DISCUSSION

Why develop interfaces to the peripheral neuromuscular system ? The need to do so is found in the development of neural prosthetic devices, where several different types of sensors (natural and artificial) may be utilized in rehabilitation prosthetics. To understand and utilize the natural sensors, and to fully integrate any artificial sensors efficiently, it is important to establish the characteristics of the physiological systems with which one is attempting to interface. Determining the physiological characteristics of neuromuscular control systems has been the goal of numerous neuroscience research projects, which typically require development of highly specialized transducer technologies. External transducers may not need to be very complex to determine intricate physiological control systems parameters, but when attempting to record *in vivo* from a mammalian neuromuscular system during voluntary awake movement, sets of rather complex implanted transducers are required (Lemon 1984, Hoffer 1990).

### *LENGTH GAUGE*

#### *Objectives of the length gauge designs*

The objective of designing a muscle length gauge based on ultrasound transit time was to improve on the mechanical and electrical characteristics of existing resistive gauges. This was done by designing gauges with two piezoelectric crystals attached at either ends of a length of fluid-filled extensible tube (Weytjens et al. 1992). The *in-vivo* dynamic performance of the ultrasound gauges was similar to previous length gauge designs, with negligible deviation of recorded length when compared to the conventional resistive gauges. The ultrasound based design had the advantage of providing a direct and precise calibration method.

#### *Comparison of developed ultrasound length gauge to existing designs*

Previous designs of resistive length gauges reported in the literature (Prochazka 1984, Loeb and Gans 1986, Hoffer 1990), had in common the undesirable feature of imposing mechanical loads on the system being measured. For mechanical measurements in a fluid filled medium, the use of ultrasound as an information carrier can reduce the mechanical loading. Ultrasound has been used for recording length changes in muscle fibers (Caputi et al. 1990, 1992, Ratcliffe et al. 1995) and a natural next step was to adapt these measuring techniques for recording

whole muscle length. This step was initiated by Caputi and co-workers, resulting in a new length gauge design as described in Chapter III.

However, this new design did not unleash the true potential of ultrasound transduction - the complete mechanical uncoupling between the recording and the measured systems. Silicone tubes were attached to the origin and insertion of the muscle in order to align the piezoelectric crystals and therefore still imposed a mechanical load on the limb.

#### *Application and future directions*

The new length gauge design should be viewed as an alternative rather than as a replacement for resistive gauges. In my opinion, implantable length gauges, based on either extensible tubes or ultrasound, are likely to remain a neurokinesiological research tool but are unlikely to be used as an artificial sensor in neuro-muscular prostheses systems. This view is based mainly on the present general state of device refinement. For the technology to mature clinically, more long-term testing and fine tuning is required, in addition to substantial advances in miniaturizing required amplifiers. Such developments are seen in the design of other length gauge transducers currently being developed such as short tendon length gauge transducers (Steven 1989, 1991). Instead of ultrasound, these gauges are based on differential reluctance of a coil and their overall size is comparatively small (10 mm in length). These transducers are anchored in soft tissue, such as tendon or muscle tissue, with stainless steel barb. The measurement is linearly related to small displacements of the tissue, rather than to the total muscle or tendon length.

#### ***NERVE CUFF RECORDING ELECTRODE***

##### *Objectives of the nerve cuff electrodes*

The objective of redesigning the nerve cuff electrode was mainly to improve on its closure mechanism. An innovative closing technique was devised, replacing existing suture closures (Kallesøe et al. 1996).

##### *Comparison of the new cuff design to existing designs*

Previous literature reported cuff closure designs based on silicone adhesive, sutures, or overlapping silicone sheeting and tubing (Stein et al. 1975, Hoffer 1990, Loeb and Peck 1996). The electrical seal along the cuff opening has always been a cause of concern, given that for

several cuff designs connective tissue was observed to grow through the wall opening. Prevention of growth of a tissue bridge had previously been attempted by attaching an external silicone "flap" that covered the opening on the outside cuff wall (Hoffer 1990). In the improved cuff design presented in this thesis, a flap was attached to the inside cuff wall. This allowed internal tissue to force the flap against the cuff wall, which sealed the opening. Cuffs with this flap arrangement and the interdigitated tubing closure had no signs of connective tissue growing through the wall opening. The cuff was, as a whole, encapsulated in connective tissue.

The new closure technique was designed to give the cuff a fixed lumen which was purposely larger than the nerve, to allow the encompassed nerve to expand as edema developed post-surgically. Contrary to this approach, cuffs based on the self-sizing concept attempt to create a variable diameter tube (Naples et al. 1986, 1988). The functionality of self-sizing cuffs remains questionable. These cuffs may be easy to install around a nerve but, to my knowledge, no conclusive evidence has been presented as to whether the forces needed to adjust the lumen size are below the threshold for nerve damage. Thus, the choice between self-sizing and fixed lumen cuff remains controversial.

In other cuff designs, various types of silicone tubing structures were used to mechanically support the internal electrodes (Loeb and Pack 1996). Commercially available silicone tubing makes for relatively stiff cuff wall and electrode structures. Installed around a nerve, the ends of a tube become mechanical transition points between the cuff wall and the neural tissue. If the mechanical impedance of the cuff wall and the neural tissue at these points is poorly matched, nerve damage is likely to occur during movements of tissue or cuff wall.

To reduce the mechanical stiffness of the tubing, a much thinner wall thickness is desirable. This was attempted in the cuff wall casting process, which included specially designed coiled electrodes embedded in the silicone material. The finished cuff assembly was extremely flexible and was successfully tested in chronic implants.

Other research groups have addressed similar transducer design issues and it has been shown that thin-walled cuffs for nerves larger than 1mm in diameter, can be produced (Walter et al. 1995, Haugland 1996). Below this diameter, the cuff is likely to become deformed and



unusable. To my knowledge, only the foil electrode techniques developed by Haugland (1996) have been successful in providing a commercially available cuff for nerves smaller than 1 mm in diameter.

#### *Application and future directions*

The new closing technique is already being applied in basic neurokinesiological research (Haugland 1996, Strange et al. in revision), but the transfer to the clinical environment remains dependent upon successful integration of nerve cuff transducers in FES systems. Initial steps have been taken in this direction (Haugland et al. 1995, Haugland and Sinkjær 1995) with the recent development of a telemetry system for nerve stimulation cuffs (Haugland 1997). However, technical limitations such as the poor match in mechanical impedance between nerve cuff and neural tissue and the lack of recording telemetry systems still hampers the more widespread use of recording nerve cuffs.

#### **SINGLE UNIT ELECTRODES**

##### *Objectives of the single unit electrodes*

The objective of designing single unit electrodes was to establish recording interfaces to single peripheral axons, to be used to characterize the discharge patterns of muscle proprioceptors.

Initially, attempts were made to transfer electrode technologies previously used for CNS and spinal root recordings. Traditional designs of fine wire and hatpin electrodes were adapted and modified for use in the peripheral nervous system. Later an innovative design of a peripheral single unit electrode (PSU) was devised using silicon micromachining techniques.

##### *Comparison of fine wire and hatpin electrodes to existing designs*

Previous literature on fine wire and hatpin electrodes had reported successful recordings for extended periods of time (days and weeks) in the spinal roots and ganglia (Prochazka et al. 1976, Loeb et al. 1977, Hoffer et al. 1987a, Gorassini et al. 1993). Using similar technology, it had proven more difficult to establish robust interfaces further distally in the peripheral nervous system (Hoffer and Weytjens 1990). This finding was unfortunately confirmed in the present thesis, where several different types of fine wire electrodes were tested. A number of small-amplitude afferent signals were successfully recorded from muscle proprioceptive organs. The fact that the electrodes were inserted in the MG fascicle exclusively, assured that

recorded signals would be related to this muscle. This was intended to be an advantage compared to single unit recordings from the spinal roots, where the complex anatomy precludes the selective positioning of electrodes to record from specific muscles, like the MG.

What could have caused the low amplitudes seen in all single unit recordings ?

A common denominator for all the single unit electrodes used in this thesis was the insertion technique. A mechanical "carrier", fine gold wire or a tungsten needle, provided the necessary mechanical strength to position an electrode intraneurally. Given that the interface sites were an integral part of the carrier, once the sites had been positioned it was not an option to withdraw the carrier from the nerve. The low signal amplitude was similar to the scenario during intramuscular single unit recordings, where an initial drop of signal amplitude has been observed during recordings from a freshly inserted electrode (Stegeman et al. 1994). It was speculated that this drop was caused by conductive fluid that gradually encompassed the electrode and its interface sites.

In my opinion this is a valid hypothesis, given personal observations from surgical procedures of immobilizing hatpin electrodes using cyanoacrylate. During insertion of many electrodes, relatively low levels of stimulation current (1-5  $\mu$ A) could be required to excite single motoneurons. However, in the minutes following the completion of the insertion procedure, the minimum stimulation current required often increased significantly. Electrodes were then either moved to other locations, with possibly the same results, or were fixed in their locations. In cases when the location was fixed using a drop of cyanoacrylate applied to the surface of the nerve around the insertion point, an immediate decrease in the minimal required current was usually observed. The required current amplitude could be reduced by an order of magnitude, but only for a limited time period (5-10 minutes).

The hypothesis of an extraneural fluid shunt along the electrode lead would explain these initial observations. Sealing the insertion point would temporarily create a high impedance barrier, forcing more of the microstimulation current to flow through the excitable neural tissue, thus lowering the minimum required stimulation amplitude. A similar argument may explain the generally low amplitude levels of all recorded signals with these electrodes.

*Comparison of silicon based electrodes to fine wire electrodes*

Silicon based electrodes have been used in the CNS both for short term (BeMent et al. 1986, Drake et al. 1988) and long term recordings (Carter and Houk 1993). In the PNS, recordings have been made with either regeneration probes, where axons were severed and encouraged to regenerate through a silicon mesh, or with dagger shaped insertion probes, as presented in this thesis.

Efforts at implementing regeneration electrodes have gained momentum in recent years (Kovacs 1992, Della Santina et al. 1997), but this technique suffers, in my view, from the drastic requirement of cutting the nerve to initiate the regeneration process. Recordings made with these devices will inevitably be affected by the altered anatomy of the regeneration. The technique may, however, find applications in situations where a peripheral nerve has been severed anyway, as in amputees. This concept has previously been proposed for other neuromuscular transducers (De Luca 1978, Hoffer and Loeb 1980, Loeb 1989). However, until the silicon device reaches a more advanced stage of clinical maturity, regeneration electrodes are more likely to remain a basic neuroscience research tool.

Most silicon dagger probes have been developed to establish interfaces to brain areas, but recently a few new designs, besides the PSU designs described in the present thesis, have been aimed primarily at the PNS. A single shank recording technique was used by Banks (1994) to perform acute recordings from unmyelinated nerves in the Locust. The electrode dimensions were significantly different than the PSU designs, with interface sites as small as  $4 \times 4 \mu\text{m}$  spaced  $200 \mu\text{m}$  apart. These dimensions were governed by the unmyelinated neuroanatomy of the locust. Unitary spikes of up to  $600 \mu\text{V}$  had been recorded with fine wire electrodes, but the silicon probe recordings did not yield much beyond  $110 \mu\text{V}$ . This was very similar to what has been shown here for the feline preparation except for the absolute recording amplitudes being larger.

A more comparable animal preparation was used by Rutten et al. (1995), recording single unit potentials from rat peroneal nerve. This was done in short-term (acute) recordings with multiple silicon shanks (128) arranged in a 3-dimensional array structure. The basic design of this electrode array was similar to an intracortical silicon array (Campbell et al. 1991),

resembling a fakir's bed of nails. It was primarily designed for selective stimulation (Rutten and Meier 1991), but single unit recordings were also reported. Similar to results described in the present thesis, signal amplitudes of less than  $20 \mu\text{V}_{\text{PP}}$  were reported.

When comparing the PSU design to CNS silicon electrodes, the largest difference is found in the significantly higher site capacitance of the PSU design (30 times higher than reported by BeMent et al. 1986). This is mainly due to a relatively larger surface area of the PSU interface sites. One advantage of this is that a higher shunt capacitance along leadout cables to front end amplifiers is acceptable. A disadvantage is that the site capacitance may load the extracellular field beyond acceptable limits. These limits remain to be determined.

Low amplitude recording levels have been speculated to be due to conductive fluid leaks along the inserted shaft (Drake et al. 1988), similar to what was hypothesized for the fine wire and hatpin electrodes.

#### *Application and future directions*

The peripheral single unit electrodes tested in the present thesis, fine wires, hatpins and silicon probes, have all proven to be fragile, delicate to implant and with extremely short *in-vivo* survival times. These electrode technologies are, at present, of interest only for basic neuroscience research. Results from this research may have indirect applications for clinically oriented rehabilitation research. However, in my view, single unit interfaces are unlikely to find applications in the grander scheme of FES control of muscles, limbs, and total body movements, given that information from single proprioceptive units carries little utility. In that context, simultaneous recordings from multiple receptors are likely to be more useful. Compared to a single unit recording, the other extreme is to record the total activity of a whole nerve, i.e. a nerve cuff recording. This kind of recording has proven useful as an event detecting feedback signal in a clinical application of FES (Haugland 1994). Other electrode designs, like intrafascicular low impedance LIFE electrodes (Yoshida and Horch 1996), are more selective than whole-nerve cuff recordings but are not restricted to single unit recordings (Yoshida et al. 1997).

The basic neuroscience applications of single unit electrodes in the PNS are questionable given the lack of performance seen here. This may in part be due to the fragility of the electrode

assemblies, typically limiting the lifetime of the electrodes to one or two weeks. Within this time frame, another large obstacle is, in my view, the current shunt along the wire or shank attachment to the recording site. In the simulations presented here (see next section) it was seen that clamping (shunting) the potential close to the recording site severely attenuates the recorded signal. Addressing this issue will require significant redesign of the present intraneural electrode technology.

### ***SIMULATION OF INTRAFASCICULAR INTERFACES***

#### *Objectives of simulation*

The objective of simulating the electrodynamics around an intrafascicular electrode was to address the performance shortfall of existing electrode designs, specifically the silicon based electrodes. A numerical simulation of the electrical interaction between peripheral axons and single unit interfaces was derived using a finite difference model. The model included myelinated axons, distributed nodes of Ranvier acting as constant current generators, and various configurations of fine wire or silicon based recording electrodes. The basic elements of the model were resistive and capacitive elements arranged in a 3-dimensional conductive universe (two spatial and one time dimension). The model was designed to compute both static and dynamic electric fields generated by a simulated action potential propagating along a myelinated or unmyelinated axon.

It was confirmed that translation of an electrode with respect to a node of Ranvier may affect the recorded signal amplitude by 5-7 dB, and that a dielectric layer around a planar silicon electrode will accentuate the potential field on one side of the shank. Special attention was paid to the conducting backplane facing away from an axon of interest. It was found that such a backplane, whether grounded or ungrounded, had a limited effect on the recording properties of an individual interface site.

#### *Comparison with existing models*

The model presented in this thesis showed that a dielectric layer inserted in an electric field accentuated potentials on the shank side facing the current source. This is in agreement with findings published on modeling silicon based neural interfaces to CNS (Drake et al. 1988) and PNS tissue (Rutten et al. 1995, Banks 1994). This is an important property of the silicon

design, given that it improves both the amplitude and the selectivity of the recorded signal. Amplitude improvement is obviously obtained by the enhanced potential levels, while selectivity is gained by the fact that the dielectric layer shields electrical events occurring on the back side of the shank, hence making the electrode more selective to sources facing the probe.

The dielectric layer in these probes was relatively wide compared to the insulating structures of other fine wire and hatpin electrode designs. Unfortunately, however, a cable still needs to be connected to the interface site and buildup of conductive fluid around the recording site may have affected the recorded potentials. As speculated by Drake et al. (1988), a low resistive electric fluid shunt to and along the silicon shank is expected to cause attenuation of surrounding fields.

Banks (1994) presented a finite element model of a silicon recording electrode in close proximity to a modeled locust nerve fiber. This model was restricted to stationary potentials from unmyelinated axons, but also confirmed the accentuation of potential fields on the front side of the insulating electrode shank.

Rutten et al. (1995) presented a model primarily designed for simulation of intrafascicular stimulation, but the model was also used for simulation of recordings. Their findings for various recording locations with respect to a node of Ranvier were generally in agreement with the present thesis results. Rutten et al. (1995) furthermore concluded that restriction of the extraneural environment, as seen with an insulating nerve cuff, would completely eliminate the selectivity of any intrafascicular recordings. This raises questions with regard to the presented recording setup, where all insertions of intraneural electrodes have been encompassed by nerve cuffs. Although the model presented here was not aimed at addressing a detailed analysis of a larger neural structure, such as whole nerve and its surroundings, indications were found in the simulation of multiple axons that confinement of action potentials changes the field pattern. This is in agreement with Rutten et al. (1995), who documented in more detail that progressively "tighter" confinement, i.e. reducing the conductivity of the surrounding environment will significantly reduce the recording selectivity properties of an intrafascicular electrode.

All models discussed so far, including the present thesis model, have been restricted to two spatial dimensions. In reality, the modeled environment is 3-dimensional, which, as noted by Drake et al. (1988), make results from any of the above simulations set an upper bound for possible recorded signal amplitudes. In simulations in 3-dimensional space, all potential amplitudes are expected to be reduced, compared to the 2-dimensional simulations due to the added direction of spreading the available current source. In addition to this, all previously presented models of silicon based interfaces were restricted to stationary potentials. To address this restriction, the present thesis model was developed in 3-dimensions - two spatial and one time dimension. This allowed the model to include capacitive elements of electrodes and conductive tissue.

#### *Applications and future directions*

The model presented has two limitations.

- 1) It is restricted to 2 spatial dimensions. Future models should be designed to have three spatial dimensions and one time dimension.
- 2) Both the spatial and the time resolutions should be increased, to give a more accurate measure of the simulated environment.

To correct both of these limitations significantly more computer power will be needed. One option would be to use parallel computing. The implementation method described in the present thesis will allow this. Other options are to optimize the implementation either through the use of a more efficient computing language and compiler, or to re-focus the entire implementation on a finite element model. However, the latter option may not be any more efficient with respect to disk storage space (Banks 1994).

On the other hand, the flexibility of the finite difference method should easily allow the model to accommodate more complex environments such as multiple active axons, inhomogeneous fascicles, and even multiple fascicles and whole nerves. The underlying computational principle is the same as for the single axon simulations. This would make direct comparisons possible between theoretical recordings from intraneural electrodes and other selective recording devices, such as multicontact nerve cuffs. Modeling effort is underway for the development of an efficient multi contact nerve cuff (Parrini et al. 1997), and given a high

degree of recording selectivity, it may very well prove to be a superior FES feedback transducer compared to the intraneural electrode.

#### *FINAL REMARKS*

In conclusion, this thesis was aimed at the development of implantable devices for recording neuromuscular activity during natural movements. A series of transducer designs was developed for use in neurokinesiological research projects. Most of these devices were developed to the point of acceptable performance with regard to providing physiological recordings of sufficient quality. However, one transducer, the peripheral single unit electrode, performed marginally and thus prevented drawing physiological conclusions on the neuroscience research project of initial interest, the characterization of proprioceptive feedback receptors. Nevertheless, other transducers were successfully developed and applied in related research projects. These transducers were designed for basic neuroscience purposes and were as such not prepared to be transferred to clinical neural prostheses applications. Clinical application may not be that far away for one of the devices, the nerve recording cuff.



## REFERENCES

- Abbas J J, Triolo R J, Experimental evaluation of an adaptive feed-forward controller for use in functional neuromuscular stimulation systems, *IEEE Trans. Rehab. Eng.* 5(1):12-22, 1997
- Agnew W F, McCreery D B, editors, *Neural prostheses: Fundamental studies*, Prentice Hall, New Jersey, 1990
- Albery J, *Electrode kinetics*, Claredon Press, Oxford, 1975
- Altman K W, *Volume conduction and fiber excitability in simulated peripheral nerve stimulation*, Ph.D. thesis, Biomedical Engineering, Duke University, Durham, NC, 1988
- Amatenik E, Measurement of bioelectric potentials with microelectrodes and neutralized input capacity amplifiers, *IRE Transactions on Medical Electronics* March:3-14, 1958
- Anderson D J, Najafi K, Tanghe S J, Evans D A, Levy K L, Hetke J F, Xue Xiaolin, Zappia J, Wise K D, Batch-fabricated thin-film electrodes for stimulation of the central auditory system, *IEEE Trans. Biomed. Eng.* 36:693-704, 1989
- Andreassen S, Rosenfalck A, Recording from a single motor unit during strong efforts, *IEEE Trans. Biomed. Eng.* 25(6):501-508, 1978
- Andreassen S, Rosenfalck A, Relationship of intracellular and extracellular action potentials of skeletal muscle fibers, *Critical reviews in Biomed. Eng.* 6:267-306, 1981
- Arendt-Nielsen L, Sinkjær T, Nielsen J, Kallesøe K, Electromyographic patterns and knee joint kinematics during walking at various speeds, *J. Electroneurography and Kinesiology* 1(2):89-95, 1991
- Arms S W, Implantable displacement sensor, US patent 4.813.435, 21 Mar. 1989
- Arms S W, Method of and means for implanting a pressure and force sensing apparatus, US patent 4.993.428, 19 Feb. 1991
- Ballin C, Gorman P H, Upper extremity applications of functional neuromuscular stimulation, *Assist Technol.* 4:31-39, 1992
- Banks D, *Modeling studies on peripheral nerve neural signal transduction using thin-film microelectrodes*, Ph.D. thesis, Department of Electronic and Electrical Engineering, Department of Mechanical Engineering, University of Surrey, United Kingdom, 1994
- Barker A T, Brown B H, Freeston I L, Modeling of an active nerve fiber in a finite volume conductor and its application to the calculation of surface action potentials, *IEEE Trans. Biomed. Eng.* 26(1):53-56, 1979
- BeMent S L, Kensall D W, Anderson D J, Najafi K, Drake K L, Solid-state electrodes for multichannel multiplexed intracortical neuronal recording, *IEEE Trans. Biomed. Eng.* 33:230-41, 1986
- Benabid AL, Pollak P, Gao DM, Hoffman D, Limousin P, Gay E, Payen I, Benazzouz A, Chronic electrical stimulation of the ventra intermedialis nucleus of the thalamus as a treatment of movement disorders, *J Neurosurg.* 84:203-214, 1996
- Benamou M, Metral S, Hort-Legrand C, Belec L, Lestrade R, In vitro model of far-field stationary potentials: boundary effects on propagated potentials, *Electroencephalography and clinical Neurophysiology*, 76:187-192, 1990
- Bernstein J J, Johnson P J, Hench L L, Hunter G, Dawson W W, Cortical histopathology following stimulation with metallic and carbon electrodes, *Brain Behav. and Evol.* 14:126-157, 1977
- Bockris J, *Comprehensive treatise of electrochemistry, Volume 1: The double layer*, Plenum Press, New York, 1980
- Bowman B, Erickson R C, Acute and chronic implantation of coiled wire intraneural electrodes during cyclical electrical stimulation, *Ann. Biomed. Eng.* 13:75-93, 1985

- Boyd I A, The mechanical properties of dynamic bag fibers, static nuclear bag fibers and nuclear chain fibers in isolated cat muscle spindles, *Prog. Brain Res.* 44:33-50, 1976
- Brunner M, Koch U T, A precision multichannel cuff electrode optimized by simulation and experiments, *J. Neuroscience Methods* 35:93-106, 1990
- Buchthal F, Rosenfalck A, Behse F, Sensory potentials of normal and diseased nerves, in *Peripheral Neuropathy*, Dyck P J, Thomas P K, Lambert E H, Bunge R (eds) Saunders W B, Philadelphia 1984
- Burns B D, Stean J P B, Web A C, Recording for several days from single cortical neurons in completely unrestrained cats, *Electroenceph. clin. Neurophysiol.*, 36:314-318, 1974
- Campbell P K, Jones K E, Huber R J, Horch K W, Normann R A, A silicon-based, three-dimensional neural interface: manufacturing processes for an intracortical electrode array, *IEEE Trans. Biomed. Eng.* 38(8):758-68, 1991
- Caputi A A, Hoffer J A, Pose I E, Sarcomeres work in the 'ascending limb' in cat medial gastrocnemius muscle during walking, *Soc. Neurosci. Abstr.* 16:891, 1990
- Caputi A A, Hoffer J A, Pose I E, Velocity of ultrasound in active and passive cat medial gastrocnemius muscle, *J. Biomech.* 25:1067-74, 1992
- Carter R R, Houk J C, Multiple single-unit recordings from the CNS using thin-film electrode arrays, *IEEE Trans. Rehab. Eng.* 1:175-184, 1993
- Chao E Y S, Justification of triaxial goniometer for the measurement of joint rotation, *J. Biomechanics*, 13:989-1006, 1979
- Christensen P R, Chen Y, Strange K D, Yoshida K, Hoffer J A, Multi-channel recordings from peripheral nerves: 4. Evaluation of selectivity using mechanical stimulation of individual digits, pp:217, Proceedings 2<sup>nd</sup> Annual IFESS Conference and Neural Prosthesis: Motor Systems 5, Burnaby, B.C. Canada, 1997
- Clark J, Plonsey R, The extracellular potential field of the single active nerve fiber in a volume conductor, *Biophysiol J.* 8:842-864, 1968
- Cleland C L, Hoffer J A, Activity patterns of spinocerebellar neurons during normal locomotion, in *Neurobiology of Vertebrate Locomotion*, Grillner S, Stein P S G, Stuart D G, Forssberg H, Herman R, eds., Macmillan, London, pp. 705-723, 1986
- Coburn B, A theoretical study of epidural electrical stimulation of the spinal cord. - Part II: Effects on long myelinated fibers, *IEEE Trans. Biomed. Eng.* 32(11):978-86, 1985
- Coburn B, Sin W K, A theoretical study of epidural electrical stimulation of the spinal cord. - Part I: Finite element analysis of stimulus fields, *IEEE Trans. Biomed. Eng.* 32(11):971-7, 1985
- Cooke I R, Brodecky V, Berger P, Easily-implantable electrodes for chronic recording of electromyogram activity in small fetuses, *J. Neuroscience Methods* 33:51-54, 1990
- Crago P E, Chizeck H J, Neuman M R, Hambrecht F T, Sensors for use with functional neuromuscular stimulation, *IEEE Trans. Biomed. Eng.* 33:256-68, 1986
- Cunningham K, Halliday A M, Jones S J, Simulation of 'stationary' SAP and SEP phenomena by 2-dimensional potential field modeling, *Electroencephalography and clinical neurophysiology* 65:416-428, 1986
- Dai R, Stein R B, Andrews B J, James K B, Wieler M, Application of tilt sensors in functional electrical stimulation, *IEEE Trans. Rehabil. Eng.* 4(2): 63-72, 1996
- De Luca C J, Control of upper-limb prostheses: a case for neuroelectric control, *J. Medical Engineering & Technology*, 2(2):57-61, 1978
- Della Santina C C, Kovacs G T A, Lewis E R, Multi-unit recording from regenerated bullfrog eighth nerve using implantable silicon-substrate microelectrodes, *J Neuroscience Methods* 72,71-86, 1997

- Dioszeghy P, Stålberg E, Changes in motor and sensory nerve conduction parameters with temperature in normal and diseased nerve, *Electroencephalography and clinical Neurophysiology* 85:229-235, 1992
- Drake K L, Wise K D, Farraye J, Anderson D J, BeMent Spencer L, Performance of planar multisite microprobes in recording extracellular single-unit intracortical activity, *IEEE Trans. Biomed. Eng.* 35:719-732, 1988
- Edin B, Quantitative analysis of static strain sensitivity in human mechanoreceptors from hairy skin. *J. Neurophys.* 67:1105-13, 1992
- Elek J, Prochazka A, Hulliger M, Vincent S, In-series compliance of gastrocnemius muscle in cat step cycle: Do spindles signal origin-to-insertion length ?, *J. Physiol.* 429:237-58, 1990
- Eng J J, Hoffer J A, Kallesøe K, Stretch reflexes elicited in standing depend on fibre velocity, not muscle velocity. *Proc. IX Can. Soc. Biomech.* pp. 396-397, 1996
- Eng J J, Kallesøe K, Qi H, Hoffer J A, Action of medial gastrocnemius muscle when cat steps over obstacle or on uneven terrain, *Soc. neurosci. abstr.*, 21:173.2, 1995a
- Eng J J, Kallesøe K, Qi H, Hoffer J A, Hindlimb muscular activity during locomotion on uneven terrain, Abstract presented at the conference Multisegmental Motor Control: Interface of Biomechanical, Neural and Behavioral Approaches (sponsored by the American Physical Therapy Association), New Hampton, New Hampshire, 15 Aug 1995b
- Fineley and Karpovich, Electrogoniometric analysis of normal and pathological gaits, *The Research Quarterly* 35(3), supplement
- Frijns J H M, ten Kate J H, A model of myelinated nerve fibers for electrical prosthesis design, *Med. & Biol. Eng. & Comput.* 32:391-398, 1994
- Ganapathy N, Clark W Jr, Extracellular currents and potentials of the active myelinated nerve fiber, *Biophysical J.* 52:749-761, 1987
- Geddes L A, *Electrodes and the measurement of bioelectric events*, Wiley-Interscience, 1972
- Geddes L A, Baker L E, The specific resistance of biologic material - A compendium of data for the biomedical engineering and physiologist, *Med. Biol. Eng. Comput.* 5:271-93, 1967
- Geselowitz D B, On bioelectric potentials in an inhomogeneous volume conductor, *Biophys. J.* 7:1-9, 1967
- Gileadi E, Kirowa-Eisner E, Penciner J, *Intrfacial Electrochemestri: An experimental approach*, Addison-Wesley, Massachusetts, 1975
- Goldman D E, Hueter T F, Tabular data of the velocity and absorption of high-frequency sound in mammalian tissues, *J. Acoustical Soc. Am.*, 28:35-37, 1956
- Goodall E V, Horch K W, Analysis of single-unit firing patterns in multi-unit intrafascicular recordings, *Med. & Biol. Eng. & Comput.* 31:257-67, 1993
- Goodall E V, Kosterman L M, Holsheimer J, Struijk J J, Modeling study of activation and propagation delays during stimulation of peripheral nerve fibers with a tripolar cuff electrode, *IEEE Trans. Biomed. Eng.* 3(3):272-282, 1995
- Goodall E V, Lefurge T M, Horch K W, Information contained in sensory nerve recordings made with intrafascicular electrodes, *IEEE Trans. Biomed. Eng.* 38(9):846-50, 1991
- Gootzen T H, Stegeman D F, van Oosterom A, Muscle electric activity. II: On the feasibility of model-based estimation of experimental conditions in electromyography, *Annals of Biomed. Eng.* 21(4):391-9, 1993
- Gorassini M, Prochazka A, Taylor J L, Cerebellar ataxia and muscle spindle sensitivity, *J. Neurophysiol.* 70:1853-62, 1993
- Grandjean P A, Lee P H J, Nerve electrode with biological substrate, US patent 5.031.621, 16 Jul. 1991

- Gregor R J, Abelew T A, Tendon force measurements and movement control: a review, *Med. Sci. Sports Exerc.*, 26:1359-72, 1994
- Griep P A M, Boon K L, Stegeman D F, A study of the motor unit action potential by means of computer simulation, *Biol. Cybernetics* 30:221-230, 1978
- Hallin R G, Ekedahl R, Frank O, Segregation by modality of myelinated and unmyelinated fibers in human sensory nerve fascicles, *Muscle and nerve*, 14(2):157-65, 1991
- Hasan Z, Stuart D G, Animal solutions to problems of movement control: The role of proprioceptors, *Ann. Rev. Neurosci.* 11:199-223, 1988
- Haugland M K, A flexible method for fabrication of nerve cuff electrodes, The 18th annual international conference of the IEEE Engineering in medicine and biology society, Amsterdam, 31 Oct. - 3 Nov., 1996
- Haugland M K, *Natural sensory feedback for closed-loop control of paralyzed muscles*, Ph.D. thesis, Department of Medical Informatics and Image analysis, University of Aalborg, Denmark, 1994
- Haugland M K, Lickel A, Riso R, Adamczyk M, Keith M, Lauge I, Haase J, Sinkjær T, Restoration of lateral hand grasp using natural sensors, 5<sup>th</sup> Vienna International Workshop on FES, pp 339-342, 1995
- Haugland M K, Sinkjær T, Cutaneous whole nerve recordings used for correction of footdrop in hemiplegic man, *IEEE Trans. Rehab. Eng.* 3(4):307-317, 1995
- Haugland M, A miniature implantable nerve stimulator, pp:221, Proceedings 2<sup>nd</sup> Annual IFESS Conference and Neural Prosthesis: Motor Systems 5, Burnaby, B.C. Canada, 1997
- Heringa A, Stegeman D F, de Werd J P C, Calculated potential and electric field distribution around an active nerve fiber, *J. Appl. Phys.* 66:2724-2731, 1989
- Heringa A, Stegeman D F, Uijen G J H, de Werd J P C, Solution methods of electrical field problems in physiology, *IEEE Trans. Biomed. Eng.* 29(1):34-42, 1982
- Hetke J F, Lund J L, Najafi K, Wise K D, Anderson D J, Silicon ribbon cables for chronically implantable microelectrode arrays, *IEEE Trans. Biomed. Eng.* 41:314-21, 1994
- Hoffer J A, Closed-loop, implanted-sensor, functional electrical stimulation system for partial restoration of motor function, US patent 4,750,499, June 14, 1988
- Hoffer J A, Techniques to study spinal cord, peripheral nerve and muscle activity in freely moving animals. In: *Neurophysiological Techniques: Applications to Neural Systems*, NEUROMETHODS, Vol. 15, Boulton A A, Baker G B, Vanderwolf C H, editors. Humana Press, Clifton, N.J., 65-145, 1990
- Hoffer J A, Caputi A A, Pose I E, Griffiths R I, Roles of muscle activity and load on the relationship between muscle spindle length and whole muscle length in freely walking cats, *Prog. Brain Res.* 80:75-85; discussion 57-60, 1989
- Hoffer J A, Haugland M K, Signals from tactile sensors in glabrous skin: Recording, processing, and applications for the restoration of motor functions in paralyzed humans, in *Neural Prostheses: Replacing motor function after disease or disability*, Stein R B, Peckham P H, Popovic D P (editors), Oxford University Press, pp. 99-125, 1992
- Hoffer J A, Loeb G E, Implantable electrical and mechanical interfaces with nerve and muscle, *Annals of Biomedical Engineering*, 8:351-360, 1980
- Hoffer J A, Loeb G E, Marks W B, O'Donovan, Pratt C A, Sugano N, Cat hindlimb motoneurons during locomotion. I. Destination, axonal conduction velocity, and recruitment threshold, *J. Neurophysiol.* 57:510-29, 1987a
- Hoffer J A, Loeb G E, Pratt C A, Single unit conduction velocities from averaged nerve cuff electrode records in freely moving cats, *J. Neurosci. Methods* 4:211-25, 1981

- Hoffer J A, Sinkjær T, A natural "force sensor" suitable for closed-loop control of functional neuromuscular stimulation, in *Proc. 2nd Vienna International Workshop on Functional Electrostimulation*, 45-50, Sep. 1986
- Hoffer J A, Stein R B, Haugland M K, Sinkjær T, Durfee W K, Schwartz A B, Loeb G E, Kantor C, Neural signals for command control and feedback in functional neuromuscular stimulation: A review, *J. Rehabilitation Research and Development*, 33(2):145-157, 1996
- Hoffer J A, Sugano N, Loeb G E, Marks W B, O'Donovan M J, Pratt C A, Cat hindlimb motoneurons during locomotion. II Normal Activity patterns, *J. Neurophysiol.* 57:530-53, 1987b
- Hoffer J A, Weytjens J L F, Alpha-motoneuron activity, afferent activity and muscle fiber movement simultaneously recorded from cat medial gastrocnemius muscle during posture and locomotion, *Soc. Neurosci. Abstr.* 16:891, 1990
- Hoogerwerf A C, Wise K D, A three-dimensional microelectrode array for chronic neural recording, *IEEE Trans. Biomed. Eng.* 41:1136-1146, 1994
- Houk J C, Henneman E, Response of golgi tendon organs to active contractions of the soleus muscle in the cat, *J. Neurophysiol.* 330:466-81, 1967
- Hulliger M, The Mammalian muscle spindle and its central control, *Rev. Physiol. Biochem. Pharmacol.* 101:1-110, 1984
- Hulliger M, Prochazka A, A new simulation method to deduce fusimotor activity from afferent discharge recorded in freely moving cats, *J. Neuroscience Methods* 8:197-204, 1983
- Hunt C C, Mammalian muscle spindle: Peripheral mechanisms, *Physiological reviews* 70(3):643-663, 1990
- Jaeger R J, Lower extremity application of functional neuromuscular stimulation, *Assist. Technol.* 4:19-30, 1992
- Jami L, Golgi tendon organs in mammalian skeletal muscle: Functional properties and central actions, *Physiol. Rev.* 72:623-666, 1992
- Ji J, Najafi K, Wise K D, A scaled electronically-configurable multichannel recording array, *Sensors and Actuators A21-A23*:589-591, 1990
- Kallesøe K, Hoffer J A, Strange K, Valenzuela I Implantable cuff having improved closure, US patent 5.487.756, 30 Jan. 1996
- Kallesøe K, Valenzuela I, Viberg D, Hoffer J A, Interfacing to single peripheral axons using flexible silicon multicontact probes, Abstr. "Neural Prostheses Workshop: Motor systems IV", Ohio, July 1994
- Kettelkamp D B, Johnson R J, Smidr G L, Chao E Y, Walker M, An electrogoniometric study of knee motion in normal gait, *J. Bone & Joint Surgery - Amer. Vol.* 52(4):775-90, 1970
- Klee M, Plonsey R, Finite difference solution for biopotentials of axially symmetric cells, *Biophys. J.* 12:1661-1675, 1972
- Kovacs G T A, Storment C W, Rosen J M, Regeneration microelectrode array for peripheral nerve recording and stimulation, *IEEE Trans. Biomed. Eng.* 39(9):893-902, 1992
- Kralj A, Acimovic R, Stanic A, Enhancement of hemiplegic patient rehabilitation by means of functional electrical stimulation, *Prosthetics and Orthotics International* 15:107-114, 1993
- Kralj A, Bajd T, *Functional electrical stimulation, standing and walking after spinal cord injury*, Boca Raton, FL: CRC Press, 1989
- Kralj A, Bajd T, Turk R, Results of FES application to 71 SCI patients, In: *Proc. of RESNA 10th Annual Conference on Rehabilitation Technology*, pp. 645-647, San Jose, CA, 1987
- Lefurge T M, Goodall E V, Horch K W, Stensaas L, Schoenberg A, Chronically implanted intrafascicular recording electrodes, *Ann. Biomed. Eng.* 19:197-207, 1991

- Lemon R, *Methods for Neuronal Recording in Conscious Animals*, IBRO handbook series; v.4, Wiley Interscience publication, 1984
- Lichtenberg B K, De Luca, C J, Distinguishability of functionally distinct evoked neuroelectric signals on the surface of a nerve, *IEEE Trans. Biomed. Eng.* 26(4):228-37, 1979
- Lindström L, Petersén I, Power spectrum analysis of EMG signals and its application, Computer-Aided Electromyography, *Prog. Clin. Neurophysiol.* Ed. Desmedt J E, Karger, Basel, 10:1-51, 1983
- Loeb G E, Peck R A, Cuff electrodes for chronic stimulation and recording of peripheral nerve activity, *J. Neurosci. Methods*, 64:95-103, 1996
- Loeb G E, Bak M J, Duysens J, Long-term unit recording from somatosensory neurons in the spinal ganglia of the freely walking cat, *Science*. 197(4309):1192-4, 1977 Sep 16.
- Loeb G E, Neural prosthetic interfaces with the nervous system, *Trends in Neurosciences*, 12(5):195-201, 1989
- Loeb G E, Gans C, *Electromyography for Experimentalists*, Univ. Chicago Press, Chicago, 1986
- Loeb G E, Hoffer J A, Activity of spindle afferents from cat anterior thigh muscles. II. Effect of fusimotor blockade. *J. Neurophys.* 54(3):565-577, 1985b
- Loeb G E, Hoffer J A, Marks W B, Activity of spindle afferents from cat anterior thigh muscles. III. Effect of external stimuli. *J. Neurophys.* 54(3):578-591, 1985c
- Loeb G E, Hoffer J A, Pratt C A, Activity of spindle afferents from cat anterior thigh muscles. I. Identification and patterns during normal locomotion. *J. Neurophys.* 54(3):549-564, 1985a
- Loeb G E, Marks W B, Beatty P G, Analysis and microelectronic design of tubular electrode arrays intended for chronic, multiple single-unit recording from captured nerve fibers, *Med. & Biol. Eng. & Comput.* 15:195-201, 1977
- Lorente de Nó, Analysis of the distribution of the action currents of nerve in volume conductors, *Studies from the Rockefeller Institute for medical research*, 132:384-497, 1947
- Lynch H W, Multi-electrode neurological stimulation apparatus, US patent 5,038,781, Aug. 13, 1991
- Malmivuo J, Plonsey R, *Bioelectromagnetism*, Oxford University Press, New York, 1995
- Marks W B, Loeb G E, Action currents, internodal potentials, and extracellular records of myelinated mammalian nerve fibers derived from node potentials, *Biophysical Journal* 16:655-668, 1976
- Mascagni M V, Numerical methods for neuronal modeling, in *Methods in neuronal modeling*, Koch C, Segev I, (eds), The MIT Press, 1989
- Matthews P B C, Evolving views on the internal operation and functional role of the muscle spindle, *J Physiol.* 320:1-30, 1981
- Matthews P B C, *Mammalian muscle receptors and their central action*, Edward Arnold, London, 1972
- Matthews P B C, Stein R B, The sensitivity of muscle spindle afferents to small sinusoidal changes of length, *J Physiol.* 200:723-43, 1969
- McIntyre J, Bizzi E, Servo hypotheses for the biological control of movement, *J. Motor Behavior*, 25:193-202, 1993
- McNeal D R, Analysis of a model for excitation of myelinated nerve, *IEEE Trans. Biomed. Eng.* 23:329-337, 1976
- McNeal D R, Nakai R J, Meadows P, Tu W, Open-loop control of the freely-swinging paralyzed leg, *IEEE Trans. Biomed. Eng.* 36(9):895-905, 1989
- Meier J H, Rutten W L, Zoutman A E, Boom H B K, Bergveld P, Simulation of multipolar fiber selective neural stimulation using intrafascicular electrodes, *IEEE Trans. Biomed. Eng.* 39:122-134, 1992

- Millesi H, Zöch G, Reihnsner R, Mechanical properties of peripheral nerves, *Clinical orthopedics and related research* 314:76-83, 1995
- Milner T, Stein R B, Gillespie J, Hanley B, Improved estimate of conduction velocity distributions using single unit action potentials, *J. Neurology, Neurosurgery, and Psychiatry*, 44:476-484, 1981
- Mirfakhraei K, Horch K, Classification of action potentials in multi-unit intrafascicular recordings using neural network pattern recognition techniques, *IEEE Trans. Biomed. Eng.* 41:89-91, 1994
- Monk P M S, Mortimer R J, Rosseinsky D R, *Electrochromism: Fundamentals and applications*, VCH, Weinheim, 1995
- Moris J R W, Accelerometry - A technique for the measurement of human body movement, *J Biomechanics* 6:729-736, 1973
- Murphy P R, Martin H A, Fusimotor discharge patterns during rhythmic movements, *TINS* 16:273-8, 1993
- Murphy P R, Stein R B, Taylor J, Phasic and tonic modulation of impulse rates in  $\gamma$ -motoneurons during locomotion in premammillary cats, *J. Neurophysiol.* 52:228-43, 1984
- Najafi K, Ji J, Wise K, Scaling limitations of silicon multichannel recording probes, *IEEE Trans. Biomed. Eng.* 37(1):1-11, 1990
- Najafi K, Wise K D, Mochizuki T, A high-yield IC-compatible multichannels recording array, *IEEE Electron Devices* 7:1206-11, 1985
- Nandedkar S D, Stålberg E, Simulation of single muscle fiber action potentials, *Med. & Biol. Eng. & Comput.* 21:158-165, 1983
- Naples G G, Mortimer J T, Scheiner A, Sweeney J D, A spiral nerve cuff electrode for peripheral nerve stimulation, *IEEE Trans. Biomed. Eng.* 35(11):905-916, 1988
- Naples G G, Sweeney J D, Mortimer J T, Implantable cuff, method of manufacture, and method of installation, US Patent 4,602,624, Jul. 29, 1986
- Nielsen J F D, *Modellering af sensoriske aktionspotentialer*, (departmental report in Danish: Sensory action potential models), R89-14, Institute for Electronic Systems, Aalborg University, Denmark, February 1989
- Panescu D, Webster J G, Stratbucker R A, A nonlinear finite element model of the electrode-electrolyte-skin system, *IEEE Trans. Biomed. Eng.* 41(7):681-687, 1994
- Park J B, Roderic S L, *Biomaterials*, 2nd ed. Plenum Press, 1992
- Parrini S, Legat V, Delbeke J, Veraart C, A modelling study to compare tripolar and monopolar cuff electrodes for selective activation of nerve fibers, pp:235, Proceedings 2<sup>nd</sup> Annual IFESS Conference and Neural Prosthesis: Motor Systems 5, Burnaby, B.C. Canada, 1997
- Patlak C S, Potential and current distribution in nerve: The effect of the nerve sheath, the number of fibers, and the frequency of alternating current stimulation, *Bulletin of Mathematical biophysics* 17:287-307, 1955
- Peckham P H, Opportunities and challenges for the clinical utilization of functional electrical stimulation, *Assist. Technol.* 4:46-48, 1992
- Peters A, Palay S L, Webster H de F, *The fine structure of the nervous system*, Harper & Row, New York, 1970
- Petrofsky J S, Phillips C A, Heaton H H, Feedback control systems for walking in man, *Comput. Biol. Med.* 14:135-49, 1984
- Pickup P G, A model for anodic hydrous oxide growth at Iridium, *J. Electroanal. Chem.*, 220:83-100, 1987
- Platt D, Wilson A M, Timbs, A Wright I M, Goodship A E, Novel force transducer for measurement of tendon force *in vivo*, *J. Biomechanics* 27(12):1489-1493, 1994

- Plonsey R, Barr R C, *Bioelectricity, A quantitative approach*, Plenum Press, New York, 1988
- Plonsey R, Barr R C, Electric field stimulation of excitable tissue, *IEEE Trans. Biomed. Eng.* 42(4):329-336, 1995
- Plonsey R, *Bioelectric phenomena*, McGraw-Hill, New York, 1969
- Plonsey R, Heppner D B, Considerations of quasi-stationarity in electrophysiological systems, *Bulletin of Mathematical Biophysics* 29:657-664, 1967
- Pollak P, Benabid A L, Limousin P, Krack P, Treatment of Parkinson's disease: New clinical treatment strategies, *European Neurology* 36(6):400-4, 1996
- Popovic D B, Stein R B, Jovanovic K L, Dai R, Kostoc A, Armstrong W W, Sensory nerve recording for closed-loop control to restore motor functions, *IEEE Trans. Biomed. Eng.* 40(10):1024-1031, 1993
- Press W H, Flannery B P, Teukolsky S A, Vetterling W T, *Numerical recipes in C*, Cambridge University Press, 1988
- Prochazka A, Chronic techniques for studying neurophysiology of movement in cats, In: Lemon R (Ed.), *Methods for neuronal recording in conscious animals*, IBRO Handbook series: Methods in the neuroscience, Vol. 4, Wiley, Chichester, 113-128, 1984
- Prochazka A, Sensorimotor gain control: a basic strategy of motor systems?, *Prog Neurobiol* 33:281-307, 1989
- Prochazka A, Wand P, Independence of fusimotor and skeltomotor systems during voluntary movement, *Prog. brain Res.* 50:229-244, 1981
- Prochazka A, Wand P, Tendon organ discharge during voluntary movements in cats, *J. Physiol.* 303:385-390, 1980
- Prochazka A, Westerman R A, Ziccone S P, Discharge of single hindlimb afferents in the freely moving cat, *J. Neurophy.* 39(5):1090-1104, 1976
- Prochazka A, Westerman R A, Ziccone S P, Ia afferent activity during a variety of voluntary movements in the cat, *J. Physiol.* 268:423-448, 1977
- Pronk C M, van der Helm F C T, The palpator: an instrument for measuring the positions of bones in three dimensions, *J. Medical Eng. and Tech.* 15(1):15-20, 1991
- Pugh J, *Design of peripheral nerve cuff and "hat-pin" microelectrodes for single unit recording*, B.Sc Honors Thesis, School of Kinesiology, Simon Fraser University, 1996
- Qi H, Kallesøe K, Hoffer J A, How muscle aponeurosis change shape during normal movement, Proceedings, Eighth Biennial Conference, Canadian Society for Biomechanics, Calgary, pp:190-1, August 18-20, 1994
- Ratcliffe M B, Gupta K B, Streicher J T, Savage E B, Bogen D K, Edmunds L H Jr, Use of sonomicrometry and multidimensional scaling to determine the three-dimensional coordinates of multiple cardiac locations: Feasibility and initial implementation, *IEEE Trans. Biomed Eng.* 42(6):587-599, 1995
- Rattay F, Analysis of models for extracellular fiber stimulation, *IEEE Trans. Biomed. Eng.* 36(7):676-682, 1989
- Robblee L S, Lefko J L, Brummer S B, Activated Ir: An electrode suitable for reversible charge injection in saline solution, *J. Electrochem. Soc.* 130:731-733, 1983
- Roberts W J, Elardo S M, Clustering of primary afferent fibers in peripheral nerve fascicles by sensory modality. *Brain Res.* 370:149-152, 1986
- Robinson D A, The electrical properties of metal micro-electrodes, *Proc. IEEE* 56:1065-1071, 1968.



- Rosenfalck P, Intra- and extracellular potential fields of active nerve and muscle fibers, *Acta Physiol. Scand. sup.* 321, 1969
- Roth B J, Altman K W, Steady-state point-source stimulation of a nerve containing axons with an arbitrary distribution of diameters, *Med & Biol. Eng. & Comput.* 30:103-108:1992
- Rothwell J C, *Control of human voluntary movement*, University Press, Cambridge, pp:86-126, 1994
- Rozman J C, Trlep M, Multielectrode spiral cuff for selective stimulation of nerve fibers, *J. Medical Eng. and Tech.* 18(2):194-203, 1992
- Rozman J, Acimovic-Janezic R, Tekavcic I, Kljajic M, Trlep M, Implantable stimulator for selective stimulation of the common peroneal nerve: a preliminary report, *J. Medical Eng. and Tech.* 18(2):47-53, 1994
- Rutten L C, Frieswijk T A, Smit J P A, Rozijn T H, Meier J H, 3D Neuro-electronic interface devices for neuromuscular control: Design studies and realization steps, *Biosensors & Bioelectronics* 10: 141-153, 1995
- Rutten W L C, Meier J H, Selectivity of intraneural prosthetic interfaces for muscular control, *Med. & Biol. Eng. & Comput.* 29:NS3-NS7, 1991
- Saad Y, *Iterative methods for sparse linear systems*, PWS Publishing Company, 1996
- Salcman M, Bak M J, Design, fabrication and in vivo behavior of chronic recording intracortical electrodes, *IEEE Trans. Biomed. Eng.* 20:253-60, 1973
- Salcman M, Bak M, A new chronic recording intracortical microelectrode, *Med. and Bio. Eng.* 42-50, 1976
- Schmidt E, Parylene as an electrode insulator: A review, *J. Electrophysiol. Tech.* 10:19-29, 1983
- Schoenberg A, Kendell J, Recruitment properties of intraneural electrodes for long-term stimulation of motor nerves to restore movement in paralyzed muscles, Final report to U.S. Department of Education, NIDRR grant No: H133G90031, University of Utah, Dec. 23, 1993
- Schoonhoven R, De Weerd J P, On the optimal choice of a recording electrode in electroneurography, *Electroencephalography & Clinical Neurophysiology.* 58(4):308-16, 1984
- Schoonhoven R, Schellen R L, Stegeman D F, Gabreels-Festen A A, Sensory potentials and sural nerve biopsy: a model evaluation, *Muscle and Nerve* 10(3):246-262, 1987
- Schoonhoven R, Stegeman D F, Model and analysis of compound nerve action potentials, *Critical reviews in Biomed. Eng.* 19(1):47-111, 1991
- Schoonhoven R, Stegeman D F, De Weerd J P, The forward problem in electroneurography. I: A generalized volume conductor model. *IEEE Trans. Biomed Eng.* 33(3):327-34, 1986a
- Schoonhoven R, Stegeman D F, van Oosterom A, The forward problem in electroneurography. II: Comparison of models, *IEEE Trans. Biomed Eng.* 33(3):335-341, 1986b
- Schoonhoven R, Stegeman D F, van Oosterom A, Dautzenberg G F M, The inverse problem in electroneurography - I: Conceptual basis and mathematical formulation, *IEEE Trans. Biomed Eng.* 35(10):769-777, 1988
- Schwan H P, Calvin F K, Capacitive properties of body tissue, *Circulation Res.* V:439-443, 1957
- Schwan H P, Calvin F K, Specific resistance of body tissue, *Circulation Res.* IV:664-670, 1956
- Sinkjær T, Hoffer J A, A computer-controlled system to perturb the ankle joint of freely standing cats trained to maintain a given force, *J. Neurosci. Methods* 21:311-20, 1987
- Smidt G L, Deusinger R H, Arora J, Albright J P, An automated accelerometry system for gait analysis, *J. Biomechanics* 10:367-375, 1977

- Snodderly D M Jr, Extracellular Single Unit Recording, in *Bioelectric Recording Techniques, Part A*, ed. Thompson R F, Patterson M M, Academic Press, New York, 137-65, 1973
- Sonn M, Fesit W M, A prototype flexible microelectrode array for implant-prosthesis applications, *Medical and Biological Eng.* 778-791, 1974
- Stegeman D F, de Weerd J P C, Modeling compound action potentials of peripheral nerves in situ. I. Model description; evidence for a non-linear relation between fiber diameter and velocity, *Electroencephalography and clinical neurophysiology* 54:436-448, 1982a
- Stegeman D F, de Weerd J P C, Modeling compound action potentials of peripheral nerves in situ. II. A study of the influence of temperature, *Electroencephalography and clinical neurophysiology* 54:516-529, 1982b
- Stegeman D F, de Weerd J P C, Eijkman E G J, A volume conductor study of compound action potentials of nerves in situ: The forward problem, *Biol. Cybernetics* 33,97-111, 1979
- Stegeman D F, Gootzen T H J M, Theeuwens M M H J, Vingerhoets H J M, Intramuscular potential changes caused by the presence of the recording EMG needle electrode, *Electroencephalography and clinical neurophysiology*, 93:81-90, 1994
- Stegeman D F, Schoonhoven R, Dautzenberg G F M, Moleman J, The inverse problem in electroneurography - II: Computational aspects and evaluation using simulated data, *IEEE Trans. Biomed. Eng.* 35(10):778-788, 1988
- Stegeman D F, van Oosterom A, E J, Colon, Far-field evoked potential components induced by a propagating generator: computational evidence, *Electroencephalography and Clinical Neurophysiology* 67(2):176-187, 1987
- Stein R B, *Nerve and Muscle*, Plenum Press, New York, 1980
- Stein R B, Charles D, Davis L, Jhamandas J, Mannard A, Nichols T R, Principles underlying new methods for chronic neural recording, *Canadian J. Neurological Sciences* 2(3),235-244, 1975
- Stein R B, Kostov A, Belanger M, Armstrong W W, Popovic D, Methods to control functional electrical stimulation in walking, in *Proc. of 1<sup>st</sup> Sendai Intern. Symp. on FES.* 130-134, 1992a
- Stein R B, Peckham P H, Popovic D P, eds, *Neural Prostheses, Replacing Motor Function After Disease or Disability*, Oxford University Press, 1992b
- Stephanova D, Trayanova N, Gydikov A, Kossev A, Extracellular potentials of a single myelinated nerve fiber in an unbound volume conductor, *Biol. Cybern.* 61:205-210, 1989
- Steven W, Implantable displacement sensor, US Patent 4,813,435, Mar 21, 1989
- Steven W, Method of and means for implanting a pressure and force sensing apparatus, US Patent 4,993,428, Feb. 19, 1991
- Strange K D, *A state controller for closed-loop functional electrical stimulation regulated by natural sensory feedback*, M.A.Sc. thesis, Simon Fraser university, April 1996
- Strange K D, Kallesøe K, Hoffer J A, Long term stability of nerve cuff signals recorded from the cat forelimb, in revision
- Struijk J J, Haugland M K, Thomsen M, Fascicle selective recording with a nerve cuff electrode, The 18th annual international conference of the IEEE Engineering in medicine and biology society, Amsterdam, 31 Oct. - 3 Nov., 1996
- Struijk J J, Holstheimer J, van der Heide G G, Boom H B K, Recruitment of dorsal column fibers in spinal cord stimulation: influence of collateral branching, *IEEE Trans. Biomed. Eng.* 39(9):903-912, 1992
- Sweeney J D, Crawford N R, Brandon T A, Neuromuscular stimulation selectivity of multiple-contact nerve cuff electrode arrays, *Med. & Biol. Eng. & Comput.* 33:418-425, 1995

- Tanghe S J, Najafi K, Wise K D, A planar IrO multichannel stimulating electrode for use in neural prostheses, *Sensors and Actuators B*1:464-467,1990
- Tasaki I, Frank K, Measurement of the action potential of myelinated nerve fiber, *Am. J. Physiol.* 182:572-78, 1955
- Teeter, J O, A review of the functional electrical stimulation equipment market, *Assist. Technol* 4:40-45, 1992
- Theeuwen M M H J, Gootzen T H J M, Stegeman D F, Muscle electric activity I: A model study on the effect of needle electrodes on single fiber action potentials, *Annals of biomedical engineering* 21:377-389, 1993
- Townsend M A, Izak M, Jackson R W, Total motion knee goniometry, *J. Biomechanics* 10(3):183-93, 1977
- Trasatti S (ed), *Electrodes of metallic oxides*, Elsevier scientific publishing company, Amsterdam, 1980
- Tyler D J, Durand D M, Corrugated inter-fascicular nerve cuff method and apparatus, US patent 5.634.462, 3 Jun. 1997a
- Tyler D, Durand D M, A slowly penetrating intrafascicular nerve electrode for selective activation of peripheral nerves, *IEEE Trans. Rehab. Eng.* 5(1), 51-61, 1997b
- UMCISC, Micromachined stimulating electrodes, *Neural Prosthesis Program*, National Institute of Health, Maryland, US, Quarterly report #9, Contract NIH-NINDS-N01-NS-2-2379, Oct.-Dec., 1995
- UMCISC, Multichannel multiplexed intracortical recording arrays, *Neural Prosthesis Program*, National Institute of Health, Maryland, US, Quarterly report #2, Contract NIH-NINDS-N01-NS-0-2396, Jan.-Mar., 1991
- van Dijk J H M, Simulation of human arm movements controlled by peripheral feedback, *Biol. Cybernetics* 29:175-186, 1978
- van Leeuwen J L, Spoor C W, Modeling the pressure and force equilibrium in unipennated muscles with in-line tendons, *Phil. Trans. R. Soc. Lond.* 324(1302),321-333,1993
- van Rotterdam, A discrete formalism for the computation of extracellular potentials, *Kybernetik* 12:223-228, 1973
- van Trigt III P, Bauer B J, Olsen C O, Rankin J S, Wechsler A S, An improved transducer for measurement of cardiac dimensions with sonomicrometry, *Am. J. Physiol.* 240 (Heart Circ. Physiol. 9):H664-H668, 1981
- Veltink P H, van Alsté J A, Boom H B K, Influence of stimulation conditions on recruitment of myelinated nerve fibers: A model study, *IEEE Trans. Biomed. Eng.* 35(11):917-924, 1988b
- Veltink P H, van Alsté J A, Boom H B K, Multielectrode intrafascicular and extraneural stimulation, *Med. & Biol. Eng. & Comput.* 27:19-24, 1989a
- Veltink P H, van Alsté J A, Boom H B K, Simulation of intrafascicular and extraneural nerve stimulation, *IEEE Trans. Biomed. Eng.* 35(1):69-75, 1988a
- Veltink P H, van Veen B K, Struijk J J, Holsheimer J, Boom H B K, A modeling study of nerve fascicle stimulation, *IEEE Trans. Biomed. Eng.* 36(7):683-92, 1989b
- Walter J S, McLane J, Cai W, Khan T, Cogan S, Evaluation of a thin-film peripheral nerve cuff electrode, *J. Spinal Cord Medicine*, 18(1):28-32, 1995
- Webster J G, editor, *Medical instrumentation. Application and design*, Houghton Mifflin Company, Boston, 1978
- Weiland J, *Electrochemical properties of iridium oxides stimulating electrodes*, Ph.D. Thesis, Biomedical Engineering, University of Michigan, 1997

- Weinberg A M, Green's functions in biological potential problems, *Bulletin of Mathematical biophysics* 4:107-115, 1942
- Weytjens J L F, Viberg D A, Caputi A A, Kallesøe K, Hoffer J A, New transducer for measuring muscle length in unrestrained animals, *J. Neurosci. Methods* 45:217-25, 1992
- Wijesinghe R S, Gielen F L, Wikoswo J P Jr, A model for compound action potentials and currents in nerve bundle I: The forward problem, *Annals of Biomed. Eng.* 19:43-73, 1991a
- Wijesinghe R S, Gielen F L, Wikoswo J P Jr, A model for compound action potentials and currents in nerve bundle II: A sensitivity analysis of model parameters for the forward and inverse calculation, *Annals of Biomed. Eng.* 19:73-96, 1991b
- Wijesinghe R S, Gielen F L, Wikoswo J P Jr, A model for compound action potentials and currents in nerve bundle III: A comparison of the conduction velocity distribution calculated from compound action currents and potentials, *Annals of Biomed. Eng.* 19:97-121, 1991c
- Wise K D, Star A, An integrated circuit approach to extracellular microelectrodes, *Proc. 8th Int. Conf. Med. Biol. Eng. Sec.* 14-5, 1969
- Xiao S, McGill K C, Hentz V R, Action potentials of curved nerves in finite limbs, *IEEE Trans. Biomed. Eng.* 42(6):599-607, 1995
- Yoshida K, Horch K, Closed-loop control of ankle position using muscle afferent feedback with functional neuromuscular stimulation, *IEEE Trans. Biomed. Eng.* 43:167-76, 1996
- Yoshida K, Horch K, Selective stimulation of peripheral nerve fibers using dual intrafascicular electrodes, *IEEE Trans. Biomed. Eng.* 40:492-4, 1993
- Yoshida K, Jovanovic K, Stein R B, Neural recordings using longitudinal intra-fascicular electrodes, pp:216, Proceedings 2<sup>nd</sup> Annual IFESS Conference and Neural Prosthesis: Motor Systems 5, Burnaby, B.C. Canada, 1997
- Zachary L S, Dellon E S, Nicholas E M, Dellon A L, The structural basis of Felice Fontana's spiral bands and their relationship to nerve injury, *J. Reconstructive Microsurgery* 9(2):131-8, 1993